JOURNAL OF THE AERONAUTICAL SCIENCES

VOLUME 11 OCTOBER, 1944 NUMBER 4

Some Two-Dimensional Adiabatic Compressible Flow Patterns

HANS KRAFT* AND CHARLES G. DIBBLE†

General Electric Company

SUMMARY

This paper presents a number of adiabatic compressible flow patterns which include subsonic and supersonic régimes at the same time. Specifically, the objective of the investigation is to obtain good records of compressible flow when it is undergoing large deflections such as occur in turbine nozzles and buckets. The patterns are analyzed so that the engineer may have a better understanding of the peculiarities of compressible flow. The velocity gradient receives special attention because of its role as originator of both jet separation and shock waves. The patterns are shown in the actual physical plane and also in the hodograph plane where magnitude and direction of the velocity vector are the polar coordinates. The hodograph variables are used because they allow the linearization and exact solution of the differential equations. The method of solution is not new. A large-scale execution of it, however, has not been previously undertaken. The patterns demonstrate effectively the relation between the hodograph and physical planes.

SYMBOLS

c = sound velocity of fluid, ft. per. sec.
c_0 = sound velocity of fluid at rest, ft. per sec.
c_1 = c/c_0, dimensionless
n = characteristic constant for fields, dimensionless
p = fluid pressure, lbs. per sq.ft.
p_0 = pressure of fluid at rest, lbs. per sq.ft.
p_1 = p/p_0, dimensionless
P = factor of flux function depending only on w_1, sq.ft. per sec.
Q = factor of flux function depending only on θ, dimensionless
r = radius of curvature of streamline, ft.
s = length of streamline path, ft.
u, v = velocity components in x and y direction, ft. per sec.
$\bar{w}$ = velocity vector, ft. per sec.
w = magnitude of velocity, ft. per sec.
w_1 = w/c_0 = velocity expressed in terms of sound velocity of fluid at rest, dimensionless
x, y = physical space coordinates, ft.
α = $(\gamma - 1)/2$
β = $\alpha - 1 = (\gamma - 3)/2$
γ = c_p/c_v adiabatic exponent of fluid, dimensionless
Δ = the Jacobian = $(\partial\varphi/\partial w)(\partial\psi/\partial\theta) - (\partial\varphi/\partial\theta)(\partial\psi/\partial w)$, cu.ft. per sec.
ϵ = $\alpha + 1 = (\gamma + 1)/2$
θ = angle (direction) of velocity vector, dimensionless
μ = viscosity of fluid, lbs. sec. per sq.ft.
ρ = mass density of fluid, lbs. sec.^{2} per ft.^{4}
ρ_0 = mass density of fluid at rest, lbs. sec.^{2} per ft.^{4}
ρ_1 = ρ/ρ_0, dimensionless
φ = velocity potential, sq.ft. per sec.
ψ = flux function, sq.ft. per sec.

Presented at the Aerodynamics Session, Twelfth Annual Meeting, I.A.S., New York, January 25–27, 1944.

* Turbine Engineering Division.
† Engineering General Division.

INTRODUCTION

EVER SINCE PRANDTL introduced the conception of the boundary layer, potential flow has held a position of great importance both in aeronautics and in turbine and compressor design. As is now well recognized, noticeable friction forces appear only as a consequence of extremely large velocity gradients. The object of good design is to relegate these forces into the boundary layer. Outside of the latter, potential theory will describe the flow phenomena to a high degree of approximation.

For a long time, until airplanes moved at high speeds, the study of the incompressible field furnished an approximation satisfactory to the aeronautical engineer. This was fortunate, since the means for obtaining mathematical solutions that describe these fields was known. Conformal transformation, properly applied, will furnish the answer to any two-dimensional problem involving incompressible potential flow. The work of obtaining these solutions is often excessively great, but many flow fields have been calculated. They serve to guide the designer's mind and hand where actual quantitative evaluation is impracticable.

The turbine and compressor designer was in a less fortunate position than the aeronautical engineer. Many of his problems deal with compressible flow

phenomena. The problem of the calculation of two-dimensional compressible flow has not yet been solved satisfactorily. True, there are a number of partial solutions and some approximate methods of attacking the problem. But there is no workable method of obtaining the general solution. In recognition of this situation, it would appear that the actual physical existence of a number of compressible flow fields should prove to be of value to the designer. They can serve in a simple way as a nucleus of correct solutions so that the behavior of compressible flow can be studied. As the art progresses, more complicated fields can be added until most flow details of interest are represented by a correct field. Proceeding in this manner, the designer may be able to acquire a "compressible flow sense" that will help in design as much as if a general solution had wrested all the secrets of compressibility from the differential equation.

This investigation is a study of a number of such partial solutions that can be readily obtained by means of the differential analyzer. As such, it does not claim any originality. All it purports to do is to take an already existing method of solution and begin to exploit it, if possible, to the limit of its usefulness. The results obtained show that even simple fields afford good opportunity to learn of, and to become accustomed to, the idiosyncrasies of this particular problem.

The mathematical derivations leading up to the differential equation and to its solution have been kept quite extensive. They are mostly a repetition of what is already contained in the literature. An effort has been made to popularize the important equations by emphasizing the physical realities of which they are the expression. A compressible flow sense is sound only when the line of thought that leads from physical law to the flow field has become second nature.

The mathematical material contained in sections marked B will be needed by the engineer who wants to employ the method actively. Engineers not so inclined may follow the trend of thought and understand the conclusions by reading only the sections marked A.

Mathematical Relations

A

The derivation of the principal equations is carried through much along the line given by Ringleb[2] in 1940. The formulas are shown in parallel for both the compressible flow and incompressible flow.

The space coordinates of the physical or actual flow plane are x and y. The velocity components are u and v in the direction of x and y, respectively. w and θ are the magnitude and direction of the velocity vector and are also the polar coordinates of the hodograph plane. It develops that the equations for compressible flow are nonlinear and involved when written in terms of the coordinates of the physical plane. But the equations are simplified and become linear when written in terms of the hodograph variables.

The basic equations ruling the behavior of the fluid are simple and generally known. They prescribe irrotationality and conservation of matter, combined with the known interrelation between gas density and velocity.

Only "irrotational" flow is considered herein. This constitutes an arbitrary limitation and, for this reason, its establishment must be justified. Physical law says that no "rotation" can be caused in a fluid by the action of mere pressure forces that are, by definition, always normal to the surface on which they are exerted. To establish so-called "rotation," tangential shear forces must be exerted such as can be furnished by the viscosity of the fluid. The viscosity of a gas is exceedingly small and can cause appreciable forces only in the presence of extremely large velocity gradients. The postulation of zero rotation is equivalent to a statement that it is the flow of a gas that is under consideration. As such, it is not a limitation but is quite universal with this one exception: The resulting solutions must be searched for near vertical velocity gradients and must be modified within these regions. All fields without such regions are physically correct flow fields where exchanges between velocity energy and pressure energy proceed without energy loss of any kind. These exchanges are by definition of the word "isentropic" and, in this investigation, are restricted to take place without heat interchanges—i.e., they are also adiabatic.

In the language of mathematical equations, irrotationality is called for by the equation

$$\text{curl of velocity} = \text{curl}\,\bar{w} = (\partial u/\partial y) - (\partial v/\partial x) = 0 \quad (1)$$

Eq. (1) is the necessary and sufficient condition for the velocity to be described as the gradient of a potential function.

$$u = \partial\varphi/\partial x; \qquad v = \partial\varphi/\partial y \quad (2)$$

A potential field is one in which a number that has magnitude but not direction can be assigned to each point in the field so that, at any point, the change of this number in unit distance in a given direction is equal to the component of flow velocity in that direction. This is the meaning of Eqs. (2) in which φ is the number or potential assigned to each point in the field. The purpose of the calculation is to find such number distributions or potential fields.

The flow is considered to be in steady state—i.e., at every space point, the flow conditions do not vary with time. Transients thus are excluded. In this case, the physical law of conservation of matter states that mass is not generated, nor can it vanish anywhere in the fluid. Mathematically, it is described as

$$\text{divergence of mass flow} = \text{div.}\,(\rho_1\bar{w}) = (\partial/\partial x)(\rho_1 u) + (\partial/\partial y)(\rho_1 v) = 0 \quad (3)$$

ρ_1 is the ratio of density to the constant value of density when the fluid is at rest. Eq. (3) clearly states that an increase in mass flow in one direction must be offset by a decrease in mass flow in the direction perpendicular to it. It can be replaced by expressing the flow in terms of the so-called stream function ψ

$$-\rho_1 v = \partial\psi/\partial x; \qquad \rho_1 u = \partial\psi/\partial y \tag{4}$$

Eqs. (4) show that changes in the magnitude ψ at any point in any direction are equal to the magnitude of the mass flow at the point in the manner of the potential described before. They are equivalent to Eq. (3) because substitution of Eq. (4) in Eq. (3) leads to an identity.

$$(\partial^2\psi/\partial x\partial y) - (\partial^2\psi/\partial y\partial x) \equiv 0 \tag{5}$$

B

Combining Eqs. (2) and (4) furnishes the relation between φ and ψ:

$$\left.\begin{aligned} \partial\varphi/\partial x &= (1/\rho_1)(\partial\psi/\partial y) \\ \partial\varphi/\partial y &= (1/\rho_1)(\partial\psi/\partial x) \end{aligned}\right\} \tag{6}$$

In the case of *incompressible* flow, $\rho_1 = 1$ and the Cauchy Riemann equations result.

$$u = \frac{\partial\psi}{\partial y} = \frac{\partial\varphi}{\partial x}; \quad v = -\frac{\partial\psi}{\partial x} = \frac{\partial\varphi}{\partial y} \tag{7}$$

Equilibrium of Forces

Bernoulli's equation for reversible adiabatic compressible flow can be written

$$p_1 = \left\{1 - [(\gamma - 1)/2](w/c_0)^2\right\}^{\gamma/(\gamma-1)} \tag{8}$$

where p_1 is the ratio of pressure to the constant value of pressure when the fluid is at rest and where γ is the adiabatic exponent, which is 1.4 for air and approximately 1.3 for superheated steam. c_0 denotes the sound velocity of the fluid at rest. The local sound velocity c at the flow velocity w is given by

$$c^2 = \gamma p/\rho \tag{9}$$

The relation between density and pressure for adiabatic flow is

$$p_1 = (\rho_1)^\gamma \tag{10}$$

The combination of Eqs. (8) and (10) gives the relation between density and velocity.

$$\rho_1 = \left\{1 - [(\gamma - 1)/2](w/c_0)^2\right\}^{1/(\gamma-1)} \tag{11}$$

Using Eq. (11) for ρ_1 and eliminating first ψ and then φ from Eqs. (6) yields the relations between φ, x, y and ψ, x, y.

$$\left(1 - \frac{u^2}{c^2}\right)\frac{\partial^2\varphi}{\partial x^2} - 2\frac{uv}{c^2}\frac{\partial^2\varphi}{\partial x\partial y} + \left(1 - \frac{v^2}{c^2}\right)\frac{\partial^2\varphi}{\partial y^2} = 0 \tag{12}$$

$$\left(1 - \frac{u^2}{c^2}\right)\frac{\partial^2\psi}{\partial x^2} - 2\frac{uv}{c^2}\frac{\partial^2\psi}{\partial x\partial y} + \left(1 - \frac{v^2}{c^2}\right)\frac{\partial^2\psi}{\partial y^2} = 0 \tag{13}$$

That these equations are not identical in form becomes apparent when u and v are expressed in terms of φ and ψ, respectively.

The corresponding equations for incompressible flow are obtained from Eqs. (7) and result in Laplace's equation.

$$\frac{\partial^2\varphi}{\partial x^2} + \frac{\partial^2\varphi}{\partial y^2} = 0; \quad \frac{\partial^2\psi}{\partial x^2} + \frac{\partial^2\psi}{\partial y^2} = 0 \tag{14}$$

Methods of solution of Laplace's equation are well established.

Eqs. (12) and (13) for compressible flow are not linear and are extremely complicated, especially in view of the fact that c is a function of w,

$$w = \sqrt{u^2 + v^2} = \sqrt{(\partial\varphi/\partial x)^2 + (\partial\varphi/\partial y)^2}$$

These complication disappear if φ and ψ are written as functions of w and θ, the hodograph variables.

Transformation into Hodograph Plane

The transformation into the hodograph plane can be made by writing

$$u = w\cos\theta; \quad v = w\sin\theta \tag{15}$$

and substituting these values into the following equations for $d\varphi$ and $d\psi$

$$\left.\begin{aligned} d\varphi &= (\partial\varphi/\partial x)dx + (\partial\varphi/\partial y)dy = udx + vdy \\ d\psi &= (\partial\psi/\partial x)dx + (\partial\psi/\partial y)dy = \rho_1(-vdx + udv) \end{aligned}\right\} \tag{16}$$

Substituting Eqs. (15) in Eqs. (16) and solving for dx and dy,

$$dx = (\cos\theta/w)d\varphi - (1/\rho_1)(\sin\theta/w)d\psi \tag{17}$$

$$dy = (\sin\theta/w)d\varphi + (1/\rho_1)(\cos\theta/w)d\psi \tag{18}$$

Since at every point on the plane there exists a definite velocity vector, x and y can be considered as functions of w and θ. This point-by-point relationship can be described as the transformation of the physical x, y plane into the hodograph w, θ plane. A streamline in the physical plane describes a continuous sequence of end points of velocity vectors (w, θ) and thus will appear as a curve in the hodograph plane. This curve is called the hodograph of the streamline (see Fig. 1).

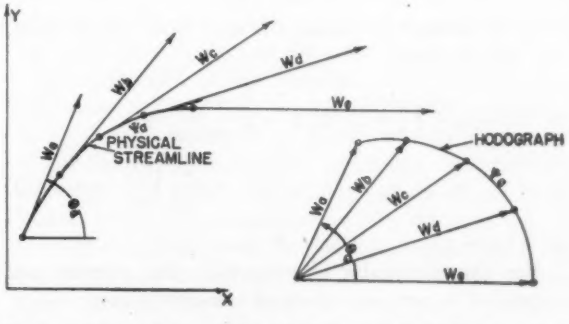

Fig. 1. Geometrical relationship between physical streamline and its hodograph.

One thing is immediately clear in these considerations: While the physical streamlines, by their definition, generally do not intersect, their hodograph pictures can do so since it is entirely possible that the same velocity vector w, θ may occur at more locations than one, either on the same streamline or on others. Hence, there is the possibility that the hodograph plane may consist of several layers or leaves. This phenomenon will lead to complications in the solution of many problems.

With these reservations, we can consider φ and ψ as functions of w and θ.

The following relations follow from Eqs. (17) and (18)

$$\left.\begin{aligned}
\frac{\partial x}{\partial w} &= \frac{\cos\theta}{w}\frac{\partial \varphi}{\partial w} - \frac{1}{\rho_1}\frac{\sin\theta}{w}\frac{\partial \psi}{\partial w} \\
\frac{\partial x}{\partial \theta} &= \frac{\cos\theta}{w}\frac{\partial \varphi}{\partial \theta} - \frac{1}{\rho_1}\frac{\sin\theta}{w}\frac{\partial w}{\partial \theta} \\
\frac{\partial y}{\partial w} &= \frac{\sin\theta}{w}\frac{\partial \varphi}{\partial w} + \frac{1}{\rho_1}\frac{\cos\theta}{w}\frac{\partial \psi}{\partial w} \\
\frac{\partial y}{\partial \theta} &= \frac{\sin\theta}{w}\frac{\partial \varphi}{\partial \theta} + \frac{1}{\rho_1}\frac{\cos\theta}{w}\frac{\partial \psi}{\partial \theta}
\end{aligned}\right\} \tag{19}$$

In order to eliminate x and y from Eqs. (19) it is necessary to make use of the following conditions:

$$\frac{\partial^2 x}{\partial w \partial \theta} = \frac{\partial^2 x}{\partial \theta \partial w}; \qquad \frac{\partial^2 y}{\partial w \partial \theta} = \frac{\partial^2 y}{\partial \theta \partial w} \tag{20}$$

Differentiating Eqs. (19) and substituting in Eqs. (20) leads to

$$\left.\begin{aligned}
\frac{\partial \varphi}{\partial w} &= -\frac{1}{\rho_1}\left(1 - \frac{w^2}{c^2}\right)\frac{1}{w}\frac{\partial \psi}{\partial \theta} \\
\partial\varphi/\partial\theta &= (1/\rho_1)w(\partial\psi/\partial w)
\end{aligned}\right\} \tag{21}$$

Eqs. (21) now take the place of Eqs. (12) and (13) and are equivalent to the Cauchy Riemann equations appearing in the case of incompressible flow.

By differentiating these equations against θ and w, respectively, and by eliminating φ, the final equation for ψ is obtained:

$$w^2\frac{\partial^2 \psi}{\partial w^2} + w\left(1 + \frac{w^2}{c^2}\right)\frac{\partial \psi}{\partial w} + \left(1 - \frac{w^2}{c^2}\right)\frac{\partial^2 \psi}{\partial \theta^2} = 0 \tag{22}$$

c can be written in terms of w and, when this is done, Eq. (22) becomes

$$w^2\left(1 - \alpha\frac{w^2}{c_0^2}\right)\frac{\partial^2 \psi}{\partial w^2} + w\left(1 - \beta\frac{w^2}{c_0^2}\right)\frac{\partial \psi}{\partial w} + \left(1 - \epsilon\frac{w^2}{c_0^2}\right)\frac{\partial^2 \psi}{\partial \theta^2} = 0 \tag{23}$$

$\alpha = (\gamma - 1)/2$; $\beta = \alpha + 1$; $\epsilon = \alpha + 1$.

For this particular investigation, the velocity was expressed in per cent of sound velocity at rest.

$$w_1 = w/c_0$$

Eqs. (21) appear then in the form

$$\left.\begin{aligned}
\frac{\partial \varphi}{\partial w_1} &= -\frac{1 - \epsilon w_1^2}{w_1(1 - \alpha w_1^2)^{\gamma/(\gamma-1)}}\frac{\partial \psi}{\partial \theta} \\
\frac{\partial \varphi}{\partial \theta} &= \frac{w_1}{(1 - \alpha w_1^2)^{1/(\gamma-1)}}\frac{\partial \psi}{\partial w}
\end{aligned}\right\} \tag{21a}$$

A

The final relationship between ψ and the velocity variables w_1 and θ results as

$$w_1^2(1 - \alpha w_1^2)\frac{\partial^2 \psi}{\partial w_1^2} + w_1(1 - \beta w_1^2)\frac{\partial \psi}{\partial w_1} + (1 - \epsilon w_1^2)\frac{\partial^2 \psi}{\partial \theta^2} = 0 \tag{24}$$

When Eq. (24) is solved, the ψ value is known for every w_1, θ combination. Then, by the use of Eqs. (21a), the φ distribution is also determined. As explained before, every point in the w_1, θ (hodograph) plane can be identified with one or more definite points in the actual x, y space; thus, a streamline (ψ = constant) can be transferred from the hodograph into the physical plane. In consequence, the flow paths, wall contours, velocities, and pressures are known at every point, and the problem is solved.

Eq. (24) is a linear partial differential equation, which, as such, possesses distinct advantages over the same equation when written in terms of the variables x and y of the physical plane. It is not difficult to see the physical cause of these advantages. Density and velocity are interconnected by the adiabatic relationship between pressure and density. This relationship, however, deals only with the magnitude of the velocity vector and is independent of the direction. The hodograph plane separates, so to speak, magnitude from direction and thus permits the density-velocity relation to enter in the simplest manner.

One consequence of the linearity of the equation is the possibility of superposing solutions. This means that two or more φ or ψ distributions can be combined by arithmetically adding the values existing at the same vector w_1, θ.

The flow patterns treated by Ringleb are product solutions of Eq. (24). They have the form

$$\psi = [P(w_1)][Q(\theta)] \tag{25}$$

where P is a function of w_1 alone and Q is a function of θ alone. This restricts the solutions that satisfy the equation to specified types. On the other hand, it greatly simplifies the calculation.

B

When Eq. (25) is substituted in Eq. (24), the independent variables w_1 and θ can be separated.

$$\left[\frac{w_1^2(1 - \alpha w_1^2)}{P(1 - \epsilon w_1^2)}\right]\left(\frac{d^2P}{dw_1^2}\right) + \left(\frac{w_1}{P}\right)\left[\frac{(1 - \beta w_1^2)}{(1 - \epsilon w_1^2)}\right] \times \left(\frac{dP}{dw_1}\right) + \left(\frac{1}{Q}\right)\left(\frac{d^2Q}{d\theta^2}\right) = 0 \quad (26)$$

This equality can exist only when the w_1 and θ relationships result in identical constants with opposite signs. Hence, the first two terms can be equated to n^2 and the last term to $-n^2$ separately.

$$\frac{d^2P}{dw_1^2} + \left[\frac{(1 - \beta w_1^2)}{w_1(1 - \alpha w_1^2)}\right]\left(\frac{dP}{dw_1}\right) - \left(\frac{n^2}{w_1^2}\right)\left[\frac{(1 - \epsilon w_1^2)}{(1 - \alpha w_1^2)}\right] P = 0 \quad (27)$$

$$d^2Q/d\theta^2 = -n^2Q \quad (28)$$

Eq. (28) can be immediately integrated. Neglecting for the time being the integration constants, its solution is

$$Q = \sin n\theta \quad (29)$$

The solution of all compressible flow fields that are within the given assumptions is thus reduced to the solution of the ordinary differential Eq. (27). Mathematically, the solution of a general problem is a series of solutions of the form of Eq. (25). The important original assumption is that for every member of this series ψ is the product of functions of w_1 and θ as given by Eq. (25). Along a streamline

$$\psi = PQ = \text{constant} \quad (30)$$

As mentioned before, $\psi = PQ$ represents a severe restriction to the usefulness of this solution. This handicap can be overcome when it is possible to calculate a large number of these solutions. Then it is possible to study the peculiarities of compressible flow under conditions sufficiently similar to those of the particular problem that must be solved. The single, but forbiddingly difficult, general solution of a problem is thus replaced by the study of a number of partial solutions bearing the important characteristics of the problem. The quantity production of solutions calls for the use of calculating machinery. In this case, the differential analyzer was employed to good advantage.

Solution in the Physical Plane

The solution of Eq. (27) together with Eq. (29) will mathematically dispose of the problem. Eventually, however, the engineer will need the actual physical streamline field.

The differential analyzer will furnish $P = f(w_1)$. Together with $Q = \sin n\theta$, this permits the calculation of the streamlines

$$\psi = PQ = \text{constant}$$

as this equation establishes the interrelation that

$$w_1 = f(\theta, \text{constant})$$

The derivative of Eq. (30) with respect to θ is

$$\partial\psi/\partial\theta = P(dQ/d\theta) = nP \cos n\theta$$

Thus, from Eq. (21a), except for constants

$$\varphi = -\int \frac{nP(1 - \epsilon w_1^2) \cos n\theta}{w_1(1 - \alpha w_1^2)^{\gamma/(\gamma-1)}}\, dw_1 \quad (31)$$

This establishes the potential function along a streamline.

The actual path of the streamlines can now be found. This is done by means of Eqs. (17) and (18), considering that along a streamline $d\psi = 0$

$$dx = \frac{\cos\theta}{w}\, d\varphi; \quad x = \int_{\varphi_0}^{\varphi} \frac{\cos\theta}{w}\, d\varphi \quad (32)$$

$$dy = \frac{\sin\theta}{w}\, d\varphi; \quad y = \int_{\varphi_0}^{\varphi} \frac{\sin\theta}{w}\, d\varphi \quad (33)$$

This is the classic way to calculate streamlines from the hodograph.

This calculation involves considerable work and may be performed best by the differential analyzer.

Meaning of Constants

The most general solution of Eq. (25) takes the form

$$\psi = [C_1P(w_1, C_2)]\ [C_3 \sin (n\theta - C_4)]$$

C_4 establishes the orientation of the zero axis for θ. C_1 is a scale factor for P; C_3 is a scale factor for Q. Hence, C_1 and C_3 can be combined into one common scale factor. This scale factor will permit a solution curve to pass through a given point. C_2 is then the constant that determines in what direction the curve passes through this point—in other words, it is given by dP/dw_1 at this point.

A

It is of interest to speculate, by means of purely physical considerations, about the number of different flow fields that must be expected as solutions.

Assume a given contour that must form one given streamline of the compressible field. The next streamline to this contour, separated from it by a given amount of flow, will have a variable distance from it depending on both the velocity and the density.

If the density can be considered to be constant (incompressible case), then the distance of the streamlines is, of course, inversely proportional to the velocity. If the flow between the two streamline boundaries is increased, the value of ψ increases as do all velocities, but *the shape of the streamline remains the same.*

If, on the other hand, the density is a function of the velocity as given by Eq. (11), then the distance between streamlines ceases to be inversely proportional to velocity. Every change in flow between two neighboring streamline points will not only change the value

of ψ but will change the shape of the whole streamline. This statement is equivalent to the result of similarity considerations of compressible flow. Two flow patterns can be similar only when Mach number and γ values are identical, in addition to the Reynolds number. The latter is irrelevant in frictionless considerations. From this we must conclude that in the case of compressible flow there exists an *infinite number of different streamline families* that fit a given contour, if they can be made to fit it at all.

B

This must mean mathematically that either parameter of the two-parameter family of solution curves has a distinct effect. Mathematically speaking, a second order differential equation describes the radius of curvature and the coordinates of the center of curvature of the curve as functions of the coordinates and of the inclination of the curve. Hence, the constant C_2 represents the inclination of the solution curve at a given point.

The disposition of the constants made in this calculation was as follows:

C_1C_3, describing a scale factor, was left open with the knowledge that the scale of the solution curves obtained could still be changed at will.

C_4 was made use of by setting the zero axis for θ on the paper in a suitable direction.

C_2 was introduced by determining the value of P'/P at an arbitrarily chosen velocity

$$P' = (dP/dw_1)$$

Choice of Solutions

A decision must still be made about the value of the constant n. This constant determines the overall flow contours of the solution. Compressible flow patterns can be considered as obtained by continuous extrapolation of incompressible patterns. Hence, the effect of the choice of n can be studied by means of the simpler equations of the latter. When the simplifications that apply to the incompressible case are made, the solutions of Eq. (26) are those represented by the complex (Schwartz-Christoffel) flow potential.

$$\varphi + i\psi = Cz^{n/(n-1)}; z = x + iy$$

A

Depending on the choice of the arbitrary constant n, the flow fields obtained from this calculation represent incompressible flow *within* wedge-shaped spaces, *past* and *around* wedge-shaped obstacles. Values of $+1 > n > 0$ result in multipoles of which the dipole ($n = +1/2$) is a special case. A pole in this case represents all flow originating from the origin and eventually returning to it. The velocity at infinity is zero for $n < +1$ and infinite for $n > +1$. The origin, which is either the corner of the wedge or the pole, represents zero velocity when the velocity at infinity is infinite and vice versa.

Speculating on the effect of compressibility, it can immediately be stated that infinite velocities cannot occur. The density becomes zero when the pressure reaches zero; this occurs at a definitely finite maximum velocity.

$$(w_1)_{max.} = \sqrt{2/(\gamma - 1)} \text{ for } \gamma = \text{constant} \quad (34)$$

This can only mean that whenever the velocity called for by the equivalent incompressible solution is infinite the compressible problem either cannot have a solution at this point at all or that the resulting streamlines will not form a sharp corner. Whenever the velocity becomes zero (flow inside the wedge space), a compressible solution is possible.

The object of the investigation was to obtain good records of compressible flow when it is undergoing large deflections such as occur in turbine nozzles and buckets. Table 1 shows in outline form the flow patterns that were studied. In general, $\gamma = 1.4$ was used as the exponent, principally to have the results in a condition where they can be checked with compressed air. In some cases $\gamma = 1.3$ was used in addition to $\gamma = 1.4$ to have results applicable to superheated steam and high-temperature air.

Table 1

γ	n	Description	Remarks
1.4	$-1/2$	360° turn	.....
1.4	$+1/2$	Dipole	Partly a repetition of Ringleb's flow picture in his paper
1.4	± 2 ($n^2 = 4$)	90° turn around (−2) and within (+2) corner	Investigation of effect of constants
1.3	± 2 ($n^2 = 4$)	90° turn around (−2) and within (+2) corner	Study of effect of γ value
1.4	± 1.5 ($n^2 = 2.25$)	120° turn around (−1.5) and within (+1.5) corner	Study of effect of magnitude of velocity

For each of the cases in Table 1 a number of streamline patterns are now available both in the hodograph and in the physical plane.

Results

The results of the investigation consist of the following material:

(1) Physical streamline patterns for all the cases mentioned in Table 1, each for a number of maximum velocities.

(2) Hodograph streamline patterns for these cases.

(3) Velocity variation along the streamlines.

(4) In one case, an extensive family of P solutions for a study of the effect of velocity on the fields.

The physical streamline patterns contain, in addition to the equipotential lines, the constant velocity lines

(isotachs), which are also constant pressure lines (isobars).

Some hodograph patterns contain the lines of constant x and y of the physical field to illustrate the distortion this field undergoes when it is mapped in the hodograph plane.

These fields are by no means easily understood. In view of this, it was decided to build some three-dimensional models for educational purposes. The physical representation of the third variable, which can be chosen to be the potential, the flux function, or the magnitude of velocity, helps to impress upon the mind the interlocking relationships that exist between path, velocity (or pressure), and potential. Furthermore, they emphasize the important fact that the simple space relationship expressed as "path" directly furnishes the important hodograph angle coordinate θ. It appears that the angle changes or streamline deflections as expressed in the curvature of the streamline are an exceedingly important variable in the case of flows that pass close to sound velocity.

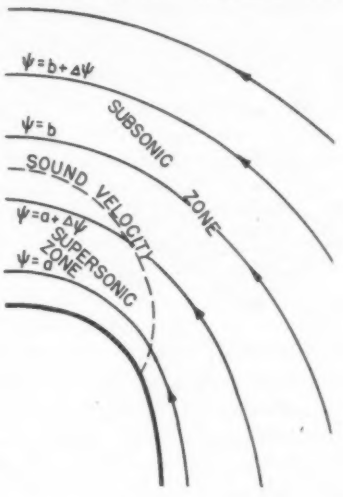

FIG. 2. Transition from subsonic to supersonic flow.

GENERAL DISCUSSION

There are some phenomena peculiar to compressible flow that are better discussed in general before the details of each pattern are studied.

The differential equations governing the flow fields have been derived from the two simple conditions.

(a) No rotation—i.e.,

$$\text{curl } \bar{w} = 0 \tag{1}$$

(b) Conservation of matter—i.e.,

$$\text{div. } (\rho_1 \bar{w}) = 0 \tag{3}$$

where ρ_1 is a function of $|\bar{w}|$ alone (isentropic, adiabatic relationship).

Two neighboring streamlines will approach each other up to sound velocity and will diverge as this velocity is exceeded. This condition is specified by Eq. (3) because the mass velocity $\rho_1 w$ has a maximum at sound velocity when ρ_1 is given by the adiabatic relationship. Because of this property, compressible and incompressible flow patterns are different and there can be compressible flow boundaries for which it is impossible to satisfy the condition of irrotational flow as given by Eq. (1).

Consider a small part of curvilinear flow (see Fig. 2). Eq. (1) calls for an increase of velocity toward the center of curvature. This increase of velocity causes closer spacing of streamlines in the direction of the center of curvature as long as the flow is subsonic. But above sound velocity the decrease in mass velocity with an increase of velocity causes wider spacing of streamlines toward the center of curvature. This is different from incompressible flow where the streamline spacing always decreases toward the center of curvature. That is, compressibility causes the streamlines to be crowded away from the center of curvature as compared with incompressible flow. Consequently, the streamline curvature for supersonic flow may be a maximum within the field, while the equivalent incompressible flow specifies continuous increase of curvature toward the center of curvature.

Some qualitative study of the effect of this phenomenon shows that above sound velocity it is likely to work at cross purposes with the postulation for zero rotation. The latter specifies a decrease of velocity with distance from the turning center to the effect that at some distance there will be sound velocity and, at greater distances, subsonic velocities. Within the inner supersonic zone, the streamlines diverge from the innermost boundary, tending to decrease the curvature. In the outer zone, the streamlines converge, stretching themselves, so to speak, to increase their curvature while circumnavigating the supersonic zone. It is to be expected that in the case of a given contour (or streamline) there can be velocities where it is impossible to satisfy both equations. In such cases, streamlines postulating ever more vigorous velocity changes run into a dead end beyond which potential flow cannot proceed. The mathematical solution yields a geometric reversal point or "cusp" of the streamline as soon as an infinite velocity change is reached. This specifies two flow patterns existing in the same space, a physical impossibility. Actually, by some means or other, the flow must acquire rotation, which in the presence of viscosity the flow of a real fluid can readily do. Since the flow is supersonic, a compression shock will be started.

There are, therefore, two conditions that can make it impossible for *potential* compressible flow to fit itself to given contours.

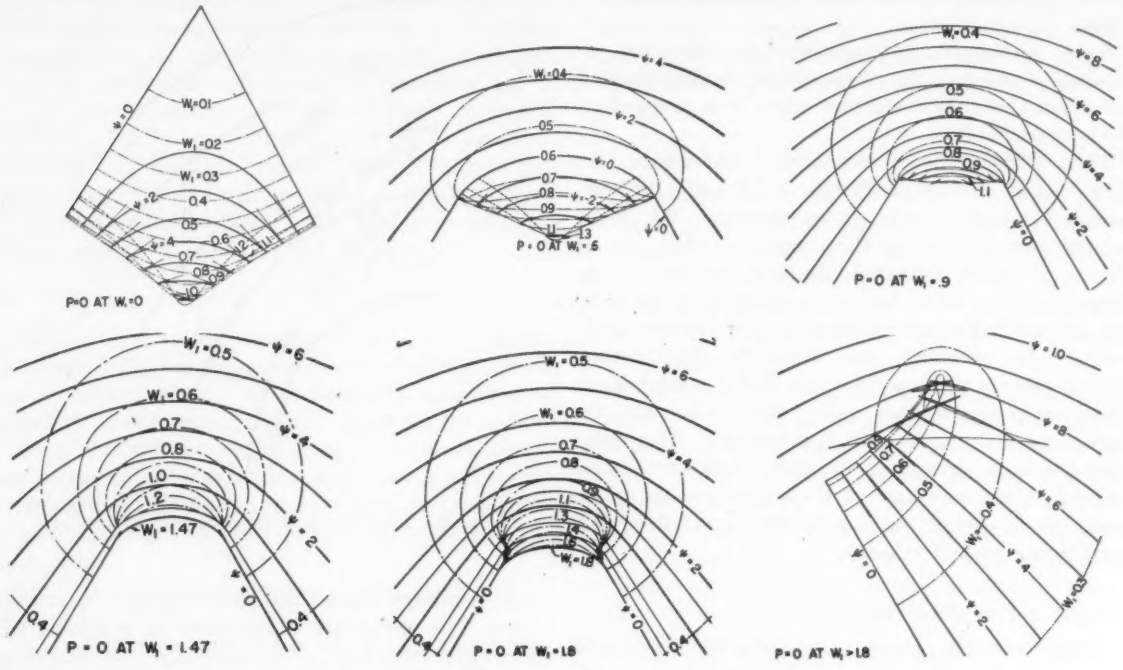

FIG. 3. Compressible fields for a 120° turn (60° wedge) at six different velocity levels.

(a) The appearance of maximum velocity constitutes a limit the flow cannot transgress. There is a minimum radius path for a compressible vortex in a given scale field once the velocity is given at a specified location. At this radius the maximum velocity prevails and the density is zero. The fluid cannot describe a smaller circle.

(b) Within certain zones of the field, zero rotation as originally specified, is incompatible with the law of conservation of matter.

Either of these conditions imposes definite restrictions on design. The second is especially important. The engineer, accustomed to calculating incompressible fields, is used to the fact that a field can be calculated for any given contour. The only limitations he respects are those introduced by viscosity. He, therefore, checks for adverse pressure gradients and wall curvature. As will be seen in the following discussion of the flow fields that were obtained in this investigation, the second limitation can appear with falling or rising pressure gradients. The first one limits the maximum curvature.

Catalog of Compressible Fields

The following information was considered as pertinent in the cataloging of results:

(1) The physical field.
(2) The hodograph field.
(3) The P function versus velocity.
(4) The velocity variation versus streamline path.

First Solution of 120° Turn or 60° Wedge

Fig. 3 shows six physical fields obtained for the following conditions: $P = 0$ at $w_1 = 0$, 0.6, 0.9, 1.47, 1.8, and >1.8. The designation of a field by the velocity at which the P value becomes zero is equivalent to a choice of the direction P' (P curve with w_1 axis) at which the P curve passes a given point P_a; in other words, it determines the integration constant C_2. As the results show, this parameter designates the maximum velocity of the flow *around* the wedge as well as the minimum velocity of the flow *within* the wedge. Obviously, this holds good only as long as an intersection of the P curve with the w_1 axis actually exists.

Thus, the fields are arranged in order of increasing velocity of the outside flow. The effect of the various velocity levels shows very clearly. A comparison with the corresponding incompressible field can be obtained by means of Fig. 4.

The inside solutions for which the $P = 0$ point represents the minimum velocity are shown only in three cases. $P = 0$ at $w_1 = 0$ has, as is obvious, only

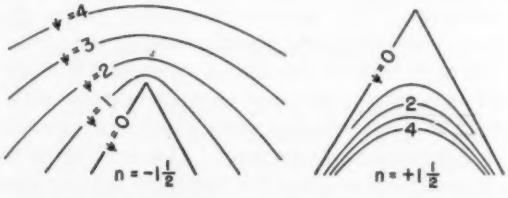

FIG. 4. Incompressible fields for a 120° turn (60° wedge).

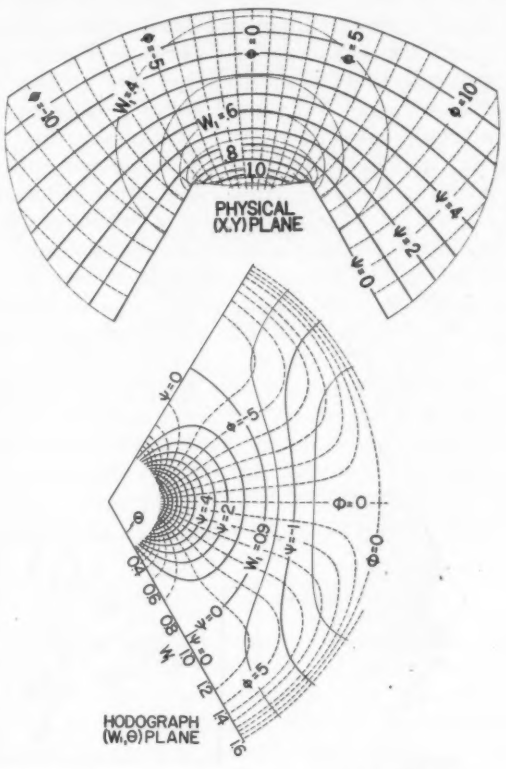

FIG. 5. Compressible 120° turn ($w_1 = 0.9$ at $P = 0$).

an inside solution. It is significant because in this case a compressible solution exists for a sharp corner.

For more detailed discussion, two of the fields are shown to larger scale. Fig. 5 shows the case $P = 0$ at $w_1 = 0.9$. Local sound velocity exists at

$$w_1 = \sqrt{2/(\gamma + 1)} = 0.913 \qquad (35)$$

thus, the maximum velocity of the outside flow is just short of sound velocity.

B

The hodograph field is, in its appearance, similar to the incompressible flow case of a tripole. However, it does not extend to infinity but is limited by a circle with the radius

$$w_1 = \sqrt{2/(\gamma - 1)} = w_{1max.}$$

It is subdivided by another circle with the radius $w_1 = 0.9$.

The streamlines within the 0.9 circle are those describing the flow around the wedge. Those between the 0.9 and the w_1 max. circle are those of the flow within the wedge.

Fig. 6 shows the P versus w_1 curves for the six fields.

The equation for the streamlines in the hodograph plane is

$$\psi = [P(w_1)](\sin n\theta) = \text{constant}$$

The values for $\psi = 0$ are obtained in one instance by a constant $P = 0$, which in this case is at $w_1 = 0.9$. At this velocity the flow can change its *direction*—i.e., the hodograph of the streamline is a circle. At $n\theta = 0$ and $n\theta = K\pi$, the ψ value likewise is zero, irrespective of the *magnitude* of the velocity. At these constant directions the velocity can change. These are the axis directions of the tripole. In the physical plane the 0-streamline consists of the two sides of the 60° wedge which, however, do not meet at the origin. As soon as $w_1 = 0.9$, the streamline turns at constant velocity until it meets the other side of the wedge. The positive ψ values are outside the wedge, while the negative values resulting from negative P values are inside. Far outside this wedge the velocities are low; the flow, therefore, has the customary incompressible characteristics. They approach each other continuously until they meet the bisectrix of the wedge. The compressible streamlines close to the wedge demonstrate the effect of decreasing density. As sound velocity is approached the streamlines cease converging. Since, in this particular case, sound velocity is not quite reached outside the wedge, the streamlines do not diverge. The effect of compressibility on streamline curvature is easily observed.

The flow *inside* the wedge shows a much different behavior. For such a flow the *minimum* velocity will occur at the line of symmetry, and the velocity will increase in a direction away from the vertex. This leads to the condition where potential flow as such cannot further exist. The solution results in streamlines with "cusps"; the field is covered with two solutions, which appear simultaneously in the same space. It is important to note that the velocity direction of the streamlines reverses as the cusp is passed. This is indicated by the fact that the potential has either a maximum or minimum. It also must be pointed out that the hodograph streamlines of these discontinuous curves are perfectly continuous curves. The reversal is

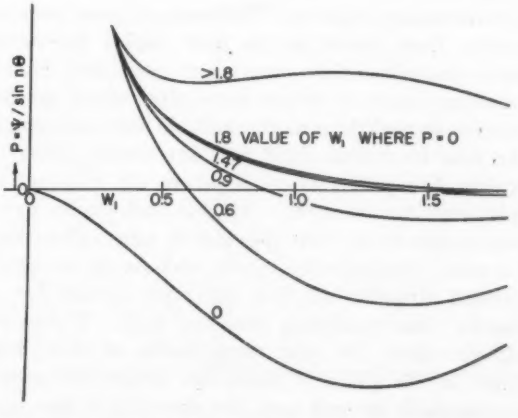

FIG. 6. P vs. w_1 functions for six compressible 120° turns.

caused by the maximum or minimum of the potential contour. This is equivalent to saying that the phenomenon occurs when the streamlines and equipotential lines in the hodograph plane have a common tangent.

Thus, it can be said that the linearization of the differential equation by means of the mapping into the hodograph plane results in the removal of singular conditions. The locus of all the reversal points (or cusps) in the physical plane is a curve that may be considered to be, with not too much mathematical precision, a kind of source or sink line. From this line will issue, or into it will disappear, two distinct types of flow. For practical application, parts of either of the two flows can be realized if the approach or leaving boundary conditions can be realized by other means than the singularities themselves.

A .

Fig. 7 shows the velocities along the streamlines of the outside solution. As sound velocity is approached, the velocity curves become steeper, rising much faster than the incompressible solution would show.

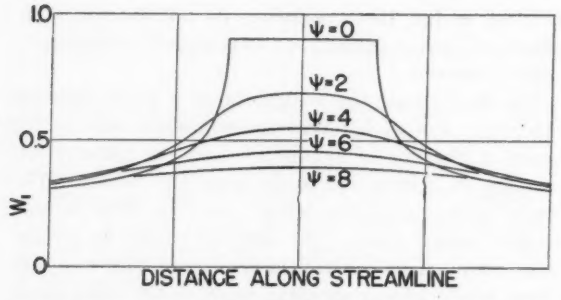

FIG. 7. Velocity distribution along streamlines for compressible 120° turn ($w_1 = 0.9$ at $P = 0$).

Fig. 8 shows the fields for a 120° turn with $P = 0$ at $w_1 = 1.8$. They bear a great similarity to those of the former case except for the fact that now, along the zero streamline, sound velocity is reached and exceeded. Within the supersonic zone the streamlines diverge with increasing velocity. Furthermore, now there are singular lines (cusps) in the field outside the wedge. Each streamline that passes one cusp also, shortly thereafter, meets a second cusp, after which the flow proceeds around the zero streamline in the usual manner. The zero streamline itself first overshoots, along the straight line path, the place where the constant velocity turn branches off. Then it back-tracks to the proper place from where it begins to turn. Thus, there is a small triangular figure with its base on the doubly traveled straight line and the sides formed by the singular lines extending into the field. Within this triangle there are now three leaves of flow fields. While in the physical plane the streamline reverses geometrically at each cusp, the direction of flow is the same on both sides of the cusp. The fluid appears to

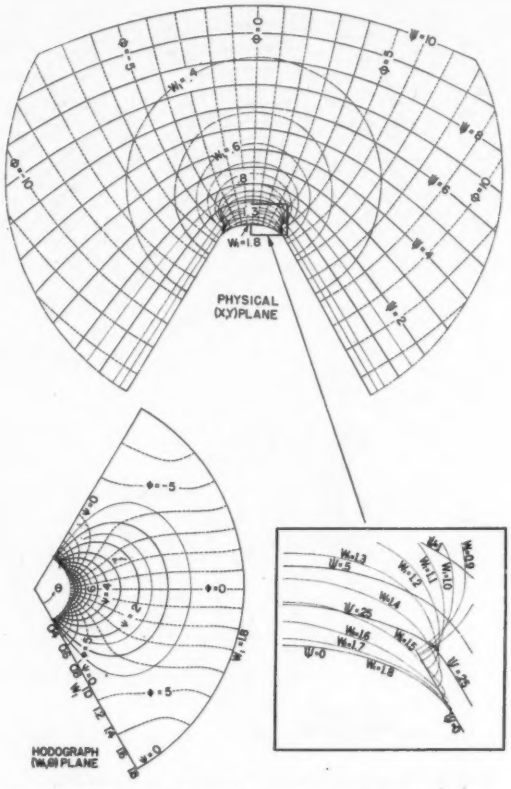

FIG. 8. Compressible 120° turn ($w_1 = 1.8$ at $P = 0$).

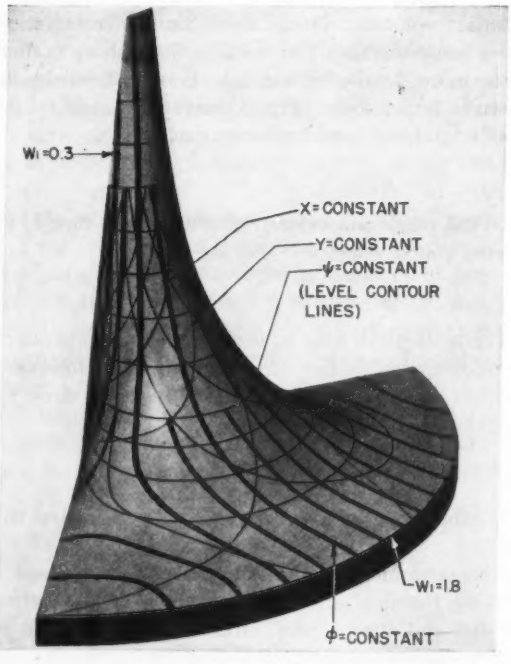

FIG. 9. Representation of streamfunction ψ distribution over hodograph (w_1, θ) plane. Compressible 120° turn ($w_1 = 1.8$ at $P = 0$). Base is hodograph plane; elevation is streamfunction.

flow into the cusp line from both parts of the field. A comparison of the hodograph field with that of the preceding case shows that the cusps are caused by streamlines and equipotential lines having common tangents in the vicinity of the two corners adjacent to the zero streamline. This condition is absent in the former case except on the negative side of the zero streamline where cusps occur in every case and for every streamline.

A three-dimensional model is available demonstrating the contour of this streamfunction in the hodograph plane. It, like Fig. 7, includes only the positive ψ values representing the flow *around* the wedge. (Fig. 9 is a photograph of this model.) The velocity plot (Fig. 10) shows again that the cusp occurs where the velocity gradient is infinite. Of the two flows directed away from the cusps, one branch is in direction of decreasing velocity, while the velocity of the other increases. The contours of the velocity distribution can be studied on the model, a picture of which is shown in Fig. 11.

Second Solution of 360° Turn

This case, even when treated as incompressible, has a field partly covering itself—i.e., part of it consists of two distinct leaves occupying the same x-y space but situated on different potential surfaces. In its entirety this field is a physical impossibility, but parts of it can be utilized to good advantage for composing solutions. The incompressible fields for the negative and positive n are shown in Figs. 12 and 13.

The compressible case for the negative n is shown on Fig. 14. The physical streamline field consists of two leaves. One-half of each is shown separately on the figure. The streamlines from 0 to about +0.96 have cusps and, hence, two branches. The streamlines above 0.96 continue around the full turn in spite of the high velocities they pass. The maximum velocity that is reached without cusps is higher than 1.6. The lines of constant velocity indicate that except for the streamlines with cusps, the velocity gradient is steepest around

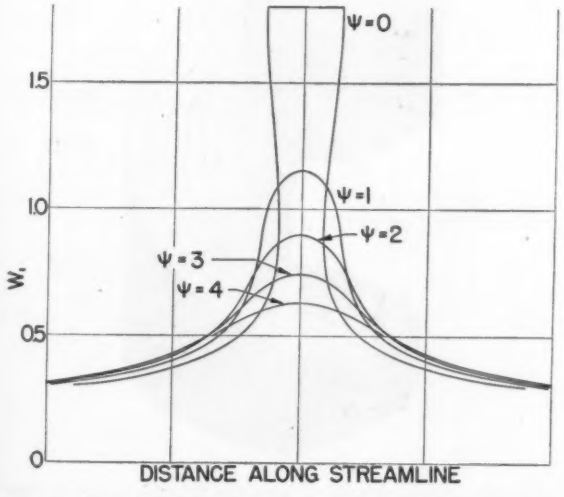

Fig. 10. Velocity distribution along streamlines for compressible 120° turn ($w_1 = 1.8$ at $P = 0$).

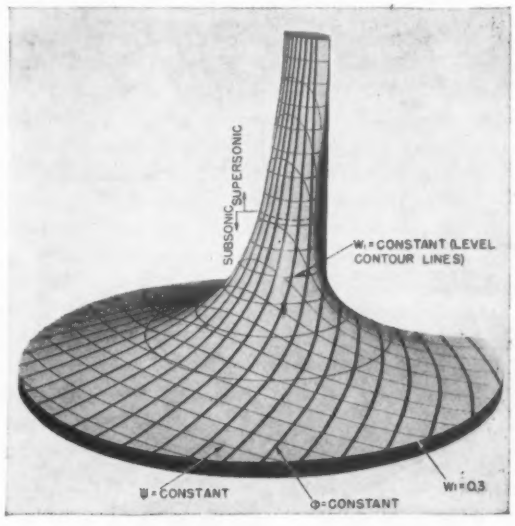

Fig. 11. Representation of velocity w_1 distribution over physical (x, y) plane. Compressible 120° turn ($w_1 = 1.8$ at $P = 0$). Base is physical plane; elevation is velocity.

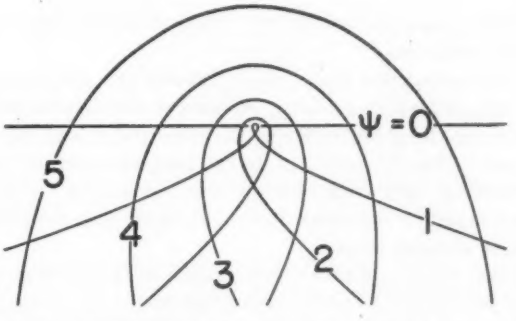

Fig. 12. Incompressible field for a 360° turn ($n = -1/2$).

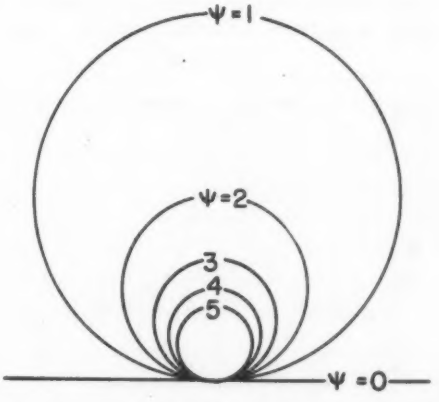

Fig. 13. Incompressible field for a 360° turn (dipole, $n = +1/2$).

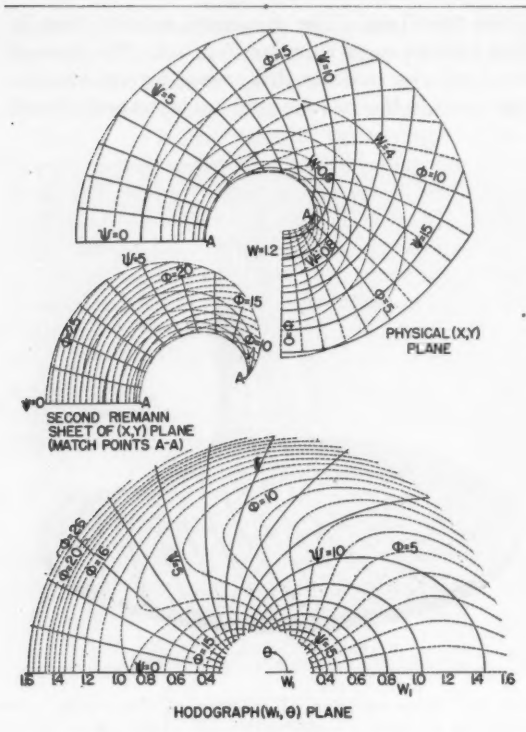

FIG. 14. Compressible 360° turn ($n = -1/2$).

the 0.9 (sound velocity) line. Fig. 15 shows the velocity variation.

The hodograph plane clearly shows the geography of the potential surface. Wherever the streamline traverses the spiral valley of the potential a cusp must occur. This is indicated by a tangent common to streamline and equipotential line. Above $\psi = 9.6$ the streamline continues down and, hence, can turn the corner without cusp.

Figs. 16 and 17 show photographs of the contour of this potential both in the hodograph and in the physical plane. The latter permits a clear visualization of the two flows emanating from, or ending in, the cusps. The two Riemann leaves are now taken apart, each of them representing a distinct potential surface. Only the

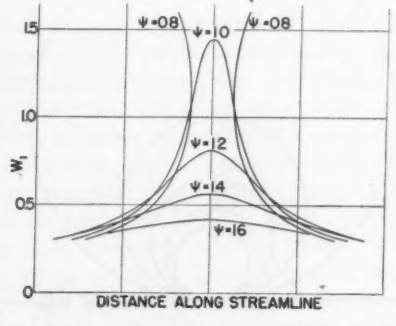

FIG. 15. Velocity distribution along streamlines for compressible 360° turn ($n = -1/2$).

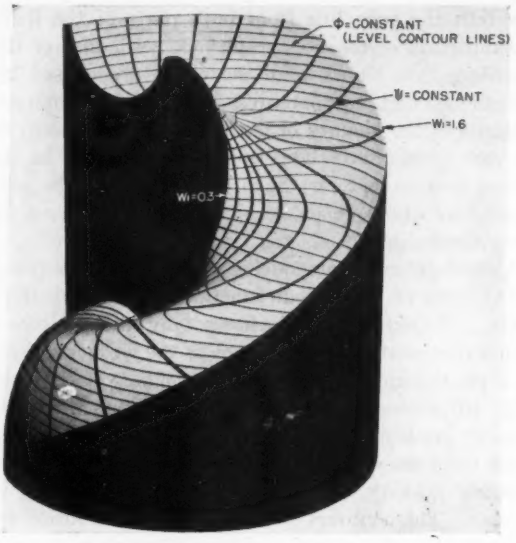

FIG. 16. Representation of potential function φ distribution over hodograph (w_1, θ) plane. Compressible 360° turn ($n = -1/2$). Base is hodograph plane; elevation is potential function.

cusp line is common to both. The two fields covering the x-y plane are but the projection of the two surfaces.

Fig. 18 represents another type of 360° turn obtained with a positive n. This is the case of the compressible dipole already familiar from Ringleb's article. All streamlines have cusps and extend beyond the cusps to infinity, there to reach the maximum velocity.

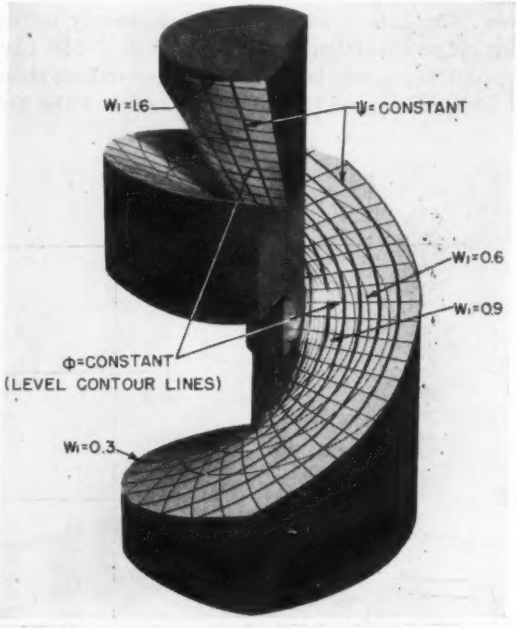

FIG. 17. Representation of potential function φ distribution over physical (x, y) plane. Compressible 360° turn ($n = -1/2$). Base is physical plane; elevation is potential function.

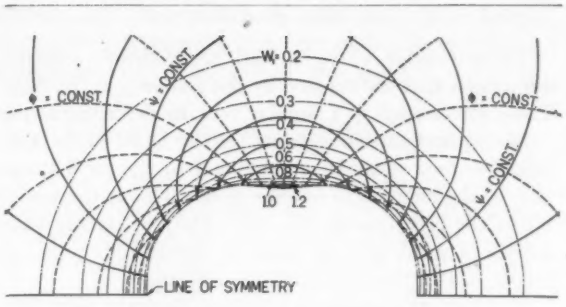

FIG. 18. Compressible 360° turn (dipole, $n = +1/2$) in physical (x, y) plane.

P-CURVE INVESTIGATION

B

One special investigation was directed toward the study of the effect of the constants on the P solution without regard to the final fields. It was seen before that for a given n each P curve represents a flow field uniquely determined by a velocity vector at a chosen location.

Once the P function is known the flow field can be relatively easily obtained. Fig. 19 is a sample of such a family of P curves for $n^2 = 4$. A number of the curves intersect the w_1 axis; in other words, P can become zero. This establishes a $\psi = 0$ streamline by other means than by $\sin n\theta = 0$.

For P'/P values smaller than about 6.3 at $w_1 = 0.3$, there is no intersection of the curves of $P = f(w_1)$ and the line $P = 0$. The streamlines in the hodograph plane have reversal points in θ. One solution for such a case has been obtained. It contains numerous cusps. It does not present anything new and, hence, is included only in Fig. 3. As w_1 increases, all P curves appear to converge into one point. It is assumed that this point is $P = 0$ at $w_{1max.} = \sqrt{2/(\gamma - 1)}$.

This family shown here for one constant value of n^2 demonstrates what a tremendous variety of different fields are possible once the flow is compressible. Many of the physical fields it represents appear to be absolutely useless by themselves. It is, however, quite possible that superpositions of their hodograph fields

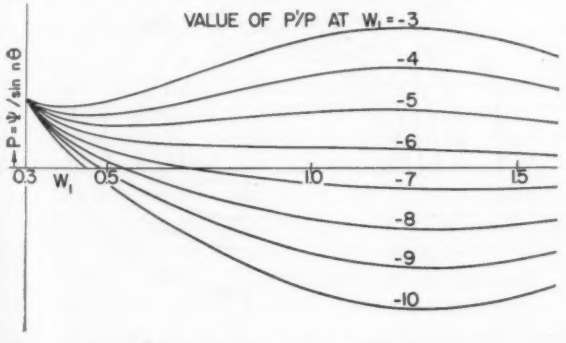

FIG. 19. P vs. w_1 function for 90° turns ($n^2 = 4$).

onto others will furnish useful results. The investigation of these solutions is still going on at present.

SUPERPOSITION

A

The fields, being linear in the hodograph plane, can be superposed in this plane. Two different fields represented by two different number distributions over the w_1–θ field can be combined to form a new and different solution. This is done simply by adding the two ψ or φ values existing at every point. The distribution resulting from this process when translated into the physical x-y plane furnishes a new physical field. This procedure permits the designer to add wanted features to, or subtract unwanted phenomena from, any particular field. An additional degree of freedom is provided by the fact that either of the two distributions can be multiplied by an arbitrary constant before the addition is made. The contributory effect of the field or fields to be added can thus be "shaded" until the proper performance is obtained. Care must be taken that only values existing at the same velocity vector are

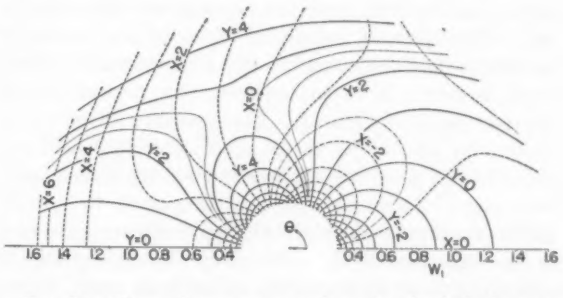

FIG. 20. Lines of constant x and y, the physical plane coordinates, plotted in the hodograph (w_1, θ) plane. Compressible 360° turn ($n = -1/2$).

added. An alternative way of superposition is given by Ringleb. If x_1, y_1 are the coordinates for one hodograph solution and x_2, y_2 are those of another, a new solution is

$$x = C_1x_1 + C_2x_2; \quad y = C_1y_1 + C_2y_2$$

This can be done easily once the x, y system is plotted in the hodograph plane. This procedure affords a close supervision of the changes in the physical x-y contours that are introduced by the superposition. On the other hand, it necessitates the plotting of the x-y contour map in the hodograph plane. A sample of such a plot is shown on Fig. 20 for the 360° turn. Work on this phase of the investigation is still in progress.

EFFECT OF γ VALUE

Not much need be said about this effect. It was small in all cases where $\gamma = 1.3$ was used in addition to $\gamma = 1.4$. The deviation of the 1.3 streamline from

the 1.4 streamline was gradual. It must be concluded that the principal difference between the two is in the relative magnitude of both the sound velocity and of the maximum velocity.

Highest Realizable Velocity

If a stream that is initially subsonic is to be deflected, the maximum velocity that is physically possible is of interest. It was found that the lower the value of n chosen, the higher the velocity obtained without cusps. In actual design this poses the problem of modifying the hodograph field in such a manner that unsatisfactory subsonic approach flow to the turn is changed to follow desired contours.

Effect of Viscosity on Fields

As in the incompressible case, a potential field will only represent a good approximation to actual flow conditions when the viscosity forces brought into play by the velocity distribution are small enough not to cause a major change in the boundaries. In other words "jet separation" or the separation of the boundary layer from the wall must not occur at any field boundary. The present solutions obtained for potential isentropic flow disregard the effect of viscosity. They must, however, be consulted when the importance of viscosity is investigated. The pressure distribution created by the inertia forces of the potential field impresses itself onto regions where viscosity forces come into play. These regions are recognized to a high approximation by the high velocity gradients appearing in the potential field. The steep velocity gradients appearing along compressible streamlines must, therefore, always be viewed with concern when the pressure gradient is adverse to the flow direction.

There is, however, in compressible flow a second viscosity term that is entirely absent in the incompressible case.

The classic Navier-Stokes equation describing viscous compressible flow contains two viscosity terms

$$\rho(d\bar{w}/dt) = -\text{grad. } p + \mu\nabla^2\bar{w} + (\mu/3)\text{ grad. div. }\bar{w} \quad (35)$$

where μ = viscosity of flowing medium. One of them, the next to the last in the equation, is the viscosity effect already familiar from the incompressible case.

The last term is zero when

$$\text{div. } \bar{w} = 0 \quad (36)$$

Eq. (36) is a basic equation for incompressible flow. At constant density, conservation of matter is identical with conservation of volume flow. No volume flow can be created nor can disappear in this case. However, when the flow is compressible, it is the actual mass flow that is conserved, and volume flow due to the density changes does appear or disappear. Then the divergence of velocity is no longer zero.

$$\text{div. } \bar{w} \neq 0 \quad (37)$$

These volume changes lead to crosswise velocity differences that are resisted by the viscosity in the fluid. These forces may, in a popular vein, be described as the "growing and shrinking pains" of the fluid. This compressible flow shear is proportional to the local variation of the changes in volume flow. This is the meaning of the last term in Eq. (35). Only extremely large values of grad. div. $\bar{w}$ need be considered, since, as mentioned in the introduction, μ is small.

To study the importance of this viscosity term, div. $\bar{w}$ is being calculated from some of the fields and plotted in the physical plane.

Fig. 21 shows a map of such a div. $\bar{w}$ contour from which the gradient can be obtained. It applies to the field of the 360° turn. The calculation has not been made to a high degree of accuracy as yet. Hence, it has descriptive rather than quantitative value.

It depicts how the divergence rises from low values in the compressible zone to infinity along the cusp lines. It must be inferred that forbiddingly high values have already appeared before the streamlines actually reach the cusps. By this token, streamlines passing through the vicinity of the cusps without actually reaching them, must trespass into a zone of high viscosity forces. Within this zone, a streamline field as given by this adiabatic solution cannot exist, because viscosity effects will prevent reversible flow. The map, however, indicates that this danger zone must be thin.

It is important to note in this connection that along with the cusp lines these viscosity forces are not connected with a solid wall as are those of boundary layers. They can exist within the field. Also, their importance is not limited to adverse pressure gradients. They can create disturbances at acceleration as well as at deceleration.

It would appear, however, from what has become known so far, that the elimination of cusp lines from

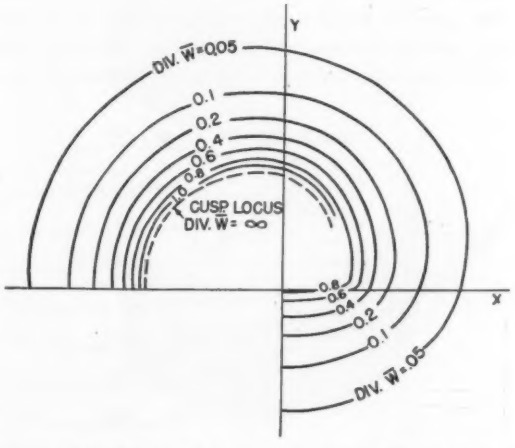

Fig. 21. Distribution of div. w_1 over physical (x, y) plane Compressible 360° turn $(n = -1/2)$.

the flow will also practically eliminate these forces. And the cusp lines must be eliminated from any design before a field can be considered as a solution.

Usefulness of Solutions in the Hodograph Plane

It is unfortunate that direct solutions can only be obtained in the hodograph plane. On the other hand, the situation can be viewed from the optimistic point of view by stating that it is fortunate that the problem *can* be solved by the means of this transformation. Following the latter line of thought, the conclusion is obvious that the engineer will have to learn to feel at home in the hodograph plane. If this is tried, it will be found that this plane has a number of desirable properties.

(a) Solutions can be superimposed. A solution once obtained can be changed into other solutions by proper manipulation until desired characteristics are obtained.

(b) The hodograph variables, magnitude of velocity, and its direction are the same as those to which the aeronautical engineer is already accustomed from the use of fields derived from the "complex velocity." They are also the variables that the turbine engineer uses in his velocity diagrams.

(c) It must be realized that the technical application that calls for a solution in all cases demands the displacement of masses of fluid—i.e., it calls for changes in velocity angle and magnitude. The form of the physical object that achieves this desired end *should be secondary* in importance and should only be a result of considerations carried through before in the hodograph plane.

(d) Those properties of the flow field that decide the physical validity of a solution can all be studied directly in the hodograph plane. The following are some properties that can be studied in the hodograph plane: (1) the pressure gradients, especially the adverse pressure gradients determined by the velocity changes along streamlines; (2) the curvature of the physical streamlines; and (3) the length of the physical streamline path.

These three quantities are needed if the boundary layer along a given streamline must be calculated. The streamline in this case represents the contour of the deflecting wall.

The boundary-layer calculation will decide whether the boundary layer will separate or not. It is, for this reason, a criterion for the validity of the solution, since separation would completely alter the flow pattern.

Another important quantity is the function that indicates the appearance of the cusps. It is the Jacobian alluded to by von Kármán.[3] To a large extent it measures large values of acceleration or deceleration in the field. It can be calculated within the hodograph field and, as such, furnishes the second criterion of the physical validity of a solution.

With good accuracy the appearance of cusps can be detected by visual observation of the combined streamline and potential hodograph field. As mentioned before, the cusps occur wherever streamlines and equipotential lines have a common tangent in the hodograph plane.

The third criterion consists of the viscosity term described in the preceding section. It is important only in the immediate vicinity of the cusps and, hence, is already detected by the Jacobian.

It is therefore possible to design any useful flow contour or passage by merely handling functions of the velocity vector—i.e., its magnitude and angle. The actual physical shape of the object does not enter the consideration at all. It merely appears at the end as the final result.

B

Mathematically these validity criteria appear surprisingly simple.

The acceleration in direction of the flow is

$$(dw/dt) = (ds/dt)(d\varphi/ds)(dw/d\varphi) = w^2(\partial w/\partial\varphi) \quad (38)$$

where the derivative is made with ψ constant.

The radius of curvature of a physical streamline is given by the following equation where the derivatives are for constant ψ:

$$r = ds/d\theta = (1/w)(d\varphi/d\theta) = (1/c_0w_1)(d\varphi/d\theta) \quad (39)$$

The lengths of the physical streamline paths are

$$s = \int_{\varphi_0}^{\varphi} d\varphi/w = 1/c_0 \int_{\varphi_0}^{\varphi} d\varphi/w_1 \quad (40)$$

Each of these magnitudes can be taken directly from the hodograph field.

The acceleration can also be written as[3]

$$dw/dt = -(w^2/\Delta)(\partial\psi/\partial\theta) \quad (41)$$

where Δ is the Jacobian given by

$$\Delta = (\partial\varphi/\partial w)(\partial\psi/\partial\theta) - (\partial\varphi/\partial\theta)(\partial\psi/\partial w) \quad (42)$$

From Eq. (41) it can be seen that the acceleration is infinite when the Jacobian is zero. That is,

$$dw/dt = \infty$$

when either

$$\partial\psi/\partial\theta = \infty \text{ or } \Delta = 0$$

The Jacobian calculated for the product solution $\psi = P \sin(n\theta)$ is

$$\Delta_{prod.} = -\frac{1-(w_1/c_1)^2}{c_0\rho_1 w_1}(nP\cos n\theta)^2 - \frac{w_1}{c_0\rho_1}(P' \sin n\theta)^2 \quad (42a)$$

a term that can be calculated from the hodograph field and the known P function.

Likewise, the acceleration becomes

$$\frac{d^2s}{dt^2} = -\frac{w^2}{\Delta}\frac{\partial\psi}{\partial\theta} = \frac{c_0^2 w_1^3 \rho_1 nP\cos n\theta}{(1 - w_1^2/c_1^2)(nP\cos n\theta)^2 + (w_1 P' \sin n\theta)^2} \quad (41a)$$

Except for θ this is a combination of three functions of w_1 which can be plotted as soon as n and $P = f(w_1)$ are known.

Conclusions

A

By means of the differential analyzer, a number of fields of adiabatic compressible flow have been obtained. Some of the results are presented for analytical study. At the present stage of the investigation, the following properties of compressible flow fields appear worth mentioning.

(a) For a given boundary contour, there exists an infinite number of different fields. Their shape is determined by the magnitude of the maximum velocity of the field.

(b) The appearance of maximum velocity (density zero) limits the maximum curvature that can be used.

(c) When sound velocity is exceeded the useful range of realizable fields is further limited by the appearance of infinite velocity gradients (cusps).

(d) Changes in γ value from 1.4 to 1.3 result only in minor changes in the properties of the fields.

(e) The additional viscosity term appearing in the general Navier-Stokes equation for compressible fluid flow becomes large only in the vicinity of the cusp lines.

(f) A great number of different flow fields can be obtained and studied by superposing the elementary fields in the hodograph plane.

(g) The smaller the constant n^2 of the calculation, the higher a physically possible supersonic velocity that can be obtained at the convex side of a flow contour.

(h) The design calculation for compressible flow contours and passages can be carried through entirely in the hodograph plane.

Acknowledgment

The data for this paper were determined by the authors for the Turbine Engineering Division in collaboration with A. Keller of the Supercharger Engineering Division. Full use was made of the General Electric Company differential analyzer. The authors are particularly indebted to C. Concordia, F. J. Maginniss, and N. R. Schultz for their help in obtaining the results from the analyzer and to Miss E. O'Connell and Mrs. H. Relihan for computing the data.

References

[1] Chaplygin, S. A., *On Gas Jets* (Russian), Scientific Annals of the Imperial University of Moscow, Physics-Mathematical Division, Pub. No. 21, Moscow, 1904.

[2] Ringleb, F., *Exakte Lösungen der Differentialgleichungen einer adiabatischen Gasströmung*, Zeitschrift für Angewandte Mathematik und Mechanik, Vol. 20, pp. 185–198, 1940. (Translated by L. A. Huguemont.)

[3] von Kármán, Th., *Compressibility Effects in Aerodynamics*, Journal of the Aeronautical Sciences, Vol. 8, p. 337, July, 1941.

Periodicals Wanted for Foreign Libraries

A committee of the American Library Association is collecting scientific and technical journals for eventual shipment to foreign libraries and institutions unable to get them now because of the war. The Committee is eager to acquire the Journal of the Aeronautical Sciences, and only through your gifts can copies be obtained. The Committee will provide storage space if necessary. If you wish to help by donating your periodicals, please write to Dorothy J. Comins, Executive Assistant, Committee on Aid to Libraries in War Areas, Library of Congress Annex, Study 251, Washington 25, D.C.

Efficiency of Lateral Stiffeners in Panels

ADAM ZAHORSKI*

Lockheed Aircraft Corporation

SUMMARY

This article discusses the "grid" analysis of flat panels reinforced by longitudinal and lateral stiffeners and subjected to the longitudinal compressive forces. Diagrams for the design of lateral stiffeners in various combinations are included.

NOTATION

ψ = $\pi^2 Bl^3/4Ds^4$, flexural stiffness index
ϕ = C_t/Ds^2, torsional stiffness index
C_t = GI_p, torsional rigidity of the lateral stiffener
l = length of the panel
s = width of the panel
D_0 = EI, flexural rigidity of the longitudinal stiffener
D = EIr/s, flexural rigidity of the longitudinal stiffener per unit width of the panel
B = EI, flexural rigidity of the lateral stiffener
I = moment of inertia of one stiffener
c = P/P_e or p/p_e, fixity coefficient
P = critical compressive load per stiffener
p = Pr/s, critical compressive load per unit width of panel
P_e = $\pi^2 D/l^2$, Euler's load
k^2 = P/D_0 or p/D
Q = force per stiffener between lateral and longitudinal stiffeners
q = force between lateral and longitudinal stiffeners per unit length of lateral stiffener
δ = deflection of the lateral stiffener
δ_0 = maximum deflection of the lateral stiffener
θ = angle of the slope of the longitudinal stiffener
M = bending moment
r = number of longitudinal stiffeners
K_ψ and K_β = correction factors for a finite number of longitudinal stiffeners
χ = correction factor for partial restraint of lateral stiffener
β = coefficient of end restraint

INTRODUCTION

AN AIRPLANE WING, from the structural point of view, is essentially a long box-beam in which the upper surface carries large compressive stresses. This surface could easily become elastically unstable save for the ribs in the wing which support it at intervals, and thus increase the strength of the wing as the whole. This function of the ribs is generally not well understood. In order to give a designer a practical method of estimating the size and spacing of the ribs in a given wing, this paper presents under stringent assumptions the analysis of lateral stiffeners in the panels. Any rib or chordwise beam is considered here as the lateral stiffener. Only flat rectangular panels subjected to longitudinal compressive loads uniformly distributed along the width are considered.

Received February 3, 1944.

* Structural Research Engineer.

There are two principal methods of analysis of reinforced panels. One is so-called "thin plate" analysis, in which it is assumed that the material of longitudinal stiffeners together with skin is uniformly and continuously distributed across the width of panel, thus permitting the use of certain differential equations derived for continuous plates. In panels, as distinct from plates, only a part of the load is carried by the skin. The skin also may buckle at small loads and by far the largest portion of the total load is carried by the longitudinal stiffener, thus the plate analysis of the panel may lead to an erroneous conclusion.

At the other extremity a "grid" analysis is one in which the panel is assumed to consist of series of longitudinal and lateral stiffeners rigidly connected at intersections, but altogether neglecting the skin and its plate effects. Obviously, for panels without lateral stiffeners, the extremes of "plate" and "grid" analyses may be quite far apart because the "grid" analysis does not allow for an interaction between the longitudinal stiffeners. However, as the number of lateral stiffeners increases, a smaller gap between "plate" and "grid" analyses can be expected, and therefore a more accurate solution of the real problem is obtained.

The buckling of "thin plates" with reinforcing ribs has been discussed by many authors.[1,2,3,4] Here the "grid" analysis of panels is developed in detail, first for the case of one lateral stiffener, then for two lateral stiffeners, and finally a general case is briefly discussed.

ONE LATERAL STIFFENER

SIMPLY SUPPORTED PANEL

A panel as shown in Fig. 1, consisting of one lateral and r longitudinal stiffeners, is subjected to the action of compressive forces. If a small displacement is given to any longitudinal stiffener normal to the panel, all stiffeners will deflect and the section through any other longitudinal stiffener will be as shown in Fig. 1a. Forces must result at each junction between lateral and longitudinal stiffeners. The free body diagram of the lateral stiffener with the forces (Q's) acting on it and the corresponding reactions to longitudinal stiffeners are also shown in Fig. 1b. The values of Q's in magnitude and variation along the span are unknown. The free body diagram of any longitudinal stiffener is shown in Fig. 2.

Let D_0 be the flexural rigidity of the longitudinal stiffener; P, the compressive force, and Q, the reaction

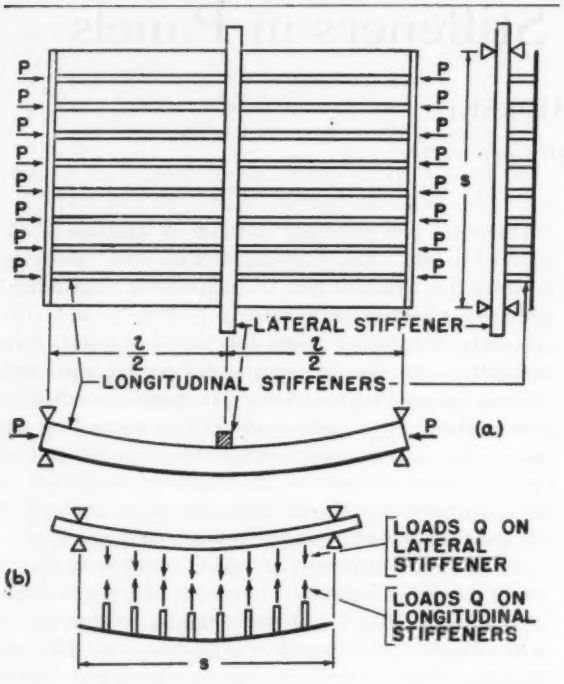

FIG. 1.

from the lateral stiffener. Then, with the system of coordinates as shown, the differential equation of the deflection curve is

$$(d^2y/dx^2) + k^2y - k^2(Q/2P) = 0 \qquad (1)$$

where $P/D_0 = k^2$.

The solution of the equation gives the deflection δ under the lateral stiffener in the form

$$\delta = \frac{Ql}{4P}\left(1 - \frac{2}{kl}\tan\frac{kl}{2}\right) \qquad (2)$$

The form of this equation is similar to beam-column formula except for the negative value of Q, and it is valid only in range $\pi < k < 2\pi$. It can be proved[5] in general that all beam-column formulas and the modified law of superposition can be applied to the analysis of the lateral stiffener, provided the value of Q is taken with the negative sign.

With the notation

$$P_e = \pi^2 D_0/l^2 \qquad c = P/P_e \qquad kl = c \qquad (3)$$

Eq. (2) can be written in the form

$$\frac{c}{1 - \frac{2}{\pi\sqrt{c}}\tan\frac{\pi}{2}\sqrt{c}} = \frac{Q}{\delta}\frac{l^3}{4\pi^2 D_0} \qquad (4)$$

On the left-hand side of the above equation we have a transcendental expression involving only the fixity coefficient c.

The use of "fixity coefficient" in this discussion is much broader than the use of a similar phrase in connection with the columns. Here the fixity coefficient depends on the end restraint of the panel, on the side restraints of the lateral stiffener and on the number of those stiffeners. The coefficient c is defined as the ratio of the panel critical load (P) to Euler's load (P_e) on the same length as that of the panel without stiffeners. Thus, the limiting value of c may be much greater than 4 which is the limit for the columns.

The value of this coefficient c depends on the unknown ratio of Q/δ. This ratio can be determined, in general, from the conditions of equilibrium between lateral and longitudinal stiffeners. Several conditions will be analyzed.

One Longitudinal Stiffener

The case of one longitudinal stiffener represents a beam with hinged ends and elastic (spring) support at the middle for which the solution is well known,[1] and is included only to illustrate here the method of solution of more complicated cases.

The free body diagram for the lateral stiffener is shown in Fig. 3, where Q is the reaction from one centrally located longitudinal stiffener, and therefore

$$Q/\delta = 48B/s^3$$

where B is the flexural rigidity of the lateral stiffener.

Substituting the above into Eq. 4

$$\frac{c}{1 - \frac{2}{\pi\sqrt{c}}\tan\frac{\pi}{2\sqrt{c}}} = \frac{12}{\pi^2}\frac{B}{D_0}\frac{l^3}{s^3} \qquad (5)$$

for any given panel, fixity coefficient c; thus the critical load can be determined.

Two Longitudinal Stiffeners

The free body diagram of the lateral stiffener will be as shown in Fig. 4. We have in this case

$$Q/\delta = (162/5)(B/s^3)$$

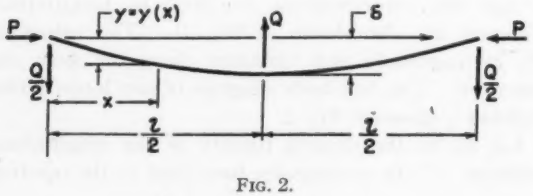

FIG. 2.

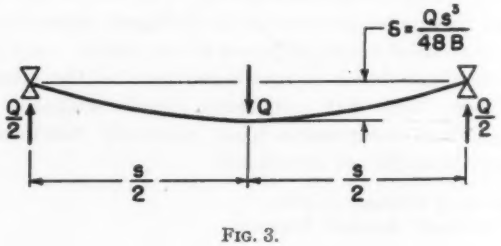

FIG. 3.

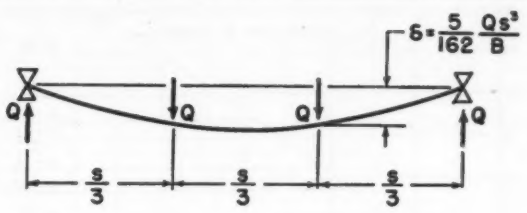

FIG. 4.

and substituting the above into Eq. (4)

$$\frac{c}{1 - \frac{2}{\pi\sqrt{c}} \tan \frac{\pi}{2\sqrt{c}}} = \frac{162}{5} \frac{2B}{4\pi^2 D_0} \frac{l^3}{s^3} \tag{6}$$

For any required fixity coefficient c, the necessary value of flexural rigidity B of the stiffener can be easily obtained.

"Many" Longitudinal Stiffeners

The use of the word "many" will imply here that there is fairly continuous shear diagram due to the reactions from longitudinal stiffeners on the lateral stiffener, so that the concentrated loads on the stiffener can be approximated by some unknown distributed load. It is then necessary to make slight modifications in Eq. (4). Differential Eq. (1) will continue to be valid if one writes q instead of Q, where q is the reaction from the longitudinal stiffeners per unit length of lateral stiffener and D for D_0 where D is the flexural rigidity of the longitudinal stiffeners per unit width of panel. With these changes the solution of Eq. (1) becomes

$$\frac{c}{1 - \frac{2}{\pi\sqrt{c}} \tan \frac{\pi\sqrt{c}}{2}} = \frac{q}{\delta} \frac{l^3}{4\pi^2 D} \tag{7}$$

The diagram of the lateral stiffener is in Fig. 5. The expression for the q/δ ratio cannot be directly determined in this case, as previously, because the distribution of the load $q(z)$ along the stiffener is not known. However, by assuming a reasonable form of the deflection curve, this ratio can be obtained from the relation

$$B(d^4\delta/dz^4) = q \tag{8}$$

It can be shown[5] that the sine curve is the deflection curve of the lateral stiffeners for the case of an infinite number of longitudinal stiffeners, and using the same curve for a finite number of stiffeners, the magnitude of error in any case can be determined in the final result (see Table 1).

Thus, taking the deflection of the lateral stiffener in the form

$$\delta = \delta_0 \sin (\pi z/s) \tag{9}$$

and substituting it into Eq. (8)

$$q/\delta = (\pi^4/s^4)B \tag{10}$$

This is the required relation by means of which the unknown factor q/δ in Eq. (7) can be eliminated. Thus,

$$\psi = \frac{c}{\left(1 - \frac{2}{\pi\sqrt{c}} \tan \frac{\pi}{2}\sqrt{c}\right)} \tag{11}$$

where

$$\psi = (\pi^2/4)(l^3/s^4)(B/D) \tag{12}$$

The curve OAC in Fig. 6 is the plot of Eq. (11). For any given panel with a lateral stiffener, *i.e.*, given ψ, the value of c and, hence, the critical buckling load, can be directly obtained from the chart. Or for the given critical load, that is, c, the solution for ψ, and thus the required value of flexural rigidity (B) of the lateral stiffener, can easily be obtained.

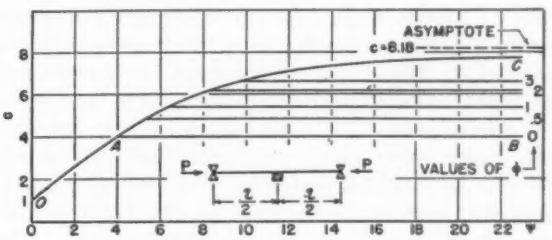

FIG. 6.

It can be seen from Eq (11) that for $(\pi/2)\sqrt{c} = 4.493$ or $c = 8.18$, the denominator on the right side becomes zero, and therefore, $\psi \to \infty$ For values of $c > 8.18$, ψ becomes negative and has no physical meaning. There is another limitation on the value of c. So far the mode of buckling as shown in Fig. 7a has been considered, but the second mode, Fig. 7b, is also pos-

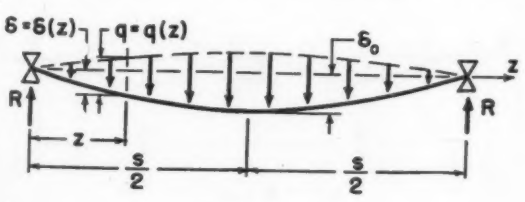

FIG. 5.

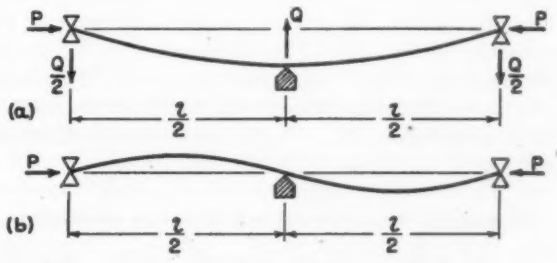

FIG. 7a

sible. Since in this mode there is no lateral displacement of the stiffener as shown in Fig. 1, the differential Eq. (1) and all subsequent equations will not apply, and it can be proved that generally a stiffener placed at a nodal point has no effect on the critical load, provided the stiffener does not have torsional rigidity. For the second mode when the stiffener has no torsional rigidity, the coefficient c must be equal to 4, which corresponds to $\psi = 4$. Thus, if $\psi = 4$, the second mode (Fig. 7b) occurs, and any further increase in the value of ψ will not increase c. Therefore, the broken line OAB (Fig. 6) should be used in the design of stiffeners. It is of interest to note that at $c = 4$

$$\psi = 4 = (\pi^2/4)(l^3/s^4)(B/D)$$

or

$$B = 16s^4D/\pi^2l^3 = 16s^4D^2P/\pi^2l^34\pi^2D$$

$$B = (4/\pi^4)(s^4/l)P$$

which is the same as Eq. (36), given by E. E. Lundquist[2] in the analysis of a built-up panel as a plate with bending rigidities different in longitudinal and lateral directions.

Fixed Ends Panel

A differential equation similar to Eq. (1) can be easily derived for the case of a panel with fixed ends, and its solution with an additional boundary condition of no rotation at the supports will be similar to Eq. (4) or (7). However, the same result may be obtained in a different way, since a modified form of the method of superposition holds for beam-column formulas. The deflection of a fixed end beam, under the load Q, can be obtained by subtracting the deflection due to moments applied at the ends of the beam of such magnitude that it just prevents the rotation of the supports, from the deflection of a simple beam. The result in either case will be an equation similar to Eq. (11) in which factor 2 will be replaced by factor 4; Eq. (10) will not change, and thus

$$\psi = \frac{c}{\left(1 - \frac{4}{\pi\sqrt{c}} \tan\frac{\pi}{4}\sqrt{c}\right)} \qquad (13)$$

This equation is plotted in Fig. 8. Thus, for any desired value of the fixity coefficient c, the corresponding value of ψ can be secured, and the required value of flexural rigidity (B) of the lateral stiffener can be obtained easily. Eq. (13), similar to Eq. (12), has two limiting values: one asymptote at $c = 32.7$ which has no practical significance, and the other, the second mode of buckling, at $c = 8.18$. This mode is shown in Fig. 9a.

Torsional Rigidity of the Lateral Stiffener

If the stiffener has no torsional rigidity, then the relation between c and ψ is represented by curves

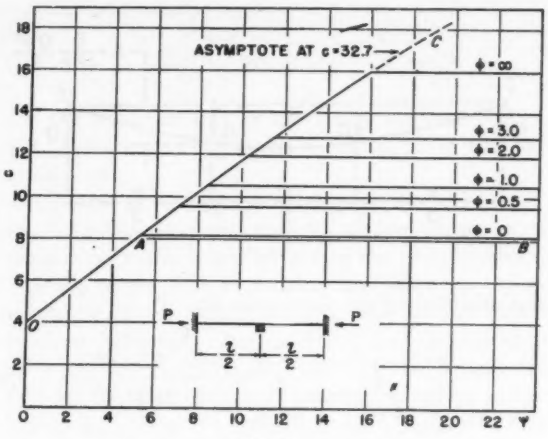

FIG. 8.

OAB, Figs. 6 and 8, and any increase in value of ψ above 4 or 5.26 does not increase the value of c above 4 or 8.18, respectively. However, it is possible to increase the value of c above 4 for simply supported ends and above 8.18 for fixed ends by providing a degree of torsional rigidity of the stiffener in addition to its flexural rigidity. If the stiffener has torsional rigidity C_t, then its rotation θ will be accompanied by a corresponding restraining moment M as shown in Fig. 9b, and will cause an increase in value of the fixity coefficient c. This increase is possible until the stiffener will not rotate, that is, when the torsional rigidity is infinite. This case is illustrated in Fig. 9c.

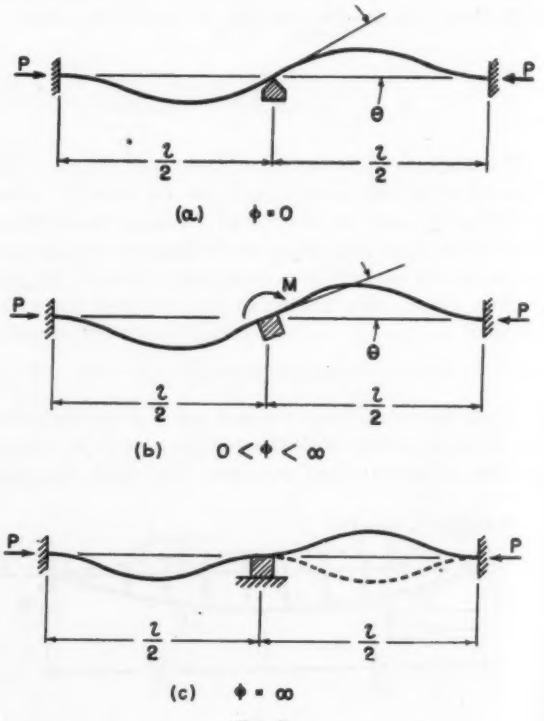

FIG. 9.

In order to find the value of c for any value of torsional rigidity of the stiffener, we can use the principle of superposition, obtaining necessary values from beam-column formulas. The results of such calculations are shown in Figs. 6 and 8, where curves are plotted for various values of the dimensionless parameter of torsional rigidity defined by

$$\phi = C_t/Ds^2 \qquad (14)$$

The diagram in Fig. 6 is for a panel with supported ends, and that in Fig. 8 is for one with fixed ends. In both figures curve OAC represents the condition for symmetrical buckling of the panel. On the portion OA of curve OAC no torsional rigidity is necessary, and the value of ϕ has no influence on the value of c, but on the portion AC, there is a definite interaction between flexural and torsional rigidities (ψ and ϕ), even though the stiffener is not twisted as it would be in antisymmetrical buckling. Since the stiffener is at the nodal point in antisymmetrical buckling, the value of c is not influenced by the value of ψ and, therefore, for lines ϕ = constant, c = constant. It is of interest to note that for fixed ends in the limiting case of $\phi \rightarrow \infty$ either form of buckling, symmetrical or antisymmetrical, may occur as shown in Fig. 9c.

Ends of Panel Partially Restrained

So far we have analyzed panels in which the ends were either free to rotate or perfectly fixed. The effect of partial restraint of the ends of the panel is shown in Fig. 10. It is assumed that the torsional rigidity of the stiffener is zero ($\phi = 0$). Then the curve $\phi' = 0$ corresponds to the case of simply supported ends; it is the same as curve OAB in Fig. 6. The curve $\phi' = \infty$ corresponds to the case of fixed ends and is the same as OAB in Fig. 8. The additional curves, $\phi' = 0.343$ and $\phi' = 1.23$, are shown. The values of ϕ''s were chosen in such a way that they pass through points $c = 2$ and $c = 3$ for $\psi = 0$.

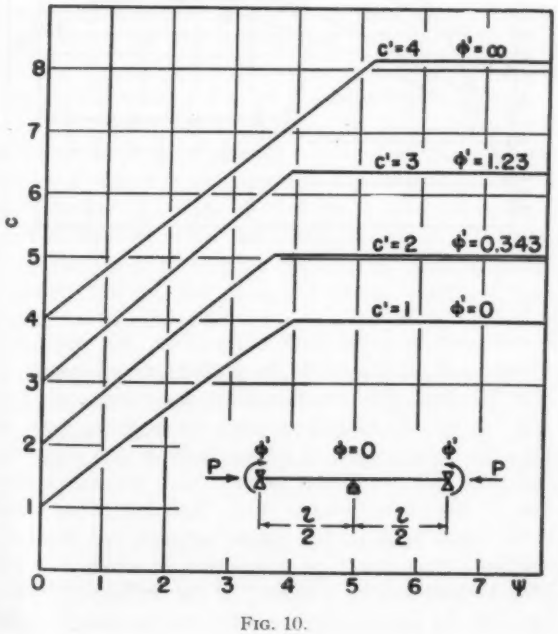

Fig. 10.

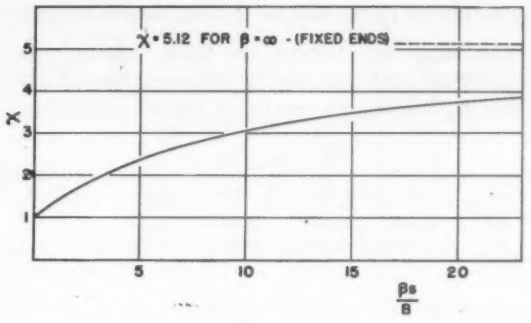

Fig. 11.

Correction Factors

In the analysis of panels with "many" longitudinal stiffeners, it was assumed that the deflection of the lateral stiffener is given by a sine curve. The same assumption is also introduced for torsional deflection. The sine curve is the deflection curve for the case of simple supported lateral stiffeners with an infinite number of longitudinal stiffeners. However, it is possible to establish the correction factors on the values of functions ψ and ϕ for any degree of end restraint of lateral stiffeners and for a finite number of longitudinal stiffeners. The proof of this is not within the scope of this paper, but it can be found in reference 5 from which the correction factors given below were obtained.

Correction for Partial Restraint of Lateral Stiffeners

The rigidity of the lateral stiffeners may be increased by a restraint at the supports, so that rotation of the ends is resisted by a moment. In effect this may be considered as an apparent increase in the value of flexural rigidity B, i.e., in the value of ψ. Let β be the coefficient of end restraint numerically equal to the bending moment per unit angle of rotation of support, χ be the correction factor due to restraint β on both ends of the stiffener; then the corrected value of ψ is given by the equation:

$$\psi_{\text{corrected}} = \chi\psi$$

The corrected value of ψ is used to enter diagrams, Figs. 6, 8 and 10. The relation between χ and parameter $\beta s/B$ is shown in Fig. 11. Note that the value of c can be directly determined if β and B are given. However, B can be determined only by successive approximation if β and c are given. For simply supported ends ($\beta = 0$) $\chi = 1$ and for fixed ends ($\beta = \infty$), $\chi = 5.12$.

Correction for Finite Number of Longitudinal Stiffeners

The correction factors for finite number (r) of longitudinal stiffeners can be obtained from Table 1, where K_ϕ and K_ψ are correction factors defined by

TABLE 1

r	1	2	3	4	$r > 4$
$K\psi$	0.493	0.662	0.750	0.80	$r/(r+1)$
$K\phi$	0.405	0.608	0.711	0.78	$r/(r+1)$

$$\psi_r = K_\psi \psi \qquad \phi_r = K_\phi \phi \tag{15}$$

In all diagrams the values of ψ_r and ϕ_r must be used instead of ψ and ϕ as given by Eqs. (12) and (14) if the effect of a finite number of longitudinal stiffeners is to be considered.

TWO LATERAL STIFFENERS

SIMPLY SUPPORTED PANEL

The analysis of a panel, reinforced at third points by two identical lateral stiffeners, does not differ fundamentally from that of one lateral stiffener. However, as the number of stiffeners increases, the work also becomes much more complicated and cumbersome, and it is essential to the solution of the problem that the mechanism of the interaction between the panel and the stiffeners is clearly understood at all times. Therefore, it is in order to discuss several special cases before the final results are presented.

First, consider the case when the two lateral stiffeners cannot resist torsion, that is, when the torsional parameter $\phi = 0$ (see Eq. (14)). In Fig. 12 are shown three possible forms of buckling.

The first form (Fig. 12a), a symmetrical case, can be analyzed easily by the method of superposition. The results of such an analysis will be the curve A_1B_1E shown in Fig. 13. The second form (Fig. 12b), an antisymmetrical case, can be handled in a similar way, and the curve $F_1B_1C_1G_1$ (Fig. 13) will result. The third form (Fig. 12c) is also symmetrical; it gives the curve EC_1D_1 which is the straight line $c = 9$. Note that in this case no vertical reaction is necessary at the stiffener to satisfy the condition of equilibrium. Since only the smallest values of c are of practicable significance, then the broken curve $A_1B_1C_1D_1$ (Fig. 13) should be used for design purposes.

Next, consider the case when the lateral stiffeners can resist torsion, i.e., when ϕ = constant illustrated in Fig. 14.

This case is similar to that in Fig. 12 and may be analyzed by the method of superposition, where in addition to the lateral load Q at each stiffener there is also a moment M which is proportional to the slope of the elastic curve. However, there is another important difference, namely, that the same analytical expression

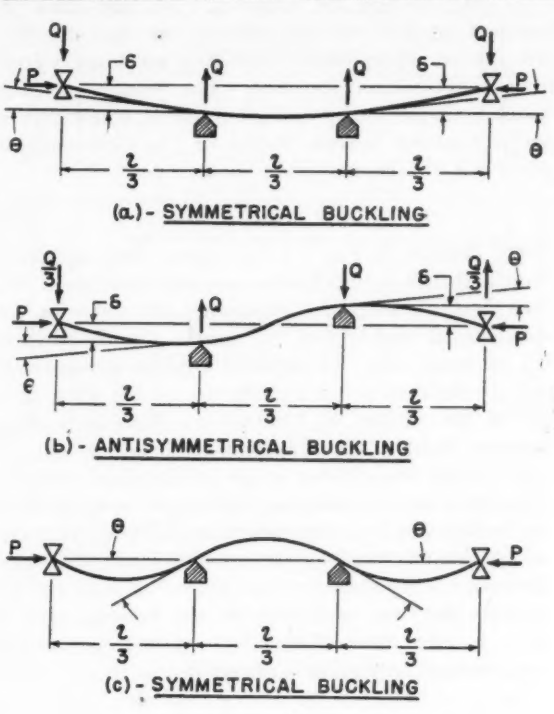

FIG. 12.

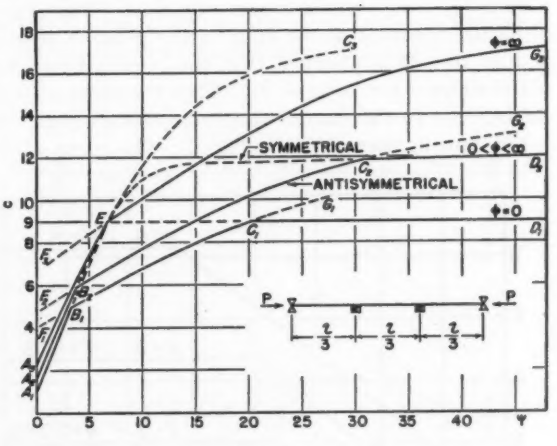

FIG. 13.

is sufficient to cover both cases (Figs. 14a and 14c) where as it is impossible to predict the existence of case 12c from the mathematical expressions of case 12a. Physically this means that the buckling form of Fig. 12c occurs with no lateral load on the stiffener, and thus has no relation to case 12a; whereas in the case of Fig. 14c, because of an unbalanced moment in the span between the simple support and the first stiffener, there must be a reaction R which in turn must be balanced by a force Q at the stiffener. Therefore, for the panels reinforced by two torsionally rigid

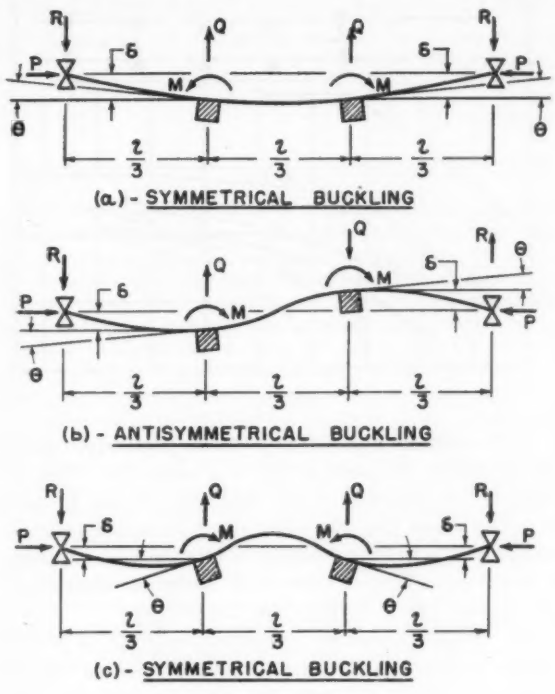

FIG. 14.

lateral stiffeners, it is impossible to have the third mode of buckling as shown in Fig. 12c. The result of the analysis of the symmetrical case (Fig. 14a) is curve $A_2B_2EC_2D_2$ (Fig. 13) and for the antisymmetrical case (Fig. 14b) curve $F_2B_2C_2G_2$. Again, since one of the smallest values of c is of practical interest, the design curve is the broken line $A_2B_2C_2D_2$.

The limiting case when $\phi \to \infty$ will give two curves, one A_3EC_3 for the symmetrical case and the other F_3EG_3 for the antisymmetrical case. Both of these curves will meet at $c = 18.41$ and $\psi \to \infty$.

By examining the diagrams in Fig. 13 it appears that all curves for symmetrical buckling intersect at the point E whose coordinates are $c = 9$ and $\psi = 6.75$. Apparently the state of the panel in this condition is independent of the torsional parameter. This can happen only if there is no twist of the stiffener, which means that the line of action of the resultant force must be on the stiffener and support as shown in Fig. 15.

In Fig. 16 there are curves similar to those in Fig. 6 computed for several values of ϕ. These are recommended to be used as design curves for a simply supported panel with two lateral stiffeners at the third points.

Ends of Panel Restrained

Similar curves for a panel with fixed ends are shown in Fig. 17.

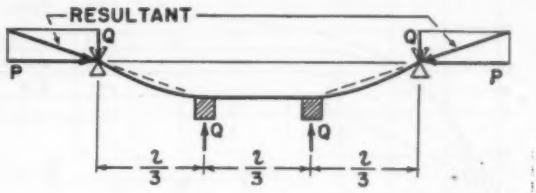

FIG. 15.

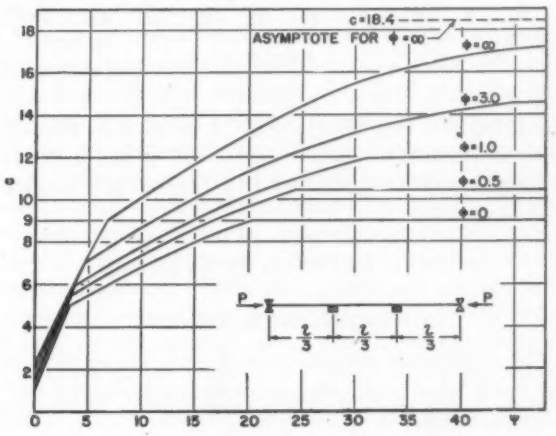

FIG. 16.

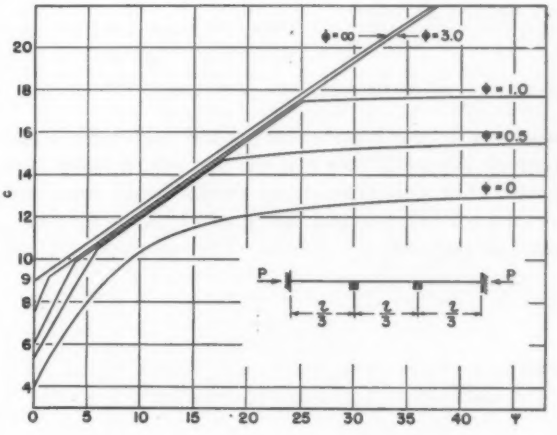

FIG. 17.

In some cases the ends of the panel might be such that they are neither simply supported nor fixed, but are partially restrained. If we denote by ϕ' this partial restraint in such a way that for simply supported ends $\phi' = 0$ and for fixed ends $\phi' = \infty$, then it is possible to get ψ vis. c diagrams for various values of end fixities ϕ'; provided that in each diagram ϕ, the torsional parameter of the stiffeners, is kept constant. In Fig. 18 there is such a diagram for $\phi = 0$ (no torsional rigidity of the stiffeners). Curve $\phi' = 0$ is obtained

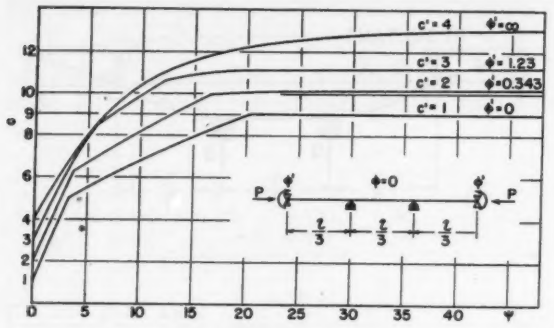

FIG. 18.

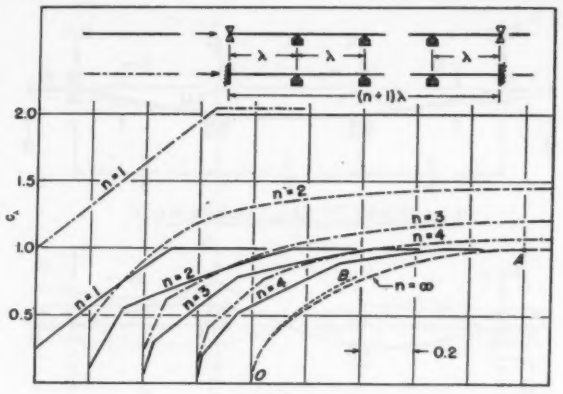

FIG. 19.

from Fig. 16, and the curve $\phi' = \infty$ is from Fig. 17. Two intermediate values of $\phi' = 0.343$ and 1.23 are chosen in such a way that for $\psi = 0$ curves pass through $c = 2$ and $c = 3$.

MANY LATERAL STIFFENERS

SOLUTION OF EQUATIONS

The solution of equations for the general case of three or more lateral stiffeners becomes quite complicated. However, for three and four stiffeners in the special case when the torsional restraint of stiffeners is neglected ($\phi = 0$), the solution has been determined.

The curves are plotted on Fig. 19. New coordinates are defined as follows

$$c_\lambda = \frac{c}{(n+1)^2} \qquad \psi_\lambda = \frac{\psi}{(n+1)^3} \tag{16}$$

where n is the number of lateral stiffeners (intermediate supports) and λ is the distance between supports. The solid lines are for panels simply supported at the ends ($\phi' = 0$) and the broken lines are for panels fixed at the ends ($\phi' = \infty$). The curves $n = 1$ and $n = 2$ are from Figs. 10 and 18, respectively. Each set of curves is displaced by one square in order to improve the clearness of the diagram. It can be seen from the figure that the effect of fixity at the ends diminishes rapidly as the number of intermediate supports is increased. The curve $n = \infty$ is the envelope of all the curves drawn through the same origin.

The correction factors for partial restraint of lateral stiffeners (Fig. 11) and for finite number of longitudinal stiffeners (Table 1) may be also applied for this case.

REFERENCES

[1] Timoshenko, S., *Theory of Elastic Stability*, pp. 103, 180 McGraw-Hill Book Company, Inc., New York, 1936.

[2] Lundquist, Eugene E., *On the Rib Stiffness Required for Box Beams*, Journal of the Aeronautical Sciences, Vol. 6, No. 7, pp. 269–277, May, 1939.

[3] Ratzerdorfer, J., *Rectangular Plates with Stiffeners*, Aircraft Engineering, September, 1942.

[4] Klemperer, W. B., and Gibbons, H. B., *Zeitschrift für angewandte Mathematik und Mechanik*, Vol. 13, pp. 251–259, August, 1933.

[5] Vega Aircraft Corporation, Report R-728, October, 1943.

Prediction of Longitudinal Dynamic Stability

H. P. LIEPMAN*

University of Cincinnati

ABSTRACT

The conventional equations of motion for disturbances from steady level flight are set up and solved in simplified form. The solution of these equations leads to a characteristic stability quartic whose coefficients determine the stability or instability of the motion. The coefficients of the stability quartic are functions of two stability parameters and the absolute angle of attack. The stability parameters can be expressed in terms of basic design and aerodynamic data, taken from an accurate and detailed static stability calculation. Graphs are constructed to facilitate the determination of the stability parameters in terms of wing and tail areas, tail length, mean wing chord, gross weight, moment coefficient slope, tail lift coefficient slope, flight speed, and lift coefficient. A stability criterion is developed, independent of the flight condition, containing geometric design data only and the slopes of the aerodynamic coefficients. This stability criterion is reduced to a single graph, which can also be used to predict stability at any altitude. The period of oscillation is also given in terms of the stability parameters and the angle of attack. The equations and graphs clearly indicate what design changes will make a dynamically unstable airplane stable. Because of the ease and rapidity of the method, it can be included in the routine static stability calculation, thus giving complete information about the stability of an airplane.

INTRODUCTION

THE NEED FOR MAKING the prediction of dynamic stability a routine calculation at an early design stage has become obvious in recent years. It is also a well-known fact that a detailed dynamic stability calculation requires many man-hours of work. This has usually kept designers and manufacturers of light airplanes from carrying out such calculations. The dynamic stability of an airplane is thus left entirely to the happy coincidence of experience and rule-of-thumb methods. In view of the future demands for safe and easily controllable airplanes it will be necessary to include the prediction of dynamic stability in the standard performance calculation of an airplane.

A great amount of valuable theoretical and practical work has been done on the subject in the past. A majority of the papers, however, have dwelt primarily on the mathematics of the subject, with no attempt to present an immediate solution for the engineer. The present paper reduces the conventional stability criteria to a form containing basic aerodynamic and design data only.

Sufficient data are available today to predict the effects of running propellers on aerodynamic coefficients. It is therefore no longer necessary to restrict the simplified discussion of dynamic stability to the power-off condition. Obviously, these power-on effects must also be included in the discussion of static stability.

The derivation of the equations of motion of an airplane can be found in any of the many books and articles on the subject. No attempt is made to repeat the derivation in detail except to point out the basic assumptions upon which these equations are based. The most general motion of an airplane in space will require six differential equations of motion. These six simultaneous equations can be reduced to two independent sets of three equations each when, and only when, small disturbances from the equilibrium position are considered. Only then is it possible to solve the symmetric or longitudinal group and the antisymmetric or lateral group separately. Another assumption is that all air forces and moments vary linearly with the angle of attack. Otherwise the equations of motion would be nonlinear and difficult to solve explicitly.

NOTATION

In addition to standard N.A.C.A. symbols and symbols defined in the text, the following notation is used:

$dc_m/d\alpha$	=	slope of total moment coefficient per rad., including effects of wing, tail, fuselage, and propellers.
$(dc_L/d\alpha)_t$	=	slope of tail lift coefficient per rad. If not available from tests, $(dc_L/d\alpha)_t = 5.7/[1 + (5.7/\pi \text{A.R.}_t)]$
S_t	=	area of horizontal tail in sq.ft.
c	=	mean aerodynamic chord in ft.
l	=	tail length in ft., distance from center of gravity of the airplane to center of pressure of tail
$I = \eta m l^2$	=	moment of inertia about the lateral axis through the center of gravity
η	=	mass distribution factor[5]
α_0	=	absolute angle of attack in rad. between mean aerodynamic chord and zero lift chord

THE EQUATIONS OF MOTION AND THEIR SOLUTION

An airplane in steady level flight with an air speed U_0 in feet per second will be in equilibrium of forces in lift and drag direction, and its resultant moment about the center of gravity will be zero (Fig. 1a). If thrust and total drag are assumed to act through the center of gravity, the only moments encountered will be those of the wing, the tail, and the fuselage. The determination of these moments is part of the static stability calculation and should include the influence of running propellers. All steady flight quantities will be denoted with a subscript zero.

Presented at the National Light Aircraft Meeting, I.A.S., Detroit, April 27–28, 1944.

* Assistant Professor in Aeronautical Engineering. Now Senior Stress Analyst, Goodyear Aircraft Corporation.

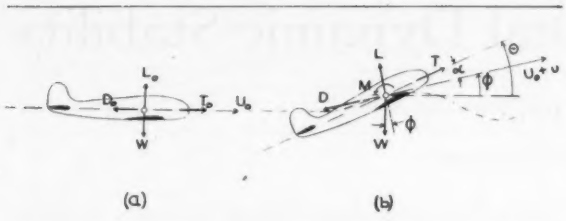

FIG. 1. The airplane in steady and disturbed level flight.

When the airplane is disturbed from its equilibrium position, changes in forces, moments, and the flight path will take place. The changes in the attitude of the airplane can best be described in terms of three variables, u, φ, and θ, where u is the change in the air speed U_0, φ is the change in the inclination of the flight path, and θ is the change in the inclination of the airplane (Fig. 1b). In addition to these variables it will be convenient to use the change in the angle of attack of the airplane, $\alpha = \theta - \varphi$, as an auxiliary variable. Since the discussion is limited to small disturbances from the equilibrium position, an angle itself may be used instead of its sine, the cosine of an angle will be unity, and small terms of higher order will be neglected.

The disturbance will change forces and moments through increments δL, δD, δT, and δM, respectively. These increments can be expressed in terms of the conventional stability derivatives. It can reasonably be assumed that the components, tangent to the flight path, of δT and δD cancel each other and that their components in lift direction are negligibly small compared to the other forces.

With these assumptions and with the velocity component $w = \alpha U_0$, normal to the flight path, the standard equations of motion for the symmetric group[1] reduce to

$$m\dot{u} = -mg\varphi \tag{1}$$

$$-mU_0\dot{\varphi} = mg - L_0 - uZ_u + \alpha U_0 Z_w \tag{2}$$

$$I\ddot{\theta} = \alpha U_0 M_w + \dot{\theta} M_q \tag{3}$$

The four stability derivatives in these equations are found in conventional manner[2]

$$Z_u = -c_L\rho SU_0$$

$$Z_w = -(dc_L/d\alpha)\rho SU_0/2 = -c_L\rho SU_0/2\alpha_0$$

$$M_w = (dc_m/d\alpha)\rho SU_0 c/2$$

$$M_q = -(dc_L/d\alpha)_t\rho S_t U_0 l^2/2$$

The derivative M_q is quite often modified to take into account the effectiveness of the tail surface, as well as a certain amount of wing damping. It is standard practice to multiply M_q by a tail efficiency factor η_t and a wing damping factor K. With the recommended average values for η_t and K, their product is close to unity. Hence, the omission of these correction factors in the expression for M_q is justified in view of the simplifications already made.

Substitution of the stability derivatives into the equations of motion (Eqs. (1), (2), and (3)), remembering that $mg = L_0 = c_L\rho SU_0^2/2$, results in the following equations

$$\dot{u} = -g\varphi \tag{4}$$

$$\dot{\varphi}U_0/g = (2u/U_0) + (\alpha/\alpha_0) \tag{5}$$

$$I\ddot{\theta} = -k_m\alpha - (k_t\dot{\theta}/U_0) \tag{6}$$

where

$$k_m = (-dc_m/d\alpha)\rho SU_0^2 c/2 \tag{7}$$

and

$$k_t = (dc_L/d\alpha)_t\rho S_t U_0^2 l^2/2 \tag{8}$$

are factors indicating the static stability and the tail damping of the airplane, respectively. Since $(dc_m/d\alpha)$ must be negative to insure static stability, both k_m and k_t, as defined in Eqs. (7) and (8), will be positive quantities.

To simplify the solution of the equations of motion, the variable u can be eliminated from Eqs. (4) and (5), and a dimensionless time parameter τ introduced,[3, 4] defined by

$$\tau = tg/U_0 \tag{9}$$

Furthermore, two stability parameters may be defined as

$$\sigma = k_m U_0^2/Ig^2 \tag{10}$$

$$\delta = k_t/Ig \tag{11}$$

where σ measures the static stability and δ the tail damping of the airplane. Both stability parameters are dimensionless and positive by definition of k_m and k_t (Eqs. (7) and (8)).

After substitution of Eqs. (9), (10), and (11) into the equations of motion (Eqs. (4), (5), and (6)), the final result will be

$$(d^2\varphi/d\tau^2) + 2\varphi - (d\alpha/\alpha_0 d\tau) = 0 \tag{12}$$

$$(d^2\theta/d\tau^2) + (\delta d\theta/d\tau) + \sigma\alpha = 0 \tag{13}$$

The solution of these two simultaneous, linear differential equations will be of the form

$$\left.\begin{aligned} \theta &= a_1 e^{\lambda\tau} \\ \varphi &= a_2 e^{\lambda\tau} \\ \alpha &= (a_1 - a_2)e^{\lambda\tau} \end{aligned}\right\} \tag{14}$$

Since the determinant of the coefficients of a_1 and a_2 must be zero, the following characteristic stability quartic in λ results:

$$\lambda^4 + [\delta + (1/\alpha_0)]\lambda^3 + [2 + \sigma + (\delta/\alpha_0)]\lambda^2 + 2\delta\lambda + 2\sigma = 0 \tag{15}$$

The four roots of λ of this stability quartic determine the type of motion the airplane will assume after a disturbance. These roots will be functions of the stability parameters δ and σ and the absolute angle of attack α_0 of steady flight. It will therefore be of value to express δ and σ in terms of basic design data.

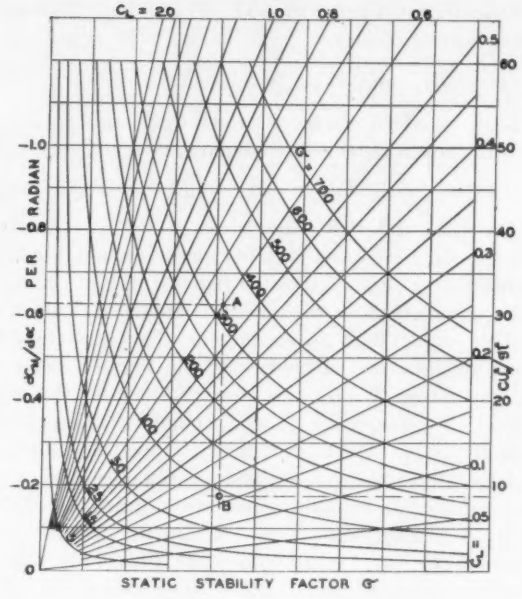

FIG. 2. Static stability parameter.

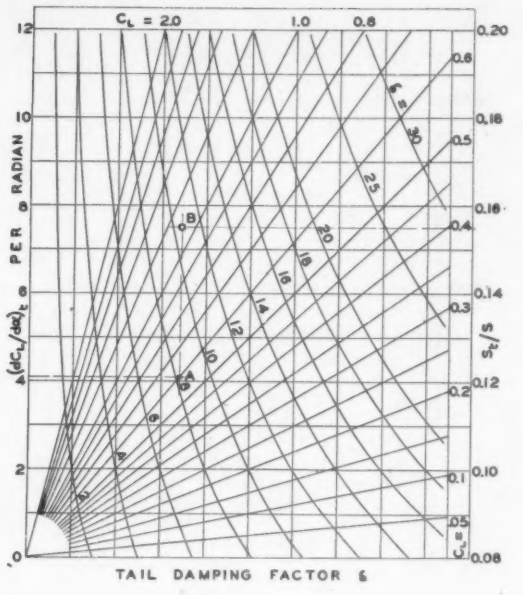

FIG. 3. Tail damping stability parameter.

THE STABILITY PARAMETERS

Substituting Eqs. (7) and (8) into Eqs. (10) and (11) and letting $I = \eta l^2 W/g$ and $W = c_L \rho S U_0^2/2$ leads to

$$\sigma = (-dc_m/c_L d\alpha)(cU_0^2/gl^2)(1/\eta) \qquad (16)$$

$$\delta = (dc_L/d\alpha)_t(1/c_L)(S_t/S)(1/\eta) \qquad (17)$$

In this form the influence of basic aerodynamic and design data on the stability parameters is easily recognized. Assuming an average value of the mass distribution factor $\eta = 0.10$ (reference 5), Figs. 2 and 3 were constructed to facilitate the rapid determination of σ and δ. To use these graphs, a point A on the straight lines, corresponding to the values of c_L and $dc_m/d\alpha$ or $(dc_L/d\alpha)_t$, is found first. Then a vertical line through this point and the value of cU_0^2/gl^2 or S_t/S will determine point B, the value of σ or δ, respectively.

If a particular airplane has a mass distribution factor η considerably different from 0.10, Figs. 2 and 3 can still be used to find the stability parameters. Simply multiply σ and δ, obtained from the graphs, by $0.10/\eta'$, where η' is the actual mass distribution factor of the airplane under consideration.

STABILITY CRITERIA

To insure dynamic stability of an airplane, the values of λ in Eqs. (14) must either be all negative, resulting in an aperiodic subsidence of the motion, or complex with negative real parts, causing damped oscillations about the equilibrium position. The values of λ depend entirely on the stability quartic (Eq. 15), which is of the form

$$A\lambda^4 + B\lambda^3 + C\lambda^2 + D\lambda + E = 0 \qquad (18)$$

The coefficients of λ can be expressed in terms of the stability parameters and the absolute angle of attack as follows (Eqs. (15) and (18)):

$$\left.\begin{array}{llll} A = 1 & B = \delta + (1/\alpha_0) & & \\ C = 2 + \sigma + (\delta/\alpha_0) & D = 2\delta & E = 2\sigma & \end{array}\right\} \qquad (19)$$

To make the roots of the stability quartic come out complex with negative real parts, all coefficients of the stability quartic must be positive, as well as Routh's stability discriminant[3]

$$R = B(CD - EB) - D^2 > 0 \qquad (20)$$

From the definitions of σ, δ, and α_0 all coefficients (Eqs. (19)) are always positive, and the only remaining criterion to be satisfied is Eq. (20), which, in terms of σ, δ, and α_0 reduces to

$$\delta\{\delta + [2\alpha_0/(\delta\alpha_0 + 1)]\} - \sigma > 0 \qquad (21)$$

Numerical evaluation of this criterion in the normal range of the absolute angle of attack shows that the second term in the bracket is negligibly small compared to δ and can be dropped. The stability criterion then reduces to the simple inequality

$$\delta^2 > \sigma \qquad (22)$$

The equality $\delta^2 = \sigma$ defines a parabolic boundary between the dynamically stable and unstable regions (Fig. 4). The approximation involved amounts to a slight reduction of the stable region and will thus give conservative results.

Although δ and σ can be found quickly from Figs. 2 and 3, they vary with the lift coefficient and the level flight speed and are therefore different for every flight condition. Fortunately, the stability parameters can

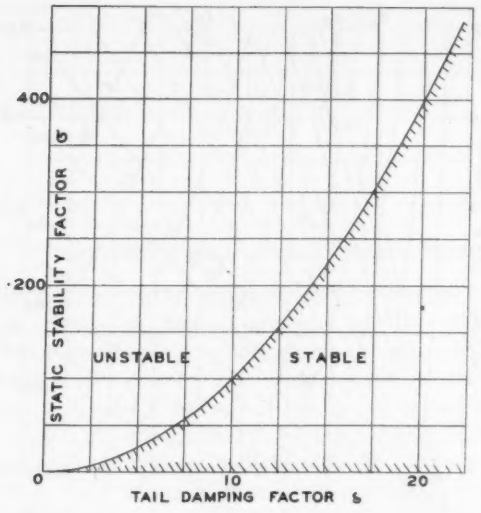

FIG. 4. Dynamic stability regions.

be expressed in terms of basic design data and substituted into the stability criterion (Eq. (22)). This criterion will then be independent of the flight condition. It is therefore possible to determine, from basic design data only, whether an airplane is dynamically stable or not. Obviously, the amount of dynamic stability, such as the period of oscillation, cannot be determined so easily.

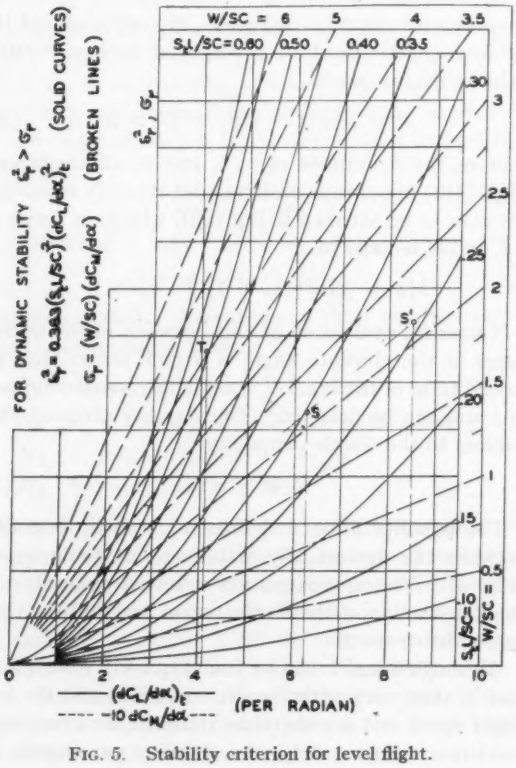

FIG. 5. Stability criterion for level flight.

Substitution of Eqs. (16) and (17) into Eq. (22) leads, after simplification, to

$$(dc_L/d\alpha)_t^2(S_t l/Sc)^2 g\rho/2\eta > (-dc_m/d\alpha)W/Sc \quad (23)$$

With standard sea-level values for g and ρ, and $\eta = 0.10$, as before, the above inequality reads

$$0.383(dc_L/d\alpha)_t^2(S_t l/Sc)^2 > (-dc_m/d\alpha)W/Sc \quad (24)$$

The left- and right-hand sides of Eq. (24) can be thought of as reduced stability parameters δ_r^2 and σ_r, respectively. Fig. 5 gives the reduced stability parameters as functions of the aerodynamic data as abscissa and the design data as parameters. Dynamic stability of an airplane is then predicted from Fig. 5 if point T, corresponding to $(dc_L/d\alpha)_t$ and $(S_t l/Sc)$ on the solid curves, is *above* point S, corresponding to $(dc_m/d\alpha)$ and (W/Sc) on the broken lines. Since the numerical values of the reduced stability parameters are of no importance, no ordinate values are indicated in Fig. 5.

If an airplane has a mass distribution factor η', different from the average value 0.10, Fig. 5 will still be valid if the abscissa for the σ_r-lines (broken lines) is taken as $10\eta'(dc_m/d\alpha)$ instead of the actual moment coefficient slope.

The dynamic stability at any altitude can also be predicted from the same graph if the value of $(dc_m/d\alpha)\rho_0/\rho$ is used as abscissa for the straight σ_r-lines instead of $(dc_m/d\alpha)$ alone (point S' in Fig. 5). The mass density ratio ρ_0/ρ of air is greater than unity at altitudes, and the question of dynamic stability is therefore more critical at higher altitudes. In case the value of $(dc_m/d\alpha)\rho_0/\rho$ should be off scale in Fig. 5, a modified value of $W\rho_0/Sc\rho$ may be used with the actual moment coefficient slope as abscissa to determine dynamic stability at any altitude.

CHARACTER OF STABILITY

Once an airplane is found to be dynamically stable, it is of further interest to know the type of damped oscillation which will follow a disturbance. This knowledge is necessary to determine the ease of maneuvering and controlling the airplane and the degree of comfort to the passengers. The factors describing a damped oscillation are the period P and the time T to damp to one-half of the amplitude.

Since the equation for the time to damp to one-half amplitude responds critically to the coefficients of the stability quartic, the simplifications introduced, although small in their overall effect, will so distort the value of the damping time T that not even an approximation can be given. However, the period of oscillation P can be found with sufficient accuracy, since the natural or undamped period is practically equal to the damped period as long as the damping is light. A reasonable value of the period can be found in terms of the stability parameters.

The stability quartic of a dynamically stable airplane will have two pairs of conjugate complex roots if

damped oscillations exist. These pairs of roots can be found through approximate factorization of the stability quartic into two quadratics.[3, 5] There exist two types of oscillations corresponding to each pair of roots. The first type is a short, heavily damped oscillation, noticeable as a bump and of little practical interest. The second type is a long, lightly damped oscillation that determines the character of dynamic stability. The period of this long oscillation can be expressed in terms of the coefficients of the stability quartic as follows:[5]

$$Pg/U_0 = 2\pi\sqrt{C/E} \tag{25}$$

The term g/U_0 on the left-hand side must be introduced to convert from the dimensionless time parameter τ to actual time t in seconds (Eq. (15)).

Substitution of the coefficients of the stability quartic in terms of δ, σ, and α_0 (Eqs. (19)) into Eq. (25) leads to

$$Pg/U_0 = 4.45\sqrt{1 + \delta'/\sigma} \tag{26}$$

where

$$\delta' = 2 + (\delta/\alpha_0) \tag{27}$$

To determine the period quickly, Fig. 6 has been constructed, giving δ' in terms of δ and α_0 on its left side and the dimensionless period Pg/U_0 as function of δ' and σ on its right side.

Since the period changes with each flight condition, it is recommended that P be calculated and plotted against flight speed or lift coefficient for the entire flight range, from stalling speed to maximum speed. If and when pilots can decide what kind of period of oscillation they want for each flight condition, the designer will be able to adjust the design parameters to the requirements.

The two most critical flight conditions are the stalling speed and the cruising speed. At the stall the dynamic stability is quite critical because of the high lift coefficient, and safety requires sufficient stability since the effectiveness of the controls at low speeds is quite often a minimum. At cruising speed the dynamic stability should satisfy passenger comfort requirements and ease of control of the airplane. It is hoped that the many flight-test results will be coordinated to give more detailed and explicit recommendations as to period and damping to the airplane designer.

Example

To illustrate the method and the use of the graphs, a small and a large aircraft have been chosen as examples. The pertinent design data and the results are collected in Table 1. The values for the small airplane (airplane I) are also indicated on Figs. 2, 3, 5, and 6. This airplane shows sufficient dynamic stability below 10,000 ft. but becomes unstable at and above that altitude. If this instability is considered undesirable, the equations indicate what kind of changes should be made. In this particular example an increase of 3 per cent in the value of $(S_t l/Sc)$ would bring the airplane into the stable range at 10,000 ft.

Table 1
Dynamic Stability Prediction

	Airplane I		Airplane II
W (lbs.)	1,200		18,000
S (sq.ft.)	140		939
c (ft.)	4		11.86
l (ft.)	13.1		36.6
S_t/S	0.155		0.165
$dc_m/d\alpha$	−0.628		−0.658
$(dc_L/d\alpha)_t$	4.1		4.0
Flight Altitude	Sea Level	10,000 Ft.	5,000 Ft.
c_L	0.6	0.6	0.3
U_0 (ft. per sec.)	111	129	250
Stability criterion Fig. 5	Stable	Unstable	Stable
δ, Fig. 3	10.6	10.6	23
σ, Fig. 2	93	125.5	375
δ', Fig. 6	81	81	354
P, Fig. 6 (sec.)	21	22.9	48.2

The results for airplane II compare favorably with other calculations[6] and flight-test results. For the flight condition investigated, a period of 50 sec. was found during flight test as compared to the predicted period of 48.2 sec.

Conclusion

The prediction of longitudinal dynamic stability from the graphs or the corresponding equations is accomplished easily and quickly. It can be made a part of the standard static stability calculation, since no new aerodynamic and design data are required. If the prediction indicates dynamic instability, the necessary changes can be easily determined from an inspection of the stability parameters. The most likely design changes are to increase either the ratios of tail area to wing area and tail length to wing chord or both. A less

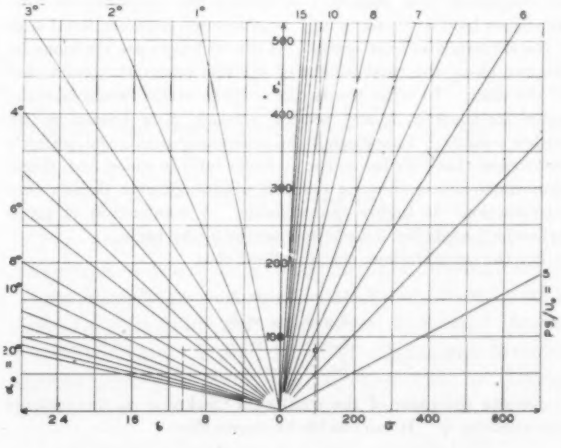

Fig. 6. Nondimensional period of oscillation.

effective and more difficult way would be to decrease the value of the moment coefficient slope. Finally, but hardly practical, a decrease in the moment of inertia through redistribution of weight items will have some beneficial effect on the stability.

Great care should be exercised in using the proper value of the slope of the moment coefficient. Hence, an accurate and detailed static stability calculation[8] is a prerequisite for the prediction of dynamic stability. The static stability discussion, from which the value of $dc_m/d\alpha$ is to be taken, should include wing, tail, and fuselage moments about the normal and extreme positions of the center of gravity.

The important but more complex problem of lateral dynamic stability has recently been exhaustively treated by Price.[7] Twenty-four stability charts are developed to determine regions of lateral stability, as well as the damping and the period.

References

[1] Durand, W. F., *Aerodynamic Theory*, Vol. V, p. 129, reprint, 1943.

[2] Metcalf, A. G. B., *Airplane Longitudinal Stability*, Journal of the Aeronautical Sciences, Vol. 4, No. 2, pp. 61–69, December, 1936.

[3] von Kármán, Th., and Biot, M. A., *Mathematical Methods in Engineering*, pp. 244–255; McGraw-Hill Book Company, Inc., New York, 1940.

[4] Munk, M. M., *Streamlining Dynamic Stability Computations*, Aero Digest, Vol. 42, No. 5, p. 205, May, 1943.

[5] Diehl, W. S., *Engineering Aerodynamics*, pp. 244 and 249; Ronald Press, 1936.

[6] Root, L. E., *Dynamic Longitudinal Stability Charts for Design Use*, Journal of the Aeronautical Sciences, Vol. 2, No. 3, p. 108, May, 1935.

[7] Price, H. L., *The Lateral Stability of Airplanes*, Aircraft Engineering, Vol. 25, No. 173–176, July–October, 1943.

[8] Liepman, H. P., *An Improved Longitudinal Stability Calculation*, Journal of the Aeronautical Sciences, Vol, 9, No. 5, p. 181, March, 1942.

Letter to the Editor

Dear Sir:

Mr. Zahorski has made an attempt to simplify panel design in his recent paper, "Effects of Material Distribution on Strength of Panels" [JOURNAL OF THE AERONAUTICAL SCIENCES, p. 247, July, 1944]. Unfortunately, the author has limited his discussion to flat panels under compressive load only. It is obvious that stiffener material will be more efficient in carrying compressive load than skin material. However, this is in general not true when shear load is present.

The curves given for panels No. 12 and No. 14 (Fig. 4 of the author's paper) do not seem to be correct. According to the expressions given in Table 1, the values of $f(\beta)$ at $\beta = 0$ should apparently be $24/\pi^2$ and $6/\pi^2$ for panels No. 12 and No. 14, respectively.

It is probably more practical to express the stiffness ratio (R_s) in terms of the unsupported width of the skin (b_s) and the skin thickness (t_s). These two quantities can never be zero in practical panel constructions.

When the strength-weight ratios of two types of construction are compared, it is necessary to confine the discussion to constructions having the same unit weight (same cross-sectional area if the materials are the same). If the stiffeners are the same in the two cases, the total weight of the skin materials should also be the same. In other words, the stiffness ratios should be compared for constant t_s and not for constant β as defined in the author's paper. Considering the above argument, the author's conclusion that "As far as the stiffness ratio is concerned, single skin construction shows a definite advantage over double skin construction" is highly questionable. A comparison is given below for panels No. 3 and No. 4 on the above basis.

For the same stiffener size, it follows that

$$\begin{aligned} t_{03} &= t_{04} = t_0 \\ b_{03} &= b_{04} = b_0 \\ b_{s3} &= b_{s4} = b_s \\ t_{s3} &= 2t_{s4} \end{aligned}$$

Denote the ratio of the total skin thickness to the stiffener thickness by γ. It can readily be shown that

$$\gamma = t_{s3}/t_0 = 2t_{s4}/t_0$$

For panel No. 3

$$R_s = \frac{1 + 2\sqrt{2}\gamma}{(\sqrt{2} + \gamma)^4}\left(\frac{b_0}{t_0}\right)^2$$

For panel No. 4

$$R_s = \frac{2 + 4\sqrt{2}\gamma + 3\gamma^2}{2(\sqrt{2} + \gamma)^4}\left(\frac{b_0}{t_0}\right)^2$$

It is obvious that Panel No. 4 always has a higher "stiffness ratio." Similar comparison can be obtained for Panels Nos. 11, 12, 13, and 14.

In discussing the skin efficiency, the load-carrying ability of the skin in the buckled state is not considered. Furthermore, the conditions prescribed in Eq. (14) are not always necessary and sufficient.

In the final discussion on "optimum stress," there has been no attempt made to differentiate the various symbols for the skin thickness (t_0 and t_s) and the skin width (b_0 and b_s). This is permissible only when their relations have been prescribed.

CONRAD C. WAN
Structure Development Engineer
Chance Vought Aircraft

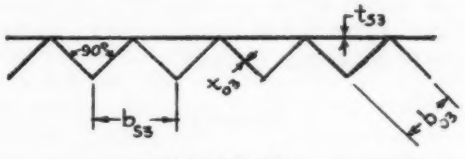

Panel No. 3

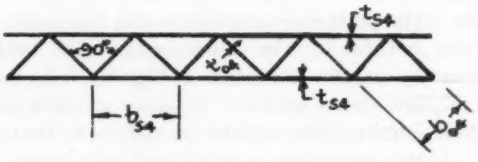

Panel No. 4

Causes of Nighttime Thunderstorms over the Middle West

D. M. CROWLEY*

Transcontinental & Western Air, Inc.

SUMMARY

Nighttime thunderstorms frequently occur during the summer months over the Middle West. This paper describes this type of thunderstorm, which is initiated and maintained by instability producing conditions other than cold fronts, warm fronts, or thermal instability.

Local superadiabatic instability initiates nighttime thunderstorms, and this instability is produced by any one of the following conditions: (1) advection of warm air at intermediate and high levels; (2) advection of cooler air at intermediate and high levels; and (3) advection of warmer air at intermediate levels and cooler air at higher levels.

Several typical occasions when these conditions prevailed and produced thunderstorms are described and analyzed.

CLASSIFICATION OF NIGHTTIME THUNDERSTORMS

THIS TYPE OF THUNDERSTORM usually occurs when the sea-level pressure decreases from the eastern or southeastern United States to the western plains or western Rocky Mountain region.

The classification of thunderstorms as high- or low-level types is made on the basis of the height of the condensation level. Primarily, the classification is determined by the intensity of the turbulence at low levels. The basis of this classification of thunderstorms will be discussed later.

With limited upper air data, considerable experience is required to forecast the intensity, time, and locality of development of nighttime thunderstorms, since three definite instability producing conditions are recognized, any one of which will cause the development of this type of thunderstorm.

These three instability-producing conditions are: (1) advection of warm air at intermediate and high levels; (2) advection of cooler air at intermediate and high levels; and (3) advection of warmer air at intermediate levels and cooler air at higher levels.

Figs. 1, 2, and 3 illustrate the initial and final temperature lapse rates and vertical wind structure common to the respective types.

During the night the stability and density of the air increase throughout the surface friction layer, permitting the energy of the existing pressure gradient to be released above the gradient level. As a result, there is a marked nocturnal decrease in winds below and increase above the gradient level (Fig. 1).

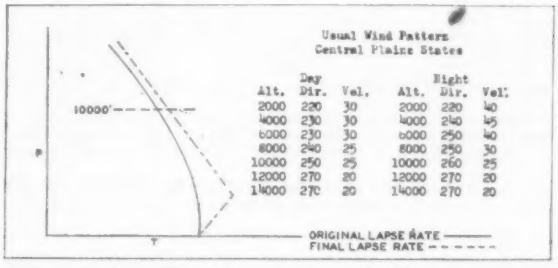

FIG. 1. Characteristic changes in lapse rate and wind structure with Type 1 instability.

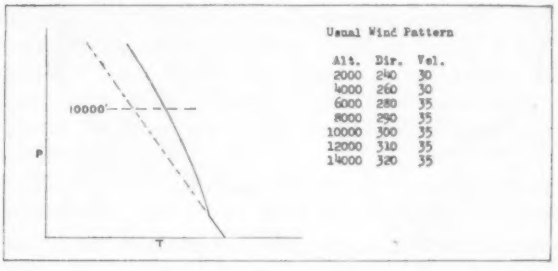

FIG. 2. Characteristic changes in lapse rate and wind structure with Type 2 instability.

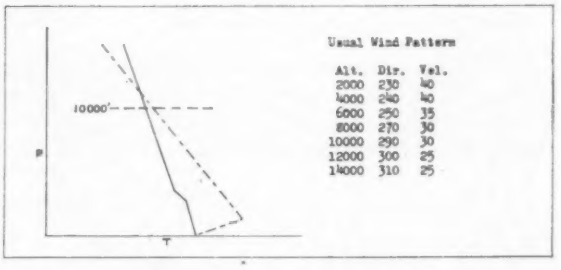

FIG. 3. Characteristic changes in lapse rate and wind structure with Type 3 instability.

TYPE 1 INSTABILITY

Fig. 4 is an illustration of Type 1 instability—i.e., advection of warm air at intermediate and high levels. These soundings were made at Olathe, Kan., and illustrate a 24-hour change between 7 AMC,† August 14, and 7 AMC, August 15, 1943. Scattered thunderstorms developed about sunrise on August 15 through central and eastern Kansas and dissipated by noon.

Presented at the Meteorology Session, Twelfth Annual Meeting, I.A.S., New York, January 25–27, 1944.

* Meteorologist.

† AMC and PMC refer to a.m. C.W.T. and p.m. C.W.T.

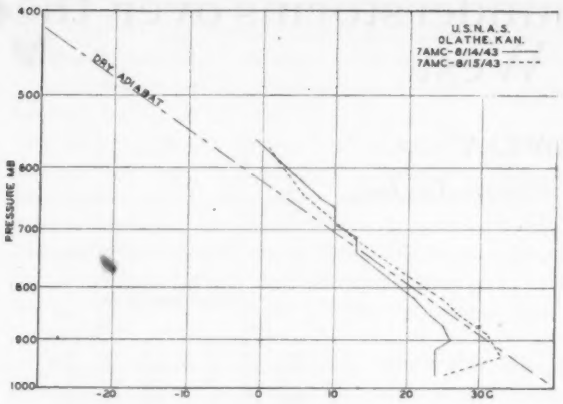

FIG. 4. An example of decreasing stability produced by the advection of warm air.

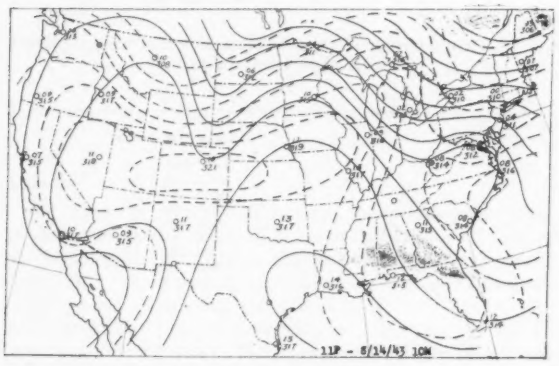

FIG. 5. Ten-thousand-ft. pressure-temperature chart illustrating a typical case of warm air advection.

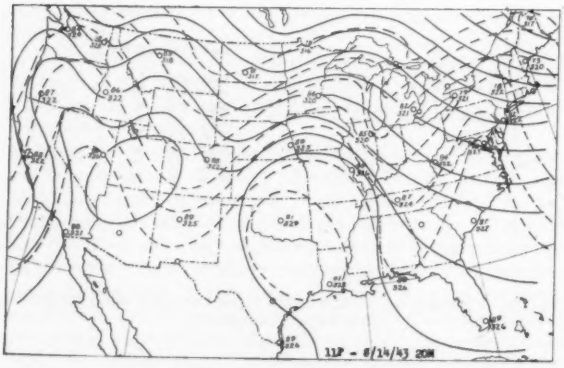

FIG. 6. A typical 20,000-ft. constant-level pressure-temperature pattern identified with high-level cooling.

The information from the 10,000- and 20,000-ft. pressure and potential temperature charts for 11 PMC, August 14 (Figs. 5 and 6), was available for this forecast. These charts show a flow of warmer air from the southwest at the respective levels. Similar charts for 11 AMC, August 15 (Figs. 7 and 8), complete this series.

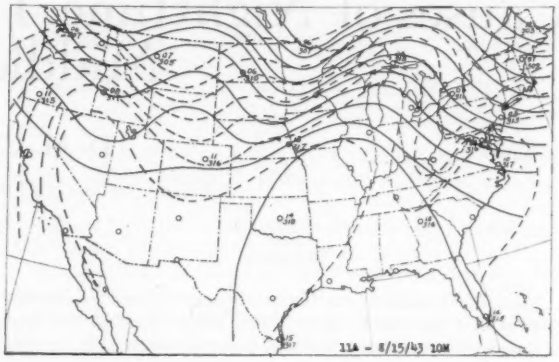

FIG. 7. Ten-thousand-ft. constant-level pressure-temperature chart at 11 a.m., August 15, 1943.

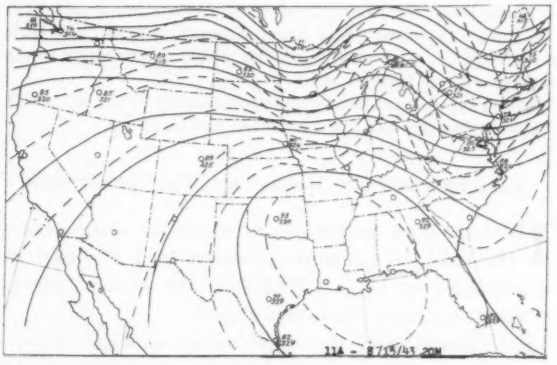

FIG. 8. Twenty-thousand-ft. constant-level pressure-temperature chart at 11 a.m., August 15, 1943.

To create sufficient instability for thunderstorms, the advection of warm air must be greater below than above 10,000 ft. This condition normally exists when the winds are southerly and veering, and the pressure gradient is increasing. The advection of warm air immediately above the gradient level increases throughout the night and is maximum near sunrise. For this reason, this type thunderstorm develops most frequently toward sunrise when the low-level warm air impulse is greatest. If conditions are ideal, this type may develop by midnight.

The warm air type of thunderstorm generally develops over a wide region but is usually widely scattered and of the high-level classification. The intensity of the individual storm varies but is most frequently light to moderate.

TYPE 2 INSTABILITY

The thunderstorms initiated by the advection of cooler air at intermediate and high levels (Type 2) can be classified as high- or low-level type and often develop during the day as well as at night. Most frequently, this type develops late in the afternoon and continues throughout the night.

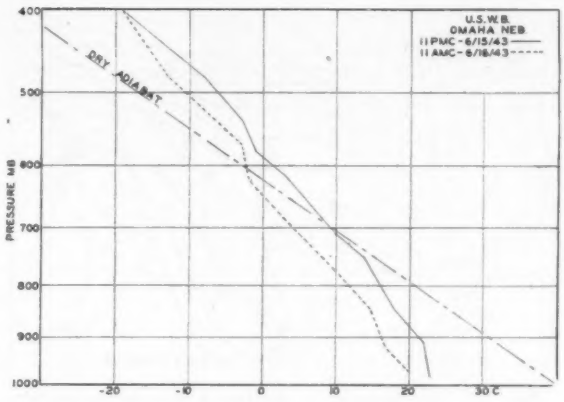

FIG. 9. A typical example of change in lapse rate produced by the advection of cooler air, Type 2 instability.

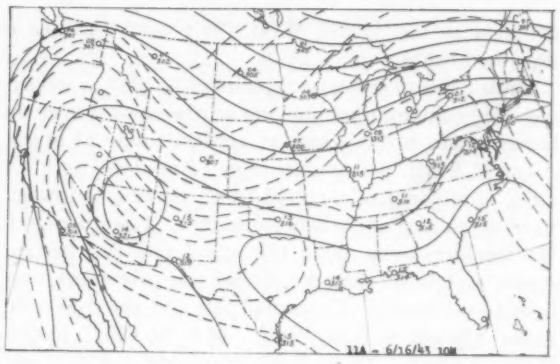

FIG. 11. Ten-thousand-ft. constant-level pressure-temperature chart for 11 a.m., June 16, 1943. At this time thunderstorms were active over Kansas, Missouri, and Oklahoma.

Fig. 9 illustrates the air mass curve before and after such a thunderstorm had passed Omaha, Neb., during the early morning of June 16, 1943. Figs. 10 and 11 are the 10,000-ft. pressure and potential temperature charts for the respective times.

Mild high-level thunderstorms were developing throughout central and southern Minnesota, western Iowa, eastern Nebraska, and northern Kansas by 11 PMC, and by 4 AMC the intensity had increased to moderate to locally severe low-level thunderstorms. The thunderstorms occurred intermittently over one locality for a period of about 6 to 8 hours.

From the 10,000-ft. chart (Fig. 10), it can be seen that cooling (increasing instability) was occurring throughout the entire area, that thunderstorms were developing, and that, as the shallow pressure trough moved eastward, the instability producing condition would continue. From this information, thunderstorms should be forecast to develop through southern and eastern Kansas, western and central Oklahoma, and Missouri the following morning.

The instability producing condition is often referred to as an upper cold front. This example is an ideal condition and easy to detect on the upper-air charts. More frequently, the temperature and pressure waves are shallow and difficult to detect when limited upper-air data are available. Often the wind aloft is the only information the forecaster has available to forecast the development of this type of thunderstorm. The usual change in vertical wind structure as an upper-air pressure trough passes a station is illustrated in Fig. 2. About 6 hours before the pressure trough passes the station, the winds at 10,000 ft. shift from the southwest to the west or from the southwest to the west-southwest.

It should be made clear that Fig. 9 represents the air mass curve before and after the thunderstorm had passed that locality. The cooling at high levels came first, creating the intense instability. The low-level cooling was caused by the downward transport of cold temperatures and the evaporational cooling of the rain.

PREFRONTAL SQUALLS

Type 2 instability—that is, advection of cooler air at high and intermediate levels—is the major cause of widespread thunderstorm activity in advance of a cold front and the development of the prefrontal squall line

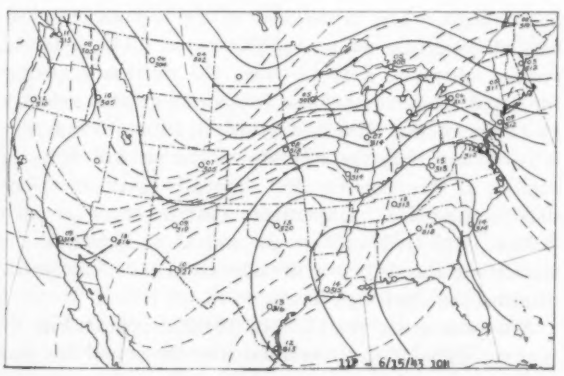

FIG. 10. Ten-thousand-ft. constant-level pressure-temperature chart for 11 p.m., June 15, 1943, showing characteristic pattern associated with Type 2 instability.

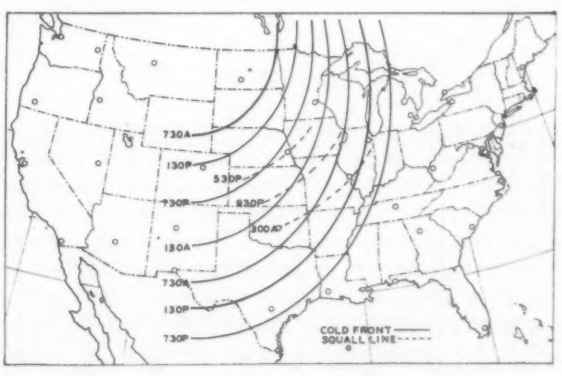

FIG. 12. Chart of the progressive positions of a cold front and associated prefrontal squall line occurring on September 5–6, 1943.

common to the Middle West. A typical example is described below.

During the morning of September 5, 1943, a moderate NPc* cold front was moving southeastward over the northwestern plains states at approximately 24 m.p.h. About 4 PMC, a moderate squall line developed 100 miles in advance of the cold front, moving southeastward at an average rate of 40 m.p.h. Toward sunset, the thunderstorms along the squall line had become severe and those between it and the cold front were light to moderate. The squall line and the cold front passed Omaha at 5:30 PMC and 9:30 PMC, respectively, Kansas City at 9:30 PMC and 4 AMC, and St. Louis at 3:00 AMC and 12 Noon. The progress of these systems is illustrated in Fig. 12. The thunderstorms were most active from 6:00 PMC to 3:00 AMC, and passed intermittently over a station between the passage of the squall line and the cold front.

The upper-air data for 11 AMC, September 5, provide ample information for the preparation of the forecast of these events. The upper air soundings for

* Transitional polar Canadian.

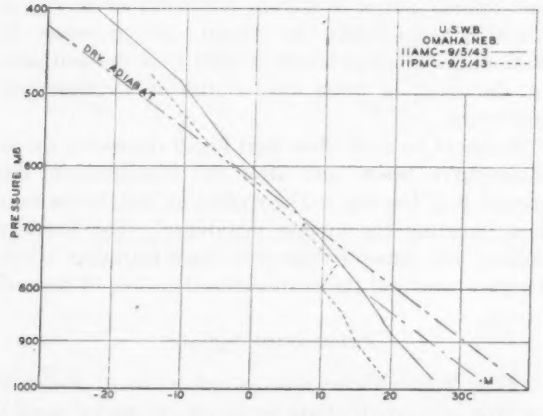

FIG. 13. An example of lapse rate change associated with Type 2 instability and typical of prefrontal squalls.

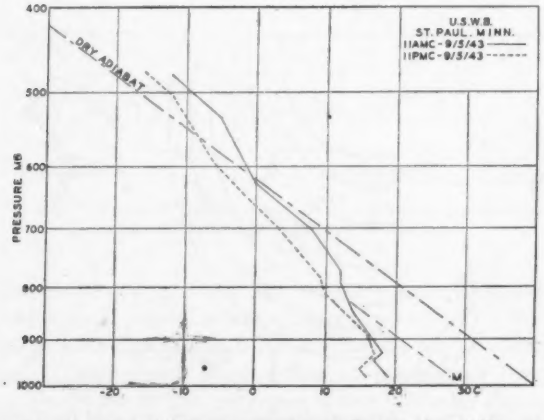

FIG. 14. An additional example of Type 2 instability observed on the same date as that illustrated in Fig. 13. Associated with the same frontal activity but farther north.

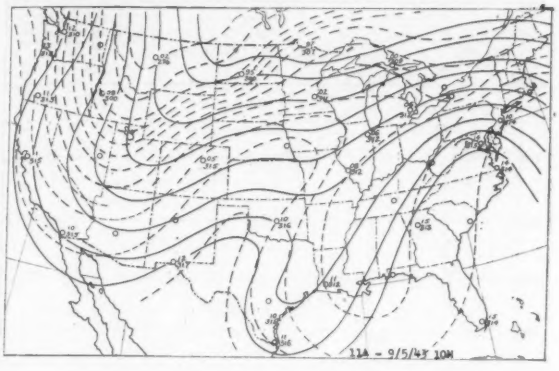

FIG. 15. Ten-thousand-ft. constant-level pressure-temperature chart immediately preceding a period of prefrontal squall activity over the Middle West.

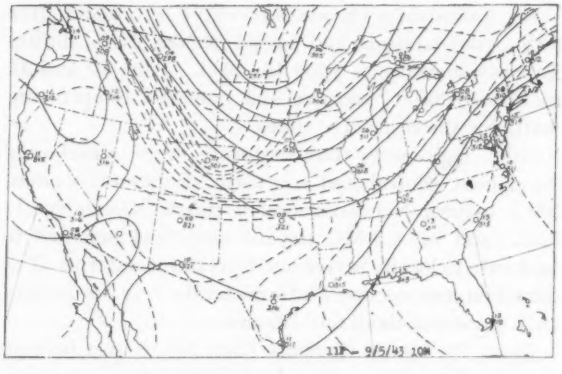

FIG. 16. Ten-thousand-ft. constant-level pressure-temperature chart during a period of prefrontal squall activity over the Middle West.

Omaha, Neb., and St. Paul, Minn., at 11 AMC and 11 PMC are illustrated in Figs. 13 and 14, respectively. The associated 10,000-ft. charts are reproduced as Figs. 15 and 16.

The 11:00 AMC 10,000-ft. chart reveals that the warm wave had reached its crest through central Kansas and Iowa and was well in advance of the pressure trough. The orientation of the isobars is "west-east" through the western plains states. The resulting strong solenoidal field provides the necessary energy for rapid movement of the cool air aloft at a velocity in excess of the indicated gradient wind. From this it is obvious that the stability of the air will decrease rapidly as the "cooling aloft" spreads eastward. The maximum surface temperature that occurred at each station is plotted on Figs. 13 and 14 to illustrate the stability of the air before the advection of cool air at the intermediate and high levels.

After examining the 11 PMC 10,000-ft. chart, Fig. 16, it is not difficult to understand why the squall line was so intense. The extent and rapidity of movement of the cool air to the east, producing local superadiabatic instability, is readily apparent from this chart.

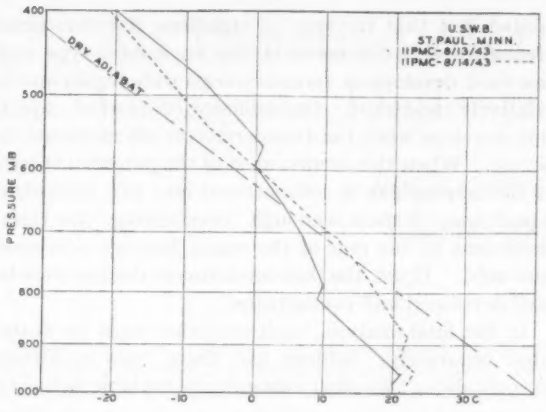

FIG. 17. An example of lapse rate change associated with Type 3 instability.

TYPE 3 INSTABILITY

The most natural instability producing conditions exist when there is an advection of warmer air at intermediate levels and cooler air at higher levels. This is Type 3 instability and is illustrated in Figs. 4 and 17.

Toward midnight on August 14, 1943, scattered thunderstorms began to develop through northern Iowa and southern Minnesota, by 5 AMC through most of Iowa and Minnesota, and by 8 AMC through western Illinois and northern Missouri. These thunderstorms dissipated 4 hours after sunrise.

Fig. 17 illustrates the changes as they occurred in the lapse rate at St. Paul between the evening of August 13 to the evening of August 14. Figs. 5, 6, 7, and 8 are the 10,000- and 20,000-ft. constant-level charts for the evening of August 14 and morning of August 15. No sounding was made at St. Paul on the morning of August 15, 1943.

Fig. 5 shows a definite advection of warm air at 10,000 ft. from the southwest through southern Minnesota, Iowa, Missouri, and Illinois. Fig. 6 shows definite advection of cooler air at 20,000 ft. through Minnesota and western Iowa and this condition moving rapidly eastward.

After making the above analysis, it is obvious that high-level thunderstorms should be forecast to develop through northern Missouri and western Illinois by morning.

It is interesting to examine the 10,000- and 20,000-ft. charts for 11 AMC, August 15, 1943, Figs. 7 and 8, respectively. The temperature wave had reached its crest at 10,000 ft. through Missouri and western Illinois (warm air impulse in low levels was a maximum), and the temperature trough at 20,000 ft. was nearly minimum over the Mississippi Valley region. This created a maximum instability impulse toward late morning throughout this region.

FLIGHT PROCEDURES

Reference was previously made to the high- or low-level classification of thunderstorms. The average commercial pilot determines this classification from the magnitude of the low-level turbulence, as well as by the height of the condensation level. Low-level turbulence is turbulence beneath the condensation level of the thunderstorm and in the immediate vicinity of the storm. It is commonly accepted that turbulence can be moderate to severe within the main cloud of a mild thunderstorm; therefore, this classification does not deal with turbulence within the cloud itself.

A knowledge of the intensity of the nighttime thunderstorm (according to this classification) is obviously desired by the pilot. With the present limited upper-air data it is not always possible to forecast accurately the magnitude of the low-level turbulence, since it depends upon the following variables:

(1) The intensity of the instability aloft and the rate of development.

(2) The individual moisture impulse, or the height of the free air convection level. (The lower the level, the greater the low-level turbulence.)

(3) The magnitude of the low-level wind squalls induced by the strong vertical currents of the thunderstorm.

(4) The degree of stability in the low levels.

Generally, nighttime thunderstorms over the central plains states are classified as the light to moderate high-level type. The proper technique to use in flying this type of thunderstorm is outlined below:

(1) Fly around the thunderstorm at an altitude below the condensation level.

(2) Fly under the thunderstorm midway between the condensation level and the ground, which is often within the relatively stable air below.

(3) Fly over the thunderstorm (not possible with present commercial equipment).

(4) Fly near the condensation level if it is absolutely necessary to fly in the cloud to clear high terrain.

IN GENERAL

After determining the approximate degree of instability to develop over a given airway, the condensation level can be determined from the nearest upper-air sounding by using the highest mixing ratio in the lower levels or the moisture content forecast for that region at the time under consideration.

The initial instability producing impulse necessary to set off the thunderstorm is caused by local irregularities in wind or local superadiabatic instability brought about by the advection process.

Weak fronts and irregular terrain will hasten the development at an earlier hour of this type of thunder-

storm, but neither of these conditions is necessary to set off the thunderstorms. Most frequently, this impulse is caused by local superadiabatic instability as explained above.

Since the nighttime thunderstorm is not "fed" by a constant instability producing source (such as surface heating, fronts, etc.), its period of activity is quite variable. It can develop into maturity and dissipate within a short period of time. This is particularly true of the mild high-level thunderstorm but is not characteristic of the moderate to severe type.

Too often the intensity of nighttime thunderstorms is erroneously measured by the amount of visible lightning. There is considerable visible lightning in the mild high-level thunderstorm, since the condensation level is high (60 to 120 m.s.l.) and the base and top of the thunderstorm are not ordinarily obscured by low or intermediate cloud decks.

Often pilots report paralleling a front into their destination, and this "front" is actually the protruding edge of a region of nighttime thunderstorms. It is repeated here that the type of nighttime thunderstorms treated in this discussion is the nonfrontal type and one that develops or spreads over a wide region and is relatively scattered. Occasionally, a marked squall line develops when the thunderstorms are moderate to severe. When this occurs, most of the potential energy of the troposphere is concentrated into this individual squall line. If there is enough "overturning," the thunderstorms to the rear of the squall line are scattered and mild. If not, the thunderstorms to the rear may be well developed and concentrated.

In the final analysis, each condition must be evaluated separately. Seldom are there two conditions exactly alike. Weather elements are variable elements.

References

[1] Byers, H. R., *Synoptic and Aeronautical Meteorology;* McGraw-Hill Book Company, Inc., New York, 1937.

[2] Taylor, G. F., *Aeronautical Meteorology;* Pitman Publishing Corporation, New York, 1938.

[3] Petterssen, S., *Weather Analysis and Forecasting;* McGraw-Hill Book Company, Inc., New York, 1940.

Letter to the Editor

Dear Sir:

Mr. H. N. Hill called my attention to the similarity between the procedure suggested in my paper "A Note on Inelastic Buckling," JOURNAL OF THE AERONAUTICAL SCIENCES, Vol. 11, No. 2, p. 163, April, 1944, and that employed in the *Structural Aluminum Handbook* published in 1940 by the Aluminum Company of America. On pp. 41, et seq., of the handbook, formulas are given for the calculation of an "equivalent slenderness ratio" of a compressed plate, shell, etc. The critical stress is then calculated by substituting the effective slenderness ratio in the pertinent column formula.

N. J. HOFF
Associate Professor of Aeronautical Engineering
Polytechnic Institute of Brooklyn

An Iterative Method for Determining Dynamic Deflections and Frequencies

N. A. BOUKIDIS* AND R. J. RUGGIERO*

Lockheed Aircraft Corporation

ABSTRACT

A solution to the problem of finding the natural modes and frequencies of vibration of a linear elastic system is given. Particular emphasis is placed on the determination of the higher modes of oscillation—i.e., modes other than the fundamental. It is found that the quantities needed to obtain the higher modes are available after the fundamental frequency and mode of vibration have been determined. This results in a saving of considerable labor.

The theory is developed in some detail after which it is applied to the calculation of the bending oscillations of the wing of a twin-engined monoplane. The necessary steps in such a procedure are summarized in a form adapted to numerical computation. This makes the process largely independent of reference to the theory previously developed.

INTRODUCTION

ONE OF THE MOST IMPORTANT PROBLEMS of vibration engineering is that of determining the natural modes and frequencies of oscillation of an elastic system. A method will be presented which applies to vibratory systems in general and which is especially useful in determining the "higher" modes of vibration. The procedure has been used by the authors in the determination of several of the bending and torsional modes of an airplane wing.

In this paper the underlying theory of the method will be sketched and its actual application will be illustrated with reference to the bending oscillations of an airplane wing.

The authors wish to point out that to the best of their knowledge the essential features of the theory as here presented are due to Biezeno and Grammel.[9] The actual method of application, however, is based on a procedure originally due to Stodola.[2] The authors also wish to take this opportunity to thank Mr. Karl Unholtz, Lockheed Research Engineer, for his numerous contributions to the solution of the problems that arose in applying the theory to airplane vibrations.

GENERAL THEORY

It is recalled that a natural mode of oscillation of a linear system is one in which all elements of the vibrating system execute simple harmonic motion at a single frequency. Thus the system may be regarded as oscillating in a single degree of freedom. Expressed mathematically, with reference to Fig. 1, this becomes

$$\Phi_k(x, t) = \varphi_k(x) \sin \omega_k t \tag{1}$$

$m(x)$ = mass per unit length (Fig. 1)
$\varphi_k(x)$ = deflection amplitude of the elastic curve for the kth natural mode (Fig. 1)
ω_k = angular frequency of the kth mode
$\Phi_k(x, t)$ = deflection as a function of position and time

From Eq. (1) the acceleration of the system is

$$\frac{\partial^2 \Phi_k(x, t)}{\partial t^2} = -\omega_k^2 \varphi_k(x) \sin \omega_k t \tag{2}$$

The elastic force acting on the system is equal to

$$m(x) \frac{\partial^2 \Phi_k(x, t)}{\partial t^2} = -\omega_k^2 m(x) \varphi_k(x) \sin \omega_k t \tag{3}$$

and therefore the inertial reaction of the system is

$$-m(x) \frac{\partial^2 \Phi_k(x, t)}{\partial t^2} = \omega_k^2 m(x) \varphi_k(x) \sin \omega_k t \tag{4}$$

The maximum inertial reaction is then $\omega_k^2 \varphi_k(x) m(x)$. This maximum force occurs at the time of maximum deflection. Thus, at each point of the system the deflection amplitude and the maximum inertia force are related by Hooke's Law. Conversely, therefore, it may be stated that if the system should be statically loaded with the force $\omega_k^2 \varphi_k(x) m(x)$ the resulting deflection would be $\varphi_k(x)$. It now follows from the superposition of forces and deflections for systems obeying Hooke's Law that the load $\varphi_k(x) m(x)$ would produce a static deflection equal to $\varphi_k(x)/\omega_k^2$. This last conclusion is important and plays a leading role in the theory to follow.

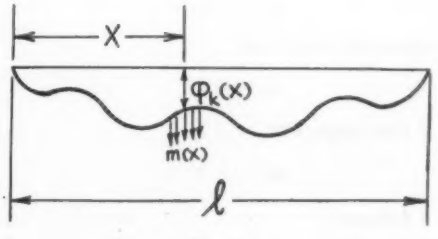

FIG. 1.

Received October 20, 1943.

* Research Engineers.

Consider now the elastic system of Fig. 1, loaded with the force

$$p_1(x) = m(x)\Psi_0(x) \tag{5}$$

The function $\Psi_0(x)$ represents an arbitrary, "possible," deflection of the system. The word possible is used simply to emphasize the fact that $\Psi_0(x)$ must satisfy all boundary conditions to which the system may be subject. It is known that any deflection of an elastic system can be expressed as a superposition of the natural elastic curves of the system.[3] These natural elastic curves are the deflection amplitude functions; thus,

$$\Psi_0(x) = a_1\varphi_1(x) + a_2\varphi_2(x) + \ldots + a_i\varphi_i(x) + \ldots \tag{6}$$

The coefficients a_i indicate the relative importance of the various modes involved in the construction of $\Psi_0(x)$. The right member of Eq. (6) has been taken as an infinite series, since the system is continuous and therefore has an infinite number of degrees of freedom. Using Eq. (6), $p_1(x)$, given by Eq. (5), may be expressed as

$$p_1(x) = a_1m(x)\varphi_1(x) + \ldots + a_im(x)\varphi_i(x) + \ldots \tag{7}$$

The deflection amplitude $\Psi_{11}(x)$ corresponding to this load is again obtained by superposition.

Since the load $\omega_k^2m(x)\varphi_k(x)$ produces the deflection $\varphi_k(x)$, the load $a_km(x)\varphi_k(x)$ will give a deflection equal to $a_k\varphi_k(x)/\omega_k^2$. Hence,

$$\Psi_{11}(x) = a_1\varphi_1(x)/\omega_1^2 + \ldots + a_i\varphi_i(x)/\omega_i^2 + \ldots \tag{8}$$

The function $\Psi_{11}(x)$ will be called the first calculated approximation to the shape of $\varphi_1(x)$. The reason for this terminology will appear subsequently. Loading the system with

$$p_2(x) = m(x)\Psi_1(x) \tag{9}$$

(the 2nd calculated approximation)

$$\Psi_{12}(x) = a_1\varphi_1(x)/(\omega_1^2)^2 + \ldots + a_i\varphi_i(x)/(\omega_i^2)^2 + \ldots \tag{10}$$

is obtained. Continuing in this fashion, it follows easily, by mathematical induction, that the load

$$p_{n+1}(x) = m(x)\Psi_{1n}(x) \tag{11}$$

will give rise to the deflection amplitude

$$\Psi_{1(n+1)}(x) = a_1\varphi_1(x)/(\omega_1^2)^{n+1} + \ldots + a_i\varphi_i(x)/(\omega_i^2)^{n+1} + \ldots \tag{12}$$

Of course,

$$\Psi_{1n}(x) = a_1\varphi_1(x)/(\omega_1^2)^n + \ldots + a_i\varphi_i(x)/(\omega_i^2)^n + \ldots \tag{13}$$

The ratio of $\Psi_{1n}(x)$ to $\Psi_{1(n+1)}(x)$ will now be determined. From Eqs. (12) and (13)

$$\frac{\Psi_{1n}(x)}{\Psi_{1(n+1)}(x)} = \frac{a_1\varphi_1(x)/(\omega_1^2)^n + \ldots + a_i\varphi_i(x)/(\omega_i^2)^n + \ldots}{a_1\varphi_1(x)/(\omega_1^2)^{n+1} + \ldots + a_i\varphi_i(x)/(\omega_i^2)^{n+1} + \ldots} \tag{14}$$

Manipulating Eq. (14) algebraically,

$$\frac{\Psi_{1n}(x)}{\Psi_{1(n+1)}(x)} = \frac{\dfrac{1}{(\omega_1^2)^n}\left[a_1\varphi_1(x) + \ldots + a_i\varphi_i(x)\left(\dfrac{\omega_1^2}{\omega_i^2}\right)^n + \ldots\right]}{\dfrac{1}{(\omega_1^2)^{n+1}}\left[a_1\varphi_1(x) + \ldots + a_i\varphi_i(x)\left(\dfrac{\omega_1^2}{\omega_i^2}\right)^{n+1} + \ldots\right]} \tag{15}$$

and, finally,

$$\frac{\Psi_{1n}(x)}{\Psi_{1(n+1)}(x)} = \omega_1^2\frac{1 + \dfrac{a_2\varphi_2(x)}{a_1\varphi_1(x)}\left(\dfrac{\omega_1^2}{\omega_2^2}\right)^n + \ldots + \dfrac{a_i\varphi_i(x)}{a_1\varphi_1(x)}\left(\dfrac{\omega_1^2}{\omega_2^2}\right)^n + \ldots}{1 + \dfrac{a_2\varphi_2(x)}{a_1\varphi_1(x)}\left(\dfrac{\omega_1^2}{\omega_2^2}\right)^{n+1} + \ldots + \dfrac{a_i\varphi_i(x)}{a_1\varphi_1(x)}\left(\dfrac{\omega_1^2}{\omega_i^2}\right)^{n+1} + \ldots} \tag{16}$$

Assuming that

$$\omega_i^2 < \omega_{i+1}^2 \tag{17}$$

for all values of i and that

$$\omega_i^2 \neq \omega_j^2 \tag{18}$$

for $i \neq j$ the inequality

$$\omega_1^2/\omega_i^2 < 1 \tag{19}$$

for $i > 1$ follows.

Hence, taking limits in Eq. (16), ω_1^2 is obtained—i.e.,

$$\lim_{n\to\infty} \Psi_{1n}(x)/\Psi_{1(n+1)}(x) = \omega_1^2 \tag{20}$$

It is to be noted that the right member of Eq. (20) is independent of x, whereas the left member is a function of x. Hence, the constancy of $\Psi_{1n}(x)/\Psi_{1(n+1)}(x)$ for values of x between 0 and l is a measure of the convergence of the ratios to ω_1^2. A quantitative idea of the accuracy with which $\Psi_{1n}(x)/\Psi_{1(n+1)}(x) = \omega_1^2$ is furnished by the fact that, for any value of n, ω_1^2 lies between the largest and smallest values of the function $\Psi_{1n}(x)/\Psi_{1(n+1)}(x)$—i.e.,

$$\left[\frac{\Psi_{1n}(x)}{\Psi_{1(n+1)}(x)}\right]_{min.} < \omega_1^2 < \left[\frac{\Psi_{1n}(x)}{\Psi_{1(n+1)}(x)}\right]_{max.} \tag{21}$$

This last result is originally due to Schwarz.[4]

For convenience, the procedure outlined above and the results obtained thus far will now be summarized:

(1) An arbitrary deflection function $\Psi_0(x)$ satisfying the boundary conditions of the system is assumed. This step will be discussed in detail in the illustrative application to be given later.

(2) The system is statically loaded in effect with $p_1(x) = m(x)\Psi_0(x)$, obtaining a deflection $\Psi_{11}(x)$. This process is successively applied; thus $p_2(x) = m(x)\Psi_{11}(x)$ gives $\Psi_{12}(x), \ldots, p_{n+1}(x) = m(x)\Psi_{1n}(x)$ gives $\Psi_{1(n+1)}(x)$.

(3) As each $\Psi_{1k}(x)$ is obtained, the ratio $\Psi_{1(k-1)}(x) \div \Psi_{1k}(x)$ is formed, and its numerical values for several values of x between 0 and l are found. The maximum and minimum values of this function are also determined.

(4) In this way two sequences of functions are constructed; viz.,

$$\Psi_0(x), \Psi_{11}(x), \ldots, \Psi_{1n}(x), \Psi_{1(n+1)}(x), \ldots$$

and

$$\frac{\Psi_0(x)}{\Psi_{11}(x)}, \frac{\Psi_{11}(x)}{\Psi_{12}(x)}, \ldots, \frac{\Psi_{1(n-1)}(x)}{\Psi_{1n}(x)}, \frac{\Psi_{1n}(x)}{\Psi_{1(n+1)}(x)}, \ldots$$

(5) The process is terminated when a ratio $\Psi_{1n}(x) \div \Psi_{1(n+1)}(x)$ is obtained so that the difference between its minimum and maximum values is within the limits of accuracy desired. This ratio is then taken as ω_1^2 and $\Psi_{1n}(x)$ is taken as $\varphi_1(x)$. This last conclusion follows from the fact that the load $m(x)\Psi_{1n}(x)$ gives the deflection $\Psi_{1(n+1)}(x)$ which, however, is equal to $\Psi_{1n}(x) \div \omega_1^2$. Hence, by virtue of the discussion following Eq. (4), it may be stated that $\Psi_{1n}(x)$ may be taken as $\varphi_1(x)$. It is, of course, understood that only the shape of $\varphi_1(x)$ can be determined in this way; the absolute magnitudes of the deflections in any natural mode depend on the initial disturbance of the system and are immaterial for the purpose at hand.

Determination of Higher Modes

To determine the higher frequencies and modes of vibration, an accurate value of ω_1^2 is required. The reason for this will appear subsequently. Such a value may be obtained from the quantities already determined by the relation

$$\omega_1^2 = \lim_{n\to\infty} \frac{\int_0^l m(x)\Psi_{1n}(x)\Psi_{1(n+1)}(x)\,dx}{\int_0^l m(x)\Psi_{1(n+1)}^2(x)\,dx} \tag{22}$$

The verification of Eq. (22) follows: substituting for $\Psi_{1n}(x)$ and $\Psi_{1(n+1)}(x)$ from Eqs. (12) and (13) and setting

$$\frac{\int_0^l m(x)\Psi_{1n}(x)\Psi_{1(n+1)}(x)\,dx}{\int_0^l m(x)\Psi_{1(n+1)}^2(x)\,dx} \equiv I(n, n+1) \tag{23}$$

the equation

$$I(n, n+1) = \frac{\int^l m(x)\left[\sum_{i=1}^{\infty} a_i\varphi_i(x)/(\omega_i^2)^n\right]\left[\sum_{j=1}^{\infty} a_j\varphi_j(x)/(\omega_j^2)^{n+1}\right]dx}{\int_0^l m(x)\left[\sum_{i=1}^{\infty} a_i\varphi_i(x)/(\omega_i^2)^{n+1}\right]\left[\sum_{j=1}^{\infty} a_j\varphi_j(x)/(\omega_j^2)^{n+1}\right]dx} \tag{24}$$

is obtained. Since the order in which the operations indicated in the right member of Eq. (24) are performed is of no consequence, this equation may be written as

$$I(n, n+1) = \frac{\sum_{i=1}^{\infty}\sum_{j=1}^{\infty}\left[\int_0^l m(x)\,\frac{a_ia_j\varphi_i(x)\varphi_j(x)}{(\omega_i^2)^n\,(\omega_j^2)^{n+1}}\,dx\right]}{\sum_{i=1}^{\infty}\sum_{j=1}^{\infty}\left[\int_0^l m(x)\,\frac{a_ia_j\varphi_i(x)\varphi_j(x)}{(\omega_i^2)^{n+1}\,(\omega_j^2)^{n+1}}\,dx\right]} \tag{25}$$

However, since the natural modes of an elastic system are orthogonal,[5]

$$\int_0^l m(x)\varphi_i(x)\varphi_j(x)\,dx = 0 \tag{26}$$

for $i \neq j$. Defining

$$\int_0^l m(x)\varphi_i^2(x)\,dx = \kappa_i \tag{27}$$

Eq. (25) becomes

$$I(n, n+1) = \sum_{i=1}^{\infty} \frac{a_ia_i\kappa_i}{(\omega_i^2)^n(\omega_i^2)^{n+1}} \Big/ \sum_{i=1}^{\infty} \frac{a_ia_i\kappa_i}{(\omega_i^2)^{n+1}(\omega_i^2)^{n+1}} \tag{28}$$

Extracting ω_1^2 and dividing through by $\kappa_1 a_1^2$, Eq. (28) becomes

$$I(n, n+1) = \omega_1^2 \frac{1 + \left(\frac{a_2}{a_1}\right)^2\left(\frac{\kappa_2}{\kappa_1}\right)\left(\frac{\omega_1^2}{\omega_2^2}\right)^{2n+1} + \ldots + \left(\frac{a_i}{a_1}\right)^2\left(\frac{\kappa_i}{\kappa_1}\right)\left(\frac{\omega_1^2}{\omega_i^2}\right)^{2n+1} + \ldots}{1 + \left(\frac{a_2}{a_1}\right)^2\left(\frac{\kappa_2}{\kappa_1}\right)\left(\frac{\omega_1^2}{\omega_2^2}\right)^{2n+2} + \ldots + \left(\frac{a_i}{a_1}\right)^2\left(\frac{\kappa_i}{\kappa_1}\right)\left(\frac{\omega_1^2}{\omega_i^2}\right)^{2n+2} + \ldots} \tag{29}$$

Since, as previously stated, $\omega_1^2/\omega_i^2 < 1$ and $\omega_i^2 \neq 0$ for all i,
Eq. (22) follows—i.e.,

$$\lim_{n \to \infty} I(n, n+1) = \omega_1^2 \tag{30}$$

For the purpose of comparison with Eq. (29), Eq. (16) will be rewritten after replacing n by $2n + 1$; thus,

$$\frac{\Psi_{1(2n+1)}(x)}{\Psi_{1(2n+2)}(x)} = \omega_1^2 \frac{1 + \frac{a_2\varphi_2(x)}{a_1\varphi_1(x)}\left(\frac{\omega_1^2}{\omega_2^2}\right)^{2n+1} + \frac{a_3\varphi_3(x)}{a_1\varphi_1(x)}\left(\frac{\omega_1^2}{\omega_3^2}\right)^{2n+1} + \ldots}{1 + \frac{a_2\varphi_2(x)}{a_1\varphi_1(x)}\left(\frac{\omega_1^2}{\omega_2^2}\right)^{2n+2} + \frac{a_3\varphi_3(x)}{a_1\varphi_1(x)}\left(\frac{\omega_1^2}{\omega_3^2}\right)^{2n+2} + \ldots} \tag{31}$$

A glance at the right members of Eqs. (29) and (31) shows that if $\Psi_{1n}(x)$ and $\Psi_{1(n+1)}(x)$ are determined and then used to compute $I(n, n+1)$ an approximation to ω_1^2 will be obtained which is as good as would be obtained by continuing the original process to $\Psi_{1(2n+1)}(x)$ and $\Psi_{1(2n+2)}(x)$ and then taking $\omega_1^2 = \Psi_{1(2n+1)}(x)/\Psi_{1(2n+2)}(x)$, at least insofar as the validity of the approximations is dependent upon the ratios $(\omega_1^2/\omega_i^2)^{2n+1}$ and $(\omega_1^2/\omega_i^2)^{2n+2}$.

Assuming now that ω_1^2 has been obtained with the accuracy required, a sequence of functions

$$\Psi_{20}(x), \Psi_{21}(x), \ldots, \Psi_{2n}(x), \ldots \tag{32}$$

approaching in the limit the shape $\varphi_2(x)$, and a sequence of ratios

$$(\Psi_{20}(x)/\Psi_{21}(x)), (\Psi_{21}(x)/\Psi_{22}(x)), \ldots, [\Psi_{2(n-1)}(x)/\Psi_{2n}(x)], \ldots \tag{33}$$

whose limit is ω_2^2, will be constructed. Proceeding by analogy, it would seem reasonable to begin with an arbitrarily chosen curve $\Psi_{20}(x)$ satisfying the boundary conditions of the system. The system would then be statically loaded with $m(x)\Psi_{20}(x)$ and a new deflection curve calculated. However, $\Psi_{20}(x)$ would be expressible in the form

$$\Psi_{20}(x) = b_1\varphi_1(x) + b_2\varphi_2(x) + \ldots + b_i\varphi_i(x) + \ldots \tag{34}$$

and therefore the process would be identical to that used in finding $\varphi_1(x)$ and ω_1^2. The process would converge to $\varphi_2(x)$ and ω_2^2 if, and only if, $\varphi_1(x)$ were absent from the right member of Eq. (34)—i.e., if $b_1 = 0$. This same conclusion can also be obtained through physical reasoning; thus, if $\varphi_1(x)$ is present in $\Psi_{20}(x)$, it will be in the loading $m(x)\Psi_{20}(x)$ and will therefore be excited when the load is applied. Hence, if $b_1 \neq 0$, the process necessarily converges to the mode of lowest frequency, $\varphi_1(x)$. There remains then the possibility of choosing $\Psi_{20}(x)$ so that $b_1 = 0$. Clearly, the probability that this would happen at random is zero. However, if $a_1\varphi_1(x)$ were known, the fundamental mode would be simply eliminated by taking

$$\Psi_{20}(x) = \Psi_0(x) - a_1\varphi_1(x) = a_2\varphi_2(x) + a_3\varphi_2(x) + \ldots \tag{35}$$

Of course $a_1\varphi_1(x)$ is not known precisely. However, the functions $\Psi_{1k}(x)$ are approximations to $a_1\varphi_1(x)/(\omega_1^2)^k$. Thus, $a_1\varphi_1(x)$ is eliminated by taking

$$\Psi_{20}(x) = \Psi_0(x) - \omega_1^2\Psi_{11}(x) \tag{36}$$

Substituting into the right member of Eq. (36) from Eqs. (6) and (8), it is found that

$$\Psi_{20}(x) = \sum_{i=2}^{\infty} a_i\varphi_i(x)[1 - (\omega_1^2/\omega_i^2)] \tag{37}$$

Loading the system with $m(x)\Psi_{20}(x)$ gives a deflection $\Psi_{21}(x)$ consisting of the superposition of the deflections due to the loads $m(x)\Psi_0(x)$ and $-\omega_1^2 m(x)\Psi_{11}(x)$

Hence,

$$\Psi_{21}(x) = \Psi_{11}(x) - \omega_1^2\Psi_{12}(x) \tag{38}$$

Continuing in this fashion the equations,

$$\Psi_{2(n-1)}(x) = \Psi_{1(n-1)}(x) - \omega_1^2\Psi_{1n}(x) \tag{39}$$

$$\Psi_{2n}(x) = \Psi_{1n}(x) - \omega_1^2\Psi_{1(n+1)}(x) \tag{40}$$

are obtained. Thus

$$\Psi_{2(n-1)}(x)/\Psi_{2n}(x) = [\Psi_{1(n-1)}(x) - \omega_1^2\Psi_{1n}(x)]/[\Psi_{1n}(x) - \omega_1^2\Psi_{1(n+1)}(x)] \tag{41}$$

Substituting for $\Psi_{1(n-1)}(x)$, $\Psi_{1n}(x)$ and $\Psi_{1(n+1)}(x)$, this last equation becomes

$$\frac{\Psi_{2(n-1)}(x)}{\Psi_{2n}(x)} = \frac{\left\{\sum_{i=1}^{\infty}[a_i\varphi_i(x)/(\omega_i^2)^{n-1}]\right\} - \omega_1^2\left\{\sum_{i=1}^{\infty}[a_i\varphi_i(x)/(\omega_i^2)^n\right\}}{\left\{\sum_{i=1}^{\infty}[a_i\varphi_i(x)/(\omega_i^2)^n]\right\} - \omega_1^2\left\{\sum_{i=1}^{\infty}[a_i\varphi_i(x)/(\omega_i^2)^{n+1}]\right\}} \tag{42}$$

Manipulating the right member of Eq. (42), the ratio becomes

$$\frac{\Psi_{2(n-1)}(x)}{\Psi_{2n}(x)} = \frac{\sum_{i=2}^{\infty}[a_i\varphi_i(x)/(\omega_i^2)^{n-1}][1 - (\omega_1^2/\omega_i^2)]}{\sum_{i=2}^{\infty}[a_i\varphi_i(x)/(\omega_i^2)^n][1 - (\omega_1^2/\omega_i^2)]} \tag{43}$$

Further algebraic transformations yield the equations

$$\frac{\Psi_{2(n-1)}(x)}{\Psi_{2n}(x)} = \frac{\left(\frac{1}{\omega_2^2}\right)^{n-1}\left[a_2\varphi_2(x)\left(1 - \frac{\omega_1^2}{\omega_2^2}\right) + \sum_{i=3}^{\infty}a_i\varphi_i(x)\left(\frac{\omega_2^2}{\omega_i^2}\right)^{n-1}\left(1 - \frac{\omega_1^2}{\omega_i^2}\right)\right]}{\left(\frac{1}{\omega_2^2}\right)^{n}\left[a_2\varphi_2(x)\left(1 - \frac{\omega_1^2}{\omega_2^2}\right) + \sum_{i=3}^{\infty}a_i\varphi_i(x)\left(\frac{\omega_2^2}{\omega_i^2}\right)^{n}\left(1 - \frac{\omega_1^2}{\omega_i^2}\right)\right]} \tag{44}$$

and

$$\frac{\Psi_{2(n-1)}(x)}{\Psi_{2n}(x)} = \omega_2^2\frac{1 + \sum_{i=3}^{\infty}\frac{a_i\varphi_i(x)}{a_2\varphi_2(x)}\left[\frac{1 - (\omega_1^2/\omega_i^2)}{1 - (\omega_1^2/\omega_2^2)}\right]\left(\frac{\omega_2^2}{\omega_i^2}\right)^{n-1}}{1 + \sum_{i=3}^{\infty}\frac{a_i\varphi_i(x)}{a_2\varphi_2(x)}\left[\frac{1 - (\omega_1^2/\omega_i^2)}{1 - (\omega_1^2/\omega_2^2)}\right]\left(\frac{\omega_2^2}{\omega_i^2}\right)^{n}} \tag{45}$$

Since as before $\omega_2^2/\omega_i^2 < 1$ for $i > 2$ and $\omega_i^2 \neq 0$ for all i, it follows that

$$\lim_{n\to\infty}[\Psi_{2(n-1)}(x)/\Psi_{2n}(x)] = \omega_2^2 \tag{46}$$

As before, the degree of accuracy to which $\Psi_{2(n-1)}(x)/\Psi_{2n}(x)$ represents ω_2^2 can be estimated by examining the constancy of the ratio for different values of x between 0 and l. Moreover, again

$$[\Psi_{2(n-1)}(x)/\Psi_{2n}(x)]_{min.} < \omega_2^2 < [\Psi_{2(n-1)}(x)/\Psi_{2n}(x)]_{max.} \tag{47}$$

An examination of Eq. (41) will show why it is that an accurate value of ω_1^2 is needed before $\varphi_2(x)$ and ω_2^2 can be found. Thus, if $\Psi_{1n}(x)/\Psi_{1(n+1)}(x)$ is taken as ω_1^2 and substituted into Eq. (41), the ratio becomes infinite. Since $\Psi_{1(n-1)}(x)/\Psi_{1n}(x)$ and $\Psi_{1n}(x)/\Psi_{1(n+1)}(x)$ are, for moderate values of n, good approximations to ω_1^2, $\Psi_{2(n-1)}(x)$ and $\Psi_{2n}(x)$ given by Eqs. (39) and (40) are the differences of quantities that are almost equal. Therefore, to obtain $\Psi_{2(n-1)}(x)$ and $\Psi_{2n}(x)$, the ω_1^2 in these equations must be, relative to the ratios $\Psi_{1(n-1)}(x)/\Psi_{1n}(x)$ and $\Psi_{1n}(x) \div \Psi_{1(n+1)}(x)$, an accurately determined number. It is to be expected, therefore, that the determination of $\varphi_2(x)$ and ω_2^2 will involve the knowledge of ω_2^2 to a greater degree of accuracy than is given by the simple ratio $\Psi_{2(n-1)}(x) \div \Psi_{2n}(x)$. A proof similar to that given by Eqs. (22) through (30) indicates that such a value is given by the relation

$$\omega_2^2 = \lim_{n\to\infty}[\textstyle\int_0^l m(x)\Psi_{2(n-1)}(x)\Psi_{2n}(x)\,dx]/[\int_0^l m(x)\Psi_{2n}^2(x)\,dx] \tag{48}$$

The procedure used to determine $\varphi_1(x)$, ω_1^2, $\varphi_2(x)$ and ω_2^2 may be extended by analogy to the determination of the third and higher modes of vibration.

General Comments on Methods of Application

A word of explanation is perhaps in order concerning the construction of the functions $\Psi_0(x)$, $\Psi_{11}(x)$, . . . , $\Psi_{1n}(x)$, ... It is recalled that $\Psi_0(x)$ is an arbitrarily assumed curve that need only satisfy the boundary conditions of the system. However, from a practical standpoint it is most desirable that $\Psi_0(x)$ resemble as closely as possible what is believed to be the probable shape of the fundamental mode. This, of course, will shorten the work required to obtain a satisfactory degree of convergence of the sequence $\Psi_0(x)$, $\Psi_{11}(x)$, . . . , $\Psi_{1n}(x)$, ... In practice, of course, a means must be found of constructing the $\Psi_{1k}(x)$. Since $\Psi_{1k}(x)$ is the

deflection corresponding to the static load $m(x) \times \Psi_{1(i-1)}(x)$, it can be determined by the methods of elasticity. The most general method is based on the concept of the influence function.[6] However, in the case of beam deflections simpler methods are available.[7]

Concerning numerical computation it may be stated that the number of significant digits to be retained in any problem depends on the number of modes required and on the relative values of $\omega_1^2, \omega_2^2, \ldots, \omega_i^2, \ldots$. Since nothing in general is known concerning the ω_i^2 save that $\omega_i^2 < \omega_{i+1}^2$ for all i, the safest procedure is to retain as many significant digits as the calculating machine to be used will handle. The authors have used this rule in all numerical work that they have undertaken.

Practical Application

Consider the pure bending oscillations of the wings of a twin-engined monoplane. By pure bending is meant a vertical motion of the wings in which each chordwise element remains parallel to its equilibrium position. In general, such oscillations are not natural modes of the wing structure and, hence, can be obtained only by applying restraints to the system. The modes of vibration to be calculated therefore are natural modes for the restrained system. Such modes are also called "primitive" modes of vibration with respect to the unrestrained system.

An idealized model of the restrained system to be considered is a beam without mass, of constant modulus of elasticity and irregular cross section, supporting concentrated masses as shown in Fig. 2. It will be noted that the notation is not that of the general theory; it has been changed to agree with accepted aircraft nomenclature. Moreover, the system shown has only a finite number of degrees of freedom, corresponding in number to the set of concentrated masses.

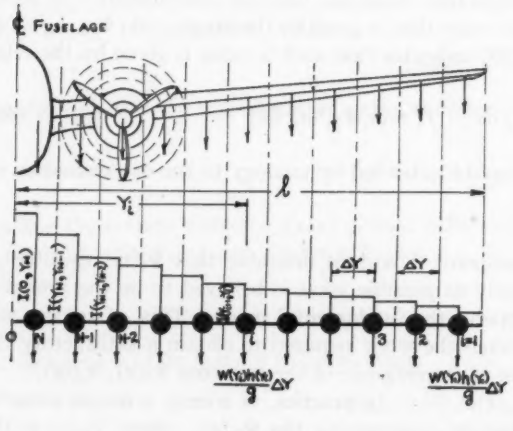

Fig. 2.

The symbols used are defined as follows:

$W(Y_i)$ ~ weight of airfoil section at station Y_i in lbs. per in.

$h(Y_i)$ ~ deflection at station Y_i, positive upward, measured in in.

E ~ modulus of elasticity of material assumed equal in tension and compression, lbs. per sq.in.

$I(Y_{i+1}, Y_i)$ ~ average cross-sectional area moment of inertia between stations

Y_{i+1} and Y_i taken about the neutral axis of the section, in.[4]

It is to be noted that the stations are numbered from the wing tip inboard. Moreover, since the natural modes of the restrained system represented can be divided into two general classes—those symmetric about the center line of the fuselage and those antisymmetric about that line—it is sufficient to consider only the wing semispan as indicated by Fig. 2. The determination of the symmetric modes only will be outlined at this time.

From beam theory it is known that the bending moment $M(Y)$, the shear $S(Y)$, the load $P(Y)$, and the deflection $h(Y)$ at the cross section of a beam are related by the equations

$$\left.\begin{aligned} P(Y) &= dS/dY \\ S(Y) &= dM/dY \\ d^2h/dY^2 &= M/EI \end{aligned}\right\} \tag{49}$$

In integral form these equations become

$$\left.\begin{aligned} S(Y) &= \int_l^Y P(Y)\,dY + S(l);\ M(Y) = \int_l^Y S(Y)\,dY + M(l) \\ \left(\frac{dh}{dY}\right)_Y &= \left.\frac{dh}{dY}\right|_0 + \int_0^Y \frac{M}{EI}\,dY \\ h(Y) &= h(0) + \int_0^Y \frac{dh}{dY}\,dY \end{aligned}\right\} \tag{50}$$

In Eqs. (50), 0 and l are the centerlines of the fuselage and the wing tip, respectively.

In line with the general theory, assume a curve $h_0(Y)$ satisfying the boundary conditions of the system. These conditions are

$$S(l) = 0; \quad M(l) = 0 \tag{51}$$

The first of these relations implies $dM/dY|_{Y=l} = 0$. Using the last of Eqs. (49), Eqs. (51) may be rewritten to read

$$d^2h/dY^2|_{Y=l} = 0; \quad d^3h/dY^3|_{Y=l} = 0 \tag{52}$$

A suitable $h_0(Y)$ may now be constructed by using Eqs. (52) to determine the relative values of the a_i in the power series below:

$$h_0(Y) = a_0 + a_2Y^2 + a_4Y^4 + a_6Y^6 + \ldots \tag{53}$$

The odd powers have been omitted in Eq. (53), since symmetry requires $h_0(-Y) \equiv h_0(Y)$. The deflection at $Y = 0$ is determined from the fact that the system is in dynamic equilibrium[8]—i.e.,

$$\sum_{\text{system}} \omega_1^2[W(Y_i)/g]h_0(Y_i)\Delta Y = 0 \qquad (54)$$

In practice, the mathematical construction of $h_0(Y)$ as described might not be desirable. An alternative procedure would be to draw a reasonably shaped curve as shown in Fig. 3 by the dotted line. To satisfy Eq. (54) and thereby determine $h_0(0)$, each point of the dotted curve must be displaced parallel to itself as indicated in Fig. 3.

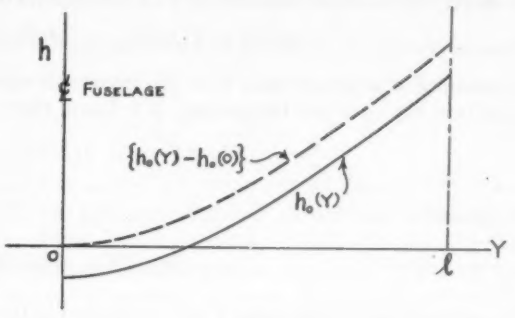

Fig. 3.

The determination of $h_0(0)$ follows from Eq. (54); thus $\sum_{i=1}^{N} W(Y_i)h_0(Y_i)\Delta Y = 0$. It follows that

$$\sum_{i=1}^{N} \{W(Y_i)h_0(Y_i)\Delta Y - W(Y_i)h_0(0)\Delta Y + W(Y_i)h_0(0)\Delta Y\} = 0$$

thus $h_0(0)$ is obtained from the relation.

$$h_0(0) = \left\{-\sum_{i=1}^{N} W(Y_i)[h_0(Y_i) - h_0(0)]\Delta Y\right\} \Big/ \left[\sum_{i=1}^{N} W(Y_i)\Delta Y\right] \qquad (55)$$

Having $h_0(0)$, $h_0(Y)$ is now found at the desired stations by adding $h_0(0)$ to the drawn curve, which is $[h_0(Y) - h_0(0)]$. The system is now loaded with

$$P_{11}(Y_6{}^1) = [W(Y_i)/g]h_0(Y_i)\Delta Y \qquad (56)$$

Since $S(l) = 0$, the shear is found by summing the load from right to left; thus

$$S_0(Y_k, Y_{k+1}) = \sum_{i=1}^{k} [W(Y_i)/g]h_0(Y_i)\Delta Y \qquad (57)$$

It is to be noted that the shear is constant between the masses—hence, the notation $S_0(Y_k, Y_{k+1})$. Eq. (57) can be written as the recurrence relation,

$$S_0(Y_k, Y_{k+1}) = S_0(Y_{k-1}, Y_k) + [W(Y_k)/g]h_0(Y_k)\Delta Y \qquad (58)$$

In particular for the final interval

$$S_0(Y_N, 0) = S_0(Y_{N-1}, Y_N) + [W(Y_N)/g]h_0(Y_N)\Delta Y \qquad (59)$$

The moments at the masses themselves are

$$M_0(Y_k) = \sum_{i=1}^{k-1} S_0(Y_i, Y_{i+1})\Delta Y \qquad (60)$$

In recurrence form Eq. (60) becomes

$$M_0(Y_k) = M_0(Y_{k-1}) + S_0(Y_{k-1}, Y_k)\ \Delta Y \qquad (61)$$

At the centerline of the airplane

$$M_0(0) = M_0(Y_N) + S_0(Y_N, 0)^1/_2\Delta Y \qquad (62)$$

since the last interval is only $^1/_2\Delta Y$ in length.

To determine the first calculated approximation $h_{11}(Y)$ it is necessary to first determine dh_{11}/dY. From Eqs. (50)

$$dh_{11}/dY|_{Y_k} = dh_{11}/dY|_0 + \int_0^{Y_k} (M/EI)\, dY \qquad (63)$$

Since the deflection curve is to be symmetric about the line $Y = 0$, $dh_{11}/dY|_0$ must be zero. Thus,

$$dh_{11}/dY|_{Y_N} = \int_0^{\Delta Y/2} (M/EI)\, dY \qquad (64)$$

However, M is a linear function of Y in the interval 0 to $\Delta Y/2$; thus,

$$M(Y) = \{[M(Y_N) - M(0)]/(\Delta Y/2)\}\ Y + M(0);\ 0 \leq Y \leq Y_N \tag{65}$$

Moreover E is constant and I over this interval is equal to a constant given as $I\ (0,\ Y_N)$. Substituting these quantities into Eq. (64) and integrating, it is found that

$$dh_{11}/dY|_{Y_N} = \{[M(Y_N) + M\ (0)]/2EI(0,\ Y_N)\}(\Delta Y/2) \tag{66}$$

In general

$$dh_{11}/dY|_{Y_k} = dh/dY|_{Y_{k+1}} + \int_0^{\Delta Y} (M/EI)dY \tag{67}$$

The integration extends from Y_{k+1}, considered as the origin, to Y_k, which is ΔY distant from it. In this interval the moment is expressible as

$$M(Y) = \{[M(Y_k) - M(Y_{k+1})]/\Delta Y\}\ Y + M(Y_{k+1});\ Y_{k+1} \leq Y \leq Y_k \tag{68}$$

(See Fig. 2.) For this interval $I \equiv I(Y_{k+1},\ Y_k)$. Substituting into Eq. (67), the following general formula is obtained:

$$dh_{11}/dY|_k = dh_{11}/dY|_{k+1} + \{[M(Y_k) + M(Y_{k+1})]/2EI(Y_{k+1},\ Y_k)\}\Delta Y \tag{69}$$

From Eqs. (50) it is known that

$$h_{11}(Y) = h_{11}(0) + \int_0^Y (dh_{11}/dY)\ dY \tag{70}$$

Since $h_{11}(0)$ is not known, $[h_{11}(Y) - h_{11}(0)]$ is first determined. Thus,

$$h_{11}(Y_N) - h_{11}(0) = \int_0^{\Delta Y/2} (dh_{11}/dY)\ dY \tag{71}$$

Substituting for dh_{11}/dY this equation becomes

$$h_{11}(Y_N) - h_{11}(0) = \int_0^{\Delta Y/2} \left\{ \int_0^Y \frac{1}{EI(0,\ Y_N)} \left[\frac{M(Y_N) - M(0)}{\Delta Y/2}\ Y + M(0) \right] dY \right\} dY \tag{72}$$

Performing the double integration gives

$$h_{11}(Y_N) - h_{11}(0) = (\Delta Y/2)^2\{[M(Y_N) + 2M(0)]/6EI(0,\ Y_N)\} \tag{73}$$

In the general case

$$[h_{11}(Y_k) - h_{11}(0)] = [h_{11}(Y_{k+1}) - h_{11}(0)] + \int_0^{\Delta Y} (dh_{11}/dY)\ dY \tag{74}$$

The interval of integration ΔY extends from Y_{k+1} to Y_k. In this interval,

$$dh_{11}/dY = dh_{11}/dY|_{Y_{k+1}} + \int_0^Y [M/EI(Y_{k+1},\ Y_k)]dY \tag{75}$$

Substituting into Eq. (74) and performing the operations indicated, there results the equation

$$[h_{11}(Y_k) - h_{11}(0)] = [h_{11}(Y_{k+1}) - h_{11}(0)] + \left.\frac{dh_{11}}{dY}\right|_{Y_{k+1}} \Delta Y + \left[\frac{M(Y_k) + 2M(Y_{k+1})}{6EI(Y_{k+1}, Y_k)} \right] (\Delta Y)^2 \tag{76}$$

In particular for $h_{11}(Y_N) - h_{11}(0)$, the relation is

$$[h_{11}(Y_N) - h_{11}(0)] = \{[M(Y_k) + 2M(0)]/6EI(0,\ Y_N)\}\ (\Delta Y/2)^2 \tag{77}$$

All that now remains is the determination of $h_{11}(0)$. This follows from the condition of dynamic equilibrium originally stated in Eq. (54).

$$\sum_{i=1}^{N} W(Y_i)h_{11}(Y_i)\Delta Y = 0 \tag{78}$$

A procedure identical to that used in obtaining $h_0(0)$ from Eq. (55) yields the relation

$$h_{11}(0) = \left\{ -\sum_{i=1}^{N} W(Y_i)[h_{11}(Y_i) - h_{11}(0)]\Delta Y \right\} \Big/ \left[\sum_{i=1}^{N} W(Y_i)\Delta Y \right] \tag{79}$$

Adding $h_{11}(0)$ to $[h_{11}(Y_k) - h_{11}(0)]$ as given by Eqs. (76) and (77) yields the values of $h_{11}(Y_k)$. The ratios $h_0(Y_i) \div h_{11}(Y_i)$ are now determined for $i = 1, 2, 3, \ldots N$.

If this ratio is fairly constant, ω_{11}^2, the first approximation to the square of the fundamental frequency, is found by taking

$$\omega_{11}^2 = \left[\sum_{i=1}^{N} W(Y_i)h_0(Y_i)h_{11}(Y_i)\,\Delta Y\right] \Big/ \left[\sum_{i=1}^{N} W(Y_i)h_{11}^2(Y_i)\,\Delta Y\right] \tag{80}$$

This equation is, of course, equivalent to the integral relation given in Eq. (22) of the general theory. The process described for obtaining $h_{11}(Y_i)$ is now repeated using $h_{11}(Y_i)$ for $h_0(Y_i)$ throughout. In this manner a second calculated approximation to the fundamental symmetric mode of the system is obtained; let it be called $h_{12}(Y_i)$. Using $h_{11}(Y_i)$ and $h_{12}(Y_i)$, a second approximation, ω_{12}^2, would be found as indicated by Eq. (80). When by this iterative process ω_1^2 has been determined to the required accuracy, the sequence of approximations to the second mode can be constructed—i.e.,

$$\left.\begin{aligned} h_{21}(Y_i) &= h_0(Y_i) - \omega_1^2 h_{11}(Y_i) \\ h_{22}(Y_i) &= h_{11}(Y_i) - \omega_1^2 h_{12}(Y_i) \\ &\vdots \qquad\quad \vdots \qquad\quad \vdots \\ h_{2n}(Y_i) &= h_{1(n-1)}(Y_i) - \omega_1^2 h_{1n}(Y_i) \end{aligned}\right\} \tag{81}$$

The last of these functions would then be taken as the second mode. Also ω_2^2 would be taken to be the ratio $h_{2(n-1)}(Y_i)/h_{2n}(Y_i)$. Before proceeding to the next mode, the accuracy to which ω_2^2 is known would be increased by taking

$$\omega_2^2 = \left[\sum_{i=1}^{N} W(Y_i)h_{2(n-1)}(Y_i)h_{2n}(Y_i)\,\Delta Y\right] \Big/ \left[\sum_{i=1}^{N} W(Y_i)h_{2n}^2(Y_i)\,\Delta Y\right] \tag{82}$$

After the desired modes and frequencies have been found it is advantageous to standardize the resulting deflection curves by assigning, in each mode, a unit deflection to the wing tip. The deflections at all other stations are then changed in proportion.

The work outlined in the preceding pages may be conveniently tabulated on the basis of the formulas given by Eqs. (55) through (82). Most of these formulas can be more easily handled by transposing all constant terms to the left members of the equations. The resulting formulas in their order of application are listed in the summary.

Summary

(1) Assume a curve of reasonable shape; call it $h_0(Y_i) - h_0(0)$.

(2) Determine $gP_{11}(Y_i)/\Delta Y = W(Y_i)\{h_0(Y_i) - h_0(0)\}$.

(3) Obtain $h_0(0) = \left\{-\sum_{i=1}^{N} W(Y_i)[h_0(Y_i) - h_0(0)]\right\} \div \left[\sum_{i=1}^{N} W(Y_i)\right]$

(4) Add $h_0(0)$ to $\{h_0(Y_i) - h_0(0)\}$ to obtain $h_0(Y_i)$.

(5) At each station find in succession $(g/\Delta Y) \times S_0(Y_k, Y_{k+1}) = (g/\Delta Y)S_0(Y_{k-1}, Y_k) + W(Y_k)h_0(Y_k)$.

(6) Next determine successively the quantities $[g/(\Delta Y)^2]M_0(Y_k) = [g/(\Delta Y)^2]M_0(Y_{k-1}) + (g/\Delta Y)S_0(Y_{k-1}, Y_k)$, noting in particular that $[g \div (\Delta Y)^2]M_0(0) = [g/(\Delta Y)^2]M_0(Y_N) + \frac{1}{2}(g/\Delta Y)S_0 \times (Y_N, 0)$.

(7) Having tabulated the quantities $I(Y_{i+1}, Y_i)$ the next step is to find

$$\frac{gE}{(\Delta Y)^3}\left.\frac{dh_{11}}{dY}\right|_{Y_N} = \frac{1}{2}\left\{\frac{[g/(\Delta Y)^2]M_0(Y_N) + [g/(\Delta Y)^2]M_0(0)}{2I(0, Y_N)}\right\}$$

and then determine

$$\frac{gE}{(\Delta Y)^3}\left.\frac{dh_{11}}{dY}\right|_{Y_k} = \frac{gE}{(\Delta Y)^3}\left.\frac{dh_{11}}{dY}\right|_{Y_{k+1}} + \frac{[g/(\Delta Y)^2]M_0(Y_k) + [g/(\Delta Y)^2]M_0(Y_{k+1})}{2I(Y_{k+1}, Y_k)}$$

(8) Finally form

$$\frac{gE}{(\Delta Y)^4}[h_{11}(Y_N) - h_{11}(0)] = \frac{1}{4}\left[\frac{gM_0(Y_N)}{(\Delta Y)^2} + \frac{2gM_0(0)}{(\Delta Y)^2}\right]\frac{1}{6I(0, Y_N)}$$

and also

$$\frac{gE}{(\Delta Y)^4}\{h_{11}(Y_k) - h_{11}(0)\} = \frac{gE}{(\Delta Y)^4}[h_{11}(Y_{k+1}) - h_{11}(0)] + \frac{gE}{(\Delta Y)^3}\left.\frac{dh_{11}}{dY}\right|_{Y_{k+1}} + \left[\frac{gM_0(Y_k)}{(\Delta Y)^2} + \frac{2gM_0(Y_{k+1})}{(\Delta Y)^2}\right]\frac{1}{6I(Y_{k+1}, Y_k)}$$

(9) Then

$$\frac{gE}{(\Delta Y)^4} h_{11}(0) = \frac{-\sum_{i=1}^{N} [gE/(\Delta Y)^4][h_{11}(Y_i) - h_{11}(0)]W(Y_i)}{\sum_{i=1}^{N} W(Y_i)}$$

(10) From steps (8) and (9) find $[gE/(\Delta Y)^4] \times h_{11}(Y_k)$.

(11) Determine $gE/(\Delta Y)^4$ and so obtain from step (10), $h_{11}(Y_k)$.

(12) Form the test ratio $h_0(Y_k)/h_{11}(Y_k)$.

REFERENCES

[1] Saibel, Edward, *A Modified Treatment of the Iterative Method*, Journal of the Franklin Institute, February, 1944.

[2] Timoshenko, S., *Vibration Problems in Engineering;* D. Van Nostrand Company, Inc., New York, 1937.

[3] Den Hartog, J. P., *Mechanical Vibrations*, pp. 194 and 195; McGraw-Hill Book Company, Inc., New York, 1940.

[4] Schwarz, H. A., *Gesammelte Werke*, Vol. I, pp. 241–265.

[5] Reference 3, pp. 193 and 194.

[6] von Kármán, Th., and Biot, M. A., *Mathematical Methods in Engineering;* McGraw-Hill Book Company, Inc., New York, 1940.

[7] Timoshenko, S., *Strength of Materials*, Vol. I; D. Van Nostrand Company, Inc., New York, 1940.

[8] Miller, R. H., *Wing Frequencies of a Multi-Engine Monoplane*, Journal of the Aeronautical Sciences, Vol. 7, No. 6, pp. 256–258, April, 1940.

[9] Biezeno, C. B., and Grammel, R., *Technische Dynamik;* Julius Springer, Berlin, 1939.

[10] Loring, S. J., *General Approach to the Flutter Problem*, SAE Journal, Vol. 29, No. 2, pp. 345–356, August, 1941.

[11] Bleakney, W. M., *Three-Dimensional Flutter Analysis*, Journal of the Aeronautical Sciences, Vol. 9, No. 2, pp. 56–63, December, 1941.

Letter to the Editor

Dear Sir:

The paper by Klemin and Walling on the "Aerodynamic Performance of the Towed Glider" (JOURNAL OF THE AERONAUTICAL SCIENCES, Vol. 10, No. 6, pp. 185–196, June, 1943) has suggested to me a method of applying the common approximate methods of analysis to this problem.

The total drag of the tug and gliders may be written

$$D_t = D_a + nD_g$$

and the total power required

$$\begin{aligned} P_{rt} &= D_t V = (D_a + nD_g)V \\ &= \rho(V^3/2)(C_{D_a}S_a + nC_{D_g}S_g) \end{aligned}$$

Replacing the polar curve of each unit by a parabola of the form $C_D = (f/S) + (C_L^2 S/\pi e b^2)$,

$$P_{rt} = \frac{\rho V^3}{2}\left(f_a + \frac{C_{L_a}^2 S_a^2}{\pi e_a b_a^2} + nf_g + \frac{nC_{L_g}^2 S_g^2}{\pi e_g b_g^2}\right)$$

Eliminating C_L and regrouping terms,

$$P_{rt} = \frac{\rho V^3}{2}(f_a + nf_g) + \frac{2}{\pi\rho V}\left(\frac{W_a^2}{e_a b_a^2} + \frac{nW_g^2}{e_g b_g^2}\right)$$

Following Mr. Klemin's lead, we may determine a fictitious total sinking speed by dividing by the weight of the tug:

$$V_{fst} = \frac{P_{rt}}{W_a} = \frac{\rho V^3}{2}\frac{(f_a + nf_g)}{W_a} + \frac{2}{\pi\rho V}\left(\frac{W_a}{e_a b_a^2} + \frac{nW_g}{W_a}\frac{W_g}{e_g b_g^2}\right)$$

We now may define performance parameters for the whole train analogous to those commonly used in analyzing the performance of an airplane alone,

$$\begin{aligned} l_{Pt} &= W_a/(f_a + nf_g) \\ l_{st} &= (W_a/e_a b_a^2) + (nW_g/W_a)(W_g/e_g b_g^2) \\ &= l_{sa} + (nW_g/W_a)l_{sg} \end{aligned}$$

and the fictitious total sinking speed becomes

$$V_{fst} = (\rho/2)(V^3/l_{Pt}) + (2/\pi\rho)(l_{st}/V)$$

which is the equation upon which the common chart methods of performance calculation are based. The power loading is not changed,

$$l_{tt} = l_{ta} = (W_a/\text{b.hp.} \times \eta)$$

since there is no power available other than that of the tug.

Using these total parameters, we may proceed to analyze the performance of the train by means of charts such as those presented by W. Bailey Oswald (*N.A.C.A. T.R. 408*) or Millikan (*Aerodynamics of the Airplane*). It should be noted, however, that we are in effect determining the performance of the tug subject to the drag of the gliders but not to their weight. This has no effect on such items as maximum speed, but the rate of climb will be too high and must be corrected by the factor W_a/W_t.

This correction may be avoided if we divide the total power required equation by the total weight instead of the weight of the tug. The total parameters then become,

$$\begin{aligned} l_{Pt} &= W_t/(f_a + nf_g) \\ l_{st} &= (W_a/W_t)l_{sa} + (nW_g/W_t)l_{sg} \\ l_{tt} &= W_t/\text{b.hp.} \times \eta = (W_t/W_a)l_{ta} \end{aligned}$$

ROBERT S. EIKENBERRY
Department of Aeronautical Engineering
University of Notre Dame

The L.P.C.* Method of Performance Computation

JOSEPH V. FOA† AND BERNARD M. LEADON‡
Curtiss-Wright Corporation

SUMMARY

Existing methods devised to simplify the tedious classic procedure of performance computation depend either upon generalized parameters or upon approximate curves valid only in a restricted range, with the result that calculations usually are not accurate even in the low-speed range and for high speeds are hardly applicable. Inasmuch as the force coefficients (C_L and C_D) become functions of the speed at high speeds, while the object of the performance computation is to determine the speed through a knowledge of these coefficients, the solution of this interlocking problem becomes extremely cumbersome by the usual analytic means.

This paper describes a new method of solution which makes direct use of the actual airplane polars without approximations. The procedure is based on an extension of the Eiffel-Rith coordinate system, and all scales can be incorporated in a simple transparent chart, thereby eliminating the necessity for specially prepared graph paper.

Compressibility effects are taken into account through the use of constant altitude variable Mach Number polars which are derived from constant Mach Number polars of the true airplane.

INTRODUCTION

A GREAT DEAL OF STUDY has been devoted to the improvement of techniques for airplane performance computation, but still more attention must be given to this investigation as the range of speeds continues to increase. So many versions and extensions of the classic performance method have been proposed that readers are a bit wary of any new paper on the subject. However, the importance of precise and rapidly computed performance data justifies the effort expended; for, if more preliminary design studies can be made in a given time without sacrifice of accuracy, the chances are that the final result will be a better airplane.

Many writers have felt that the attribute of rapidity in performance calculations is more worthy than that of exactness. The methods now being used accomplish their purpose quite successfully for current airplane designs and speeds, but there is every reason to anticipate their failure when applied to high-speed aircraft of advanced design and with new propulsion systems.

THE CLASSIC SOLUTION

The so-called classic solution consists of a point by point comparison of powers available and required obtained by direct computation from the engine and airplane data. The limit of accuracy depends only upon that of the data employed and upon the care of the user, but the computation time required is almost prohibitive for preliminary work. So the resourceful engineer has introduced a series of approximations enabling him to attain certain neat results from three basic equations. Thus, the lift equation for steady, level flight,

$$W/S = C_L(\sigma V^2/391) \tag{1}$$

the power required equation,

$$\eta \text{b.hp.}/S = C_D(\sigma V^3/391)\cdot(1/375) \tag{2}$$

and the approximating parabolic polar,

$$C_D = C_{D_0} + kC_L^2 \tag{3}$$

made possible an entirely analytic solution. Many ingenious devices have been conceived to help speed up this process, but, when time permits and greater accuracy is sought, we still find the engineer checking points by the old classic method.

COMPRESSIBILITY EFFECTS

As airplane velocities increase, the effects of air's compressibility loom large. Compressibility effects become appreciable at Mach Numbers above about 0.4—that is, at speeds that are already well exceeded by many present-day airplanes. Consideration of these effects is of paramount importance in performance computation, because the magnitude of the lift and drag coefficients and the nature of their relation with each other are radically influenced. Eq. (3), which is sometimes acceptable as a simple expression for the polar curve at low Mach Numbers, is certainly not valid in the high-speed range. In the future it might become possible to extend the validity of this analytic relation to the high-speed range by introducing M (Mach Number) into it as an additional parameter. But this is not possible at present, since the data available on compressibility effects are still so meager that any attempt to "freeze" them into an empirical formulation of this sort would be entirely unjustifiable. Indeed, so much uncertainty still exists in this branch of applied aerodynamics that the correct interpretation of the results of flight tests and high-speed wind-tunnel experiments of a given airplane is an accomplishment in itself.

Received January 6, 1944.

* L.P.C. = Logarithmic Performance Computer.

† Senior Design Engineer, Research Laboratory.
‡ Senior Aerodynamicist, Research Laboratory.

Analyzing Experimental Results

When this analysis is made, it is found that constant-Mach-Number polar curves of an airplane for various Mach Numbers often differ from each other much more than the polar curves of entirely different airplanes at the same Mach Number. It is then obvious that all short-cut methods that are based on approximations of the nature of Eq. (3) would result in gross errors in the high-speed range. Nor can it be said that the use of different equations for the different constant-Mach-Number polars would extend the validity of these methods, because at high Mach Numbers not only does the speed depend on the polar curve but the polar curve itself depends on the speed, so that the computation of performance becomes an interlocking problem.

The classic method can be modified to take care of this through the use of a different polar curve for each speed in the computation of the power required. However, the simple relation that exists in the low-speed range between the curves of power required at different altitudes (i.e., that the "indicated power required" curve is constant) ceases to be valid at high speeds, as the Mach Number changes with altitude at any given speed. The curves of power required for different altitudes must be computed one by one, each point of them being related to a different polar curve. Thus, the classic method, always cumbersome, becomes even more formidable and inelegant when carried into the domain of compressibility.

In the early development of performance analyses a method was proposed in France by Eiffel and Rith which utilized the two analytic expressions given in Eqs. (1) and (2) in combination with the true C_D vs. C_L polar as found by experiment or synthesis. Thus, they restricted the approximations to those mild ones that the two equations demand and avoided the often gross inaccuracy of the analytic polar. Their method, which depends upon logarithmic coordinates, attained the classic method's accuracy and was found to exceed its speed immensely. Logarithmic charts became well known and were widely used, especially in Europe. In many countries they are used almost exclusively even today.

An extension of the Eiffel-Rith system provides for extremely rapid and accurate computations in all speed ranges, solving the problem as easily and logically in the high as in the low velocity region. First, let us consider briefly the Eiffel-Rith coordinate system.

The Eiffel-Rith Coordinate System

In logarithmic form Eqs. (1) and (2) may be written:

$$\log C_L = \log (W/S) - \log \sigma - 2 \log V + \log \text{const.} \quad (4)$$

$$\log C_D = \log (\eta \text{b.hp.}/S) - \log \sigma - 3 \log V + \log \text{const.} \quad (5)$$

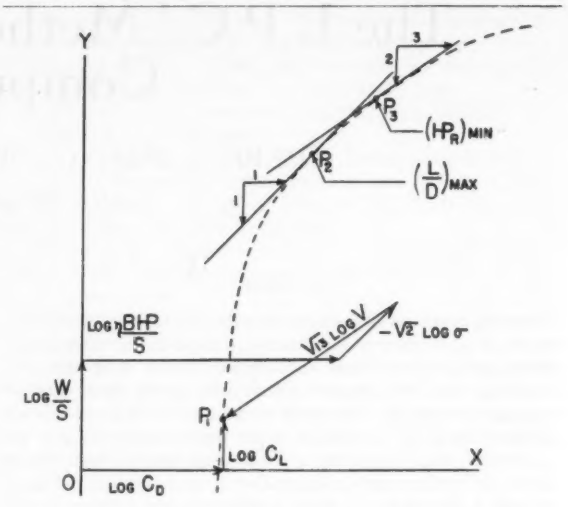

Fig. 1. Eiffel-Rith vectors.

If Eqs. (4) and (5) are considered as vectorial sums made, respectively, along the vertical and horizontal axes of a Cartesian coordinate system, then

$$\overline{\log C_L} + \overline{\log C_D} = \overline{\log (W/S)} + \overline{\log (\eta \text{b.hp.}/S)} - \overline{\sqrt{2} \log \sigma} - \overline{\sqrt{13} \log V} + \overline{\log \text{const.}} \quad (6)$$

This vectorial equation is represented in Fig. 1 where point P_1 is a point on the polar curve. This construction, in which the order of addition is of no consequence, provides a simple means of finding one or more of the parameters when the others are given. It is seen that the scales for density and velocity necessarily have the slopes 1 and $^2/_3$, respectively, and also have scale lengths in cycles per inch which are $\sqrt{2}$ and $\sqrt{13}$ times the scale length of the orthogonal axes. The sense of direction corresponds to the signs of the terms in Eq.

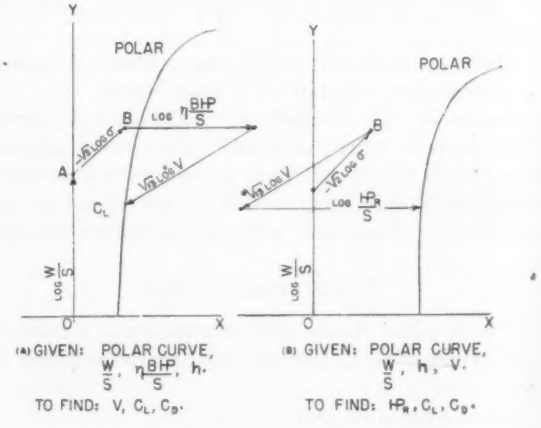

Fig. 2. Use of Eiffel-Rith nomogram.

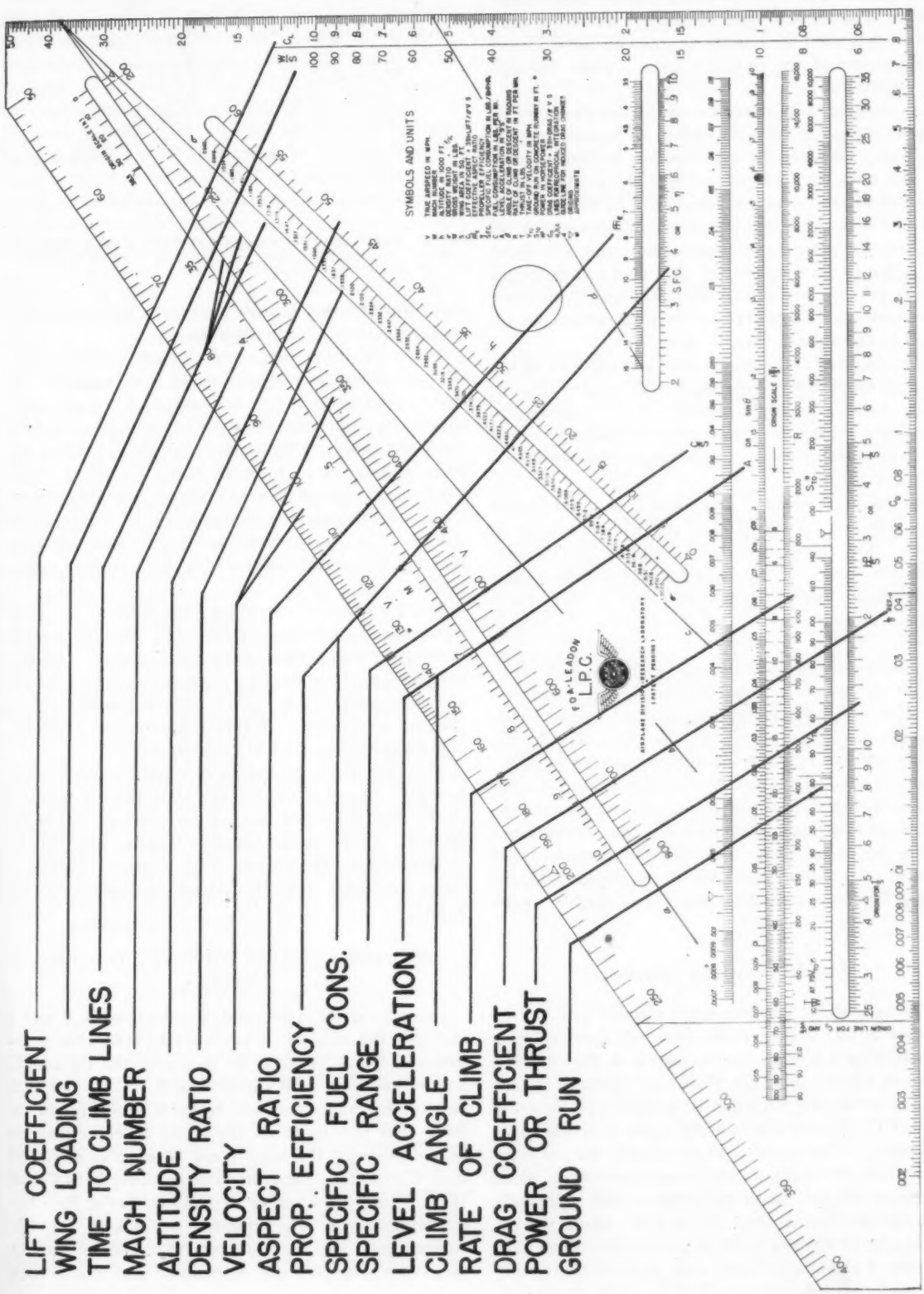

FIG. 3. The logarithmic performance computer.

(6). In the preparation of the logarithmic nomogram, the origins of the V and σ scales can be chosen arbitrarily. The chosen origin values of V and σ are then used to determine the relative position of the W/S and C_L scales and of the ηb.hp./S and C_D scales through Eqs. (4) and (5).

As examples to illustrate the use of this chart, let us suppose the polar curve is plotted in logarithmic coordinates. Knowing the wing loading and thrust power per unit area, the speed at any altitude and the corresponding lift and drag coefficients can be found by direct vector composition, Fig. 2(A). Conversely, if we are given the polar curve, wing loading, and altitude of flight, the power required per unit area can be found for any velocity, Fig. 2(B). Thus the logarithmic polar curve assumes the role of power required curve when referred to the oblique velocity scale.

The preceding two examples give an indication of the inherent simplicity of the system and its advantage in aiding visualization of the influence of the separate performance parameters. The method is therefore much less tedious and just as accurate as any that have been devised in the past.

The familiar points of maximum L/D and of minimum power are as easily found on this diagram as on others. The reader can verify that for (L/D) maximum the slope of the logarithmic polar is 1 and for minimum power required the slope is $^2/_3$. These points are shown in Fig. 1 as P_2 and P_3, respectively.

An investigation of the properties of the Eiffel-Rith coordinate system reveals that the simple addition of one scale makes the logarithmic method uniquely suitable for quick and direct consideration of compressibility effects. It is also found that the speed and accuracy of the method are greatly improved if all scales are incorporated in a transparent rule and that the use of such an instrument makes possible many other time-saving scales enabling the user to compute quick answers to most performance problems, thereby saving days in computation time for a complete analysis.

The Performance Computer

The logarithmic performance computer (L.P.C.) developed by the writers at the Research Laboratory of Curtiss-Wright Corporation is shown in Fig. 3. The scales of C_D, C_L, b.hp./S, W/S, and altitude are the same as in the original Eiffel-Rith chart. However, in the L.P.C. version the velocity scale is divided into two parts: a low-speed scale principally for velocities lower than 198 m.p.h.; and a high-speed scale, along the upper left slot (with the origin at the right end), for velocities higher than 198 m.p.h. Along the opposite edge of this slot is the Mach Number scale. The location of the origin of this scale depends on the altitude under consideration, so that the origin is not indicated by the usual triangle defining a point but by a small scale graduated in altitudes.

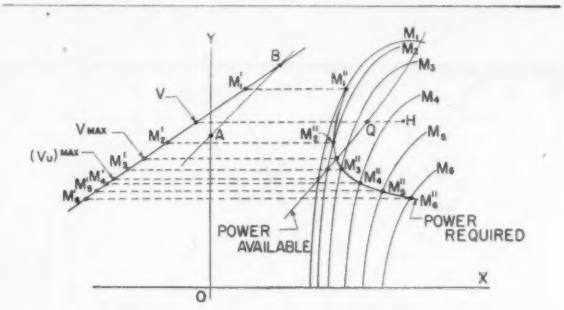

FIG. 4. Power required and power available curves, maximum speed, and compressibility correction at a given altitude.

Above the lower horizontal slot are several scales: (1) take-off distance, consisting of three segments divided in terms of thrust per pound of weight, take-off velocity, and take-off distance; (2) and (3) rate of climb and angle of climb, whose origins depend on the wing loading (so as to serve both, a scale of origin locations, graduated in wing loadings, is found between them); (4) fuel consumption per mile, C; (5) propeller efficiencies, η, or alternatively, specific fuel consumption, S.F.C.; and (6) induced drag for a range of aspect ratios.

This instrument provides the answer to most performance problems *directly*—i.e., through simple readings on scales, without any computation. The data required are, as in the classic method, airplane weight and wing area, a few constant-Mach-Number polars, the curves of thrust or thrust horsepower available, and curves of specific fuel consumption.

The following is the outline of a performance computation by means of the L.P.C. Only the computation of the most important items of performance will be described. As the reader becomes familiar with this instrument, he will discover that a great number of other problems can be solved by means of the L.P.C.

Plotting of Polars and Power Available Curves

Draw a pair of orthogonal coordinate axes X and Y and plot the constant-Mach-Number polars for a few different Mach Numbers by means of the C_D and C_L scales (lower and right edges of the L.P.C.). The location of the origins in these scales is arbitrary, in the sense that any point on them can be chosen as the origin, provided the same point be used as origin for both C_D and hp./S and the same point for both C_L and W/S. However, in order to avoid confusion, it is recommended that the origins be taken on the "origin line" for the C_D and hp./S scales and on the lower edge of the instrument for the vertical scales.

On the Y-axis mark a point at the W/S of the computation (point A in Fig. 4). Then bring the origin of the altitude scale to this point and mark the point which, on the 45° altitude scale, corresponds to the altitude under consideration (point B). Draw a line through these points, A and B, and a velocity line parallel to the velocity scales through B, and set the Mach Number scale along it, with the origin on B. It must be remembered that the location of the origin in this scale depends on the altitude: For instance, at an altitude of 20,000 ft., the point 20 at the upper right end of the scale must be used as origin. Now mark on the velocity line the points M_1', M_2', M_3', etc., corresponding to the same Mach Numbers as those of the polar curves used. These points are projected horizontally to their respective polars forming the curve which is a constant-altitude variable-Mach-Number polar passing through M_1'', M_2'', M_3'', etc. Repeat this process for several altitudes and/or for several wing loadings as desired.

Now $M_1'\,M_1''$ is the power required per unit area at the velocity corresponding to the Mach Number M_1. This velocity is obtained by setting the velocity scale along BM_1', with the origin at B and reading at M_1'. The power required is obtained by setting the power scale along $M_1'\,M_1''$, with the origin at M_1' and reading at M_1''. Likewise, $M_2'\,M_2''$ is the power required at the velocity corresponding to the Mach Number M_2 and so on. Thus, the polar curve, when referred to the velocity and power axes, is the curve of power required.

The curve of power available at any altitude is obtained as follows. Mark a point H as measured from V equal in length to the brake horsepower per unit wing area for that particular speed and altitude, and adjust the point back to Q by placing 1 on the "η" scale at H and marking Q at the propeller efficiency found for that particular speed and altitude. Continue to plot these points in rapid order until the power available curve is indicated clearly enough to fair it in. Proceed in this manner for all altitudes and/or wing loadings for which constant-altitude polar curves have been constructed.

Maximum Speed

The maximum speed at any altitude and with any wing loading occurs when the corresponding curves of power required (polar) and power available intersect each other ($V_{max.}$ in Fig. 4).

An interesting feature of this representation is that the effect of compressibility can be estimated at a glance. In Fig. 4, if compressibility effects were not taken into consideration, the maximum speed would be found to be $(V_u)_{max.}$ at the intersection of the power-available curve with the low Mach Number polar. Hence, $(V_u)_{max.} - V_{max.}$ is the compressibility effect on maximum speed.

Rate of Climb

The rate of climb, in feet per minute is

$$\frac{dh}{dt} = \frac{(\text{hp.}_{\text{Available}} - \text{hp.}_{\text{Required}})33{,}000}{W} = \frac{[(\text{hp.}_A/S) - (\text{hp.}_R/S)]33{,}000}{W/S} = \frac{(\text{hp.}_R/S)[(\text{hp.}_A/\text{hp.}_R) - 1]33{,}000}{W/S}$$

In logarithmic terms,

$$\log dh/dt = \text{const.} + \log (\text{hp.}_R/S) + \log [(\text{hp.}_A/\text{hp.}_R) - 1] - \log (W/S)$$

It appears that the rate of climb is maximum where

$$\log (\text{hp.}_R/S) + \log [(\text{hp.}_A/\text{hp.}_R) - 1]$$

is maximum. In Fig. 5, VP is $\log (\text{hp.}_R/S)$; PQ is $\log (\text{hp.}_A/S) - \log (\text{hp.}_R/S) = \log (\text{hp.}_A/\text{hp.}_R)$. Place the power scale horizontally with the point 1.0 at P and read on the scale at Q (this reading is the ratio $(\text{hp.}_A/\text{hp.}_R)$. Mentally subtract 1.0 from this reading and mark the difference at R. Then, PR is $\log [(\text{hp.}_A/\text{hp.}_R) - 1]$, and $VR = \log (\text{hp.}_R/S) + \log [(\text{hp.}_A/\text{hp.}_R) - 1] = \log$ (excess horsepower/S). If the process is repeated for several speeds, the curve of excess horsepower (dotted curve in Fig. 5) can be easily traced. At the point of the curve where the slope is the same as that of the velocity scale, the excess horsepower is a maximum and the corresponding velocity is that of best rate of climb (V_c). Having determined this velocity, set the origin of the rate of climb scale at V_c and read the rate of climb directly on the rate of climb scale at R_c. The origin in this case corresponds to the wing loading as read on the wing loading scale, which adjoins the rate of climb scale.

Ceiling and Time to Climb

Although the absolute ceiling can be found directly on the logarithmic graph, the quickest way is still that

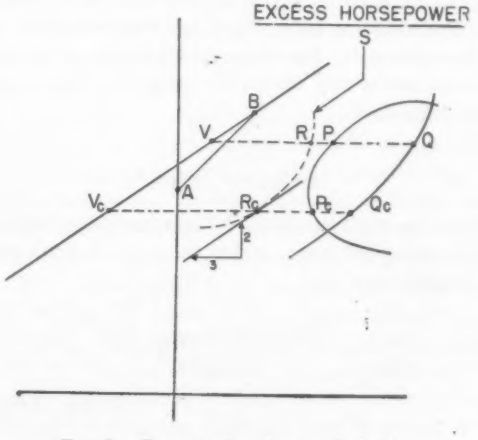

FIG. 5. Computation of rate of climb.

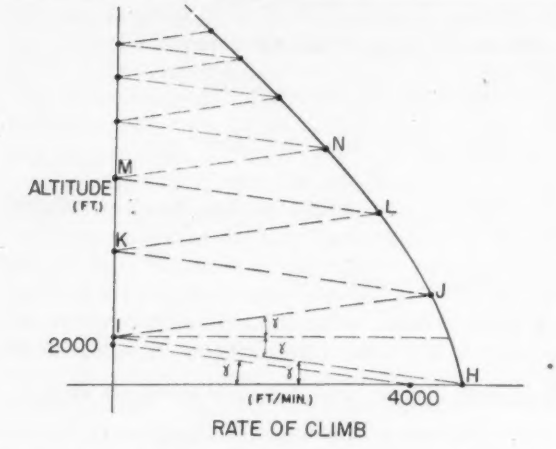

FIG. 6. Determination of time to climb by reciprocal integration.

of plotting the rate of climb versus altitude on common graph paper and extending the curve to the point at which the rate of climb becomes zero. Once this graph has been prepared, the time to climb to any altitude can be rapidly computed as follows:

Draw a line through 4,000 on the dh/dt axis and 2,000 on the h axis (or 5,000 and 2,500, or 6,000 and 3,000, and so on, respectively). Then draw the line HI, parallel to the former, through the point H (rate of climb at sea level). Measure the angle γ, and draw the line IJ, with the same slope with respect to the horizontal. Then draw the lines JK, KL, LM, MN, and so on, alternately parallel to HI and to IJ. It is readily seen that tan γ is an interval of time, as tan $\gamma = \Delta h/(\Delta h/\Delta t) = \Delta t$. In the present example, tan γ is $^1/_2$ min. In other words, J indicates the altitude at which the airplane will be after 1 min. of climb, L the altitude at which the airplane will be after 2 min., and so on. In order to facilitate this graphic computation, the three lines a, b, and c have been incorporated in the computer. They can be used on the usual graph of dh/dt vs. h, when the scales are selected so that the scale of rate of climb in feet per minute is five times the scale of altitude in feet. Their use is obvious and need not be explained. The time to climb thus computed is not exact but is well within the limits of approximation of the data used.

Angle of Climb

If θ is the angle of climb, V the speed along the flight path in miles per hour, and w the rate of climb in feet per second, then

$$\sin\theta = \frac{w}{1.467V} = \frac{550(\text{excess horsepower})}{1.467VW} = \frac{(\text{excess thrust}/S)}{W/S}$$

In logarithmic terms,

$$\log\sin\theta = \log\left(\frac{\text{excess horsepower}}{S}\right) - \log V - \log\frac{W}{S} + \text{const.}$$

In Fig. 5, VR = log (excess horsepower/S) + const. On the other hand, VN is log V + const., as VN is one-third of the horizontal projection of the velocity vector. Hence, NR = log (excess horsepower/S) − log V + const.

The steepest angle of climb is achieved when NR is a maximum—i.e., at the point of the excess horsepower curve at which the slope is that of the altitude scale (45°). In order to find the angle of climb, set the angle of climb scale along VR, with its origin (wing loading) at N, and read the angle of climb at R.

Acceleration in Horizontal Flight

If the excess thrust is used to accelerate the airplane along its horizontal path, instead of for climb, then the acceleration in g's is:

$$\text{acceleration in } g\text{'s} = \text{excess thrust}/W$$

Hence, the horizontal acceleration in g's, when the excess thrust is entirely used for acceleration along a horizontal path, equals the sine of the angle of climb when the excess thrust is entirely used for climb without change of speed along the trajectory. Therefore, the horizontal acceleration is computed in exactly the same manner as the angle of climb and by means of the same scale.

Sinking Speed and Angle of Descent—Power On

When the power available is less than the power required, the airplane descends. There is no essential difference between sinking speed and rate of climb except for sign. If sinking speed is considered positive,

$$\left(\frac{dh}{dt}\right)_s = \frac{[(\text{hp}_{\cdot R}/S) - (\text{hp}_{\cdot A}/S)]33{,}000}{W/S} = \frac{(\text{hp}_{\cdot A}/S)[(\text{hp}_{\cdot R}/\text{hp}_{\cdot A}) - 1]33{,}000}{W/S}$$

Point Q will be to the left of point P (Fig. 7). The power scale will be set with 1 at Q and the reading will be taken at P. Through a mental subtraction of 1 from this reading, point R will be located as in the computation of the rate of climb. The rate of descent can be read directly on the rate of climb and descent scale at R by placing the origin corresponding to the given wing loading at V. Analogously, the angle of descent is obtained at R on the angle of climb and descent scale when the origin is set at N.

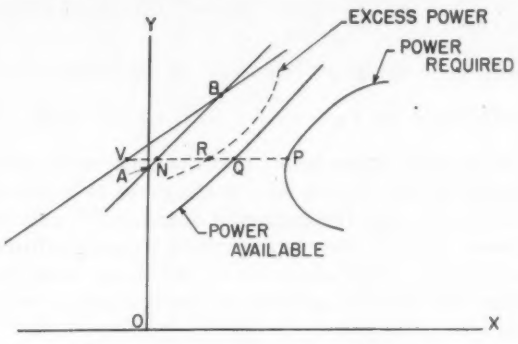

FIG. 7. Computation of sinking speed.

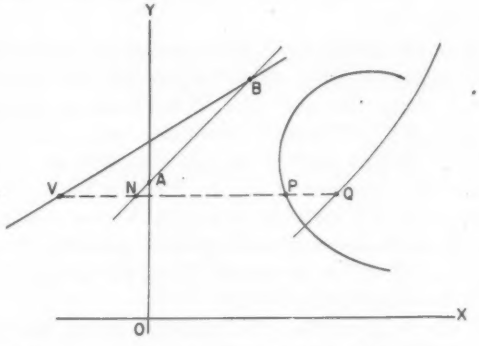

FIG. 8. Use of thrust instead of thrust horsepower.

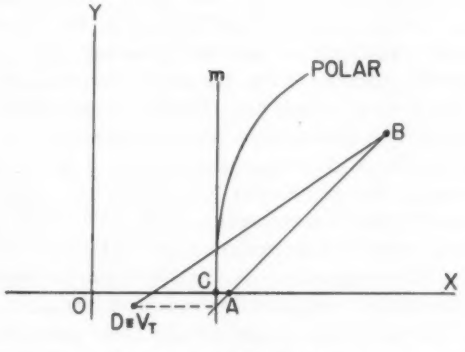

FIG. 9. Terminal velocity.

RATE OF DESCENT AND GLIDE ANGLE—POWER OFF

For the particular case of descent with no power the term $hp._A/S$ is zero and the point R as determined by the previously described method coincides with P. Hence, the horizontal distance from the velocity scale to the polar curve read on the rate of climb and descent scale gives the rate of descent. By the same reason the angle of glide is found from the angle of climb and descent scale as the horizontal distance between the altitude scale and the polar curve. It appears that the minimum glide angle is achieved when the airplane is flying at the angle of attack corresponding to the point on the logarithmic polar curve at which the slope is equal to that of the altitude scale (45°). This was to be expected since this point defines the angle of attack for maximum L/D.

USE OF THRUST INSTEAD OF THRUST HORSEPOWER

It is often considered convenient to use thrust instead of thrust horsepower in the computation of performance. The L.P.C. method is particularly well suited to such a representation of the propulsive force in that the same scale may be used to measure values of T/S as is ordinarily used for $hp./S$ simply by referring all measurements to another origin that differs only by a constant from the usual origin. Since the thrust required is proportional to the square and not to the cube of the speed as is the power required, the velocity line will have in this case a slope of 1 and will therefore coincide with the altitude line. Hence, the velocities can still be measured along the usual line of $^2/_3$ slope, but all thrust available and thrust required measurements must be made from the 45° line. In Fig. 8 the distances NP and NQ when read in the thrust scale are, respectively, the thrust required and thrust available at the speed V, whereas the distances VP and VQ when read in the power scale are, respectively, the power required and power available at the speed V. The interested reader can revise the performance computation to this basis using as a guide the procedure heretofore outlined.

TERMINAL VELOCITY

In a zero lift dive with power off the thrust is furnished by the weight of the airplane and, therefore, the thrust per unit area is equal to the wing loading. The point of zero lift does not appear in a logarithmic chart since it is located at minus infinity. On the assumption that the drag coefficient is that corresponding to the lowest C_L on the chart, a vertical "minimum drag" line m can be drawn through C as in Fig. 9. OA is the wing loading (W/S) read in the T/S scale, AB is the altitude, and BD is the terminal velocity at the given altitude. D is read horizontally from the intersection of BA, extended, and the line m.

In general, the terminal velocity will be high enough to make the consideration of compressibility effects imperative. This can be done as follows (Fig. 10): Several lines m_1, m_2, m_3, are drawn for different Mach Numbers (they are the verticals through the intersections of the various constant-Mach-Number polars with the X-axis). Following the procedure illustrated in Fig. 4 for level flight, the constant-altitude polar is constructed. The curve of thrust available becomes in this case the line BA extended. The intersection of this line with the constant-altitude polar when projected horizontally upon the velocity line determines the point M. The Mach Number M thus determined is

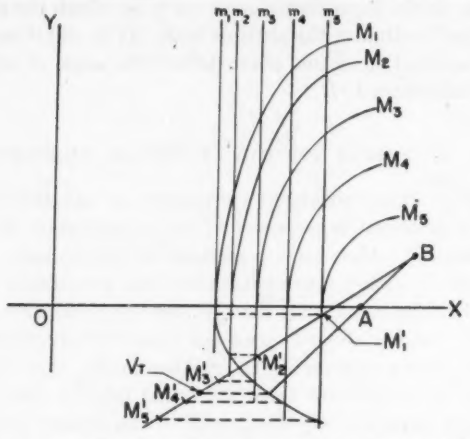

FIG. 10. Terminal velocity with consideration of compressibility effects.

that corresponding to the terminal velocity at the given altitude, and the corresponding velocity can be immediately obtained by measuring BM on the velocity scale.

It is clear that this case differs from that of level flight in only two ways: (1) W/S is practically zero, (2) $T/S = W/S$. In Fig. 10 the arrangement of work is somewhat simpler than in Fig. 4.

RANGE

The weight of fuel dW (in pounds) consumed during the time dt (in hours) when the airplane is flying horizontally at the velocity V (in miles per hour) is

$$dW = \text{hp.}_R(\text{S.F.C.}/\eta)dt = \text{hp.}_R(\text{S.F.C.}/\eta)(ds/V)$$

where S.F.C. is the specific fuel consumption in pounds per horsepower hour, η is the propeller efficiency, hp._R is the power required (in horsepower), and s is the distance covered during the time t, in miles. Hence, the fuel consumption in pounds per mile is

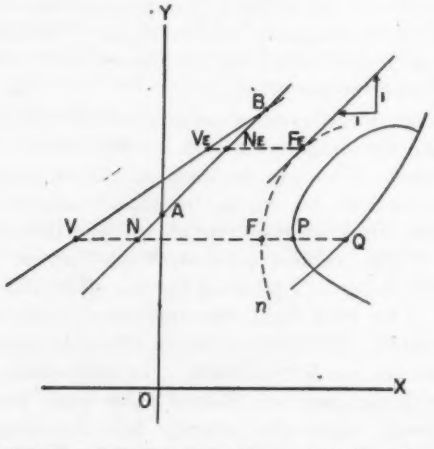

FIG. 11. Use of the L.P.C. for the computation of range.

$$C = \frac{dW}{ds} = (\text{hp.}_R/V)(\text{S.F.C.}/\eta) = (1/375)T_R(\text{S.F.C.}/\eta)$$

where T_R is the thrust required. In logarithmic form,

$$\log dW/ds = \log T_R + \log \text{S.F.C.} - \log \eta + \text{const.} \quad (7)$$

It has been shown before that the polar curve, when referred to the altitude line, is the curve of thrust required—i.e., that the horizontal distance NP from the altitude line to the corresponding constant-altitude polar curve, when measured on the thrust scale, furnishes the thrust required at the speed V and at the altitude h.

Now set the S.F.C. scale horizontally with the point corresponding to the propeller efficiency at P and mark the point F corresponding to the specific fuel consumption (Fig. 11).

Then, the distance NF, when measured on the thrust scale, is log $(T_R\text{S.F.C.}/\eta)$. To expedite the computation of range, the scale of C/S has been incorporated in the L.P.C. This scale is nothing but a (thrust/S) scale, so shifted with respect to its origin as to take care of the constant of Eq. 7. Thus, if the C/S scale is set along NF with the origin at N, the reading at F is the fuel consumption in (pounds per mile/S)—i.e., $[(1/S)(dW/ds)]$ at the speed V and the altitude h and with the wing loading W/S.

If one wants to find the maximum range, the speed of minimum fuel consumption per mile must be determined. The procedure for this determination follows immediately from the above considerations: Several points such as F are located in the chart for different values of V, and the locus of such points (curve n) is drawn; then, the most economic speed is the speed V_e at which the tangent to the curve n is parallel to the altitude line (45° inclination).

As the flight progresses, the weight of the airplane decreases. Hence, in order to compute the range, the above-described determination of the fuel consumption per mile must be repeated for a few different values of W/S. Then a graph of C/S vs. W/S can be prepared and the range computed by means of the lines a, b, and c of the L.P.C., following the same procedure as for the computation of the time to climb (in the present case, $\tan\theta = \Delta(W/S)/[\Delta(W/S)/\Delta s] = \Delta s$. The scales can be so chosen as to give Δs any desired value), or a graph of the reciprocal function $S(ds/dW)$ vs. W/S can be prepared and integrated to give the range.

The above method is general in the sense that it can be used in the computation of any kind of range. The computation of the maximum range, described above, is the only one that requires the plotting of an auxiliary curve, such as n. The range at constant speed, or constant power, or constant angle of attack, can obviously be computed directly.

With a little practice, the user of the L.P.C. not only learns to perform any range computation in a short time but also discovers that he can determine such

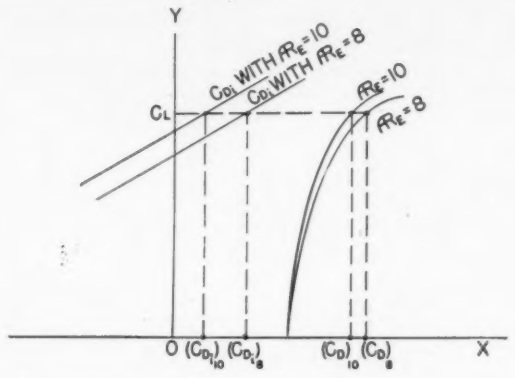

FIG. 12. Correction of logarithmic polar for a change of aspect ratio.

basic design parameters as the optimum wing loading or the most economical flight altitude almost at a glance.

INDUCED DRAG AND EFFECT OF CHANGE OF ASPECT RATIO

The evaluation of the effect of a change of aspect ratio is often of great importance in preliminary design. The aspect ratio scale of the L.P.C. makes this evaluation possible in a quick way.

From the definition of induced drag coefficient, it follows that

$$\log C_{D_i} = 2 \log C_L - \log \text{A.R.}_e - \log \pi$$

where A.R._e is the effective aspect ratio. Hence, with any given A.R._e, the curve of C_{D_i} vs. C_L becomes a straight line with slope $1/2$. The position of this line on the chart is determined as follows: The L.P.C. is placed on the chart with the lower right corner at the intersection of the X and Y axes and the right edge along the Y-axis, the point corresponding to the given A.R._e is marked on the chart, and a line with the slope indicated by the line d of the L.P.C. is drawn. This line represents the function $C_{D_i}(C_L)$. A change of aspect ratio will merely shift this line horizontally by the amount indicated on the aspect-ratio scale.

In Fig. 12 the aspect ratio is changed from 8 to 10. As a result, at the lift coefficient C_L, the induced drag decreases from $(C_{D_i})_8$ to $(C_{D_i})_{10}$. Then, at the given C_L,

$$(C_D)_{10} = (C_D)_8 - [(C_{D_i})_8 - (C_{D_i})_{10}]$$

$(C_D)_{10}$ for several values of C_L should be plotted to obtain the new polar for $\text{A.R.}_e = 10$.

TAKE-OFF DISTANCE

For the computation of ground run simply mark on a sheet of paper the distance between the values, E and F, of thrust at $0.75V_{t_0}$ divided by the gross weight and V_{t_0} as shown in the figure, where V_{t_0} is the take-off speed. Then set the origin of the ground run scale at E and take the reading at F. This reading is the approximate value of the ground run. No take-off computation can be exact because too much uncertainty exists as to the effect of certain factors such as pilot technique, runway condition, ground effect, angle of attack during run, propeller efficiency, etc. The take-off scale of the L.P.C. is based upon the charts developed in reference 4.

The distance to clear an obstacle of given height after the take-off is found from the angle of climb whose computation has already been described.

MISCELLANEOUS COMPUTATIONS

There are many other computations that can be performed on the L.P.C. Once the basic principles have been understood the procedures become evident and the user of the instrument can derive them by himself as obvious corollaries of the above-explained properties of the logarithmic performance nomogram. Thus, such items of performance as the speed corresponding to a given lift coefficient at a given altitude and with a given wing loading (e.g., stalling speed, landing speed, take-off speed), the maximum acceleration attainable in a sudden pull-up, the optimum wing loading and/or optimum altitude for best range, the absolute ceiling, the magnitude of compressibility effects, the influence of flap deflection upon performance, the landing distance, the radius of turn, and such values as the density at any altitude, the Mach Number at any speed and altitude, and many others can be readily obtained by means of the L.P.C., whose scales, incidentally, can also be used to perform ordinary multiplications and divisions.

The interested reader is referred to a book (four volumes) that a French enthusiast wrote to describe all performance items that can be obtained by means of the original Eiffel-Rith nomogram.[3] His list includes such problems as sideslip, circular glide, circular climb, and what not. Yet, the field of application of the L.P.C. is much broader than that of the original Eiffel-Rith nomogram, for the L.P.C. can solve all the problems that could be solved by the original nomogram and many more.

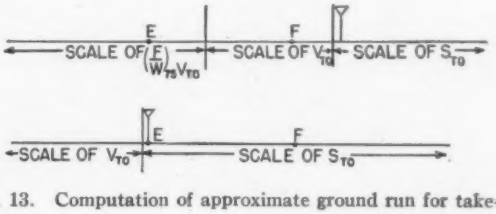

FIG. 13. Computation of approximate ground run for take-off.

REFERENCES

[1] Eiffel, G., *Nouvelles Recherches sur la Résistance de l'Air et l'Aviation*, Paris, 1914.

[2] Durand, W. F., *Aerodynamic Theory*, Vol. V, Div. O, Chapter VIII; J. Springer, Berlin, 1935.

[3] Bilbault, G. *Cours d'Aérodynamique et Calcul des Performances par la Méthode Graphique a Échelles Logarithmiques*, 4 vols.; R. Constant-Pinel, Paris, 1932.

[4] Foa, J. V., *Abachi per il Calcolo dello Spazio e del Tempo di Decollo degli Aeroplani*, L'Aerotecnica, January, 1937.

Letter to the Editor

Dear Sir:

The following remarks may be of interest in connection with Donald A. duPlantier's paper, "Analysis of Fuselage Rings by the Column Analogy," JOURNAL OF THE AERONAUTICAL SCIENCES, Vol. 11, No. 2, p. 137, April, 1944. Men well versed in the analysis of fuselage rings will hardly need the column analogy, since the numerical work is the same whether the calculations are based upon the column analogy, Castigliano's principle, or any equivalent method. The advantage of the analogy is that it can be learned much easier than the classic methods. In this regard Mr. duPlantier makes a contribution by presenting the subject in a manner easily understandable to the nonspecialist. Unfortunately, some of the statements and proofs in the paper are lacking in accuracy and rigor.

In particular the writer objects to Mr. duPlantier's use of the plus and minus ($\pm$) sign which may lead to incorrect results. The statement that "all ambiguity (namely, in the sign to be used) will be definitely removed....by applying the fundamental principle that M_i must reduce M_s numerically at the point where M_s is a maximum" is erroneous as may be seen from the numerical example that follows:

Because of the symmetry of ring and loading shown in Fig. 1(a) only one-half of the ring need be considered in the analysis. The ring is assumed to be cut at the point where the 2-lb. load is acting, and the unknown force H and the unknown moment N are applied in the section. The bending moment M_s caused in the cut ring by the actual external loads alone is

$$M_s = -r \sin \varphi \qquad \text{when } 0 \leq \varphi \leq 168°$$
$$M_s = r(2.079 - 11 \sin \varphi) \qquad \text{when } 168° \leq \varphi \leq 180°$$

The bending moment M_i caused by the unknowns is

$$M_i = N + Hr(1 - \cos \varphi)$$

With the customary assumptions the strain energy stored in the ring can be written as

$$U = (1/EI) \int_0^\pi (M_s + M_i)^2 r d\varphi$$

From Castigliano's theorem

$$(\partial U/\partial N) = 0 \text{ and } (\partial U/\partial H) = 0$$

Since

$$\partial(M_s + M_i)/\partial N = 1$$
$$\partial(M_s + M_i)/\partial H = r(1 - \cos \varphi)$$

the two requirements following from Castigliano's theorem may be written in the form

$$\int^\pi (M_s + M_i) d\varphi = 0$$
$$\int_0^\pi (M_s + M_i) \cos \varphi \, d\varphi = 0$$

After substitution, integration, and solution of the two simultaneous linear equations, the following values are obtained for the unknowns:

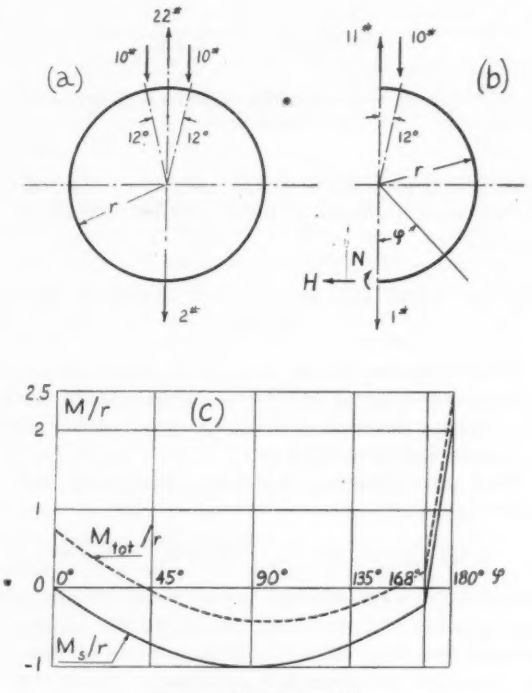

FIGS. 1 (a), (b), and (c).

$$H = -0.137 \qquad N = 0.707r$$

The bending moment M_s and the final bending moment $M_{tot.} = M_s + M_i$ are plotted against the angle φ in Fig. 1(c). The moment is a maximum when $\varphi = 180°$. Its value in the cut ring is $2.079r$, and in the actual statically indeterminate ring $2.510r$. Consequently, in this case M_i increased the maximum value of M_s.

Other examples can be devised in which the same is true. The reason is that the unknown quantities make the total strain energy stored in the ring, not the maximum moment, a minimum. If the signs are used consistently, however, there is no need for a principle of the reduction of the maximum moment, when the bending moments in a fuselage ring are calculated by the column analogy.

N. J. HOFF
Associate Professor of Aeronautical Engineering
Polytechnic Institute of Brooklyn

Periodic Aerodynamic Forces on Rotors in Forward Flight

CHARLES SEIBEL*
Bell Aircraft Corporation

SUMMARY

A new explanation is advanced for the cause of vibrations in rotary wing systems in forward flight, based on the fact that the down-wash is greater in the rear part of the swept disc than in the front part. An estimate of the magnitude of the down-wash variation at different forward speeds is made with the aid of data previously published by the N.A.C.A. on tests of a 10-ft. gyroplane rotor. This nonuniform down-wash causes a periodic change in the drag force on a blade and is a cause of forced vibrations, especially noticeable in two-bladed rotors at low air speeds.

INTRODUCTION

IN THE COURSE OF FLIGHT TESTING Model 30, the Bell Helicopter, a principal characteristic of which is the two-bladed rotor supported on a universal joint hub, pronounced vibrations were observed to occur at low forward speeds. These vibrations were of sufficient severity to prevent further increase of forward speed and to cause the pilot to land the machine. Flight testing was discontinued until an explanation could be found.

Oehmichen[3] has discussed the effect of the down-wash gradient on the flapping of a rotor in forward flight, and not until cognizance was taken of this gradient across the rotor disc from front to rear was a satisfactory explanation forthcoming. It was recalled that any pressure-actuating element—whether it be a propeller, a wing, or a rotor—generated a force by changing the momentum of a portion of the operating medium. Furthermore, the theory indicated that half of the momentum change is imparted to the medium before it reaches the actuating element, the other half being added after the medium has passed the element. Proceeding to the problem of a rotor operating in transverse flow, it became evident that the down-wash through the rear portion of the swept rotor disc was greater than through the front portion. It followed that the induced drag of the blade was varying with azimuth position. Pursuance of this line of thought led to the conclusion that at higher forward speeds, when the total induced flow was reduced, the gradient would become smaller and the vibration less severe.

This conclusion warranted an attempt to "pass through" the region of maximum vibration in flight, and it was found that this could be done. Above 30 m.p.h. the magnitude of the vibration began to die down and became unnoticeable at higher speeds around 70 m.p.h.

Although this evidence seemed conclusive, a quantitative estimate of the magnitude of the impressed periodic force was desired.

REFERENCE TO N.A.C.A. REPORT NO. 536

Not having facilities available for accurate force or down-wash measurements on models in forward flight, a search was made for data that could be used to make a quantitative estimate of the periodic aerodynamic forces involved. These data were found in *N.A.C.A. Report No. 536*.[2] In this report Wheatley and Bioletti present data obtained from a series of wind-tunnel tests on a 10-ft. gyroplane rotor.

The rotor was operated at full-scale tip speeds over a large range of tip-speed ratios. Cyclic pitch change was used to balance any tendency for the rotor to roll due to forward motion. The pitching moment was not balanced by cyclic pitch change; however, it was measured.

The gyroplane rotor was equipped with cyclic feathering control and did not employ flapping hinges to balance the unsymmetrical lift. With this setup a pitching moment can arise from two sources. First, because of coning in the rotor blades there will be a positive pitching moment; second, if the induced velocity through the rear portion of the rotor is greater than at the front, there will be a positive pitching moment. The pitching moment due to coning is proportional to the coning angle and to the forward velocity. Since the rotor was rigidly mounted it could carry bending at the hub and the coning was small. At low speeds the pitching moment due to coning is a small part of the total moment; however, it may become important at high speeds.

For simplicity of analysis the coning effect is neglected, and it is assumed that the down-wash variation is linear from the front of the rotor disc to the rear. In addition, it was found convenient to limit the analysis to low air speeds by assuming v small compared with ωR. This latter assumption is justified by the severity of the observed vibrations at low air speeds.

The following notation is used by Wheatley and Bioletti:

L = rotor lift, lbs.
T = rotor thrust, lbs.

Received January 10, 1944.
* Research Engineer.

M = pitching moment, lbs. ft.
V = air speed, ft. per sec.
ρ = air density, slugs per cu.ft.
Ω = angular velocity of rotor
R = radius of rotor
$C_L = L/{}^1/_2\rho V^2\pi R^2$
$C_T = T/\rho\Omega^2\pi R^4$
$C_m = M/{}^1/_2\rho V^2\pi R^3$

Determination of Down-Wash Variation

Notation

m_L' = pitching moment of a blade element resulting from down-wash distribution
m_L = total pitching moment of rotor
w_0 = average hovering down-wash
ψ = blade azimuth angle measured from down-wind position in direction of rotation
v = velocity of helicopter
ω = angular speed of rotor
x = blade element distance from hub
C_{D_P} = parasite drag coefficient of the blade
D' = drag of blade element
L' = lift of blade element
M_L' = lift moment of blade element about the hub
k_1 = flapping angle to rear due to forward motion
k_2 = flapping angle to the side due to down-wash variation
β = geometric blade angle
a = slope of lift curve
w = down-wash velocity at blade tip for a given blade azimuth position
R = radius of rotor
c = chord of blade
w_1 = down-wash at front of rotor disc
w_2 = down-wash at rear of rotor disc
μ = tip speed ratio $= v/\omega R$

Writing the equation for the pitching moment of a blade element with the assumption that the down-wash variation from the front of the rotor disc to the rear is linear,

$$m_L' = \frac{\rho}{2}(\omega x + v\sin\psi)^2\left(a\frac{w_2 - w_1}{2\omega R}\cos\psi\right)(c\,dx)\,x\cos\psi$$

Since v is small compared to ωR,

$$m_L' = \frac{\rho}{2}\omega^2 a\frac{w_2 - w_1}{2\omega R}cx^3\cos^2\psi\,dx + \frac{\rho}{2}2\omega a v\,\frac{w_2 - w_1}{2\omega R}cx^2\cos^2\psi\sin\psi\,dx$$

for a four-bladed rotor is

$$m_L = 4\left[\frac{\rho}{2}\omega^2 a\frac{w_2 - w_1}{2\omega R}c\int_0^R\frac{1}{\pi}\int_{-\pi/2}^{\pi/2}x^3\cos^2\psi\,dx\,d\psi + \rho\omega a v\,\frac{w_2 - w_1}{2\omega R}c\int_0^R\frac{1}{\pi}\int_{-\pi/2}^{\pi/2}x^2\cos^3\psi\sin\psi\,dx d\psi\right]$$

$$m_L = \rho\omega a c(w_2 - w_1)R^3/8$$

Expressing the measured moment in terms of the moment coefficient,

$$m_L = C_m(\rho/2)V^2\pi R^3$$

Equating the two expressions for m_L,

$$C_m(\rho/2)V^2\pi R^3 = \rho\omega a c(w_2 - w_1)R^3/8$$
$$w_2 - w_1 = (4\pi\omega R^2/ac)C_m\mu^2$$

The following numerical constants of the rotor are given in reference 2: $\omega = 550$ r.p.m., $R = 5$ ft., and $C = 6.28$ in. Assuming $a = 5.7$/rad., it is possible to compute the value of $(w_2 - w_1)$ from the curves of C_m vs. μ of reference 2, Fig. 12, by picking corresponding values of C_m and μ.

In order to obtain the down-wash distribution for various forward speeds it is necessary to obtain the average down-wash velocity as a function of forward speed. This relation has been presented in several performance analyses[1] and is plotted in Fig. 2. The value of the hovering down-wash w_0 can be computed from the following relation:

$$w_0 = \sqrt{C_T/2}(\omega R)$$

Wheatley and Bioletti give values of C_T for various blade angles, reference 2, Fig. 7. It is now possible to draw the induced velocity distribution over the rotor disc as it would appear when viewed perpendicular to the flight path. However, the induced velocity is not the total velocity perpendicular to the rotor disc for all conditions. During high-speed flight the rotor plane must be tipped forward to provide the necessary thrust to overcome parasite drag. Thus a component of velocity arises perpendicular to the rotor disc which

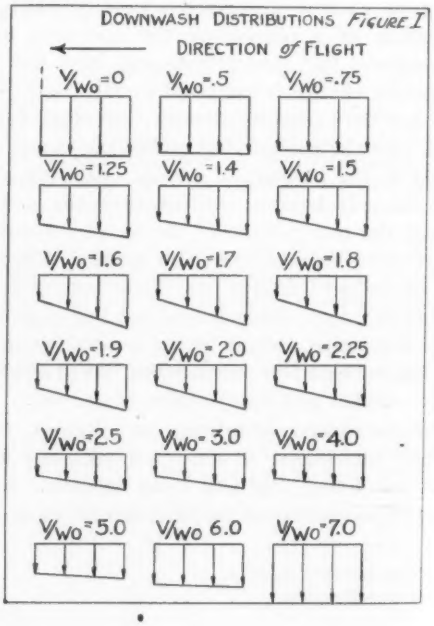

is uniformly distributed over the disc. For the example considered the parasite area of the fuselage was assumed to be 7.0 sq.ft. On the basis of this value the velocity component perpendicular to the rotor disc was computed and added to the induced velocities to give the velocity diagrams shown in Fig. 1.

Writing the equation for lift on a blade element of a flapping rotor.

$$L' = \frac{\rho a c}{2}\left[(\beta - k_1 \sin\psi + k_2 \cos\psi)(v \sin\psi + \omega x)^2 - \frac{wx}{\omega R x + vR \sin\psi}(v \sin\psi + \omega x)^2\right]dx \qquad (1)$$

Since the rotor cannot transmit any rolling or pitching moments into the fuselage because of the presence of the flapping hinges or universal joint, it is necessary to adjust the values of flapping angles k_1 and k_2 so that the rolling and pitching moments of the rotor are zero.

To obtain the lift moment of the blade element about the hub the former equation is multiplied by x.

$$M_L' = \frac{a\rho c}{2} x\left[(\beta - k_1 \sin\psi + k_2 \cos\psi)(v \sin\psi + \omega x)^2 - \frac{wx}{R(\omega x + v \sin\psi)}(v \sin\psi + \omega x)^2\right]dx \qquad (2)$$

Integrating this expression with respect to x,

$$M_L = \frac{a\rho c}{2}\left[(\beta - k_1 \sin\psi + k_2 \cos\psi)\left(\frac{v^2R^2 \sin^2\psi}{2} + {}^2/_3 v\omega R^3 \sin\psi + \frac{\omega^2 R^4}{4}\right) - \frac{w}{R}\left(\frac{vR^3 \sin\psi}{3} + \frac{\omega R^4}{4}\right)\right] \qquad (3)$$

Equating the lift moment of the blade when $\psi = 90°$ to the moment when $\psi = 270°$, the value of k_1 is found to be

$$k_1 = [{}^8/_3\beta\mu - {}^4/_3(w/\omega R)\mu]/(1 + 2\mu^2) \qquad (4)$$

Equating the lift moment of the blade when $\psi = 0°$ to the moment when $\psi = 180°$, the following value of k_2 is obtained:

$$k_2 = (w_2 - w_1)/2\omega R \qquad (5)$$

The equation for the drag of the blade element can be written as follows:

$$D' = \left[\frac{C_{D_P}\rho c}{2}(\omega x + v \sin\psi)^2 + \left(\frac{wx}{\omega x R + vR \sin\psi}\right)L'\right]$$

$$D' = \frac{C_{D_P}\rho c}{2}(\omega^2 x^2 + 2\omega v x \sin\psi + v^2 \sin\psi) + \frac{a\rho c}{2}\left[(\beta - k_1 \sin\psi + k_2 \cos\psi)\frac{w}{R}(\omega x^2 + vx \sin\psi) - \frac{w^2 x^2}{R^2}\right] \qquad (6)$$

Integrating with respect to x,

$$D = \frac{C_{D_P}\rho c}{2}\left(\frac{\omega^2 R^3}{3} + \omega v R^2 \sin\psi + Rv^2 \sin^2\psi\right) + \frac{a\rho c}{2}\left[(\beta - k_1 \sin\psi + k_2 \cos\psi)\frac{w}{R}\left(\frac{\omega R^3}{3} + \frac{R^2 v \sin\psi}{2}\right) - \frac{w^2 R}{3}\right] \qquad (7)$$

To compute the drag on the blade the following procedure is used. First k_1 is determined from Eq. (4). Next, determine the values of k_2 for a series of forward speeds by referring to the velocity diagrams of Fig. 1. Since the angle of attack of the blade is $(\beta - k_1 \sin\psi)$, the parasite drag coefficient is a function of ψ. Values of C_{D_P} are taken from suitable experimental curves that give the parasite drag coefficient as a function of angle of attack. Now, with the values of k_1, k_2, and C_{D_P} the drag of a blade can be determined by substituting in Eq. (7).

Example

The following example is chosen as a typical helicopter:

R = 16 ft.
ω = 300 r.p.m.
c = 0.833 ft. (Blade airfoil N.A.C.A. 0012)
β = 6°

The drag curves are plotted in Fig. 3. Each curve represents the blade drag as a function of forward speed for a given azimuth position. The drag increment between the upwind and downwind positions is shown at the bottom of the figure. It will be noted that the maximum amplitude is found at 25 m.p.h. From Fig. 3 it is also found that the curves for $\psi = 90°$ and 270° cross each other at air speeds in excess of about 60 m.p.h. However, the original assumption that v is small in comparison with ωR limits the validity of the results, and Fig. 3 is an indication of the general trend

at low air speeds only. It should be emphasized that the phenomenon has not been accurately determined by the foregoing analysis and that more experimental work is urgently needed before reliable quantitative results can be obtained.

It was necessary to assume a down-wash distribution in order to use the data of *N.A.C.A. Report No. 536*. It is quite evident that the linear distribution is only an approximation to the reality and may lead to appreciable errors in the final results. Furthermore, the effects of the wind-tunnel boundaries on the flow pattern are unknown and uncorrected.

It was assumed that the pitching moment was solely a result of the down-wash distribution. This would be correct if the coning angle were zero. Coning will lead to a positive pitching moment that will be proportional to the forward speed. Since the coning increases with increased pitch of the blades, this effect will be more pronounced for the high pitch settings, reference 2, Fig. 12.

Conclusions

(1) The problem involved in this paper is by no means solved but has merely been introduced. It is hoped that experimental research programs will be initiated in the near future in an attempt to bring more light on the subject.

(2) With increasing air speed the flow through a rotor is in a state of transition from pure axial flow to a state that is principally transverse flow. During this transition the down-wash velocities are large and unsymmetrical; thus, large variation in induced drag can be expected. These periodic drag forces have not hitherto been considered as a cause of vibrations.

(3) The vibration in two-bladed helicopter rotors observed by several designers and having the characteristic maximum at low air speeds is quite possibly a result of the flow pattern at these low air speeds.

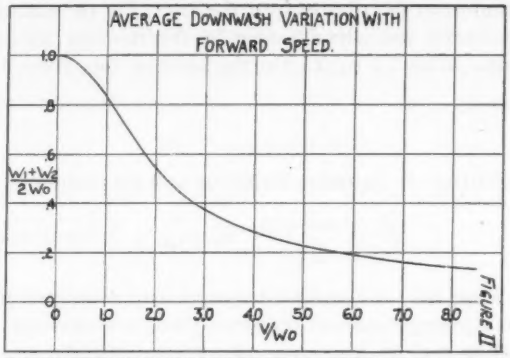

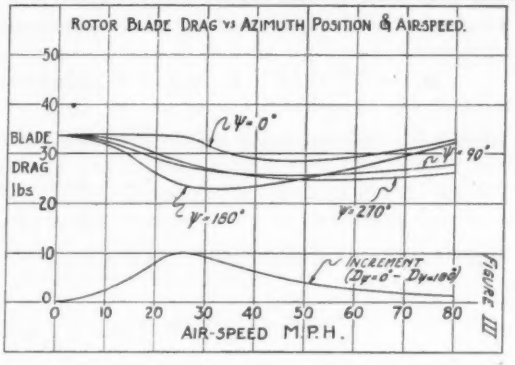

References

[1] Wald, Quentin, *A Method for Rapid Estimation of Helicopter Performance*, Journal of the Aeronautical Sciences, Vol. 10, No. 4, p. 131, April, 1943.

[2] Wheatley, John B., and Bioletti, Carlton, *Wind Tunnel Test of a 10 Foot Diameter Gyroplane Rotor*, N.A.C.A. Report No. 536.

[3] Oehmichen, Etienne, British Patent 303,769.

Stress Analysis of Open Cylindrical Membranes

LEON BESKIN*

Consolidated Vultee Aircraft Corporation

Introduction

It is known that axial stresses in open cylindrical membranes are not completely defined by the axial load and the bending moments in two directions and that supplementary stresses may exist, which are generally ascribed to torque.

Those stresses, in the case of conventional approximations, can generally be neglected for closed membranes. They cannot be neglected for open membranes since they are necessary to insure the local equilibrium under general loading. As those stresses may exist even when no torque is applied, in the same manner as stresses due to bending exist in pure bending (without shear), a method of determination of the distribution of axial stresses which would generalize the formula My/I for pure bending is developed hereafter. Those axial stresses can be combined by addition (superposition) with the stresses due to axial load and bending.

In order to obtain this result a new mechanical concept must be introduced. This concept is called a bicouple (B) and it has the same relationship with the warping curvature $d^2\theta/dz^2$ (θ = angle of twist; z = ordinate along generators) as a couple has with the conventional curvature $d^2\theta/dz^2 = B/EI_0$, in which I_0 is the torsion bending constant.

Under nonuniform warping without bending or axial load, the axial stresses constitute a bicouple. In the case of uniform warping curvature ($d^2\theta/dx^2$ = Const.) the distribution of axial stresses, f, is completely defined by the value of the bimoment, following the relation: $f = BA/I_0$, in which A is an area.

In the case of symmetrical profiles, the analogy with bending can easily be developed by introducing a "conjugate beam" placed in the plane of symmetry, the center of gravity of which is the shear center of the given section, and the moment of inertia of which is equal to I_0. For unsymmetrical profiles, a conjugate beam can also be introduced, but its location has no definite relationship with the given section and it has a less important physical significance than in the case of symmetrical profiles.

The concept of the bicouple and the relations which are its consequences are "true" in the sense of the theory of elasticity provided the membrane has no thickness and deflections are infinitely small. The extension of the theory to the condition of a membrane under applied end torque is similar to the extension of pure bending distribution to cantilevers under applied transversal end load. A uniform warping curvature due to constant shear distribution does not affect the distribution of axial stresses. Those stresses still constitute a bicouple but as they are proportional to the distance to the end section, the bicouple is proportional to the product of the torque by the distance to the end section, and the definition of a bicouple is such that the two quantities are equal. This product will be called the bimoment of the torque in respect to the section and in any section the bicouple of the axial loads is equal to the bimoment of the torque.

The relationship between bimoment and torque can be conventionally extended to any loading condition, the torque being the opposite of the derivative of the bimoment taken along the axis of the membrane, but for an arbitrary loading the relation between distribution of stress and bicouple is not absolutely correct; however, it can be applied in the same manner as the formula My/I is applied for any load distribution in conventional stress analysis.

Received January 12, 1944.

* Structures Engineer, San Diego Division.

Notations

A	= areas from the shear center and a polar line, limited to the directrix
A^*	= same areas from an arbitrary line
A_0	= $A - A^*$
A'	= areas inside a contour (Fig. 6)
A_D	= area inside directrix (closed membrane)
a, a'	= finite area of a member; area between two generators
a_0	= total area of a section
B	= bimoment in respect to the shear center; bicouple
B_α	= bimoment in respect to an arbitrary point 0
B', B'', B_α', B_α''	= bimoments at the ends of a membrane
B_1	= bimoment in respect to center of rotation
b	= bimoment due to a unit load
b_b, b_m, b_z, b_y, b_x, b_c, b_k	= bimoment due to a unit bicouple, couple, load in x, y, z direction, redundant load X_c, X_k
b_m', b_z', b_y' b_x'	= corresponding bimoment for the statically indeterminate system
D	= length of the directrix
d	= distance from shear center (Fig. 6)
d_0	= depth of the conjugate beam (Eq. (44))
E	= modulus of elasticity
f	= axial stress
$f(s)$	= substitution function (Eq. (2))
G	= modulus of rigidity
g_x, g_y, g_z, g_m	= load coefficients for unit loads in x, y, z directions and unit couple
$g(s)$	= substitution function (Eq. (3))
h, h_1, h_2	= thickness of a membrane
I_0	= moment of inertia in torsion bending (Eq. (25))
I_0', I_0''	= corrected values of I_0 (*see* Example of Application)
I_α	= moment of inertia in torsion bending in respect to an arbitrary point
I_x, I_y	= principal moments of inertia
J_b	= shear rigidity coefficient for torsion bending
J_1, J_2, J_{12}, J_{21}	= various shear rigidity coefficients (*see* Example of Application)
L	= length of generators
L_1, L_2	= length of generators (*see* Example of Application)
M	= torsional moment in respect to shear centers; torque
M_α	= torsional moment in respect to an arbitrary point 0
M_x, M_y	= bending moments in respect to the principal axes x, y

M_ξ, M_η = bending moments in respect to arbitrary axes ξ, η
m = local couple (Eq. (30))
m_y, m_m = couples due to unit loads y, m (*see* Examples of Application)
N_1 = axial stress flow along directrix
N_2 = axial stress flow along generators
N_2', N_2'' = axial stress flow at the ends of a membrane
N_{12} = shear flow along directrix and generators
P = concentrated load in a member
P', P'' = symmetrically located loads (Eq. (43))
Q = shearing force on an element of directrix (Figs. 4, 6)
q = unit shear flows
q_x, q_y = unit shear flows for X and Y forces
q_0, q_1, q_2, q_3 = unit shear flows (*see* Example of Application)
r = ratio of load increase (*see* Example of Application)
$S = ay^2$ = *see* (Eq. (31))
s = arc along the directrix
s_{12}, s_{23} = lengths along directrix (Fig. 4)
T, T', T'', T_y, T_y', T_y'', T_m, T_m', T_m'' = multiplicators for strain energy coefficients (*see* Example of Application)
W = strain energy
X, Y = shearing forces along axes x, y
X_c, X_k = redundant unknowns (*see* Example of Application)
x, y = principal coordinates through center of gravity, in a section
x_0, y_0 = coordinates of the shear center
x_1, y_1 = coordinates of center of rotation
x' = coordinates in the conjugate beam, from center of gravity (Fig. 6)
x_T = coordinate from thrust line (*see* Example of Application)
x_{T0}' = coordinate of shear center, from thrust line
x_T' = coordinate in the conjugate beam, from thrust line
$\bar{x}$, $\bar{y}$ = coordinates with origin at shear center, parallel to principal coordinates
Z = force along direction of generators
z = coordinate along generators
α = areas from an arbitrary point 0 (*see* A)
α_0 = difference of areas (Eq. (45))
$\bar{\alpha}$ = area from center of rotation
Γ = arbitrary quantity (Eq. (60))
δ = distances to shear center (Fig. 4)
η, ξ = arbitray coordinates in the plane of the directrix
θ = angle of twist
λ = a function (Eq. (60))
U, L = (indices) refer to upper and lower longeron (*see* Example of Application)

General Principles of Stress Analysis Under Torsion Bending for Unsymmetrical Sections

Consider an open cylindrical membrane limited by two plane sections on which edge loads are applied (Fig. 1). The coordinates on the cylinder are s along the directrix and z along the generators (length L). It is assumed that only inplane stresses exist in the membranes which is limited by two bulkheads.

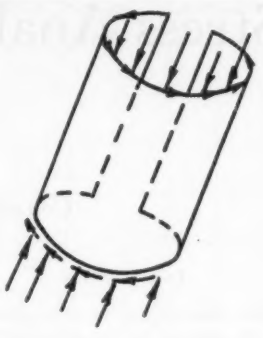

Fig. 1.

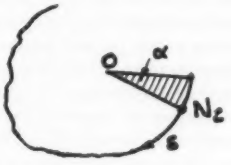

Fig. 2.

The stresses are expressed in terms of stress flows (stress × thickness): N_1 = axial flow along directrix; N_2 = axial flow along generator (given values N_2', N_2'' at the ends); N_{12} = shear flow along directrix and generator.

The conditions of equilibrium of the membrane are

$$\frac{\partial N_1}{\partial s} + \frac{\partial N_{12}}{\partial z} = 0 \qquad \frac{\partial N_2}{\partial z} + \frac{\partial N_{12}}{\partial s} = 0 \tag{1}$$

When there are no surface loads, there is no hoop tension N_1. Then Eqs. (1) can be successively integrated

$$N_{12} = N_{12}(s) = -(1/L)\int f(s)ds \text{ say} \tag{2}$$

$$N_2 = (z/L)f(s) + g(s) \tag{3}$$

These equations signify that along a generator, the shear flow is constant and the axial flow varies uniformly.

At the ends $z = 0$ and $z = L$ the conditions of equilibrium are

$$N_2 = g(s) = N_2' \qquad N_2 = f(s) + g(s) = N_2'' \tag{4}$$

Thus

$$f(s) = N_2'' - N_2' \tag{5}$$

$$N_{12} = \int_0^s [(N_2' - N_2'')/L]ds \tag{6}$$

In an open membrane, the shears along the end generators must be equal to zero. The index D standing for the integration along the total length of the directrix, this condition of zero end shear is

$$\int_D [(N_2' - N_2'')/L]ds = 0 \tag{7}$$

Call α the area taken from an arbitrary origin 0 and limited by the arc of directrix between the extremity

and a given point, and by two radii extending from 0 to the ends of the arc (Fig. 2). The condition of equilibrium of moments on the bulkheads is

$$2\int_D N_{12}d\alpha = M_\alpha \tag{8}$$

M_α being the moment of the forces applied in the plane of each bulkhead taken in reference to 0.

The integral in Eq. (8) can be transformed by integration by parts, using Eq. (6) for N_{12}, and introducing the condition of zero shear along the end generators

$$\begin{aligned} 2N_{12}\alpha]_0^D - 2\int_D \alpha dN_{12} &= M_\alpha \\ 2\int_D \alpha[(N_2'' - N_2')/L]ds &= M_\alpha \end{aligned} \tag{9}$$

The last expression is equivalent to

$$2\int_D \alpha N_2''ds = 2\int_D \alpha N_2'ds + M_\alpha L = B_\alpha''say \tag{10}$$

The quantity B_α'' is the bimoment of forces N_2'', acting on the section $x_2 = L$ in respect to the origin of the areas α.

Thus, introducing the general definition of a bimoment B_α

$$B_\alpha = 2\int_D \alpha N_2 ds \tag{11}$$

it appears that when a torque is applied, the relationship between torque and bimoment is

$$B_\alpha'' = B_\alpha' + M_\alpha L \tag{12}$$

and when no torque is applied

$$B_\alpha'' = B_\alpha' \tag{12a}$$

Those equations show the equivalence between bimoments and torques multiplied by lengths of application along open membranes. Thus, when a torque M is applied at one end of an open membrane, at the opposite end the axial forces constitute a bimoment B_α'' such as

$$B_\alpha'' = M_\alpha L \tag{12b}$$

The definition of a bimoment B can be extended for a semimonocoque structure; with general distributed axial flow N_2, and concentrated forces P along some of the generators (longerons or stiffeners), the bimoment is

$$B_\alpha = 2\int_D \alpha N_2 ds + 2\Sigma \alpha P = 2\int_D \alpha f da \tag{13}$$

where f = axial stress and da = elemental area.

It is to be noted that the definition of the bimoment is independent of the pole and origin radius only if the resultant and couple of the axial forces are zero, in which case the axial forces constitute a bicouple, in the same manner as the value of moment of axial forces is independent of the axis of reference only when there is no resultant of the axial forces.

The results obtained thus far show that for an open cylindrical membrane, the three conventional conditions of equilibrium are insufficient to define axial loads in a section. To these conditions, it is necessary to add the condition of "equilibrium of bimoments" (Eq. (12)) or its two special cases (Eqs. (12a) and (12b)), which can be also called "condition of open membranes."

Knowing applied loads at the end of a solid of elongated shape, it is possible to determine the stress distribution at some distance from the end by means of the conventional formulas for bending and axial loads, because of Saint Venant's principle. Since for open membranes an equation of equilibrium of bimoments must be added to the conventional equations of equilibrium, it is necessary to modify Saint Venant's principle to cover that case.

St. Venant's Principle for Open Membranes With Bulkheads

Two statically equivalent systems of axial loads applied at one end directrix, which satisfy the condition of equivalence for membranes, produce approximately the same axial stresses at a distance from the end directrix which satisfies the following conditions: (1) It is equal to several times the greatest dimension in the plane of the directrix; (2) it includes at least two bulkheads.

Saint Venant's principle indicates that there is a privileged distribution of axial loads, but does not define it. For any given end distribution of axial loads the actual distribution along the generators, which at some distance from the end becomes the privileged distribution, must satisfy the theorem of minimum energy under axial loads, which gives a method of determination of these loads.

If constant shearing forces and torques are applied, the distribution of axial forces is not affected, since for two dimensional problems with constant transversal loads, shear produces a distortion of the plane sections without producing a curvature of the generators, which are simply displaced by translation in respect to one another. The solutions considered here presuppose the existence of bulkheads for redistribution. When the redistribution is effected, the following bulkheads are not loaded, which shows that the asymptotic privileged distribution is the one for which the shape of the cross section of the cylinder does not change, thus giving a second method for determining the distribution. This does not necessarily mean that a bulkhead remains plane; if there are applied torques or if the shearing forces do not have a resultant passing through the shear center, the bulkheads will come out of plane (warping of the sections). Conventional methods initiated by Wagner[1, 2] and developed by Kappus[3] and clarified by Goodier[4, 5] and by Hoff[6] give the privileged distribution of axial loads under bimoment when the latter is caused by shearing forces or a torque. From consideration of the deformation because of the warping caused by a rotation around an axis passing through an arbi-

trary point 0 (Fig. 2), it is found that the longitudinal stresses f are given by a relation of the type

$$f = K\alpha \tag{14}$$

The axes of coordinates being the principal axes of inertia x, y of the section and the origin for areas α being the shear center of the section, with a suitable choice of the polar line origin of α, Eq. (14) can be written as

$$f = \frac{Z}{a_0} - \frac{M_y x}{I_y} + \frac{M_x y}{I_x} + \frac{B 2A}{I_0} \tag{15}$$

in which

a_0, I_x, I_y = area and principal moments of inertia of the section
Z, M_x, M_y = axial load and bending moments on the section
A = areas α in reference to shear center and polar line indicated above, the end point of which is called "neutral point"
I_0 = torsion bending constant
B = bimoment in respect to shear center

Calling X, Y, M the shearing forces and torque (in reference to the shear center), the shear flow is

$$N_{12} = \int_0^s da \frac{\partial f}{\partial z} = X \int_0^s \frac{x da}{I_y} + Y \int_0^s \frac{y da}{I_x} + M \int_0^s \frac{2A da}{I_0} \tag{16}$$

The summations are carried from one end generator to the generator along which the shear is computed.

Eq. (15) is the generalization of formulas established in references cited above by substitution of the bimoment B to the product Mz. Since the torque M is to be taken in respect to the shear center, the bimoment B, which is a generalization of the product Mz (see Eq. (12)), is also to be taken in respect to the shear center. Such generalization of previous results to Eq. (15) may appear dubious. Also, in the conventional methods, various assumptions are made: warping is considered as being caused by axial strain only, and shearing strain is omitted, which is in contradiction with the fact that torsion bending is ascribed to torque and presupposes nonuniform warping due to nonuniform shear distribution; transversal strain is also disregarded. As no infinitesimal geometry is introduced there may be doubt on the validity of the results, since it is not possible to find the limitations of the conventional methods which are actually valid only for constant or uniformly varying rate of twist.

An analysis, solely based on considerations of energy, which are valid only in case of constant shearing forces (as indicated above), is developed in the appendix, and gives directly Eq. (15).

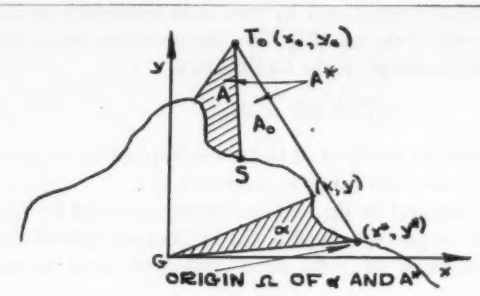

FIG. 3.

PRACTICAL DETERMINATION OF SECTION PROPERTIES AND LOAD DISTRIBUTIONS UNDER GENERAL LOADING

1. Determine the total area a_0, the principal axes of inertia of the section and the principal moments of inertia (I_x, I_y).

2. Determine the center of shear in respect to the principal axes by its coordinates (x_0, y_0)

$$y_0 = -\int 2\alpha x da / I_y \qquad x_0 = \int 2\alpha y da / I_x \tag{17}$$

in which da are the elemental areas of the section. The polar areas α can be taken from the centroid or any other point. They are positive if the polar line rotates in a direction which brings the axis ox on the axis oy.

3. Determine the areas A having the shear center T_0 and a polar line T_0S ending at a neutral point S for origin. "Neutral points" S, so called because, under pure bicouple, there is no strain at these points, are defined by the condition

$$\int 2A da = 0 \tag{18}$$

For a convex section, there are three neutral points and any of them can be taken for the origin.

A temporary origin line for areas A being chosen, for instance corresponding to the same origin point on the profile as for the areas α, the areas A, called A^* in that case, are related to α by

$$2A^* = 2\alpha - x_0 y + y_0 x + x_0 y_* - y_0 x_* \tag{19}$$

in which (x_*, y_*) are the coordinates of the origin Ω common to α and A. Then the areas A are defined by

$$2A = 2A^* - (2\int A da / a_0) = 2A^* - 2A_0 \tag{20}$$

It is immaterial to find, by means of Eq. (20), the actual location of a neutral point.

4. Determine the torsion bending constant I_0 by

$$I_0 = \int (2A)^2 da \tag{21}$$

I_0 can be defined by

$$I_0 = \int (2A^*) da - a_0 (2A_0)^2 = \int (2\alpha)^2 da - a_0 (2A_0)^2 - I_x x_0^2 - I_y y_0^2 \tag{22}$$

5. Eq. (15) gives the values of axial stresses in each point and Eq. (16) gives the values of shear flow along each generator. The moments in Eq. (15) are those of

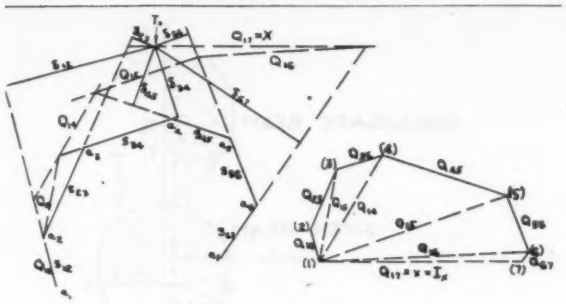

FIG. 4.

the resultant axial force Z in respect to the axes passing through the center of gravity; the bimoment is equal to the value of the resultant shearing force multiplied by its distance to the shear center line (giving the torsion) and by its distance to the section.

6. *Graphical determination of the shear center* (Fig. 4). The shear center is the point through which shearing forces pass in bending without torsion bending. Thus, the problem is that of determining the resultants of forces $Q = qs$, the unit shears q being given by the expressions

$$q_x = \sum xa \qquad q_y = \sum ya \tag{23}$$

s being the distances between the successive finite areas a. The computation is repeated in two directions (x, y) which are not necessarily the principal directions. It is to be noted that I_x, I_y have been omitted in Eq. (23) since they are constants of proportionality. Fig. 4 shows the procedure for one direction, x. The membrane being defined by the directrix $a_1a_2 \ldots a_7$, the forces Q parallel to the sides of the membrane are computed, the quantities x being taken from the centroid along an arbitrary direction. A force polygon (1)–(7) is drawn. The resultants Q from one end are shown in dotted lines, and the resultants in position are determined by the conventional method (for instance, Q_{14}, Q_{15} intersect on a_4a_5). The general resultant is finally located in position. Its value gives the moment of inertia I_y, which can be determined by this method. Operating in the same manner in direction y, the second direction of resultant is obtained, and the intersection gives the shear center T_0.

7. *Graphical determination of stress distribution in torsion bending with the use of a conjugate beam.* Consider the areas $2A$ as ordinates along the web of a fictitious beam, with members of areas da or finite areas a being placed at each ordinate $2A$. Then, if M and B are the shear and the moment applied to the conjugate beam, it is obvious that

$$f = B2A/I_0 \qquad N_{12} = M\int_0^s 2Ada/I_0 \tag{24}$$

since the centroid of the beam is at the origin of the ordinates (Eq. (18)).

From Fig. 4 it appears that

$$2A = 2A^* + 2A_0 = \sum s\delta + A_0 \tag{25}$$

the areas $2A^*$ being taken from one end of the directrix, and the distances δ being taken from the shear center to the successive sides s. Adding along an axis the products $s\delta$, as shown on Fig. 5, and affecting the end points with the areas a, the conjugate beam is determined.

As the quantities $s\delta$ change sign where the lines a_na_{n+1} pass from one side to the other of the shear center, the beam appears to have a folded web and is expanded sideways for clarity. The quantities $2A^*$ are taken, for instance, from the origin point a_1, and the quantities $2A$ are taken from the centroid of the beam. It is obvious that since the web intersects the neutral line three times, there are three neutral points which are directly determined by dividing the distances from the center of gravity of the conjugate beam to the nearest areas a by the corresponding δ, thus locating the neutral points on the actual contour.

The moment of inertia I_0 of the conjugate beam (Eq. (21)) and the axial stresses and shear flows (Eqs. (24)) are determined in a conventional manner.

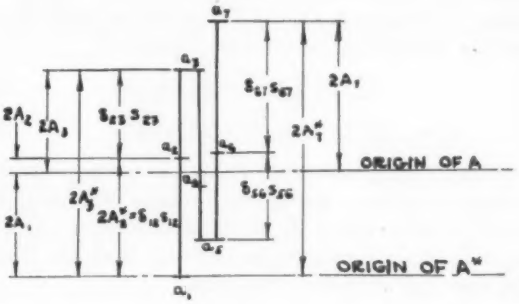

FIG. 5.

SIMPLIFIED TORSION BENDING THEORY FOR SYMMETRICAL PROFILES

In the case of a symmetrical profile a direct analysis can be made as follows, considering torsion bending only, without introducing symmetrical bending and normal forces. Assuming a section as shown, consider two small areas a, a, along the profile, these areas being submitted to forces P, $-P$ (axial forces) caused by a shearing force Q applied at a distance z from the section. This shearing force is located at a point T, the distance of which to the line aa is (Fig. 6)

$$d = 2A'/2y = A'/y \qquad x' = x + (A'/y) \tag{26}$$

A' = area enclosed by the profile and the chord aa; (x, y) = coordinates of a; x' = coordinate of T. The relation between P and Q is

$$P = Qz/2y \tag{27}$$

The applied forces are given, thus the forces Q have a resultant equal to a given couple M_a and a given force Y (with the centroid as reference point).

The conditions of equilibrium are

$$\sum Q = Y \qquad \sum Qx' = M_\alpha \tag{28}$$

An analogy with a beam problem defines the distribution of the stresses. The condition of minimum strain energy is

$$\sum (P^2/a) = \text{minimum} \tag{29}$$

Replacing P in function of the couple m

$$m = 2Py = Qz \tag{30}$$

and introducing the notation

$$S = ay^2 \tag{31}$$

Eqs. (28) and (29) become

$$\sum m = Yz = M_x \qquad \sum mx' = M_\alpha z = B_\alpha \tag{32}$$

$$\sum (m^2/S) = \text{minimum} \tag{33}$$

This is the same set of conditions as those existing in a beam defined by areas S, ordinates x', submitted to an axial load M_x, a couple B_α, the axial loads on the areas S being called m. The centroid of that beam, called "conjugate beam" is T_0; it has an ordinate x_0, and the moment of inertia of the beam is I_0

$$x_0 = \sum Sx'/\sum S = 2\sum ay^2x'/I_x \tag{34}$$

$$I_0 = 2\sum S(x' - x_0)^2 = 2\sum ay^2(\bar{x})^2 \tag{35}$$

in which $\bar{x}$ is the distance TT_0, and $I_x = 2\Sigma ay^2$ (area of conjugate beam). Using the formulas of beams, and referring the moment M_α and bimoment B_α to the centroid T_0 of the conjugate beam which from Eq. (34) is the shear center of the given beam

$$m = B(2ay^2\bar{x}/I_0) + M_x(2ay^2/I_x) \tag{36}$$

Using relations between m, N_{12} and P

$$P = B\frac{ay\bar{x}}{I_0} + M_x\frac{ay}{I_y} \qquad N_{12} = M\sum\frac{ay\bar{x}}{I_0} + Y\sum\frac{ay}{I_x} \tag{37}$$

M and B are to be taken in respect to the shear center T_0.

Relationship Between the General Method and the Method for Symmetrical Sections

General Eq. (17), giving the shear center, can be identified with special Eq. (34) for symmetrical profiles. From the definition of α it appears that (Fig. 7)

$$2\alpha = A' - xy = dy - xy = x'y$$

Thus, Eq. (17) becomes:

$$x_0 = \int 2\alpha y da/I_x = 2\sum y^2x'a/I_x$$

As the summation of the general formula is made for both sides and the summation for symmetrical profiles is made for one side, a coefficient 2 must be introduced into the numerator and the above equation becomes identical with special Eq. (34).

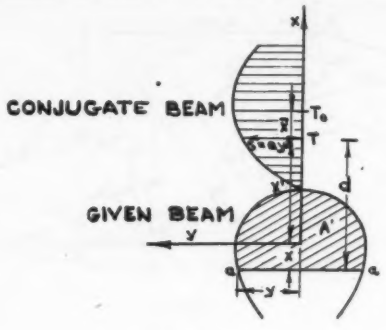

Fig. 6.

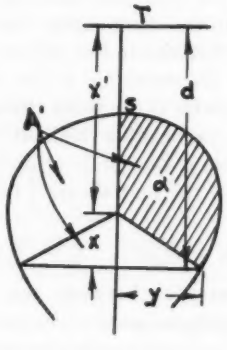

Fig. 7.

Practical Determination of Section Properties and Load Distribution of Symmetrical Profiles

(1) Introduce a conjugate beam of the open profile, determined as follows: For each couple of areas a of the profile there is a corresponding area $2ay^2 = 2S$ of the conjugate beam. This area is located at the center of torsion of the couple of areas a, in respect to the given profile (i.e., at a distance A'/y from the line of areas a, on the center line, A' = area enclosed by the profile from one area a to the other; with a straight closing line, $2y$ = distance between the two areas a).

(2) The centroid of the conjugate beam coincides with the center of shear of the given profile. The area of this conjugate beam is equal to the moment of inertia I_y of the profile in respect to the center line. The moment of inertia I_0 of the conjugate beam is the torsion bending constant.

(3) The distribution of the shearing forces related to a couple of areas a, and the distribution of the moments and the normal forces acting on the areas a, under given lateral load Y (perpendicular to the axis of symmetry) and couple M_x, and a moment M and bicouple B (taken in reference to the center of shear), are given by Eqs. (36) and (37).

(4) *Graphical method of determination of shear centers and construction of the conjugate beam for symmetri-*

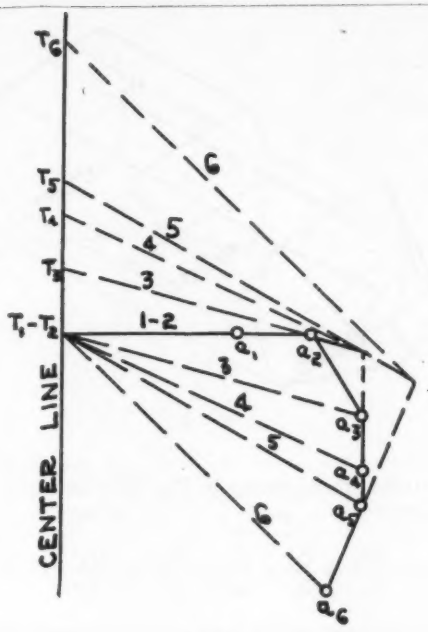

FIG. 8.

cal sections(Fig. 8). The shear center of two symmetrically located areas is placed at the intersection of the resultant of a uniform shear acting along the membrane between the two points, and the center line. Taking a shear flow equal to one unit force per unit length, the shearing forces along elements of the profile are proportional to those elements. Thus a force polygon is given by the profile itself. In order to determine the location of the forces, proceed as follows (Fig. 8): The force acting on Sa_1 is equal to Sa_1 and is applied along Sa_1. The same holds true for a_1a_2; thus the resultant is along Sa_2 and is equal to Sa_2, and the shear cehters T_1T_2 of a_1 and a_2 are both in S. The force acting on a_2a_3 is applied on a_2a_3 and is equal to a_2a_3. The resultant of Sa_2 and a_2a_3 passes through a_2 and has the magnitude and direction given by Sa_3.

Thus, drawing the parallel 3 through a_2 to Sa_3, the point T_3 on the center line is determined, which is the intersection of two symmetrically located resultants for the two halves of the profile. Thus the resultant of the shearing forces between symmetrical points a_3 passes by T_3, which is the shear center of the profile between points a_3. Adding the shear between a_3a_4 to the previous shear, take the intersection of a_3a_4 with the resultant T_3-3 of the shears between S and a_3, and through this intersection draw the parallel 4-T_4 to the resultant of the forces acting between S and a_4, which is Sa_4. Line T_4-4 gives the location of the resultant and T_4 is the shear center of the profile between symmetrically located points a_4. The process can be repeated as shown until the whole profile is explored and the different points $T_1 \ldots . T_n$ of the conjugate beam are located. Affecting the points with areas $a_n y_n^2$ (note that for points which correspond to a skin point of noneffective area, $a_n = 0$), it is easy to determine the section properties of the conjugate beam.

Definition of the Bicouple for Symmetrical and Nonsymmetrical Membranes with the Help of a Conjugate Beam

The definition of the bicouple acting on a given section is given by Eq. (13) in which the origin of polar areas is *arbitrary if there is no external load applied* ($Z = 0$, $M_x = 0$, $M_y = 0$), and in which the origin of polar areas *must be taken from the sheat center and a polar line passing through one neutral point if there are external loads applied.* In that case Eq. (13) is to be replaced by

$$B = 2\int_D AN_z ds + 2\sum AP \tag{38}$$

Nonsymmetrical Membranes

Introducing the conjugate beam, apply at each area a of the conjugate beam the load P and the following relations hold between the loads the moments and the bimoment

$$\sum P = Z \qquad \sum P2A = B \tag{39}$$

$$\sum Py = M_x \qquad \sum Px = -M_y \tag{40}$$

From Eqs. (39) the bimoment is represented by the moment of a force Z acting on the conjugate beam since the quantities $2A$ are ordinates on the beam. If the end loads P are known, Eqs. (39) and (40) give the components of the load acting on the section in terms of statics and the additional quantity called bimoment. Applied loads do not necessarily follow distributions corresponding to the theory of beams, but at some distance from the end the distribution will correspond to the beam theory. Since Eqs. (39) and (40) give all the necessary components at the end, the components at any section will be (affecting with a prime (′) the end components)

$$\left.\begin{aligned} Z = Z' \quad B = B' + Mz \\ M_y = M_y' - Xz \quad M_x = M_x' + Yz \end{aligned}\right\} \tag{41}$$

Symmetrical Membranes with Antisymmetrical Loading

Introducing the conjugate beam, apply at each area S of the beam the load defined by the moment $m = 2Py$, thus obtaining the relations

$$\sum m\bar{x} = B \qquad \sum m = M_z \tag{42}$$

The bicouple B acting on an open symmetrical profile is represented by a fictitious couple acting on its conjugate beam, and the couple M_z is represented by a fictitious axial load acting on its conjugate beam, the fictitious forces acting at each point of the conjugate beam being equal to the couples acting at the corresponding pairs of points of the given beam. The sum

of these couples is equal to the total couple M_z, and the moment in respect to the general shear center of these couples located at the local shear centers is equal to the total bicouple B.

Symmetrical Membranes with General Loading

In that case, each couple, $m = 2Py$, will be replaced by a moment $(P' - P'')y$, P' and P'' being the axial forces applied to symmetrically located areas. Thus

$$B = \sum(P' - P'')y\bar{x} \qquad M_z = \sum(P' - P'')y \quad (43)$$

For a four-flanged open membrane, submitted to a pure bicouple, the moments $m = 2Py$ for both pairs of flanges are opposite, and the bicouple is equal to the common moment $(2Py)$ multiplied by the distance between the two shear centers of the pairs of flanges, which is the depth d_0 of the conjugate beam

$$B = 2Pyd_0 \quad (44)$$

Statics of Bimoments and Moments of Inertia in Torsion Bending

When the pole and polar line from which areas for bending moments are computed are changed from the shear center to a point having the coordinates $(\bar{x}, \bar{y})$ in respect to the shear center, and keeping the coordinates (x, y) of the directrix in respect to the centroid, the following relationship may be written for the areas α as functions of the areas A

$$2\alpha = 2A + (\bar{x}y - \bar{y}x) + 2\alpha_0 \quad (45)$$

If the origin on the directrix is the same for A and α, α_0 represents the area of the triangle defined by that origin, the center of gravity and the shear center.

Applying Eqs. (15) and (13) and using the definitions of A_0, I_x, I_y, I_0, $\bar{x}$, $\bar{y}$, the value of the bimoment B_α is

$$B_\alpha = \int_D 2f\alpha da = B + \bar{x}M_x + \bar{y}M_y + 2\alpha_0 Z \quad (46)$$

which is an expression of the type of those used for moments when the origin of coordinates is changed. This relation is valid only when principal coördinates are used. When B can be replaced by Mz, Eq. (46) becomes

$$B_\alpha = Mz + M_x\bar{x} + M_y\bar{y} + 2Z\alpha_0 \quad (47)$$

which is an entirely symmetrical formula.

There exists a point in respect to which Eq. (15) becomes

$$f = B2\bar{\alpha}/I_0 \quad (48)$$

The coordinates of that point being (x_1, y_1) in respect to the centroid.

Identifying Eq. (48) with Eq. (15)

$$y_1 = \frac{M_y}{B}\frac{I_0}{I_y} \qquad x_1 = \frac{M_x}{B}\frac{I_0}{I_x} \qquad 2\bar{\alpha}_0 = \frac{Z}{B}\frac{I_0}{a_0} \quad (49)$$

$$2\bar{\alpha} = 2A + (x_1y - y_1x) + 2\bar{\alpha}_0 \quad (50)$$

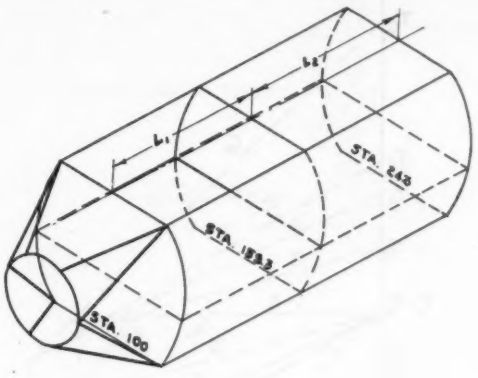

FIG. 9.

Substituting those values in Eq. (47), in which B_α becomes B_1.

$$\frac{BB_1}{I_0} = \frac{B^2}{I_0} + \frac{Z^2}{a_0} + \frac{M_x^2}{I_x} + \frac{M_y^2}{I_y} \quad (51)$$

That expression can be used in strain energy computations. The point (x_1, y_1) is the center of rotation in complex torsion bending, and the points corresponding to $\bar{\alpha} = 0$ are the neutral points in complex torsion bending (i.e., torsion bending with bending and axial load). It is to be noted that an expression of the type used for transformation of moments of inertia can be established for I_α

$$I_\alpha = \int(2\bar{\alpha})^2 da = I_0 + \bar{x}^2I_x + \bar{y}^2I_y + a_0(2\alpha_0)^2 \quad (52)$$

In this expression, I_x and I_y are taken in respect to the center of gravity, and I_0 in respect to the shear center.

Example of Application

The following example is taken from an airplane fuselage analysis (Fig. 9).

The fuselage is an open membrane from the firewall of the engine mount (station 100) to the main spar (station 159.3) and a closed membrane from the main spar to a bulkhead (station 243). The engine mount has a dissymetrical structure and is assembled by four points to the fuselage, the points of attachment corresponding to the four longerons. Fig. 10 shows a cross section of the open part, the floor being the horizontal shear web. The closed section has a web at the level of the upper longerons. On Fig. 10 are determined the local shear centers, by the general method of Fig. 8.

Axial Loads

Table 1 gives the computations of section properties in torsion bending for distribution of axial load. Column 11 gives the load coefficients per longeron or stringer. The complete structure being redundant, strain energy coefficients must be computed. If a torque is applied at the firewall, the rigidity coefficient

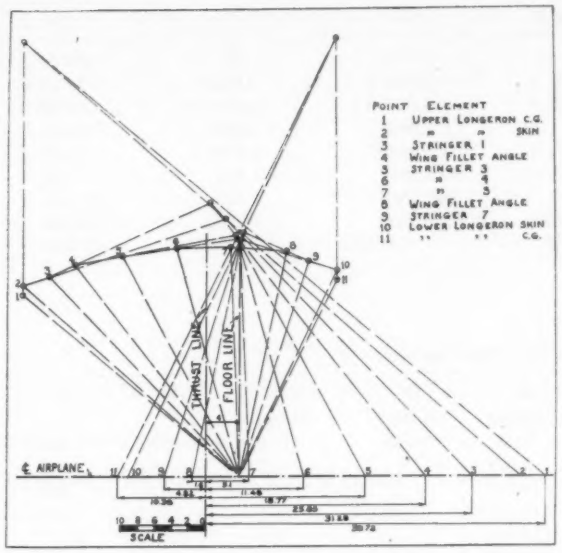

FIG. 10. Torsion bending between stations 100 and 243. Determination of shear centers.

is I_0. If a bicouple is applied at the firewall, the load being transmitted by the four longerons only and then redistributed to the whole structure between stations 100 and 159.3, the rigidity is smaller than if the loads were distributed at station 100 according to the torsion bending theory. The redundant loads in the engine mount produce bicouples only, since they are in equilibrium inside the engine mount. For distribution at longerons only the loads under $B = 1$ are indicated in Table 1, reference VIII.

Let L_1 and L_2 be the lengths of the open and closed section ($L_1 = 59.30$; $L_2 = 83.70$). X_c, X_k are the redundant loads in the engine mount; $g_z \ldots g_y$ are the load coefficients multiplying symmetrical and antisymmetrical unit load conditions, respectively; b_c, b_z, b_y are the bicouples at the firewall caused by a unit redundant load, a unit symmetrical load, and a unit antisymmetrical load (calculated by means of Eqs. (43) and (44)); and m_y is the couple at the firewall caused by a unit antisymmetrical load (in respect to shear center).

The bimoment B is of the type:

$$B = \sum b_c x_c + \sum b_z g_z + \sum b_y g_y + z \sum b_y m_y$$

By integration of the quantity B^2/I_0 along the structure, strain energy terms are obtained. They can be written in the following form (see Table 2), in which numerical coefficients T', T_y' are given hereafter.

TABLE 2

Terms	Coefficients
$X_c^2 b_c^2 T'$; $X_c X_k b_c b_k T'$ ..... $X_c g_z b_c b_z T'$	$T' = \dfrac{L_1}{I_0'} + \dfrac{L_2}{3I_0}$
$X_c g_y b_c T_y'$	$T_y' = \dfrac{L_1 b_y}{I_0'} + \dfrac{L'^2 m_y}{I_0''} + \dfrac{L_2(b_y + m_y L')}{3I_0}$

$T' = 0.00004998$; $T_y' = 443.2$; $T_m' = 464.4$

The quantities I_0', I_0'' replacing I_0 are caused by the

TABLE 1

Determination of Axial Load Distributions

Point	Element	a (1)	y (2)	S = ay^2 (3)	ay/I_x (4)	x_T (I) (5)	x_T' (II) (6)	Sx_T' (7)	$\bar{x} = x_T' - xT_0'$ (III) (8)	$S\bar{x}$ (9)	$S\bar{x}^2$ (10)	$(ay\bar{x}/I_0)$ 10^8 (V) (11)
1	*UL* c.g.	1.239	21.30	562.12	0.00494	21.52	−39.72	−22,327	−27.528	−15,474	425,968	−36,896
2	*UL* skin	0	. .	....	.....	.....	.....	....	....	....	....	....
3	S1	0.264	23.44	145.05	0.00116	18.40	31.28	−4,537	−19.088	−2,769	52,855	−6,001
4	W1	0.511	24.78	313.78	0.00237	15.48	−25.85	−8,111	−13.658	−4,285	58,525	−8,782
5	S3	0.211	25.81	140.56	0.00102	9.86	−18.77	−2,638	−6.578	−925	6,085	−1,821
6	S4	0.215	26.78	154.19	0.00108	3.42	−11.48	−1,770	0.712	110	78	211
7	S5	0.219	26.87	158.12	0.00110	−2.96	−5.1	−806	7.092	1,121	7,950	2,118
8	W2	0.651	26.33	451.32	0.00321	−9.58	1.60	722	13.792	6,225	85,855	12,006
9	S7	0.232	25.18	147.09	0.00109	−12.12	4.82	709	17.012	2,502	42,564	5,046
10	*LL* skin	0	...	....	.....	.....	.....	.....	....	....	....	....
11	*LL* c.g.	1.134	22.96	597.80	0.00488	−15.50	10.38	6,205	22.572	13,494	304,587	29,852
One side				2,670.03				−32,553		−1	984,467	
Both sides			Iy =	5,340.06				−65,106		I_0 =	1,968,934	

References

(I) x_T = ordinates from thrust line.
(II) x_T' = ordinates of local shear centers, from Fig. 10.
(III) Shear center $x_{T0}' = \Sigma S x_T'/\Sigma S = (-32{,}553)/2{,}670.03 = -12.192$.
(IV) Torque box area above floor $(x_T' + x_T)y = (39.72 + 21.52)21.3 = 1{,}304 = A_D$.
(V) Coefficients for axial load: $P = B \cdot ayx/I_0$ (Col. 11).
(VI) $(-\bar{x}_U + \bar{x}_L) = 27.528 + 22.572 = 50.1 = d_0$ (Col. 8).
(VII) Longeron areas at firewall $a_U' = a_L' = 1.066$.
(VIII) Loads in longerons at firewall for $B = 10^8$: $-10^8/2d_0y_U = -46{,}850$; $10^8/2d_0y_L = 43{,}470$.
Increase r in comparison with Col. 11: $r_U = 1.270$; $r_L = 1.456$.

TABLE 3

		X_c	X_k	g_z	g_y	g_x	g_m
Loads on	U'	0.506	−0.157	726.4	−1,015.3	2,632.6	−2,712.6
	U''	−0.506	0.157	787.1	1,015.3	2,717.6	2,712.6
	L'	−0.470	0.146	1,071.6	5,368.7	−2,636.7	2,516.5
	L''	0.470	−0.146	1,011.9	−5,368.7	−2,715.5	−2,516.5
	M_U	21.6	−6.69	−1,293	−43,250	−1,810	−115,560
	M_L	−21.6	6.69	1,293	246,530	1,810	115,560
	b	−1082	335	64,780	6,755,000	90,700	5,789,000
	m	0	0	0	131.4605	0	100,000

TABLE 4

Determination of Stress Flow Distributions

Panel	(1)	(2)	(3)	(4)	(5)	(6)	(7)	(8)	(9)
Truss	....	21.30	...	....	38,343	0.0045	69,589	.....	...
UL-S1	36,896	4.39	0.051	1,171.5	1,447	0.040	2	9,959	494
S1-W1	42,897	3.21	...	1,158.1	−4,554	....	17	3,958	610
W1-S3	51,679	5.72	...	2,995.7	−13,336	....	254	−4,824	847
S3-S4	53,500	6.49	...	3,642.0	−15,157	....	375	−6,645	949
S4-S5	53,289	6.38	...	3,552.8	−14,946	....	356	−6,434	1,057
S5-F1	51,171	1.09	0.051	559.5	−12,828	0.040	45	−4,316	1,167
Floor	4,267	26.90	0.055	88.0	34,076	0.0166	18,817	−879	2,085
F1-W2	46,904	5.48	0.051	2,363.9	−46,904	0.040	3,014	−3,437	−918
W2-S7	34,898	2.86	0.051	683.0	−34,898	0.040	871	8,569	−597
S7-LL	29,852	4.76	0.051	831.6	−29,852	0.040	1,061	13,615	−488
One side				17,046.1			94,400		
Two sides				34,092.2			188,000		
(Symbol)				$(10^8/J_0)$			$(10^8/J_1)$		
Rigidity coefficient				2,933.2			532		
(Symbol)				(J_0)			(J_1)		

References

(1) Unit shear flows q_0 in torsion bending in open section (summation of Col. 11, Table 1, from longerons to floor) (values $10^8\ q_0$).
(2), (3), (6) Panel length s and thickness h_0 and h_1 in open and closed sections (for top truss, equivalent web is used).
(4) Summation for rigidity coefficient J_0 (coefficients $10^8 q_0^2 s/h_0$).
(5) $q_1 = 1/2A_D - q_0$ (closed box); $q_1 = -q_0$ (below floor) (shear flow under bimoment equal to L_2 at station 159.3 and zero at station 243; A_D = Area of closed box, see Table 1) (values $10^8 q_1$).
(7) Summation for rigidity coefficient J_1 (coefficients $10^8 q_1^2 S/h_1$).
(8) Unit shear flow q_2 for redistribution of bimoment equal to L_1 applied at the longerons at station 100.
$(1/2d_0y_u - q_0)$ or $(1/2d_0y_L - q_0)$ (values $10^8 q_2$).
(9) Unit shear flow under side bending (summation of Col. 4, Table 1, from longerons to floor) (values $10^8 q_3$).

stress concentration in the longerons near the firewall. It is found that

$$I_0/I_0' = 1.189 \qquad I_0/I_0'' = 1.019$$

Example: Two redundancies X_k, X_c, four unit loads corresponding to accelerations g_z, g_y, g_x, and torque g_m (g_y, g_m are antisymmetrical). The values of the loads at the longerons for unit loads are given in Table 3, with the corresponding moments M_U, M_L at top and bottom ($M_U = y(P_U' - P_U'')$) and the bicouples $b = M_U\bar{x}_U + M_L\bar{x}_L$; ($\bar{x}_U$ and $\bar{x}_L$ from Table 1, Col. 8).

Shear Stresses

Table 4 gives the computations for shear flow and the corresponding rigidity, which cannot be neglected in comparison with the energy under axial loads. In addition to the coefficients of rigidity J_0, J_1 calculated on Table 4, the following rigidity coefficients can be considered:

J_2—redistribution of axial loads between stations 100 and station 159.3 (shear q_2).

J_{02}—interaction between redistribution shears q_2 and shears q_0.

J_{23}—interaction between redistribution shears q_2 and shears q_3 because of side load.

It is found that

$$J_2 = 107{,}770 \quad J_{02} = 116{,}461 \qquad J_{22} = -1{,}608$$

A tabulation similar to that of Table 2 gives for shear the terms and coefficients (Table 5), in which d is the arm of the load giving the torque m in respect to the shear center (for g_y, $d_y = 13.1$; for g_m, $d_m = 0$). The coefficients T'' are comparable to coefficients T'; they are combined together

TABLE 5

Terms	Coefficients
$X_c^2 b_c^2 T''; X_c X_k b_c b_k T''; \ldots\ldots$ $X_c g_y b_c b_y T''; \ldots\ldots$	$T'' = \dfrac{1}{J_2 L_1} + \dfrac{1}{J_1 L_2}$
$X_c g_y T_y''; \ldots\ldots$	$T_y'' = \dfrac{b_y}{J_2 L_1} + \dfrac{M_x}{J_{02}} + \dfrac{M_x/d_y}{J_{23}} + \dfrac{b_y + M_x L_1}{J_1 L_2}$

$T'' = 0.0000226; \quad T_y'' = 230; \quad T_m'' = 267$

$$T = (T'/E) + (T''/G)$$

$10^6 T = 0.00001056 \quad 10^6 T_y = 101.2 \quad 10^6 T_m = 112.7$

Strain Energy Factors

Multiplying the coefficients T by the products of the type

$$b_c^2; \quad b_c b_k; \ldots; \quad b_c b_z \ldots; \quad b_c b_y \ldots .$$

the energy coefficients are obtained (Table 6).

Results

The coefficients of Table 6 being added to the coefficients of the other parts of the structure, the solution of the simultaneous equations in X_c, X_k gives the values of the redundant loads, and the values of the loads at the four longerons are determined. At station 100, unit and total bicouples are of the types

$$b_z' = b_z + X_c b_c + X_k b_k$$
$$B' = b_z' g_z + b_y' g_y + b_x' g_x + b_m' g_m$$

The bimoment at station 159.3 is B''

$$B'' = B' + ML_1$$

and the loads in the members at station 159.3 are determined by multiplying B by Col. 11, Table 1.

These loads vary uniformly from the values at station 100 (zero for stringers, applied loads for longerons) to the values at station 159.3, and from those values to zero at station 243. Shears are given by Table 7.

TABLE 7

Shear Flows

Unit Load	Stations 100–159.3	Stations 159.3–243
g_z	$q_2 b_z'/L_1$	$q_1 b_z'/L_2$
g_y	$q_2 b_y'/L_1 + q_0 m_y$	$q_1(b_y' + L_1 m_y)/L_2$
g_x	$q_2 b_x'/L_1$	$q_1 b_x'/L_2$
g_m	$q_2 b_m'/L_1 + q_0 m_m$	$q_1(b_m' + L_1 m_m)/L_2$

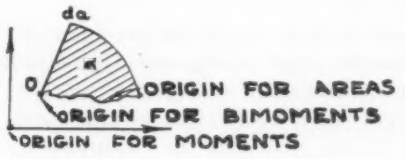

FIG. 11.

APPENDIX

APPLICATION OF THE METHOD OF LEAST WORK TO THE DETERMINATION OF THE DISTRIBUTION OF STRESSES IN TORSION BENDING

The problem is the following: Being given an open cylinder, with applied normal force Z, bending couples, M_ξ, M_η, and bicouple B_α, determine the stress distribution. The moments and bimoments are taken from an arbitrary origin, corresponding to the coordinates ξ and η and to the areas α. The conditions of equilibrium are

$$\left\{\begin{array}{ll} \int f\,da = Z & \int 2f\alpha\,da = B_\alpha \\ \int f\xi\,da = -M_\eta & \int f\eta\,da = M_\xi \end{array}\right\} \tag{53}$$

The principle of least work gives

$$W = \int f^2 da/2E = \text{Minimum} \tag{54}$$

In order to obtain Eqs. (53) independent from one another (i.e., orthogonalized conditions), a change of orthogonal coordinates and polar areas is made. The coordinates (x, y) and areas A correspond to new values B, M_y, M_x, of bicouples and couples

$$\begin{array}{c|c|c|c} \text{(a)} & \text{(b)} & \text{(c)} & \text{(d)} \\ \int f\,da = Z & \int fx\,da = -M_y & \int fy\,da = M_x & \int 2fA\,da = B \end{array} \tag{55}$$

with the condition of orthogonalization between the terms

$$\left|\begin{array}{c|c|c} \text{(a, b)} & \text{(a, c)} & \text{(b, c)} \\ \int x\,da = 0 & \int y\,da = 0 & \int xy\,da = 0 \\ \text{(a, d)} & \text{(b, d)} & \text{(c, d)} \\ \int 2A\,da = 0 & \int 2Ax\,da = 0 & \int 2Ay\,da = 0 \end{array}\right| \tag{56}$$

M_x, M_y, B are taken in reference to origins of coordinates and areas which satisfy the six conditions of orthogonalization. The first three conditions are well known: They determine the centroid of the section and the principal axes of inertia. The last two conditions determine the coordinates (x_0, y_0) of a point T_0, origin of the areas. Calling α the areas from a point different from T_0, then

TABLE 6

Coefficient of	X_c	X_k	g_z	g_y	g_x	g_m
Equation in X_c	$b_c^2 T = 12.36$	$b_c b_k T = -3.83$	$b_c b_z T = -0.000740$	$b_c T_y = -0.1034$	$b_c b_x T = -0.001036$	$b_c T_m = -0.1219$
Equation in X_k	$b_c b_k T = -3.83$	$b_k^2 T = 1.185$	$b_k b_z T = 0.000229$	$b_k T_y = 0.0339$	$b_k b_x T = -0.000321$	$b_k T_m = 0.0378$

$$2A = 2\alpha + 2\alpha_0 - x_0 y + y_0 x \tag{57}$$

and condition (b, d) becomes

$$\int 2\alpha x da + 2\alpha_0 \int x da - x_0 \int xy da + y_0 \int x^2 da = 0 \tag{58}$$

The second and third quantities are zero if the initial axes are the principal axes of inertia. Then Eq. (58) becomes

$$y_0 = -\int 2\alpha x da / I_y \tag{59}$$

Condition (c, d) gives the second coordinate of T_0 which shows that the origin of the areas coincides with the shear center (defined by Eqs. (17)).

Condition (a, d) defines the neutral points and is identical to Eq. (18). As the conditions have been orthogonalized, the distribution can be calculated for each component independently of the others. If there are shearing forces, the moments M_x, M_y must be taken in respect to the center of gravity, while the bimoment B must correspond to a torsional moment taken in respect to the center of shear T_0 and the polar line T_0S.

It is now known that if Eq. (54) is satisfied, together with a relationship of the type

$$\int f \lambda da = \Gamma \tag{60}$$

Γ being a given quantity and λ being a quantity attached to da, the distribution of the unknowns f is given by

$$f = \lambda\Gamma / \int \lambda^2 da \tag{61}$$

Thus, with the conditions of Eq. (55), in which λ is successively 1, x, y, $2A$, using the well-known constants total area a_0 and principal moments of inertia I_x, I_y, and defining a constant I_0,

$$I_0 = \int (2A)^2 da \tag{62}$$

the values of f for each component are defined by equations of the type of Eq. (61). Addition of these values leads to Eq. (15), which is thus completely proved. Substituting this value of f in Eq. (54) giving the strain energy W, and integrating, it is found, using conditions of orthogonalization, Eq. (56), that

$$W = \frac{1}{2E}\left(\frac{Z^2}{a_0} + \frac{M_x^2}{I_x} + \frac{M_y^2}{I_y} + \frac{B^2}{I_0}\right) \tag{63}$$

This expression generalizes the conventional formula of strain energy in beams by the introduction of the bimoment B.

Using Eq. (51), the strain energy can be written

$$W = BB_1/2EI_0 \tag{64}$$

Deflections in Torsion Bending

In Eqs. (63) and (64), EI_0 can be considered as a rigidity, exactly as EI, and all formulas for deflections hold. A bimoment corresponds to a twist, as can be seen by applying a couple M and calculating the twist θ_b at a point z_0, by the method of virtual work

$$\left.\begin{aligned} \theta_b(z_0) &= \int_{z_0}^{L} \frac{Mz(z - z_0)dz}{EI_0} \\ \theta_b(z_0) &= \frac{M}{EI_0} z_0^2 \left(\frac{L}{2} - \frac{z_0}{6}\right) \end{aligned}\right\} \tag{65}$$

The second derivative of Eq. (65) gives the relationship between θ_b and B. Replacing z_0 by $z = L - z_0$, with the conventional relations of sign between moment and shear, it is found that

$$d\theta_b(z)/dz^2 = Mz/EI_0 = -B(z)/EI \tag{66}$$

This relationship is similar to that existing between deflection and bending moment. Therefore all considerations relating deflection to bending are valid for torsion bending. For instance

$$d\theta_b/dz = \int (Bb_b/EI_0)dz \tag{67}$$

in which b_b is the bimoment caused by a unit bimoment applied at the point where $d\theta/dz$ is computed. For a cantilever membrane, $b = 1$ and under constant bimoment (no torque)

$$d\theta_b/dz = -Bz/EI_0$$

Twists θ_b can be directly calculated by the expression

$$\theta_b = \int (Bb_m/EI_0)dz \tag{68}$$

in which b_m is the bimoment caused by a unit couple applied at the point where θ is computed.

If the distribution of shear is taken into consideration, that distribution under unit torque gives a coefficient of rigidity in torsion J_b, which is different from the coefficient of rigidity J_t in St. Venant's twist. Using Eq. (16) for a unit torque M, the shears are

$$N_{12} = \int 2Ada/I_0 \tag{69}$$

Calling h the thickness of the membrane which resists in shear, the coefficient J_b is given by

$$\int_D N_{12}^2 ds/h_s = 1/J_b \tag{70}$$

Because of this effect, a supplementary deflection θ_s is added to the principal deflection. Between θ_s and M the relation is

$$d\theta_s/dz = M/GJ_b \tag{71}$$

Adding θ_s and θ_b, the total value of θ is found.

$$\frac{d^2\theta}{dz^2} = \frac{d^2\theta_b}{dz^2} + \frac{d^2\theta_s}{dz^2} = -\frac{B}{EI_0} + \frac{1}{GJ_b}\frac{dM}{dz} = -\frac{B}{EI_0} - \frac{M'}{GJ_b} \tag{72}$$

Quantities M' are the couples applied per unit length. If the rigidity GJ_t is taken into consideration, the total moment M must be divided in such a way that deflections θ in torsion bending and in twist be the same.

Calling M_1 the part of the moment M taken in torsion bending, it is found, by derivation of Eq. (72)

$$d^3\theta/dz^3 = -(M_1/EI_0) + (d^2M_1/dz^2)(1/GJ_b)$$

TABLE 8
Location of the Axis of Rotation

Load Condition	No torque or bimoment	Applied torque or bimoment	
Membrane Condition	Uniform torsion	Nonuniform torsion	Combined torsion
No end load	Indetermined axis	Axis at shear center	Indetermined axis
Axial thrust	Axis at center of gravity	Axis at shear center	Axis on the line connecting points defined on left
Bending couple	Axis at infinity in a definite direction	Axis at center of rotation (Eq. 49)	
General thrust	Axis on line of action of thrust	Axis at center of rotation	

and, for pure twist

$$d\theta/dz = (M - M_1)/GJ_t$$

By elimination of M_1 between the two relations above, the differential equation for twist becomes

$$EI_0\left(1 + \frac{J_t}{J_b}\right)\frac{d^3\theta}{dz^3} - GJ_t\frac{d\theta}{dz} = -M + \frac{EI_0}{GJ_b}\frac{d^2M}{dz^2} \quad (73)$$

If $1/J_b$ is neglected Eq. (73) simplifies to the conventional equation for torsion bending. For thin sections, J_t is negligible and Eq. (72) can be applied in the form

$$EI_0\frac{d^3\theta}{dz^3} = -M + \frac{EI_0}{GJ_b}\frac{d^2M}{dz^2} \quad (74)$$

For thicker sections, I_0 must be corrected, as indicated in references 1, 2 and 3. It is to be noted that M must be constant between bulkheads, since shears must remain constant. Thus, all the expressions above, in which derivatives of M are taken, presuppose a uniform distribution of rigid frames. This is in contradiction with the hypotheses of the membrane theory. This contradiction does not affect the results relative to the distribution under bending or torsion bending, and is necessary for the solution of problems related with general instability. If local instability is taken into consideration, the expressions must be revised. If a structure with a definite number of frames is taken into consideration, between two frames M is constant, and Eq. (66) must be used. At a frame there is a discontinuity δ in the slope of twist $d\theta/dz$ (δM, applied local couple)

$$\delta(d\theta/dz) = \delta M/GJ_b \quad (75)$$

Combined, Eqs. (66) and (75) solve the general problem of torsion bending for thin membranes with frames. Combined, Eqs. (72) and (75) solve the same problem when distributed loads are applied, together with concentrated loads on frames.

LOCATION OF THE AXIS OF ROTATION IN TORSION AND COMBINED LOADING FOR OPEN MEMBRANES

Some misunderstandings have often occurred relative to the location of the axis of rotation in torsion. The following points summarize the problem:

1. In the absence of torque or bimoment, the axis of rotation giving a uniform torsion is indetermined and has no relationship with the shear center or the center of gravity. An applied thrust defines the axis of rotation which must be along the line of application of the thrust. Otherwise, the line of application of the thrust becomes a helix, and nonuniform torsion appears.

2. With torque or bimoment, the axis of rotation coincides with the line of centers of rotation defined by Eqs. (48) and (49), provided there is no uniform torsion added to the nonuniform torsion due to bimoment.

3. In superposed uniform and nonuniform torsion, the center of rotation is on the line between the centers of rotation in (2) and (1), above. The results can be tabulated as shown in Table 8.

REFERENCES

[1] Wagner, H., *Torsion and Buckling of Open Sections*, N.A.C.A. T.M. No. 807, 1936.

[2] Wagner, H., and Pretschner, W., *Torsion and Buckling of Open Sections*, N.A.C.A. T.M. No. 784, 1936.

[3] Kappus, R., *Twisting Failure of Centrally Loaded Open-Section Columns in the Elastic Range*, N.A.C.A. T.M. No. 851, 1938.

[4] Goodier, J. N., *Buckling of Compressed Bars by Torsion and Flexure*, Engineering Experiment Station, Cornell University, Bulletin No. 27, December, 1941.

[5] Goodier, J. N., *Flexural-Torsional Buckling of Bars of Open Section*, Engineering Experiment Station, Cornell University, Bulletin No. 28, January, 1942.

[6] Hoff, N. J., *Stresses in Spaced-Curved Rings Reinforcing Edges of Cut-Outs in Monocoque Fuselages*, Journal of the Royal Aeronautical Society, Vol. 47, No. 386, pp. 35–83, February, 1943.

Contracting Cones Giving Uniform Throat Speeds*

RICHARD H. SMITH† AND CHI-TEH WANG‡

Massachusetts Institute of Technology

SYNOPSIS

A difficult problem in fluid mechanics which comes up frequently, especially in the design of venturi meters and wind tunnels, is to find the geometric form of contracting cones having uniform flow speeds at the throat. The solution given in this report** makes use of the exact analogy between the magnetic field that is created by two coaxial and parallel coils carrying electrical current and the velocity field that is created by two corresponding ring vortices. The high uniformity of the magnetic field over a core area when the coils are suitably arranged is well known. A corresponding uniformity of the velocity field over the same core area is here obtained by simply translating the electromagnetic solution into an aerodynamic one and by choosing one of the stream surfaces as a flow boundary. The geometric form of the stream surfaces is found without difficulty. A family of these contracting cones is developed, the inner eight of which give throat speed distributions that are uniform theoretically within a fifth of 1 per cent. The distributions become less uniform for the outer cones, but variations from uniformity are still less than 1 per cent even for the outermost one. Essentially, the same throat uniformities will occur in the case of real airflows, provided the upstream flow is uniform and the downstream, or diffuser, flow does not separate.

THEORY

CONSIDER A NONVISCOUS INCOMPRESSIBLE FLUID enclosed within a fixed boundary surface S (Fig. 1). Let the vorticity $\vec{\zeta}$ be given everywhere at some instant of time.

Take any points P and Q within the fluid and let $\vec{q}_P$ and $\vec{q}_Q$ be the velocities at P and Q, respectively. Then, by reference 3:

$$\vec{q}_P = \nabla \times \vec{\varphi}_P \tag{1}$$

where $\nabla = \vec{i}\,\frac{\partial}{\partial x} + \vec{j}\,\frac{\partial}{\partial y} + \vec{k}\,\frac{\partial}{\partial z}$ and $\vec{\varphi}_P$ is the vector potential at P defined by

$$\vec{\varphi}_P = (1/4\pi)\,\nabla \times \int_V (\vec{q}_Q/r)\,dv \tag{2}$$

In Eq. (2), r is the distance $\overline{PQ}$, where P is fixed, and the integration is taken through the volume V, which is enclosed by S.

Extend the boundary surface S to infinity. It is shown in reference 4 that

$$\vec{\varphi}_P = (1/4\pi)\int_V (\vec{\zeta}_Q/r)\,dV \tag{3}$$

and that

$$\vec{q}_P = (1/4\pi)\int_V (\vec{\zeta}_Q \times \vec{r}/r^3)\,dV \tag{4}$$

Consider now an infinite domain where the vorticity is concentrated on a vortex filament and is zero elsewhere. The strength of a vortex filament may be defined as

$$\Gamma = \vec{\zeta} \cdot d\vec{\sigma} \tag{5}$$

where Γ is the circulation and $d\sigma$ is the cross-sectional area of the filament. Since, by definition, the direction of the vorticity is the same as the direction of the element of the vortex filament, the direction of the vector potential $\vec{\varphi}$ is in this direction also. By Eqs. (4) and (5)

$$\begin{aligned} \vec{q}_P &= (1/4\pi)\int_V (\zeta_Q/r^3)\vec{s} \times \vec{r}\,d\sigma\,ds \\ &= (1/4\pi)\int_C \Gamma(\vec{s} \times \vec{r}/r^3)\,ds \end{aligned} \tag{6}$$

where the integration C is taken along the vortex filament. From Eq. (6) it is seen that the velocity induced by a vortex element can be defined as

$$d\vec{q}_P = (\Gamma/4\pi)(\vec{s} \times \vec{r}/r^3)\,ds \tag{7}$$

The rate of outflow through a circle C, Fig. 2, can be expressed in terms of the vector potential as follows: If we close over the circle by a surface S, the flux across S is:

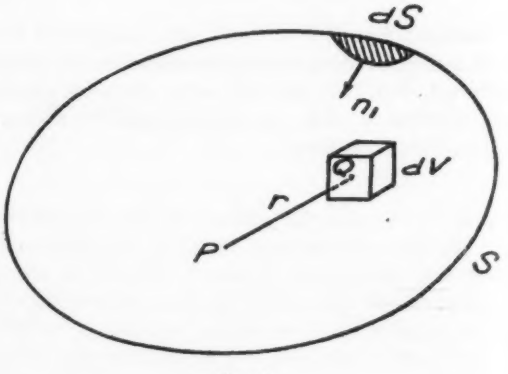

FIG. 1.

Received May 1, 1944.

* Mr. Wang prepared this report at Brown University, with the coauthor's permission, to satisfy their thesis requirement for the degree of Master of Science in the Department of Mathematics, with the understanding that the two authors would later publish the results jointly. The authors acknowledge their indebtedness to Drs. Lipman Bers and L. J. Savage for the valuable criticisms they gave Mr. Wang while this work was in progress.

† Professor of Aeronautical Engineering.

‡ Candidate for the Sc.D. degree in Aeronautical Engineering at M.I.T.

** Two recent solutions have been published.[1, 2]

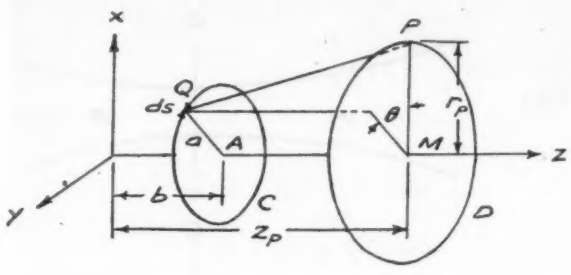

FIG. 2.

$$\begin{aligned}\int_s \vec{n}_1 \cdot \vec{q}\,dS &= \int_s \vec{n}_1 \cdot (\nabla \times \vec{\varphi})dS \\ &= \int_s (\vec{n}_1 \times \nabla) \cdot \vec{\varphi}\,dS \\ &= \int_C \vec{\varphi} \cdot \vec{s}\,ds\end{aligned} \tag{8}$$

where the right-hand integration is taken around the circle C. The last step is obtained by the use of Stoke's theorem.

A stream function can always be defined for axisymmetrical incompressible flows. Take an arbitrary point P, Fig. 2, whose cylindrical coordinates are $(r_p, 0, z_p)$. If we close over the circle $r = r_p$ by any surface and denote the flux across the surface by $2\pi\psi_P$, then ψ_P is called the Stoke's stream function for the point P. Consider the vortex ring whose core is C, Fig. 2. Since $\vec{\varphi}$ is tangent to the vortex ring and has the same magnitude φ at every point on the circle because of symmetry, Eq. (8) becomes:

$$\text{Flux} = \int_D \vec{\varphi} \cdot \vec{s}\,ds = 2\pi r\varphi \tag{9}$$

Therefore, by definition

$$\psi = r\varphi \tag{10}$$

Let Γ be the strength of the ring vortex, let a be the radius of its core, and let the C circle be normal to the z axis centered at A, a distance b from the origin. Then the element of arc at Q is $ad\theta$ and the vorticity vector at Q is tangent to C. Expressing $\vec{\zeta}$ at Q in terms of its components along x and y, which are perpendicular and parallel, respectively, to the meridian plane,

$$\vec{\zeta} = \vec{j}\zeta \cos\theta - \vec{i}\zeta \sin\theta \tag{11}$$

where $\vec{i}$ and $\vec{j}$ are unit vectors parallel to x and y, respectively.

Following Eq. (3)

$$\vec{\varphi}_P = 1/4\pi \int_V \frac{\zeta_Q}{r} \vec{s}\,d\sigma\,ds = \frac{\Gamma}{4\pi}\int_0^{2\pi} \frac{\vec{j}\cos\theta - \vec{i}\sin\theta}{\overline{PQ}}\,ad\theta$$

where

$$\overline{PQ}^2 = (z-b)^2 + a^2 + r^2 - 2ar\cos\theta$$

Upon performing the integration, the coefficient of $\vec{i}$ vanishes. The magnitude of $\vec{\varphi}$ is therefore the coefficient of $\vec{j}$, and the stream function becomes

$$\psi = (\Gamma/4\pi)ra\int^{2\pi} \cos\theta d\theta/\overline{PQ} \tag{12}$$

After some transforming,

$$\overline{PQ}^2 = [(a+r)^2 + (z-b)^2][1 - k^2\cos^2(\theta/2)]$$

where,

$$k^2 = 4ar/[(a+r)^2 + (z-b)^2]$$

Then,

$$\psi = \frac{\Gamma}{4\pi}\frac{ar}{\sqrt{(a+r)^2+(z-b)^2}}\int_0^{2\pi}\frac{\cos\theta d\theta}{\sqrt{1-k^2\cos^2(\theta/2)}}$$

By the relation $\cos\theta = 2\cos^2(\theta/2) - 1$ and after certain transformations,

$$\begin{aligned}\psi = \frac{\Gamma}{4\pi}\frac{ar}{\sqrt{(a+r)^2+(z-b)^2}} \times \\ \left[-\frac{4}{k^2}\int_0 \sqrt{1-k^2\cos^2\alpha}\,d\alpha + \left(\frac{4}{k^2}-2\right)\int_0^{\pi}\frac{d\alpha}{\sqrt{1-k^2\cos^2\alpha}}\right] \\ = \frac{a\Gamma}{\pi k}\sqrt{\frac{r}{a}}\left[\left(1-\frac{k^2}{2}\right)K - E\right]\end{aligned} \tag{13}$$

where K and E are the complete elliptical integrals of the first and second kind, respectively. Letting $R = r/a$, $Z = z/a$ and $B = b/a$,

$$\psi = \frac{a\Gamma}{\pi}\frac{\sqrt{R}}{k}\left[\left(1-\frac{k^2}{2}\right)K - E\right] \tag{14}$$

and

$$k^2 = \frac{4R}{(1+R)^2 + (Z-B)^2}$$

It is evident from the above derivation that the stream function due to several vortex rings can be obtained by simple arithmetic addition.

ELECTROMAGNETIC ANALOGY

The magnetic field intensity at a field point P, Fig. 2, induced by an element ds of a conductor carrying electrical current at Q is given by the Biot and Savart Law[5] as

$$d\vec{H}_P = (I/4\pi)(\vec{s} \times \vec{r}/r^3)ds \tag{15}$$

where

$\vec{H}_p$ = field intensity at P
I = total electrical current carried by the conductor
$\vec{s}$ = unit vector in the direction of the current element ds
$\vec{r}$ = vector distance of $\overline{PQ}$, r being its magnitude.

It is evident that Eqs. (7) and (15) are exactly analogous, with $d\vec{H}_p$ corresponding to $d\vec{q}_P$ and I corresponding to Γ. In this analogy a vortex filament corresponds

to a circuit of electric current and the field velocity to a field of magnetic force. Certain electromagnetic phenomena, therefore, will be paired with exactly corresponding aerodynamic phenomena in the analogous vortex motion in ideal fluids.

It is well known[6] that a pair of Helmholtz coils produces a magnetic field of uniform intensity over a core area in the neighborhood of the magnetic axis and in the common median plane. Shaw[7] has shown theoretically that a uniform field intensity at any desired point off the axis can be secured by reducing the Helmholtz separation. It has been calculated and verified experimentally[8] that a pair of circular coils of 30.776 cm. radius and separated a distance of 14.445 cm. produce a field intensity in the median plane which is uniform to within one part in 500 over a core area of radius 13 cm.

It follows from these last studies that a pair of equal vortex rings separated by a distance $14.445/30.776 = 0.46936$ radius will give a velocity distribution over a core area of $13/30.776 = 0.42241$ radius, in the median plane between the rings, which will likewise be uniform to within one part in 500. One only needs to build a boundary that follows the shape of one of the stream surfaces inside the core to obtain contracting cones whose velocity distribution over the throat section is uniform within the same precision.

Design of Contracting Cones to Give Uniform Velocity at the Throat

Before the design of a venturi tube or a wind tunnel having uniform throat speeds is discussed, the principle according to which different flows can be pieced together may be mentioned. Consider Fig. 3, where tubes in (a) and (b) give the same velocity distributions across the sections C–C and C'–C'. Then from boundary value considerations it is evident that there will be the same velocity distribution at section C''–C'' if we let the portion of tube A at the left side of C–C be connected to the portion of tube B' at the right side of section C'–C'.

These principles can be utilized in the design of a venturi tube or a wind tunnel in the following way: Let the contracting cone follow one of the inner stream surfaces produced by the two ring vortices up to the median plane. Let it be joined there by a straight tube which, in the case of a wind tunnel, will be the test section. Finally, let there follow a divergent cone of some convenient design. It would seem at first that the divergent cone should also follow another appropriate stream surface chosen from the same family. However, to escape separation everywhere a cone of this type would generally have to be much longer than space limitations would permit. Therefore, in practice the usual straight line diffuser cone is preferable. The combination is shown in Fig. 4.

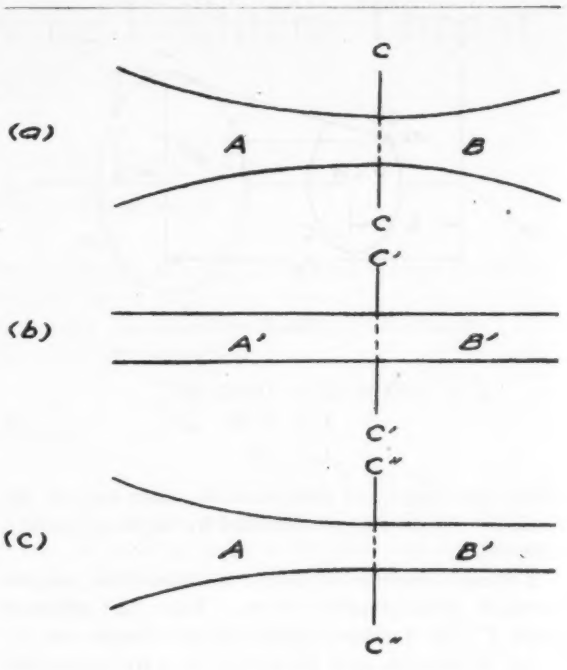

Fig. 3.

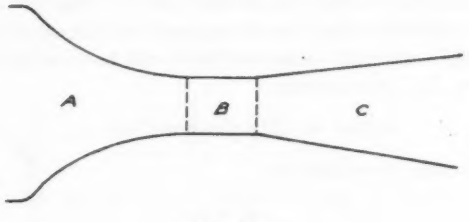

Fig. 4.

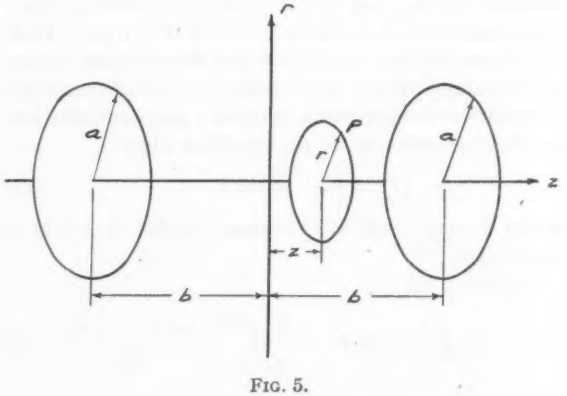

Fig. 5.

Construction of the Contracting Cones

When there are two vortex rings of equal core radii, a, and with centers at $(0, b)$ and $(0, -b)$, respectively (Fig. 5), the stream function at a point $P(r, z)$ is, from Eq. (14):

$$\psi = \frac{a\Gamma}{\pi}\sqrt{R}\left\{\frac{1}{k_1}\left[\left(1-\frac{k_1^2}{2}\right)K_1 - E_1\right] + \frac{1}{k_2}\left[\left(1-\frac{k_2^2}{2}\right)K_2 - E_2\right]\right\}$$

where

$$k_1^2 = \frac{4R}{(1+R)^2+(Z-B)^2}$$

$$k_2^2 = \frac{4R}{(1+R)^2+(Z+B)^2}$$

and where K_1, E_1 correspond to argument k_1 and K_2, E_2 correspond to k_2.

The problem is now to find the stream cones which are given by ψ = constant. This can be done graphically as follows:

(1) Tabulate k_1^2 and k_2^2 for many values of R and Z.

(2) Find $M_1/\sqrt{R}a$ and $M_2/\sqrt{R}a$ from tables in reference 9 where

$$\frac{M}{\sqrt{R}a} = 8\pi\frac{1}{k}\left[\left(1-\frac{k^2}{2}\right)K - E\right]$$

(3) Since the numerical values of Γ and a are irrelevant in finding the ψ = constant lines, we can assume $\Gamma a/\pi = 8\pi$. Then find ψ by

$$\psi = \sqrt{R}[(M_1/\sqrt{R}a) + (M_2/\sqrt{R}a)] \qquad (16)$$

(4) Plot ψ against Z for constant R's and read off the (Z, R) coordinates for constant values of ψ. The stream cones can then be plotted.

Sample Calculations

The values of ψ, Eq. (16), are computed for many values of R and Z.

For example, for $R = 0.38$ and $Z = 0.2$

$$\begin{aligned} k_1^2 &= 4R/[(1+R)^2 + (Z-B)^2] \\ &= (4)(0.38)/[(1+0.38)^2 + (0.2-0.46936)^2] \\ &= 0.768857 \\ k_2^2 &= 4R/[(1+R)^2 + (Z+B)^2] \\ &= (4)(0.38)/[(1+0.38)^2 + (0.2+0.46936)^2] \\ &= 0.646138 \end{aligned}$$

Values of $M_1/\sqrt{R}a$ and $M_2/\sqrt{R}a$, corresponding to the arguments k_1^2 and k_2^2 are found from tables in reference 9 by interpolation.

$$M_1/\sqrt{R}a = 4.30351$$
$$M_2/\sqrt{R}a = 2.59100$$

and

$$\begin{aligned} \psi &= \sqrt{R}[(M_1/\sqrt{R}a) + (M_2/\sqrt{R}a)] \\ &= 0.616441(4.30551 + 2.59100) \\ &= 4.25006 \end{aligned}$$

Values of ψ to six significant places have been computed in this way for 0.1 increments of Z over the useful range, which required from 10 to 16 values, and for 34 different values of R ranging from 0.28 to 1.40. This table can be secured if needed from the Department of Aeronautical Engineering at M.I.T.

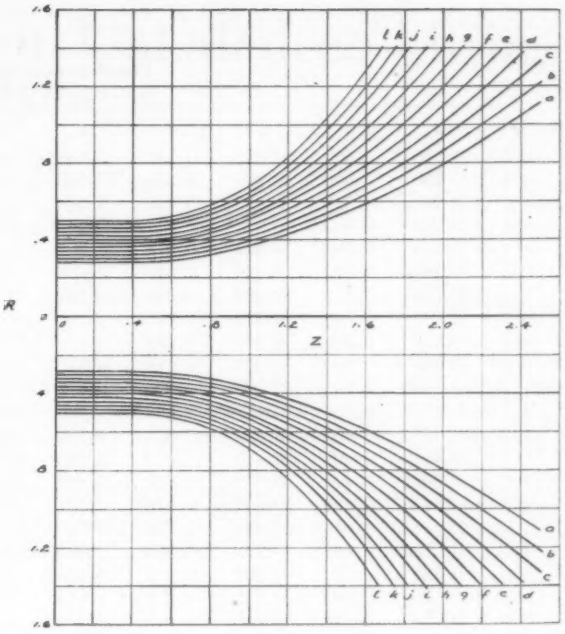

Fig. 6. Precision of uniformity of throat speed: a to h within 0.2 per cent; i within 0.4 per cent; j within 0.6 per cent; k within 0.9 per cent; l within 1 per cent.

Results

The values of ψ so found were plotted to large scale against Z for constant R's for accurate reading. Then values of (R, Z), which give the geometric form of the stream surfaces, were read from the curves ψ = constant. The cone forms so found are plotted in Fig. 6. The degree of uniformity of the speed at the throat sections of the various cone forms is noted in the figure. Finally, the coordinates (R, Z), from which Fig. 6 was drawn, are given in Table 1.

Application to Airflows

The behavior of these cones when used for contracting real airflows is the same as their theoretical behavior, for all practical purposes, provided the velocity of the upstream flow is fairly uniform over a normal section and provided the flow is not allowed to separate in the diffuser. Uniformity of the oncoming flow is often difficult to achieve in practice. Fortunately, any nonuniformity in the upstream flow is greatly reduced by the contraction and is a minimum at the throat.[10] Separation of real flows is impossible in the contracting cone and the throat because of the falling pressure gradient and the natural stream form of the surface. On the other hand, flow separation can hardly be avoided in the diffuser. Its effect on the uniformity of the throat flow, however, can be made negligibly small by keeping

TABLE 1

Coordinates of Stream Cone Sections

	R											
Z	a	b	c	d	e	f	g	h	i	j	k	l
0.0	0.280	0.300	0.320	0.340	0.360	0.380	0.400	0.420	0.440	0.460	0.480	0.500
0.1	0.280	0.300	0.320	0.340	0.360	0.380	0.400	0.420	0.440	0.460	0.480	0.500
0.2	0.280	0.300	0.320	0.340	0.360	0.380	0.400	0.420	0.440	0.460	0.480	0.500
0.3	0.282	0.302	0.322	0.342	0.362	0.382	0.402	0.422	0.440	0.460	0.480	0.500
0.4	0.284	0.304	0.324	0.344	0.364	0.384	0.404	0.424	0.442	0.461	0.480	0.500
0.5	0.289	0.309	0.329	0.349	0.369	0.389	0.409	0.429	0.450	0.464	0.488	0.506
0.6	0.298	0.318	0.338	0.358	0.381	0.401	0.421	0.442	0.462	0.482	0.502	0.522
0.7	0.310	0.330	0.352	0.375	0.396	0.418	0.448	0.461	0.482	0.504	0.525	0.547
0.8	0.317	0.339	0.360	0.383	0.406	0.429	0.450	0.474	0.511	0.534	0.556	0.581
0.9	0.345	0.370	0.394	0.419	0.445	0.469	0.496	0.519	0.547	0.571	0.598	0.626
1.0	0.369	0.396	0.422	0.450	0.478	0.505	0.531	0.561	0.590	0.619	0.650	0.681
1.1	0.397	0.426	0.455	0.484	0.516	0.546	0.577	0.610	0.644	0.676	0.712	0.750
1.2	0.428	0.460	0.492	0.526	0.557	0.594	0.631	0.665	0.704	0.743	0.785	0.830
1.3	0.464	0.499	0.533	0.572	0.606	0.648	0.687	0.730	0.774	0.817	0.870	0.922
1.4	0.502	0.541	0.579	0.622	0.664	0.708	0.753	0.802	0.853	0.907	0.967	1.032
1.5	0.543	0.586	0.630	0.676	0.724	0.775	0.827	0.883	0.940	1.008	1.078	1.160
1.6	0.588	0.636	0.684	0.736	0.790	0.846	0.905	0.970	1.037	1.115	1.197	1.294
1.7	0.635	0.689	0.742	0.800	0.860	0.921	0.989	1.064	1.144	1.237	1.330	
1.8	0.685	0.744	0.804	0.866	0.935	1.005	1.082	1.168	1.265	1.370		
1.9	0.738	0.803	0.868	0.938	1.014	1.093	1.182	1.280	1.396			
2.0	0.793	0.865	0.936	1.016	1.100	1.190	1.290	1.405				
2.1	0.852	0.930	1.009	1.096	1.190	1.292	1.406					
2.2	0.915	0.997	1.084	1.180	1.286	1.401						
2.3	0.979	1.069	1.164	1.269	1.386							
2.4	1.046	1.144	1.246	1.364								
2.5	1.116	1.222	1.331									

the local double divergent angle of the diffuser surface everywhere below 6°.[11]

A precise application of these contracting cones to real fluid flows would require that their surfaces be swollen by normal displacements equal everywhere to the displacement thickness of the local boundary layer. In practice, however, the displacement thickness of the boundary layer over the contracting cone surface is negligibly small and tends, furthermore, to be uniform. Normally, no appreciable error is made in neglecting it.

REFERENCES

[1] Tsien, H. S., *On the Design of the Contraction Cone for a Wind Tunnel*, Journal of the Aeronautical Sciences, Vol. 10, No. 2, pp. 68–70, February, 1943.

[2] Szcaeniowski, B., *Contraction Cone for a Wind Tunnel*, Journal of the Aeronautical Sciences, Vol. 10, No. 8, pp. 311–312, October, 1943.

[3] Milne-Thomson, L. M., *Theoretical Hydrodynamics*, p. 489; Macmillan and Company, London, 1938.

[4] *Ibid.*, p. 490.

[5] Joos, G., *Theoretical Physics*, p. 290; Stechert & Co., New York, 1934.

[6] Maxwell, J. C., *A Treatise on Electricity and Magnetism*, p. 357, Vol. II, Third Edition; 1892.

[7] Shaw, A. E., *A New Precision Method for the Determination of e/m for Electrons*, Physical Review, Vol. 54, pp. 193–209, August 1, 1938.

[8] Terence, M., Shaw, A. E., and Stephenson, R. J., *The Production of Annular Magnetic Fields of Great Uniformity*, The Review of Scientific Instruments, Vol. 11, pp. 57–62, February, 1940.

[9] Nagaoka, H., and Sakurai, S., *Tables for Facilitating the Calculation of Self-inductance of Circular Coil and of Mutual Inductance of Coaxial Circular Currents*, Table No. 2, Scientific Papers of the Institute of Physical and Chemical Research, Tokyo, September, 1927.

[10] Abramovich, G., *Principles of Aerodynamical Design of Wind Tunnel Nozzle*, Publication 231, Moscow Central Aero-Hydrodynamical Institute, 1935.

[11] Peters, H., *Energieumsetzung in Querchnettserweiterungen bei verschieden Zulanfbedingenngen*, Ingenieur-Archiv, Vol. 2, pp. 92–107, 1931–1932.

Aero-Elastic Instability in Unbalanced Lifting Rotor Blades

REINHARDT ROSENBERG*

Bell Aircraft Corporation

SUMMARY

Lifting rotor blades, which are unbalanced (tail heavy) about the quarter chord, are subject to flutter. Because of the action of the centrifugal force, additional energies which do not occur in the flutter analysis of fixed wings must be considered when the equations of motion are written. The equations of motion, their solution, and three-dimensional expressions for the elements of the stability determinant are derived. The treatment of the air forces is similar to that given by Smilg and Wasserman[5] as derived from the works of Theodorsen[1] and Küssner.[2] The fact, unfamiliar in classical flutter theory, is developed that the mechanical terms of the determinant elements as well as the aerodynamic terms, are functions of the reduced frequency. In addition, a labor-saving two-dimensional approach is indicated. In conclusion, expressions are derived from which the speed of torsional divergence can be determined.

The treatment of the subject is classical; it rests on standard methods in dynamics and is in part based on the development of other investigators, most of whom are mentioned in the list of references.

INTRODUCTION

THE BLADES OF LIFTING ROTORS are airfoils in an air stream. Therefore, they are susceptible to flutter if they have tail-heavy unbalance about the quarter chord line.

Neither the critical flutter speed nor the flutter mode can be predicted by applying without modification the methods of flutter analysis which were developed for fixed wings. An analysis of this instability in rotary wings is more tedious than that of fixed wings because of several factors: (a) the air velocity varies over the span; (b) new forces which are functions of the rotational speed must be considered; (c) the restoring forces, i.e., the frequencies in bending and torsion vary with rotational speed.

In the present paper the mechanism of this instability is treated and three-dimensional methods are developed which permit (within the limits of the assumptions) the determination of the critical speed and of the flutter mode.

The air forces are those developed by Theodorsen,[1] Küssner,[2] and others[3,4] for the oscillating airfoil of infinite span. These are applicable to lifting rotor blades only in flight without side wind, i.e., in hovering, climb, and descent. The development presented here is, therefore, restricted to the named conditions of flight.

The treatment of the problem is classical, i.e., the equations of motion are developed, and these are solved with the aid of the assumptions of harmonic motion and of complete linearity. Some of the material presented in this paper may be found elsewhere in the literature. It has not been given here with the intent of claiming originality but rather to make, at least, the treatment of the mechanical forces self-contained.

NOMENCLATURE

The nomenclature deviates from that common in flutter analysis. It incorporates ideas of many workers and was chosen: (a) so as to permit later additions without the necessity of revisions, (b) so as to be consistent with mathematical operations and physical concepts and, (c) so as to permit application to the widest possible variety of flutter modes and structures.

dK/dy	=	oscillatory aerodynamic lift per unit span in pounds per foot
dM/dy	=	oscillatory aerodynamic torque per unit span about the elastic axis in lb.-ft. per ft.
K_A	=	$-(V/b\omega)^2 k_a$
K_B	=	$-(V/b\omega)^2 k_b$
M_A	=	$-(V/b\omega)^2 m_a$
M_B	=	$-(V/b\omega)^2 m_b$
		Defined in reference 5 as L_h, L_α, M_h, and M_α, respectively
k_a, k_b, m_a, m_b		are coefficients in the aerodynamic forces and are defined by Küssner[2]
V	=	velocity in ft. per sec.
V_{FL}	=	linear flutter velocity in ft. per sec.
A	=	bending displacement of elastic axis in feet perpendicular to the air stream (positive when down)
B	=	torsional displacement in radians (positive for increasing angle of attack)
ω	=	flutter frequency in radians per sec.
ρ	=	density of air in slugs per cu.ft.
dm/dy	=	mass per unit span in slugs per ft.
dS_1/dy	=	static mass moment per unit span about the elastic axis in slug-feet per ft.
dI_1/dy	=	mass moment of inertia per unit span about the elastic axis in slug-(feet)^2 per foot
w	=	elemental mass of unit span in slugs per (ft.)^3 per ft.
b	=	half chord in feet
br	=	distance of w from elastic axis in feet
bx_1	=	distance between elastic axis and center of gravity in feet (positive when elastic axis is forward of center of gravity)
br_1	=	radius of gyration about elastic axis in feet
ba	=	distance of elastic axis from mid-chord point in feet (positive when elastic axis is aft of mid-chord point)

Presented at the Rotating Wing Aircraft Session, Twelfth Annual Meeting, I.A.S., New York, January 25–27, 1944.

* Now Design Specialist, Stout Research Division, Consolidated Vultee Aircraft Corporation.

$(dC/dy)_c$ = centrifugal force per unit span in lbs. per ft.
$(dC/dy)_n$ = component of centrifugal force normal to span per unit span in lbs. per ft.
ω_1 = natural "uncoupled" frequency of rotor in bending in radians per sec.
ω_2 = natural "uncoupled" frequency of rotor in torsion in radians per sec.
dC_1/dy = bending stiffness per unit span in lbs. per sq.ft.
dC_2/dy = torsional stiffness per unit span in lb.-ft. per radian per ft.
C_{TR} = coefficient of torsional rigidity in pound-(ft.)^2 per radian
f_1 = bending vibration deflection in terms of tip deflection as a function of y
f_2 = torsional vibration deflection in terms of tip deflection as a function of y
g_n = damping coefficient in the n-degree of freedom
m_R = value of m at the rotor blade root
m_T = value of m at the rotor blade tip
$m(y)$ = m as a function of y
ν = angular velocity of rotor in radians per sec.
N = angular velocity of rotor in r.p.m.
L = distance from center of rotation to blade tip in feet
L_0–L_0 = distance from blade root to blade tip in feet
j = $\sqrt{1}$

Positive forces oppose positive displacements and velocities.

The Centrifugal Force

Let a rotor blade oscillate in flutter; then a change in angle of attack will cause a change in lift and a resulting translatory motion of the elastic axis of A feet, as shown in Fig. 1. Now consider an elemental mass of the unit span w such that

$$\int\int w dx dz = dm/dy$$

If the rotor spins with an angular velocity ν the centrifugal force on w

$$(dC/dy)_c = wy\nu^2 \qquad (1)$$

The component of the centrifugal force normal to the span

$$(dC/dy)_n = wy\nu^2 \sin d\theta$$

which, for small values of $d\theta$, becomes

$$(dC/dy)_n = wy\nu^2 d\theta \qquad (2)$$

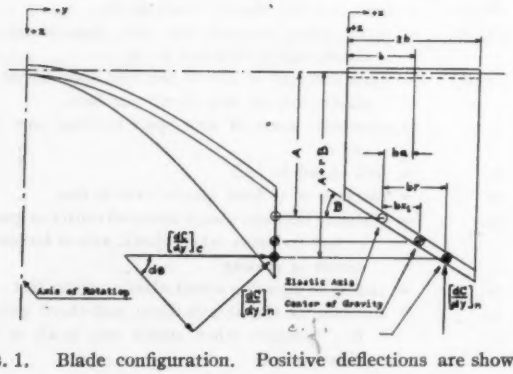

Fig. 1. Blade configuration. Positive deflections are shown.

It is self-evident that

$$(dC/dy)_n \propto d\theta$$

From Hooke's law it follows that

$$d\theta \propto -dK/dy$$

Therefore,

$$(dC)_n \propto -dK$$

or, expressed in words, the component of the centrifugal force which opposes translatory deflection is opposite in direction to, and varies as, the oscillatory aerodynamic lift.

Eq. (2) will now be put into a form more useful in flutter computations. The translatory displacement of the elemental mass w is $(A + rB)$ and $d\theta$ is approximately given by

$$d\theta = (A + rB)/y$$

The above expression for $d\theta$ is identically true only for blades which are hinged at the root and whose translatory deflection is caused entirely by motion in the hinge. For blades which deflect elastically (as shown in Fig. 1) and which are fixed at the root this expression is an approximation similar to the so-called "semi-rigid" wing theory used with good results by many British investigators. The error involved is conservative and is seen to be small if the magnitude of the actual component of the centrifugal force is compared with the assumed one as shown in Fig. 2.

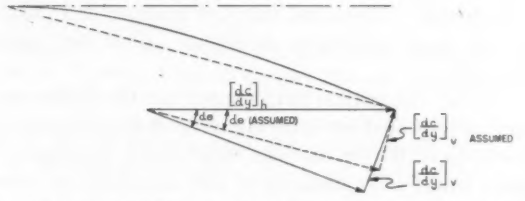

Fig. 2. Approximation of vertical component of centrifugal force for blades fixed at the root.

Substituting the above expression for $d\theta$ in Eq. (2)

$$(dC/dy)_n = w\nu^2(A + rB) \qquad (3)$$

When the integration $\int\int w dx dz$ is carried out

$$\left(\frac{dC}{dy}\right)_n = \frac{dm}{dy}\frac{V^2}{y^2}A + \frac{dS_1}{dy}\frac{V^2}{y^2}B \qquad (4)$$

where

$$dS_1/dy = (dm/dy)x_1$$
$$V^2/y^2 = \nu^2$$

Eq. (4) evaluates the normal component of the centrifugal force per unit span acting on a spinning rotor blade. This same force, also, exerts a moment about the elastic axis. This moment is, obviously, equal to

$$(dM/dy)_e = w(V^2/y^2)r(A + rB)$$

When the integration $\int\int wdxdz$ is carried out

$$\left[\frac{dM}{dy}\right]_e = \frac{dS_1}{dy}\frac{V^2}{y^2}A + \frac{dI_1}{dy}\frac{V^2}{y^2}B \qquad (5)$$

Eq. (5) evaluates the moment per unit span which the vertical component of the centrifugal force exerts about the elastic axis. From Eq. (5) it appears that, when the elastic axis and the center of gravity coincide, there is still a moment equal to $(dI_1/dy)(V^2/y^2)B$ because of the centrifugal force which tends to produce wash-out at the blade tip. Since the centrifugal force acts on the center of gravity, it is, perhaps, difficult to see how it can have a moment about the elastic axis when the center of gravity and the elastic axis coincide. This apparent inconsistency is cleared up when an angular deflection about the elastic axis is assumed. In that case restoring moments in the same direction exist on either side of the elastic axis as shown in Fig. 3.

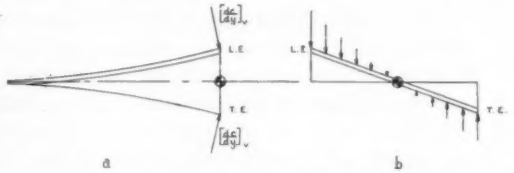

FIG. 3. Moment tending to produce washout when elastic axis and center of gravity coincide.

The sum of these moments is, clearly, not equal to zero and produces wash-out.

THE INERTIA FORCE

The inertia force exerted by the elemental mass is its mass times its acceleration. The deflection has been shown to be $(A + rB)$. Therefore, the inertia force

$$d(I.F.)/dy = w(\ddot{A} + r\ddot{B})$$

When the integration $\int\int wdxdz$ is carried out

$$d(I.F.)/dy = (dm/dy)\ddot{A} + (dS_1/dy)\ddot{B} \qquad (6)$$

Eq. (6) evaluates the inertia force per unit span acting on the rotor blade.

The elemental mass w also exerts an inertia couple about the elastic axis. This moment is

$$d(I.C.)/dy = wr(\ddot{A} + r\ddot{B})$$

When the integration $\int\int wdxdz$ is carried out

$$d(I.C.)/dy = (dS_1/dy)\ddot{A} + (dI_1/dy)\ddot{B} \qquad (7)$$

Eq. (7) evaluates the inertia couple per unit span acting on the rotor blade.

THE RESTORING FORCE

The restoring force in bending is familiar (from the common differential equation of motion of a vibrating system) as kx. Since the bending stiffness is dC_1/dy and the deflection is A, the restoring spring force is $(dC_1/dy)A$. This force is, however, augmented by damping. Theodorsen[6] has introduced damping in the form of a new force which is proportional to the elastic force (say, it is g_1 times the elastic force) and which lags the displacement by 90°, i.e., it is a coefficient of the velocity. The damping force in bending is, therefore, $g_1(dC_1/dy)jA$, and the total restoring force per unit span

$$d(R.F.)/dy = (dC_1/dy)(1 + jg_1)A \qquad (8)$$

In the twisting degree of freedom there is a restoring couple whose value is

$$d(R.C.)/dy = (dC_2/dy)(1 + jg_2)B \qquad (9)$$

and it is derived in a similar manner as Eq. (8).

EQUATIONS OF MOTION

For equilibrium the sum of the forces normal to the span must equal zero, or

$$-\frac{dm}{dy}\ddot{A} - \frac{dS_1}{dy}\ddot{B} - \frac{dm}{dy}\frac{V^2}{y^2}A - \frac{dS_1}{dy}\frac{V^2}{y^2}B - \frac{dC_1}{dy}(1 + jg_1)A + \frac{dK}{dy} = 0 \qquad (10a)$$

and the sum of the moments about the elastic axis must equal zero, or

$$-\frac{dS_1}{dy}\ddot{A} - \frac{dI_1}{dy}\ddot{B} - \frac{dS_1}{dy}\frac{V^2}{y^2}A - \frac{dI_1}{dy}\frac{V^2}{y^2}B - \frac{dC_2}{dy}(1 + jg_2)B + \frac{dM}{dy} = 0 \qquad (10b)$$

In order to solve these differential equations it is convenient to assume harmonic motion, or

$$\left.\begin{aligned} A &= A_0e^{j\omega t} \\ B &= B_0e^{j(\omega t + \phi_B)} \end{aligned}\right\} \qquad (11a)$$

where ϕ_B = phase angle between A and B.

From Eqs. (11a) it follows that

$$\left.\begin{aligned} \ddot{A} &= -\omega^2 A \\ \ddot{B} &= -\omega^2 \ddot{A} \end{aligned}\right\} \qquad (11b)$$

Furthermore, the spring stiffnesses

$$\left.\begin{aligned} dC_1/dy &= (\omega_1)^2(dm/dy) \\ dC_2/dy &= (\omega_2)^2(dI_1/dy) \end{aligned}\right\} \qquad (11c)$$

Substituting Eqs. (11) into the differential equations of motion, these become

$$\frac{dm}{dy}\omega^2 A + \frac{dS_1}{dy}\omega^2 B - \frac{dm}{dy}\frac{V^2}{y^2}A - \frac{dS_1}{dy}\frac{V^2}{y^2}B - (\omega_1)^2\frac{dm}{dy}(1 + jg_1)A + \frac{dK}{dy} = 0 \qquad (12a)$$

and

$$\frac{dS_1}{dy}\omega^2 A + \frac{dI_1}{dy}\omega^2 B - \frac{dS_1}{dy}\frac{V^2}{y^2}A - \frac{dI_1}{dy}\frac{V^2}{y^2}B - (\omega_2)^2\frac{dI_1}{dy}(1 + jg_2)B + \frac{dM}{dy} = 0 \quad (12b)$$

Multiplying throughout by $(1/\omega^2)dy$ and taking like terms together

$$dm\left[1 - \left(\frac{V}{y\omega}\right)^2 - \left(\frac{\omega_1}{\omega}\right)^2(1 + jg_1)\right]A + dS_1\left[1 - \left(\frac{V}{y\omega}\right)^2\right]B + \frac{dK}{\omega^2} = 0 \quad (13a)$$

and

$$dS_1\left[1 - \left(\frac{V}{y\omega}\right)^2\right]A + dI_1 \times \left[1 - \left(\frac{V}{y\omega}\right)^2 - \left(\frac{\omega_2}{\omega}\right)^2(1 + jg_2)\right]B + \frac{dM}{\omega^2} = 0 \quad (13b)$$

Some algebraic manipulations are required for the final form of the equations. These are obvious when Eqs. (14a) and (14b) are compared with Eqs. (13a) and (13b).

$$dm\left[1 - \left(\frac{b}{y}\right)^2\left(\frac{V}{b\omega}\right)^2 - \left(\frac{\omega_1}{\omega_2}\right)^2\left(\frac{\omega_2}{\omega}\right)^2(1 + jg_1)\right]A + dS_1\left[1 - \left(\frac{b}{y}\right)^2\left(\frac{V}{b\omega}\right)^2\right]B + \frac{dK}{\omega^2} = 0 \quad (14a)$$

and

$$dS_1\left[1 - \left(\frac{b}{y}\right)^2\left(\frac{V}{b\omega}\right)^2\right]A + dI_1\left[1 - \left(\frac{b}{y}\right)^2\left(\frac{V}{b\omega}\right)^2 - \left(\frac{\omega_2}{\omega}\right)^2(1 + jg_2)\right]B + \frac{dM}{\omega^2} = 0 \quad (14b)$$

Eqs. (14) do not show immediately the increase in bending and torsional frequencies with rotational speed. That the frequencies do change with rotational speed may be visualized as follows:

In fixed wings the elastic force in bending is defined as

$$(\omega_1)^2 dm = dC_1$$

Eq. (13a) shows that the bending stiffness may be considered increased by the $(V/y)^2$ term, or

$$dm(V/y)^2 + (\omega_1)^2 dm = \text{stiffness}$$

from which it follows (when $(V/y)^2$ is replaced by ν^2) that the blade bending frequency in flight

$$\omega_1' = \sqrt{\nu^2 + (\omega_1)^2} > \sqrt{(\omega_1)^2}$$

It can be shown similarly that the blade torsional frequency in flight

$$\omega_2' = \sqrt{\nu^2 + (\omega_2)^2} > \sqrt{(\omega_2)^2}$$

This paper assumes that the aerodynamic terms in Eqs. (14) are identical with those which act on the fixed oscillating wing. This assumption is based on the fact that, in both cases, the distance between the wing (or rotor) tip and a shed vortex increases with time. Furthermore, in both cases, the airflow is normal to the span when the lifting rotor analysis is restricted to the flight conditions of hovering, climb, and descent.

Analytical expressions for the aerodynamic terms in Eqs. (14) may be found in references 1 and 2. It will suffice here to state that each contains (for the degrees of freedom of the case at hand) only terms which are either linear in A or B. The coefficients of these variables are functions of the reduced wave length $V/b\omega$ and of the lift vector $(F + jG)$.

Eqs. (14) are, therefore, linear, homogeneous equations in A and B. It is necessary and sufficient for the existence of a nontrivial solution that the determinant of their coefficients vanish.

Stability Determinant

Let Eqs. (14) be equal to

$$dV_{11}A + dV_{12}B = 0 \quad (15a)$$

and

$$dV_{21}A + dV_{22}B = 0 \quad (15b)$$

where

$$dV_{mn} = dM_{mn} + dA_{mn}$$

Then, the component parts of the determinant elements are

$$dM_{11} = dm\left[1 - \left(\frac{\omega_1}{\omega_2}\right)^2\left(\frac{\omega_2}{\omega}\right)^2(1 + jg_1)\right] - dm\left(\frac{b}{y}\right)^2\left(\frac{V}{b\omega}\right)^2 \quad (16a)$$

$$dM_{12} = dS_1 - dS_1(b/y)^2(V/b\omega)^2 \quad (16b)$$

$$dM_{21} = dS_1 - dS_1(b/y)^2(V/b\omega)^2 \quad (16c)$$

$$dM_{22} = dI_1\left[1 - \left(\frac{\omega_2}{\omega}\right)^2(1 + jg_2)\right] - dI_1\left(\frac{b}{y}\right)^2\left(\frac{V}{b\omega}\right)^2 \quad (16d)$$

$$dA_{11} = \pi\rho b^2 K_A \quad (17a)$$

$$dA_{12} = \pi\rho b^3[K_B - (1/2 + a)K_A] \quad (17b)$$

$$dA_{21} = \pi\rho b^3[1/2 - (1/2 + a)K_A] \quad (17c)$$

$$dA_{22} = \pi\rho b^4[M_B - (1/2 + a)K_B - (1/2 + a)1/2 + (1/2 + a)^2 K_A] \quad (17d)$$

Eqs. (16) demonstrate the dependence of the mechanical terms on the reduced frequency. This phenomenon which is an immediate consequence of the variation of centrifugal force with speed is new in flutter theory. Eqs. (17) are the same as those of classical flutter theory.

For those who prefer this treatment, the determinant elements are given below in their nondimensional form, and in the nomenclature introduced by Theodorsen.[1]

$$dM_{11} = \frac{1}{\kappa}\left[1 - \left(\frac{\omega_h}{\omega_\alpha}\right)^2\left(\frac{\omega_\alpha}{\omega}\right)^2(1 + jg_h)\right] - \frac{1}{y^2\kappa}\frac{b^2}{k^2} \quad (18a)$$

$$dM_{12} = \frac{x_\alpha}{\kappa} - \frac{x_\alpha}{y^2\kappa}\frac{b^2}{k^2} \quad (18b)$$

$$dM_{21} = \frac{x_\alpha}{\kappa} - \frac{x_\alpha}{y^2\kappa}\frac{b^2}{k^2} \quad (18c)$$

$$dM_{22} = \frac{r_\alpha^2}{\kappa}\left[1 - \left(\frac{\omega_\alpha}{\omega}\right)^2(1 + jg_\alpha)\right] - \frac{r_\alpha^2}{y^2\kappa}\frac{b^2}{k^2} \quad (18d)$$

$$dA_{11} = A_{ch} \quad (19a)$$

$$dA_{12} = A_{c\alpha} \quad (19b)$$

$$dA_{21} = A_{sh} \quad (19c)$$

$$dA_{22} = A_{s\alpha} \quad (19d)$$

Three-Dimensional Approach

The development presented above describes the three-dimensional case when the time rate of change of energy vanishes, i.e., when the magnitude of the amplitude of oscillation does not vary with time. This condition can be satisfied numerically only if the deflection curves in flight of those uncoupled modes are known which participate in the flutter mode. It has been quite generally accepted[5,7,8,9] that these deflection curves are sufficiently similar to those excitable on the ground that the substitution of one by the other is permissible.

Let the sum of all forces acting in the bending degree of freedom per unit span be dF' and the sum of all moments in the twisting degree of freedom per unit span be dM'. Then, the equations of motion become three-dimensional if

$$\left.\begin{aligned} A &= A_0 f_1 e^{j\omega t} \\ B &= B_0 f_2 e^{j(\omega t + \phi_B)} \\ \dot{E}_B &= j\omega A_0 \textstyle\int_{L_0}^{L_5} f_1 dF' = 0 \\ \dot{E}_T &= j\omega B_0 \textstyle\int_{L_0}^{L_5} f_2 dM' = 0 \end{aligned}\right\} \quad (20)$$

where E_B = energy in the bending degree of freedom
E_T = energy in the torsional degree of freedom

Substituting Eqs. (20) in Eqs. (10), linearized equations of motion in A and B are obtained whose coefficients are $V_{mn} = M_{mn} + A_{mn}$ and

$$M_{11} = \left[1 - \left(\frac{\omega_1}{\omega_2}\right)^2\left(\frac{\omega_2}{\omega}\right)^2(1 + jg_1)\right]\int_{L_0}^{L_5} f_1^2 dm - \int_{L_0}^{L_5}\left(\frac{b}{y}\right)^2\left(\frac{V}{b\omega}\right)^2 f_1^2 dm \quad (21a)$$

$$M_{12} = \int_{L_0}^{L_5} f_1 f_2 dS_1 - \int_{L_0}^{L_5}\left(\frac{b}{y}\right)^2\left(\frac{V}{b\omega}\right)^2 f_1 f_2 dS_1 \quad (21b)$$

$$M_{21} = \int_{L_0}^{L_5} f_2 f_1 dS_1 - \int_{L_0}^{L_5}\left(\frac{b}{y}\right)^2\left(\frac{V}{b\omega}\right)^2 f_2 f_1 dS_1 \quad (21c)$$

$$M_{22} = \left[1 - \left(\frac{\omega_2}{\omega}\right)^2(1 + jg_2)\right]\int_{L_0}^{L_5} f_2^2 dI_1 - \int_{L_0}^{L_5}\left(\frac{b}{y}\right)^2\left(\frac{V}{b\omega}\right)^2 f_2^2 dI_1 \quad (21d)$$

$$A_{11} = \pi\rho\textstyle\int_{L_0}^{L_5} K_A b^2 f_1^2 dy \quad (22a)$$

$$A_{12} = \pi\rho\textstyle\int_{L_0}^{L_5}[K_B - (1/2 + a)K_A]b^3 f_1 f_2 dy \quad (22b)$$

$$A_{21} = \pi\rho\textstyle\int_{L_0}^{L_5}[1/2 - (1/2 + a)K_A]b^3 f_2 f_1 dy \quad (22c)$$

$$A_{22} = \pi\rho\textstyle\int_{L_0}^{L_5}[M_B - (1/2 + a)K_B - (1/2 + a)1/2 + (1/2 + a)^2 K_A]b^4 f_2^2 dy \quad (22d)$$

Eqs. (22) are based on aerodynamic theory of the oscillating airfoil of infinite span. This theory is in most cases conservative. It is considered more nearly correct for lifting rotor blades than for most fixed wing aircraft because of the large aspect ratio of rotor blades.

A simplification of Eqs. (21a) and (21d) is possible if the conservative assumption is made that the damping coefficients are zero. However, at best, the numerical work is much greater for the problem at hand than is usual in the flutter analysis of fixed wings.

In the latter case it is common to assume a representative half-chord for the entire wing and to obtain, thus, a representative value of the reduced frequency for all spanwise sections of the airfoil. This procedure is nearly correct when only the chord is a span function. The widespread use of this practice has, perhaps, obscured the fact that the three-dimensional determinant elements are rigorously correct (within the limits of the assumptions) with no restrictions of constancy, linearity, or even continuity on the function $(V/b\omega)(y)$.

In lifting rotor blades, both V and b are span functions. Since V varies from zero at the center of rotation to a maximum at the rotor tip, the use of a constant value of the reduced frequency for all sections of the blade cannot be expected to describe properly the occurrence or character of flutter.

It seems necessary, therefore, to determine the function $(V/b\omega)(y)$ before Eqs. (21) and (22) can be evaluated numerically. This function is easily obtained (for straight tapered blades without spanwise discontinuities in plan form) as

$$(V/b\omega)(y) = [V(y)/b(y)\omega] \quad (23)$$

where

$$V(y) = V_T(y/L)$$

$$b(y) = b_R + (b_T - b_R)/(L_5 - L_0)y$$

By means of Eq. (23) the three-dimensional determinant elements can be evaluated numerically for any assumed value of $(V/b\omega)_T$. The integrations are most easily carried out tabularly.

Expansion of the stability determinant

$$\Delta = \begin{vmatrix} V_{11} & V_{12} \\ V_{21} & V_{22} \end{vmatrix} = 0 \quad (24)$$

results in a quadratic equation in ω_2/ω whose complex coefficients are given in terms of $(V/b\omega)_T$. This equation which, by virtue of the vanishing of the stability determinant, equals zero, may be solved in several ways.[1, 5, 7] The one suggested by Theodorsen[1] is to consider the binomial as consisting of a real and of an imaginary equation which must both equal zero independently. The critical value of $(V/b\omega)_T$ is that for which ω_2/ω satisfies both the real and the imaginary equation. The critical flutter speed of the tip is then

$$V_{FL} = (V/b\omega)_T(\omega/\omega_2)\omega_2 b_T \text{ ft. per sec.} \qquad (25)$$

The critical angular flutter velocity is easily found from Eq. (25) as

$$N_{FL} = 0.955\ V_{FL}/L \text{ r.p.m.} \qquad (26)$$

The flutter mode may be computed by substituting the numerical values of the determinant elements in the equations of motion of the form

$$\begin{aligned} V_{11}A + V_{12}B &= 0 \\ V_{21}A + V_{22}B &= 0 \end{aligned} \qquad (27)$$

and by assuming a given torsional deflection. This permits the solution of Eqs. (27) explicitly for the translatory deflection A. Such calculations, made for a representative blade, have shown that a torsional deflection at the tip of 10 degrees is associated with a translatory displacement at the tip of 0.08 inch. It is characteristic for flutter in lifting rotor blades that considerable twist is associated with very small translatory motion.

Two-Dimensional Approach

In view of the large amount of labor involved in solving the integrals of the three-dimensional determinant elements, it would be desirable to reduce the problem to a two-dimensional analysis, i.e., to find a section along the blade whose flutter speed, when analyzed two-dimensionally, is its true velocity at flutter angular velocity.

It will now be shown that a section exists somewhere between the root and the tip of the blade whose flutter speed, analyzed two-dimensionally, fulfills that condition. For proof it need only be shown that the flutter speed of the tip, analyzed two-dimensionally, is lower than the actual flutter speed of the blade.

It is apparent without rigorous analysis that this is the case. Consider a blade with constant section all along the span. Two-dimensional analysis implies that the blade (of infinite aspect ratio) moves parallel to itself. Three-dimensional analysis, on the other hand, considers its actual motion, i.e., rotation about the root. The air forces are in either case proportional to the square of the velocity. In the first instance, the velocity is for all sections of the blade equal to the maximum whereas, in the second instance, the velocity is for all sections of the blade less than the maximum, i.e., the tip value. It follows that, for the two-dimensional case, the effect of the air forces is larger and, therefore, the flutter speed lower than for the three-dimensional case. Since the "two-dimensional" flutter speed is smaller than the linear velocity of the blade tip at the flutter angular velocity and larger than the velocity at the center of rotation (which is zero) it follows that the "two-dimensional" flutter speed is equal to the air velocity over some blade section between root and tip. In flutter analysis of fixed wings, the section located at a distance three-quarters of the half span from the center line of the airplane has been found to be nearly representative of the wing. It follows from the difference in assumed motion between two- and three-dimensional analysis that this same section cannot be the representative one in rotor blades and that the representative section must be further inboard. At the present stage of the investigation, it seems that this representative section is located approximately at a distance of one-quarter to one-half the blade radius from the center of rotation.

Blade Divergence

There is still another possible instability because of aerodynamic forces which has not been discussed as yet; blade torsional divergence.

Torsional divergence is nonoscillatory in character. It may be described as follows: In an airfoil of finite torsional stiffness whose elastic axis is aft of the aerodynamic center, the twisting moment due to an increase in lift is in such a direction as to increase the angle of attack. This will cause an additional increase in lift further twisting the airfoil. At the torsional divergence speed, this process continues until the airfoil fails in torsion, i.e., until it diverges.

The speed at which divergence occurs is found from the moment equation which is, for convenience, repeated here.*

$$\frac{dS_1}{dy}\omega^2 A + \frac{dI_1}{dy}\omega^2 B - \frac{dI_1}{dy}(\omega_2)^2 B - \frac{S_1 d}{dy}\frac{V^2}{y^2}A - \frac{dI_1}{dy}\frac{V^2}{y^2}B + \frac{dM}{dy} = 0 \qquad (28)$$

Since torsional divergence is nonoscillatory, the technique of determining the divergence speed from Eq. (28) is, obviously, to write this equation for nonoscillatory conditions, i.e., to let the flutter frequency approach zero.

It has been shown elsewhere[10] that

$$\lim_{\omega \to 0} \frac{dM}{dy} = 2\pi\rho V^2 b^2 (1/2 + a)B \qquad (29)$$

Executing the step of $\omega \to 0$ and substituting Eq. (29) in Eq. (28), the moment equation becomes

* Because of the nonoscillatory character of the motion the damping term has been omitted.

$$-\frac{dI_1}{dy}(\omega_2)^2B - \frac{dS_1}{dy}\frac{V^2}{y^2}A - \frac{dI_1}{dy}\frac{V^2}{y^2}B + 2\pi\rho V^2b^2(1/2 + a)B = 0 \quad (30)$$

Reintroducing $\nu = V/y$, multiplying by (dy) and taking like terms together

$$-dS_1\nu^2A - [dI_1(\omega_2)^2 + dI_1\nu^2 - 2\pi\rho(by)^2\nu^2(1/2 + a)dy]B = 0 \quad (31)$$

Divergence occurs when

$$dI_1(\omega_2)^2 + dI_1\nu^2 - 2\pi\rho(by)^2(1/2 + a)\nu^2dy = 0 \quad (32)$$

where

$$dI_1(\omega_2)^2 = dC_2$$

A relation between dC_2/dy and C_{TR} as used elsewhere[10] can be established as follows:

When the blade is vibrated in torsion at a frequency of ω_2 radians per second, the kinetic energy per unit span is given by

$$K.E. = dI_1(\omega_2)^2/2 = dC_2/2 \quad (33)$$

The strain energy per unit span at the same instant is given by

$$U = T(B/y)/2 \quad (34)$$

where T is the torque in foot-pounds.

But by definition, $C_{TR} = T(y/B)$ or

$$T = C_{TR}(B/y) \quad (35)$$

Substituting Eq. (35) in Eq. (34)

$$U = C_{TR}(B/y)^2/2 \quad (36)$$

and, equating the kinetic and strain energies

$$dC_2 = C_{TR}(B/y)^2dy \quad (37)$$

The substitution of Eq. (37) in Eq. (32) yields

$$C_{TR}(B/y)^2dy + [dI_1 - 2\pi\rho(by)^2(1/2 + a)dy]\nu^2 = 0 \quad (38)$$

The three-dimensional form of Eq. (38) is obtained in the following manner:

Let

$$B = B_T[f_T(y)] = f_T(y)$$

where B_T = torsional deflection at the blade tip = unity.

Then

$$\int_{L_0}^{L_1} C_{TR}(1/y^2)[f_T(y)]^2dy + \nu^2\int_{L_0}^{L_1}[dI_1 - 2\pi\rho(by)^2 \times (1/2 + a)dy] = 0 \quad (39)$$

and the divergence angular velocity

$$\nu_D = \sqrt{\frac{\int_{L_0}^{L_1} C_{TR}(1/y^2)[f_T(y)]^2dy}{2\pi\rho(1/2 + a)\int_{L_0}^{L_1}(by)^2dy - \int_{L_0}^{L_1}dI_1}} \text{ radians per second} \quad (40)$$

where $f_T(y)$ may be found by successive convergent approximations as shown by Shornick.[11]

Conclusions

Methods have been presented which permit the determination of the flutter and divergence angular velocities of lifting rotor blades. From these developments certain conclusions can be drawn which are listed below. Some of them are mentioned here for the first time but they may be readily verified by an inspection of the determinant elements.

(a) All mechanical terms of the determinant elements contain addends which are functions of the reduced frequency. These are contributed by the centrifugal force.

(*b*) The contribution of the centrifugal force has the effect of raising the flutter speed as well as the divergence speed.

(c) The actual flutter speed of a rotor blade is much higher than would be the case if it were traveling parallel to itself.

(d) Theoretically, at least, flutter extends over a speed range below and above which the blade will not flutter.

(e) A blade which is mass-balanced about the quarter chord line will not flutter.

(f) A blade, regardless of whether or not it is mass-balanced about the quarter-chord line, may experience divergence if the blade elastic axis is aft of the quarter-chord line.

Care must be used in applying the development presented here because blades have, usually, two axes about which they can twist, (1) the hinge which permits changes in angle of attack, and (2) the elastic axis. Since the mechanical arrangement may provide interconnected motion of several blades, it may be necessary to consider some or all blades in the flutter analysis. Strictly speaking, the theory presented here considers only elastic deformations of a single blade. It is, however, immediately adaptable to other modes much in the same manner in which classical flutter theory may be applied to symmetrical as well as antisymmetrical modes. The analyst must consider the motions of all components which participate in the mode and he must use judgment in deciding which motions can couple with one another.

References

[1] Theodorsen, T., *General Theory of Aerodynamic Instability and the Mechanism of Flutter*, N.A.C.A. T.R. No. 496, 1935.

[2] Küssner, H. G., and Schwartz, L., *Der Shwingende Flügel Mit Aerodynamisch Ausgeglichenem Ruder*, Luftfahrtforschung, Vol. 17, Number 11/12, pp. 337–354, December, 1940.

[3] Cicala, P., *Le Azione Aerodinamiche Suit Profili De Ala Oscillanti in Presenza Di Corrente Uniforme*, Mem. Royal Accad.

Scienza Torino, Series 2, Pt. I, t. 68, pp. 73–98, 1934–1935.

[4] Lyon, H. M., *Review of Theoretical Investigations of the Aerodynamic Forces on a Wing in Non-Uniform Motion*, R. & M. 1768, 1937.

[5] Smilg, B., and Wasserman, L. S., *Application of Three-Dimensional Flutter Theory to Aircraft Structures*, A.C.T.R. No. 4798, July, 1942.

[6] Theodorsen, T., and Garrick, I. E., *Mechanism of Flutter*, N.A.C.A. T.R. No. 685, 1940.

[7] Loring, S. J., *General Approach to the Flutter Problem*, S.A.E. Journal, Vol. 49, No. 2, pp. 345–356, August, 1941.

[8] Bleakney, W. M., *Three-Dimensional Flutter Analysis*, Journal of the Aeronautical Sciences, Vol. 9, No. 2, pp. 56–63, December, 1941.

[9] Lombard, A. E., *An Investigation of the Conditions for the Occurrence of Flutter in Aircraft*, Thesis, Guggenheim Aeronautics Laboratory, California Institute of Technology, Pasadena, Cal., Galcit Publication No. 116.

[10] Rosenberg, R., *Loss in Aileron Effectiveness Because of Wing Twist and Considerations Regarding the Internal Pressure Balanced Aileron*, Journal of the Aeronautical Sciences, Vol. 12, No. 1, pp. 41–47, January, 1944.

[11] Shornick, L. H., *The Computation of the Critical Speeds of Aileron Reversal, Wing Torsional Divergence and Wing-Aileron Divergence*, Army Air Forces Memorandum Report Serial No. Eng.-M-51/VF-18, Add. 1, December 19, 1942.

I. A. S.

National Meetings Schedule

1944-1945

AIR TRANSPORT MEETING	**October 20, 1944**	WASHINGTON, D.C.
FALL MEETING	**November 9–10, 1944**	DAYTON, OHIO
WRIGHT BROTHERS LECTURE	**December 17, 1944**	WASHINGTON, D.C.
THIRTEENTH ANNUAL MEETING	**January 30–31, February 1, 1945**	NEW YORK
SPRING MEETING	**April, 1945**	DETROIT, MICHIGAN

The Officers and Council of the Institute invite participation in the Technical Sessions of the Meetings of the Institute.

The Meetings Committee will consider for inclusion on the program complete papers, or outlines or summaries of proposed papers.

Information for Participants

(1) Complete papers or outlines or summaries should be submitted in triplicate at least four months prior to the meeting at which it is proposed to present the paper. Outlines or summaries should not exceed 1,000 words.

(2) Each paper should be so planned that it may be presented within a time limit of 45 minutes.

(3) All papers submitted will be considered for publication in the **Journal of the Aeronautical Sciences** or the **Aeronautical Engineering Review.** While a paper should be planned to take only 45 minutes for presentation at a meeting, the written presentation may have a maximum length of approximately 15,000 words.

(4) All material received will be submitted to the Meetings Committee. Authors will be notified, in ample time to prepare the complete paper, whether or not their papers can be scheduled for presentation.

All correspondence should be addressed to

The Meetings Committee

Institute of the Aeronautical Sciences
1505 RCA Building West
30 Rockefeller Plaza
New York 20, N. Y.

Drag of Airfoils in Grids of High Solidity

J. R. WESKE*

Case School of Applied Science

Introduction

AIRFOIL GRIDS OF HIGH SOLIDITY are applied in duct bends, in the blading of turbines and compressors, in heat exchangers, and in numerous applications, such as scavenging ports of two-cycle Diesel engines. The present investigation deals with grids of zero stagger, operating at zero lift and consisting of symmetrical airfoils, profile N.A.C.A. 0012. An analysis has been undertaken of the drag of airfoils in grid arrangement.

Earlier Investigations

Grids of this type have been investigated both theoretically and experimentally by a number of investigators. An early investigation by Kirschmer[1] was undertaken to furnish design data for the design of rakes in hydraulic installations. Further data are found in an N.A.C.A. report by Biermann and Herrnstein[2] in connection with an investigation of the interference between two struts. Grids quite similar to the type under discussion were analyzed theoretically and experimentally by Keller.[3] Grids of related type are treated by Ruden.[4] Although not dealing with airfoils in grid arrangement, Squire and Young[5] developed calculations for the profile drag of airfoils which are of direct interest for the present investigation.

In addition to these investigations, mention should be made of theoretical and experimental work on two-dimensional diffusers, since certain characteristics of the flow in diffusers may be related readily to the flow through grids. A list of literature of fairly recent date in regard to the latter has been compiled by Polzin.[6] Reference will be made to certain results of these investigations in subsequent sections of the paper.

Flow Through Grids, General Aspects

In analyzing the profile drag of airfoils, whether in grid arrangement or in indefinite flow, distinction may be made between two component parts, namely, the drag produced by normal pressures and the drag produced by skin friction. Of special interest among the causes contributing to the profile drag are those which arise in the wake downstream of the trailing edge.

In airfoils in indefinite flow operating at high Reynolds Numbers, the drag arising from normal pressures generally is small, since the flow pattern closely conforms to the potential flow pattern. Such deviations as do occur are caused by the displacement of the main flow caused by the boundary layer. In the case of airfoils in grid arrangement the flow outside the boundary layer is of finite extent laterally, hence the displacement caused by the development of the boundary layer is capable of producing a pronounced deviation of the flow pattern of the main flow from potential flow and a corresponding rise in the relative magnitude of the part of profile drag resulting from normal pressures.

A further aspect of the flow through grids as affecting profile drag is of interest, namely, the conditions influencing the development of the wake. It is known that in the case of the individual airfoil in indefinite flow, the static pressure at the trailing edge, approaching the stagnation pressure, is larger than the pressure of undisturbed flow. The wake and the adjacent main flow leaving the trailing edge therefore are subjected to acceleration. On airfoils in grids of high solidity a corresponding rise of static pressure at the trailing edge is exceedingly slight, if at all noticeable, again as a result of the finite extent of the main flow. In place of the pressure drop, a pressure rise occurs in the wake. This is caused by the decrease of the mean velocity of main flow as a result of the decay of the wake. This decrease of mean velocity follows by continuity relation from the gradual disappearance of the area of low velocities in the wake. The wake and the adjacent main flow, upon passing the trailing edge, therefore are subjected to deceleration. It is of interest to investigate what effect the pressure rise in the wake of airfoils in grid arrangement has upon the development of the wake and upon the profile drag.

Theoretical Treatment

The coefficient of the drag C_D of an airfoil may be expressed in terms of the momentum thickness Θ as follows:

$$C_D = 2\Theta_0/C \qquad (1)$$

where

C = chord

$\Theta_0 = \int_0^\delta \frac{u}{U_0}\left(1 - \frac{u}{U_0}\right)dy$, the subscript $_0$ denoting a plane far downstream

y = distance normal to the direction of flow

u = $f(y)$ velocity in the boundary layer

U = velocity of free stream just outside the boundary layer.

Presented at the Aerodynamics Session, Twelfth Annual Meeting, I.A.S., New York, January 25–27, 1944.

* Professor of Aerodynamics.

If the growth of the momentum thickness with distance in the direction of flow were known, the contributions of various regions of the airfoil and of the wake could at once be calculated. Calculations of the momentum thickness for the individual airfoil in indefinite flow have been carried out by Squire and Young[5] for the three distinct regions, namely, the region of laminar boundary layer, the region of turbulent boundary layer, and the wake. In applying this calculation to airplanes in indefinite flow, it is found that the location of the point of transition from the laminar to the turbulent regime in the boundary layer has an appreciable effect upon the profile drag. Tests on airfoils in grid arrangement, on the other hand, have shown that for grids of high solidity which are considered in this paper, the location of the transition point may be assumed with good accuracy to be at the point of maximum thickness of the airfoil.

The momentum equation for the turbulent boundary layer is as follows:

$$\tau = \frac{d}{dx}(\rho U^2\Theta) - \delta^x\frac{dp}{dx} \tag{2}$$

where

p = static pressure
τ = shear stress on the surface
$\delta^x = \int_0^\delta[(U-u)/U]dy$ displacement thickness of the boundary layer

The pressure gradient is related to the variation of velocity outside the boundary layer by Bernoulli's equation, which is valid at the edge of the boundary layer

$$dp/dx = -\rho UU'$$

where $U' = dU/dx$.

Substitution of the ratio $H = \delta^x/\Theta$, which may be interpreted as the reciprocal of the mean wake velocity in per cent of main stream velocity and which constitutes an effective parameter indicative of the wake velocity profile, leads to the following form of the above equation, replacing the shear stress by the coefficient of skin friction:

$$f = (\tau/\rho U_0^2)/2$$

$$2f = \frac{d\Theta}{dx} + \frac{U'}{U}(H+2)\Theta \tag{3}$$

An estimate is made of the relative magnitude of the quantities of Eq. (1) on the basis of the following data representing mean experimental values:

$$\tau = 0.002\rho(U_0^2/2)$$
$$\delta^x = 0.01\,ft$$
$$\frac{dp}{dx} = 1.0\rho(U_0^2/2)$$

Hence

$$\delta^x(dp/dx) \approx 5\tau$$

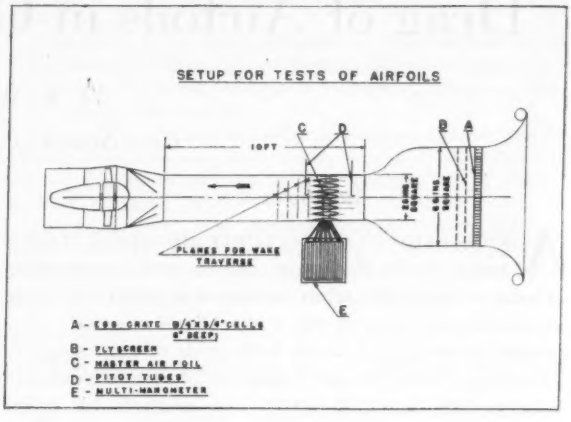

FIG. 1. Test setup.

The momentum equation for the wake which may be derived from the momentum equation of the turbulent boundary layer (Eq. (3)), simply by deleting the term representing the shear stress, is

$$\frac{d\Theta}{dx} + \frac{U'}{U}(H+2)\Theta = 0 \tag{4}$$

In order to determine the coefficient drag of the airfoil, Eq. (1), it will be necessary to calculate the ultimate momentum thickness of the wake Θ_0. This requires an integration of Eq. (4). To do this, it is necessary to state the ratio H, as a function of the ratio of velocity in the main stream just outside of the wake to the ultimate velocity U/U_0.

In the case of the airfoil in indefinite flow, Squire and Young cite test data, shown in Fig. 4, obtained in free flight, from which these authors, after showing that the effect of variation of H is limited to a narrow range, derive the following relation:

$$H - 1 = \text{const.}\,\log_e(U_0/U)$$

and when substituting this relation into Eq. (4) and integrating, obtain for the ultimate momentum thickness

$$\Theta_0 = \Theta_3(U_3/U_0)^{(H_3+5)/2}$$

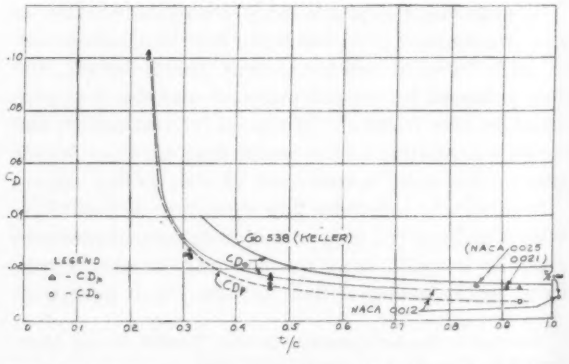

FIG. 2. Measurements of drag for grids of various solidity ratios.

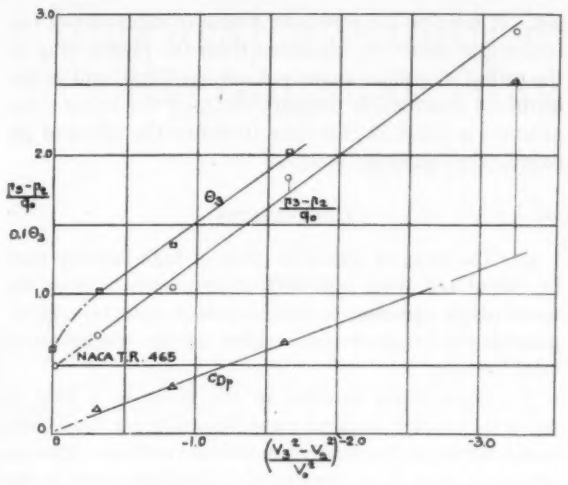

FIG. 3. Analysis of the drag produced in the turbulent boundary layer.

where the subscript $_3$ refers to the plane of measurement of wake traverse.

In discussing the general aspects of flow through grids it was pointed out that the main flow downstream of the trailing edge of airfoil grids is retarded and not accelerated, as in the case of the individual airfoil in indefinite flow, the quantity $\log_e (U/U_0)$ therefore covers a range of negative instead of positive values.

An experimental investigation was undertaken to determine the functional relation between H and $\log_e (U/U_0)$ and thus to establish a basis for the integration of Eq. (4) and, by this means, for the determination of the profile drag of airfoils in grids of high solidity. The results are shown in Fig. 5.

Experimental Investigation

Experimental work was conducted in a wind tunnel shown in Fig. 1. This wind tunnel, of NPL type, has a carefully designed inlet producing a uniform pattern of flow of low turbulence. Its working section is closed and of constant cross-sectional area. No adjustment has been made on the lateral walls to compensate for the frictional pressure drop, since the exact magnitude of the latter as affected by the presence of the grid was unknown and probably of minor influence compared with the "jet contraction" referred to later. The airfoil grid consists of profiles N.A.C.A. 0012 of 15-in. chord and 28-in. span. Half airfoils were fastened to the lateral walls. The solidity of the grid, i.e., the ratio of pitch to chord, was varied by installing a successively larger number of airfoils, their number being from one to eight. Intermediate grid spacings could be obtained by narrowing the working section through false side walls.

The center or master airfoil had a metal section at midspan provided with 50 pressure holes distributed over both sides from leading to trailing edge. Each of these pressure taps was connected individually to a tube of a multimanometer. The pressure distribution was recorded for each test by photoprinting the fluid columns on sensitized paper.

Pitot tube readings were taken upstream of the grid at a point one chord length ahead of the leading edge. The profile drag of the central airfoils and, in a few instances, of adjacent airfoils was obtained from wake traverses using a small total-static pitot tube in several transverse planes at $0.15C$, $0.3C$, $0.6C$, and $1.0C$ downstream of the trailing edge.

Results

The results obtained from tests and from calculations based on measured data are shown in Fig. 2, namely, the drag coefficient of the airfoil as a function of the solidity ratio. Also shown are the component parts of the drag coefficient, namely, the pressure drag calculated by integrating the static pressure distribution over the airfoil in direction of flow and the additional drag produced by turbulent momentum exchange in the wake. For comparison there are plotted in this diagram the experimental data given by Keller.[8] Furthermore there are included in this figure the profile drags of certain symmetrical airfoils of various thickness ratios from wind-tunnel tests in indefinite flow. These latter were correlated with the grid data by means of potential flow theory.

The curves of Fig. 3 show the effect of the flow in the main stream of airfoil grids upon the pressure gradient and upon the momentum thickness Θ_3, measured 0.15 C downstream of the trailing edge.

The development of the wake of airfoils in grids of the various solidity ratios investigated is represented graphically in Fig. 4, showing curves of momentum thickness Θ, displacement thickness δ^* and of the ratio H.

Finally a plot has been prepared (Fig. 5) of the variation of the ratio H with $\log_e (U/U_0)$, where values of the latter quantity were calculated from the measured

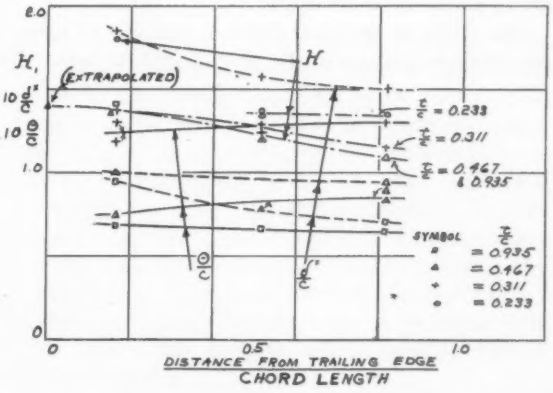

FIG. 4. Variations of quantities defining the development of the wake.

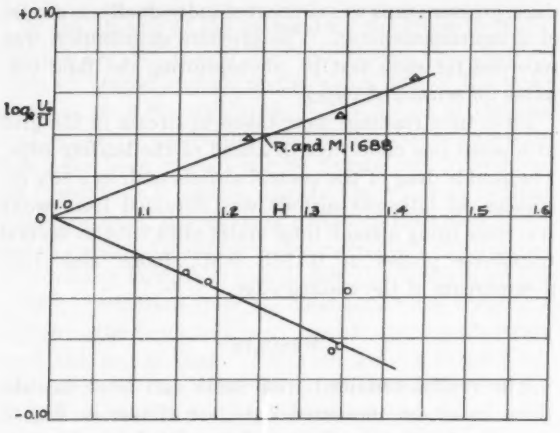

FIG. 5. Variations of the ratio H with $\log_e (U_0/U)$.

displacement thickness by means of the continuity relation. For comparison this graph also shows the test points for free flight from reference 5.

It was observed that for grids of the highest solidity ratio investigated, $t/c = 0.234$, separation did not occur, although in a similar investigation by Keller,[3] at lower Reynolds Numbers, separation occurred at a smaller solidity ratio. There was evidence, however, that the development of the wake for this grid differed from that of smaller solidity ratios, chiefly by the fact that the expected static pressure rise failed to occur.

It is to be recalled that wake traverse measurements were taken at midspan of the airfoil only. The above irregularities therefore may have their cause in variations of flow along the span. In fact, from a comparison of the velocity measurements upstream and downstream of the grid, the conclusion is reached that the grid has the effect of diverting the initially uniform airstream from both spanwise ends of the grid toward the midspan portion. This jet contraction, which was observed and discussed by Keller, appears to cause acceleration of the flow on midspan downstream of the grid. Its development is closely related to the transverse contamination observed in the boundary layer of flat plates placed between end plates.

The effect of jet contraction is believed to cause a considerable increase of the drag of grids of high solidity. It may be the foremost source of discrepancy between grid losses as calculated from the profile drag of the airfoil in grid arrangement, on one hand, and as determined from static pressure drop, on the other. No attempt is made at this time to define the effect of jet contraction quantitatively.

CONCLUSIONS

1. The drag of airfoil in grids of high solidity may be calculated with sufficient approximation from the momentum equation of the turbulent boundary layer, assuming a constant mean value for the coefficient of skin friction.

2. Momentum transfer in the wake in a field of adverse pressure gradient causes losses larger than those encountered in the wake of individual airfoils. This increase of drag is of significance, however, only in the case of grids of very large solidity ratio.

3. In grids of high solidity ratio there is evidence of displacement of the flow from the ends of the airfoils toward the midspan portions, observed previously and referred to as jet contraction. This phenomenon, which may be related to transverse contamination of the boundary layer, produces a condition of flow at the ends resembling separation while the flow on midspan still adheres. It is believed to increase the drag of grids of high solidity above values which might be expected on the basis of profile drag alone.

REFERENCES

[1] Kirschmer, O., *Investigation of the Loss of Head of Rakes*, Communication, Munich, Inst. of Techn., Vol. 1, p. 21, 1926.

[2] Biermann, D., and Herrnstein, W. H., Jr., *The Interference between Struts in Various Combinations*, N.A.C.A. T.R. No. 468, 1933.

[3] Keller, C., and Marks, L. S., *The Theory and Performance of Axial-Flow Fans*, p. 66; McGraw-Hill Book Company, Inc., New York, 1937.

[4] Ruden, P., *Investigations of Single Stage Axial-Flow Blowers*, Luftfahrtforschung, Vol. 14, pp. 325–346 and 458–473, 1937.

[5] Squire, H. B., and Young, A. D., *The Calculation of the Profile Drag of Airfoils*, R. & M. No. 1838, 1937.

[6] Polzin, J., *Flow Investigations in a Two-Dimensional Diffuser*, Ingenieur-archiv, Vol. 11, No. 5, pp. 361–385, October, 1940. R.T.P. Translation No. 1286, British Ministry of Aircraft Production.

Flexural Strength in the Plastic Range of Rectangular Magnesium Extrusions

F. A. RAPPLEYEA* AND E. J. EASTMAN†

The Dow Chemical Company

ABSTRACT

A problem exists in the use of magnesium alloys in aircraft of determining the resisting moment in bending. Special methods and theories have to be used in order to predict these values because of the lower yield strength of wrought magnesium alloys in compression as compared to tension. The standard classic formula $f = Mc/I$ is not applicable, and some other formula is necessary. Experimental tests were made which agreed fairly well with the theoretical formula:

$$M_r = bh^2(\Sigma Q_c + \Sigma Q_t)/(\epsilon_c + \epsilon_t)^2$$

where

M_r = moment of resistance
b = width of beam
h = depth of beam
ΣQ = first moment of stress-strain curve about stress axis
ϵ = strain in outermost fiber

Subscripts c and t refer to compression and tension, respectively.

The tests were made on various magnesium alloys of several different sizes. The deviations of experimental results from theory were not excessive.

INTRODUCTION

IT HAS BEEN the general engineering practice to use the classic bending theory to determine the strength of beams in bending. This classic theory states that plane sections before bending remain plane after bending, and, in the elastic range, the stress is proportional to the strain. The stress is expressed mathematically by the conventional formula

$$f_b = Mc/I$$

where f_b = stress at a fiber located at a distance c from the neutral axis, M = applied bending moment, and I = moment of inertia about the neutral axis. The stress computed by this formula when used in the plastic range is a fictitious stress and is called the modulus of rupture. The modulus of rupture varies with the width and shape of the cross section, and a form factor is introduced to take account of the shape.

In present practice there are a number of aircraft materials which have low proportional limits. Since the classic formula no longer holds above the proportional limit, it is evident that some more accurate method of analysis should be developed. Some investigators[1, 2] have already recognized that the above-mentioned discrepancy is due to the difference in stress distribution from the classic theory when the plastic range is reached. Methods for determining the allowable flexural resistant moment have been developed.[7]

Wrought magnesium alloys usually have a compressive yield strength less than the tensile yield strength. Consequently, when a beam is subjected to flexure, symmetrical about a horizontal axis, the outermost fibers on the compression side of the beam may be strained in the plastic region, while the outermost fibers on the tension side are still strained elastically. The position of the neutral axis then shifts toward the tension side to compensate for this difference in strain of the outermost fibers. This shift of the neutral axis means that more material is in compression than in tension.

In most cases, the ultimate strength of magnesium beams, like steel beams, cannot be developed, since bending deflections become excessive when plastic flow occurs. It has been previously proposed[1] that design for material with low proportional limits be based on an allowable resisting moment when the outermost fiber on the tensile side is strained to the yield strain as the criterion rather than the classic formula, $f = Mc/I$.

TEST PROCEDURE

A jig was designed so that third-point loading could be obtained. This is a type of loading which gives pure bending without shear across the center third of the beam. The discussion of test results is confined to the middle third of the beam, which is under constant bending moment.

Loads and reactions were applied through knife edges. The supports at the ends were carried on ball bearings to allow longitudinal movement with a minimum of friction. Figs. 1 and 2 show details of the test setup. Electric strain gauges of the SR-4 type were mounted on the sides, top, and bottom of the specimens to determine the strain distribution across the section of constant moment. The strains were read at a number of different loads. The results were plotted over the cross section of the beam, as shown in Figs. 3b and 4b. The distribution of strain is seen to be linear, thus proving that plane sections before bending remain plane after bending.

The strains were converted to stresses by means of stress-strain curves, such as Fig. 5, which were obtained

Presented at the Structures Session, Twelfth Annual Meeting, I.A.S., New York, January 25–27, 1944.

* Engineer.
† Engineer.

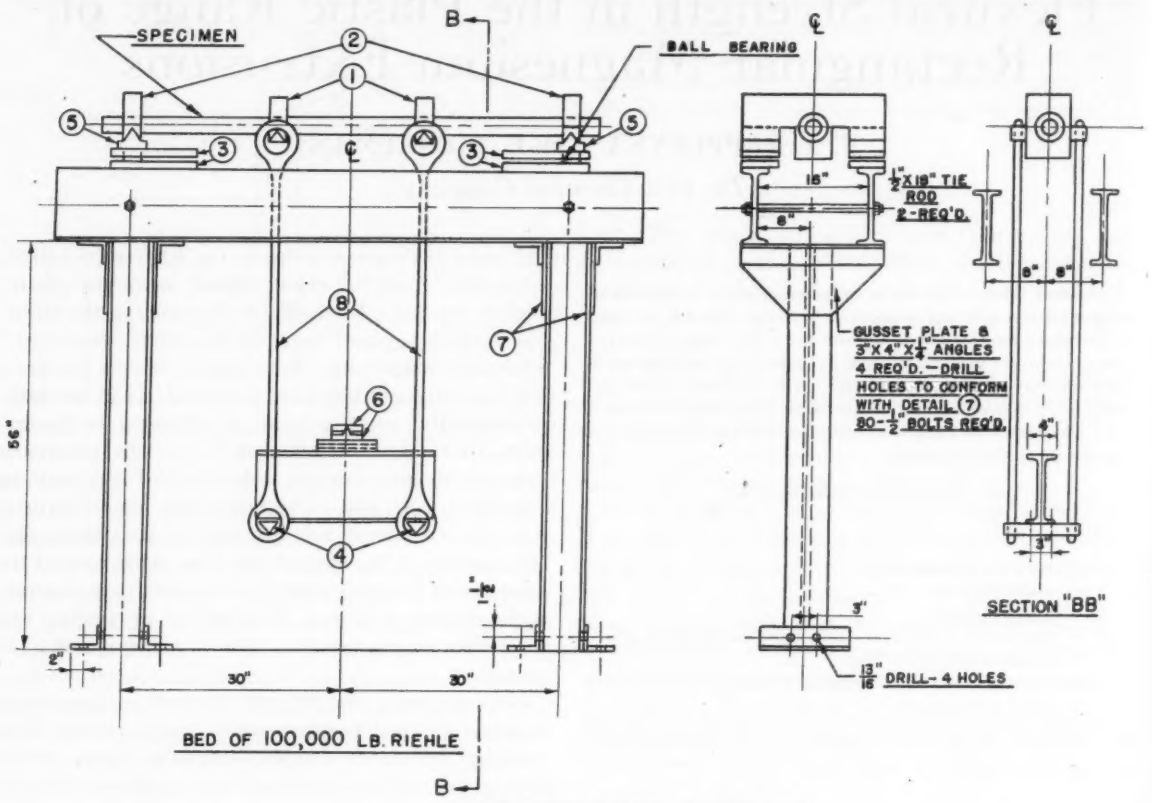

BEND TEST FRAME & FIXTURES FOR 100,000 LB. RIEHLE

FIG. 1.

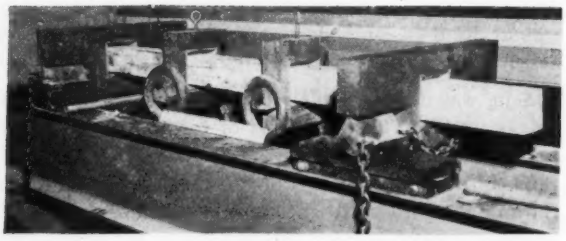

FIG. 2.

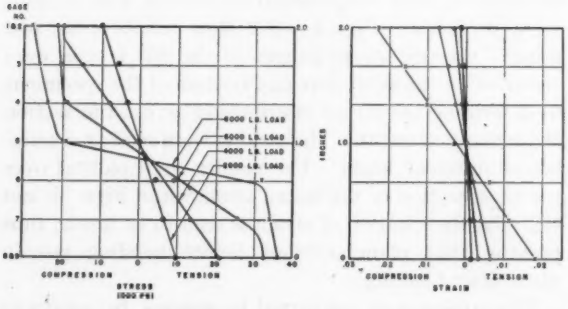

FIG. 3. Bending beyond the yield point. J-1 alloy; 2 in. by 2 in. Spec. No. 25621.

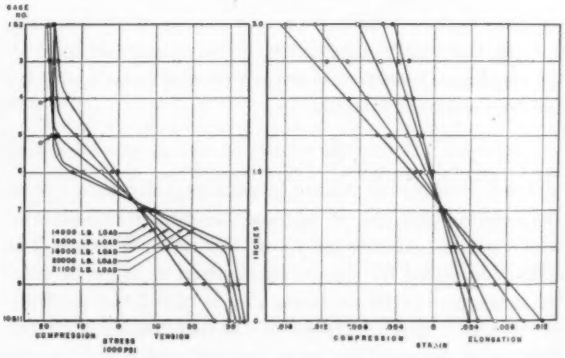

FIG. 4. Bending beyond the yield point. J-1 alloy; 3 in by 3 in. Spec. No. 25689-1.

by tensile and compressive tests of the specimens cut from the beam. The resulting distribution of stresses is shown in Figs. 3a and 4a.

THEORY

The moment of resistance of a cross section of a rectangular beam subjected to pure bending is given by the following formula (Eq. 15, p. 165 of reference 7):

TABLE 1
Calculation of Static Moment and Area of Compression Stress-Strain Curves

	(1) Item	(2) Strain, In. per In.	(3) Mean Strain, In. per In.	(4) Stress, Lbs. per Sq.In.	(5) Mean Stress, Lbs. per Sq.In.	(6) Interval Area, Lbs. per Sq.In.	(7) ΣQ, Lbs. per Sq.In.	(8) ΣA, Lbs. per Sq.In.
Compression	0	0	0	0	0	0	0	0
	1	0.0022		14,500		16.0*	0.023†	16.0
			0.0026		15,750			
	2	0.0030		17,000		12.6	0.056	28.6
			0.0035		17,200			
	3	0.0040		17,400		17.2	0.116	45.8
			0.0070		17,700			
	4	0.0100		18,000		106.0	0.858	151.8
			0.0150		19,500			
	5	0.0200		21,000		195.0	3.790	346.8
			0.0250		22,250			
	6	0.0300		23,500		222.5	9.360	567.3
			0.0350		25,000			
	7	0.0400		26,500		250.0	18.11	819
			0 0450		28,000			
	8	0.0500		29,500		280.0	30.71	1,099
			0.0550		31,750			
	9	0.0600		34,000		317.5	48.11	1,417
			0.0650		37,000			
	10	0.0700		40,000		370.0	72.21	1,787
			0.0750		43,250			
	11	0.0800		46,500		432.5	104.50	2,220
			0.0850		49,500			
	12	0.0900		52,500		495.0	146.50	2,715
Tension	0	0	0	0	0	0	0	0
	1	0.0047		25,000		58.7‡	0.184**	58.7
			0.0048		25,875			
	2	0.0050		26,750		7.8	0.220	66.5
			0.0055		28,000			
	3	0.0060		29,250		28.0	0.374	94.5
			0.0065		29,750			
	4	0.0070		30,250		29.8	0.568	124.3
			0.0075		30,625			
	5	0.0080		31,000		30.6	0.897	155
			0.0085		31,250			
	6	0.0090		31,500		31.2	1.162	186
			0.0095		31,750			
	7	0.0100		32,000		31.8	1.480	217
			0.0150		34,250			
	8	0.0200		36,500		342.0	6.610	560
			0.0250		37,500			
	9	0.0300		38,500		375.0	16.000	935
			0.0350		39,150			
	10	0.0400		39,800		391.5	29.700	1,327
			0.0450		40,400			
	11	0.0500		41,000		404.0	47.900	1,731
			0.0550		41,350			
	12	0.0600		41,700		413.5	70.600	2,145
			0.0650		42,100			
	13	0.0700		42,500		421.0	98.00	2,566
			0.0750		42,750			
	14	0.0800		43,000		427.5	130.00	2,944
			0.0850		43,250			
	15	0.0900		43,500		432.5	166.80	3,427
			0.0950		43,600			
	16	0.1000		43,700		436.0	208.30	3,963
			0.1050		43,750			
	17	0.1100		43,800		437.5	254.30	4,401

Columns (2) and (4)—taken from stress-strain curve of material.
Columns (3) and (5)—arithmetic average of items m and $m - 1$ in columns (2) and (4), respectively.
Column (6)—difference in strain of items m and $m - 1$ multiplied by value for m in column (5).
Column (7)—value in column (6) multiplied by value in column (3) and summed progressively.
Column (8)—summation of values in column (6).
* $(0.0022)(14,500)/2$.
† $(0.0022)^2(14,500)/3$.
‡ $(0.0047)(25,000)/2$.
** $(0.0047)^2(25,000)/3$.

$$M = bh^2 \int_{\epsilon_c}^{\epsilon_t} f(\epsilon)\epsilon d\epsilon/(\epsilon_c + \epsilon_t)^2$$

where

For purposes of numerical integration this can be reduced to

$$M_r = bh^2(\Sigma Q_c + \Sigma Q_t)/(\epsilon_c + \epsilon_t)^2 \qquad (1)$$

M_r = moment of resistance
b = width of beam
h = depth of beam

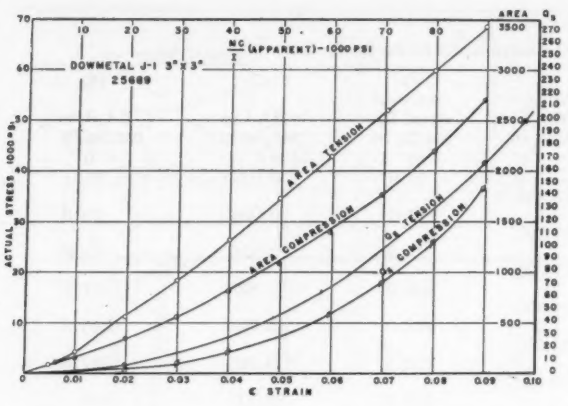

FIG. 5.

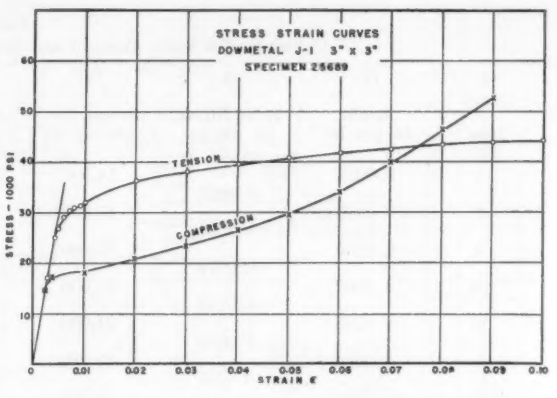

FIG. 6.

ΣQ = first moment of stress-strain curve about stress axis

ϵ = strain in outermost fiber

Subscripts c and t refer to compression and tension, respectively.

For materials with identical stress-strain curves in tension and compression $\epsilon_c = \epsilon_t$, the moment of resistance in the plastic range can easily be calculated by Eq. (1). When the compressive yield strength is lower than the tensile yield strength, the compressive strain in the outermost fiber no longer equals the tensile strain in the outermost fiber. Therefore, if an allowable strain on the tension side is assumed, the corresponding strain on the compression side must be determined. By the law of statics, the load on the compression side of the beam must equal the load on the tension side of the beam. In a beam of constant width this means that the area under the tensile stress-strain curve up to a strain, ϵ_t, must equal the area under the compressive stress-strain curve up to a strain, ϵ_c. Knowing what portions of each stress-strain curve to use, the first moment of these areas about the neutral axis can be calculated. Therefore, all items in Eq. (1) are known, and the moment of resistance can be calculated.

To illustrate the above procedure, one specimen will be followed through completely. Tensile and compressive stress-strain curves of specimen 25689, Dowmetal J-1, are given in Fig. 5. These curves were integrated as shown in Table 1.

Stress-strain curves in tension and compression of the beam material are divided into a triangle and number of trapezoids. The areas under the curve of each item are determined and summed, and the first moment of each increment of area about the stress axis is calculated and summed.

From the values in columns (2), (7), and (8), the curves plotting area versus strain and the static moment versus strain for both tension and compression were drawn in Fig. 6. Now, when the tensile yield strength is reached on the outermost tensile fiber of the beam, a strain, ϵ_t, of 0.0077 results. This corresponds to an area of 124 under the tensile stress-strain curve. (See Fig. 7 for lower part of area-strain curves of Fig. 6 enlarged.) For an equal area under the compressive stress-strain curve, a strain, ϵ_c, of 0.0097 in the outermost compressive fiber is found. The lower portions of the static moment curves are also replotted on Fig. 7. Entering the respective static moment plots at strains corresponding to ϵ_c and ϵ_t, static moments for ΣQ_c and ΣQ_t are found to be 0.780 and 0.760. All values in the formula are now known, and it is a matter of substitution to find the moment of resistance.

$$b = 3.0 \text{ in.}$$
$$h = 3.0 \text{ in.}$$
$$\Sigma Q_c = 0.780 \text{ lb. per sq.in.}$$
$$\Sigma Q_t = 0.760 \text{ lb. per sq.in.}$$
$$c = 0.0097 \text{ in. per in.}$$
$$t = 0.0077 \text{ in. per in.}$$
$$M_r = \frac{3 \times 3^2 \times (0.780 + 0.760)}{(0.0097 + 0.0077)^2}$$
$$M_r = 137{,}000 \text{ in.lbs.}$$

Referring to the actual test of this specimen, when

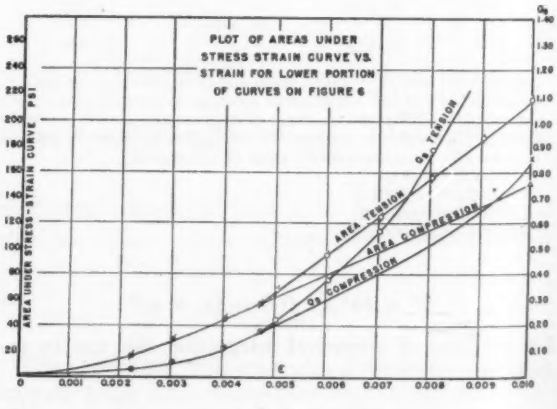

FIG. 7.

TABLE 2
Test Results and Predicted Results

Dowmetal Alloy	Size	Tensile Yield Strength, Lbs. per Sq.In.	Compressive Yield Strength, Lbs. per Sq.In.	Applied Moment at ϵ_t = Yield Strain, In.Lbs.	Predicted Moment at ϵ_t = Yield Strain, In.Lbs.	Center Deflection in Middle Third of Beam at ϵ_t = Tensile Yield Strength	
						Actual, in.	Predicted, in.
O-1	4 by 4	34,300	24,900	366,000	370,000	0.0882	0.0960
O-1	3 by 3	26,500	19,000	123,900	126,000	0.1090	0.1020
O-1	2 by 2	32,900	21,000	47,600	45,500	0.210	0.205
J-1	4 by 4	30,000	19,800	297,000	298,000	0.114	0.103
J-1	3 by 3	30,600	17,100	136,000	137,000	0.144	0.152
J-1	2 by 2	33,400	22,000	41,300	42,700	0.191	0.181
FS-1	4 by 4	30,500	15,700	283,000	289,000	0.088	0.0955
FS-1	3 by 3	27,700	12,200	103,000	97,000	0.124	0.125
FS-1	2 by 2	30,000	20,800	39,600	37,100	0.209	0.2410
M	3 by 3	35,100	11,100	114,700	108,600	0.143	0.1733
M	2 by 2	28,400	8,800	28,490	25,800	0.330	0.2820

the strain gauge on the outermost tensile fiber registered a strain equal to the tensile yield strain, the actual measured applied moment was 136,000 in.lbs. Similar calculations of predicted allowable moments of resistance were made for all specimens tested and the predictions compared to the actual tests. A good agreement is shown in Table 2 for the various magnesium alloys tested.

The differences between applied and predicted moments at the yield strain were on the conservative side with few exceptions. The exceptions do not exceed 4 per cent. These variations can be caused by the variation of material properties across the cross section of the extrusion and also by inherent errors in accuracy of testing equipment. For design purposes, if the specified minimum stress-strain curves were used, the allowable moments of resistance obtained would be satisfactory.

There may be some question as to whether under the allowable flexural yield resisting moment the deflection will be excessive. For that reason the center deflection in the middle third of the beam was measured and recorded in Table 2 for the points at the flexural yield strength. This deflection for the beam loaded at the third points can also be predicted, either in the elastic or plastic range by means of a formula[7]

$$\delta = 1^2(\epsilon_c + \epsilon_t)/2h \qquad (2)$$

Permanent set at this flexural yield strength was of the order of 0.01 in. and could well be considered within the limits of assembly tolerance of any structure. Fig. 8 shows the curves of center deflection in the middle third of the beam as measured and as calculated.

REFERENCES

[1] Cozzone, Frank P., *Bending Strength in the Plastic Range*, Journal of the Aeronautical Sciences, Vol. 10, pp. 137–151, May, 1943.

[2] Beilschmidt, J. L., *The Stresses Developed in Sections Subjected to Bending Moment*, Journal of The Royal Aeronautical Society, Vol. 46, pp. 161–181, July, 1942.

[3] Gilkey, H. J., *Materials Testing;* McGraw-Hill Book Company, Inc., New York, 1941.

[4] Davis, Troxwell, Wiskocil, *Testing and Inspection of Engineering Materials;* McGraw-Hill Book Company, Inc., New York, 1941.

[5] Churchill, H. D., *Physical Testing of Material;* A series of five educational lectures on the physical testing of metals presented to the members of the A.S.M. during the eighteenth National Metal Congress and Exposition, Cleveland, 1936.

[6] Timoshenko, S., *Strength of Materials, Part I;* D. Van Nostrand Company, Inc., New York, 1930.

[7] Nadai, A., *Plasticity;* McGraw-Hill Book Company, Inc., New York, 1931.

[8] Volterra, E., *Results of Experiments on Metallic Beams Bent Beyond the Elastic Limit*, Journal of the Institution of Civil Engineers, No. 5, 1942–43, March, 1943.

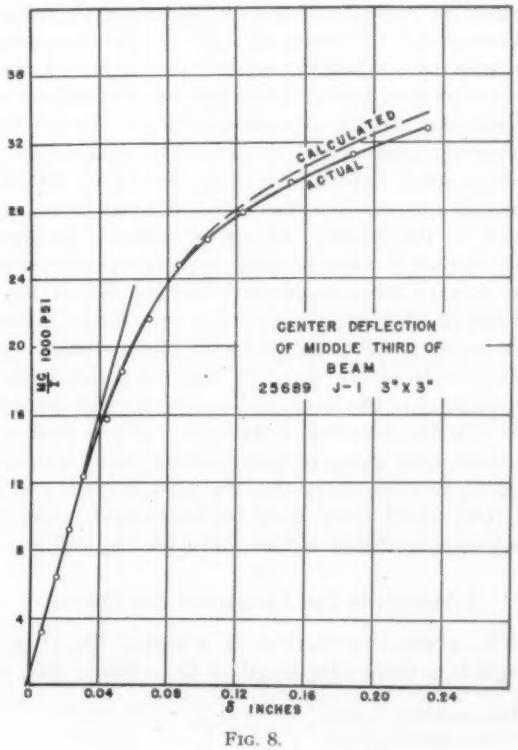

FIG. 8.

Corrections for Lengths of Columns Tested Between Knife Edges

WILLIAM R. OSGOOD*

National Bureau of Standards

Introduction

More often than not when a column tested between knife edges is supported on carriers between the knife edges and the ends of the column, the length of the column is taken as the distance between knife edges. When this is done, only a small error is introduced if the column specimen is long relative to the distance between knife edges, but the error may amount to several per cent for short columns. There are two practical ways of avoiding this error in tests made under eccentrically applied loads when it is desired to obtain column curves corresponding to a series of constant eccentricities.

Testing Groups of Columns

One method consists of making tests of groups of columns, each column specimen of a given group having the same length, $\overline{DF}$, Fig. 1, and thus the same ratio of slenderness and each column of the group being tested with a different initial eccentricity e. With the depth d of the carrier and the initial eccentricity e known, the angle of rotation ϕ of the end of the column is measured at the maximum load, and the eccentricity at the maximum load is computed as $d \sin \phi + e \cos \phi$. Then a series of curves can be plotted of average stress against eccentricity at maximum load. From these curves the customary curves can be constructed of average stress against ratio of slenderness for different constant eccentricities, the ratios of slenderness being based on the lengths, $\overline{DF}$, of the column specimens. This method involves plotting an extra series of curves, the average stress-eccentricity curves, and it has a further disadvantage if instead of the ratio of slenderness use is made of the preferable dimensionless variable $\lambda = (1/\pi)(\overline{DF}/i)\sqrt{S/E}$, where i is the radius of gyration, S is the compressive secant yield strength, and E is the modulus of elasticity. If λ is used as a variable, each group of tests must be made with constant λ, and this means that the yield strength and the modulus of elasticity must be determined before the specimens can be cut to the proper lengths, $\overline{DF}$.

Correcting the Length of the Column

The alternative method of avoiding the error in length is to correct the length of the column. The correction may be made rationally by the following considerations. In Fig. 1 let an eccentrically loaded column under a load P be represented by $CDFG$. Rigid carriers of depth d are assumed at each end, and the initial eccentricity of the load is e. The rotation of each end of the column is ϕ. The column would behave somewhat differently if the same material and section as the rest of the column were substituted for the rigid ends CD and GF over their entire lengths, and the problem is to substitute for the ends the proper lengths to make the column so formed behave like the test column. The end CD (and similarly FG) can be replaced by a portion of a sine curve DJ tangent to CD at D if the stresses near the ends of the column specimen at D and F are elastic or if the effective modulus near the ends is sensibly constant. The length of the equivalent column so formed is less than that of the original column by the amount $2\overline{CJ} = 2(d \cos \phi - d_0)$, and it is now a question of determining d_0. Since, ordinarily, the depth of the carriers is small relative to the length of the specimen and the angle ϕ will rarely exceed 10°, the assumption of a constant effective modulus in the short portions at the ends may be considered reasonable.

Under the assumed conditions the equivalent centrally loaded column of constant modulus would be represented by the sine curve $OJDKL$ of (half-wave) length l_0, passing through the point J with coordinates $x = l_0/2 - (l/2 + d_0)$, $y = e \cos \phi$. Its equation is

$$y = \frac{e \cos \phi}{\cos (\pi/l_0)(l/2 + d_0)} \sin \frac{\pi x}{l_0} \qquad (1)$$

where the axes and $l/2$ are as indicated in the figure, K being the midpoint of the centrally loaded column. By the equivalent centrally loaded column is meant the centrally loaded column, failing at the load P, that has the same cross section as the given column specimen and a constant effective (double) modulus equal to that at the ends of the column specimen. From the first derivative of y with respect to x (Eq. (1)) taken at the point D,

$$\tan \phi = \frac{\pi e \cos \phi}{l_0} \frac{\sin [\pi l/(2l_0)]}{\cos (\pi/l_0)(l/2 + d_0)} \qquad (2)$$

and from the geometry of the figure,

$$\tan \phi = \frac{\dfrac{e \cos \phi}{\cos \dfrac{\pi}{l_0}\left(\dfrac{l}{2} + d_0\right)} \sin \dfrac{\pi}{l_0}\left(\dfrac{l_0}{2} - \dfrac{l}{2}\right) - e \cos \phi}{d \cos \phi}$$

Received May 1, 1944.

* Materials Engineer.

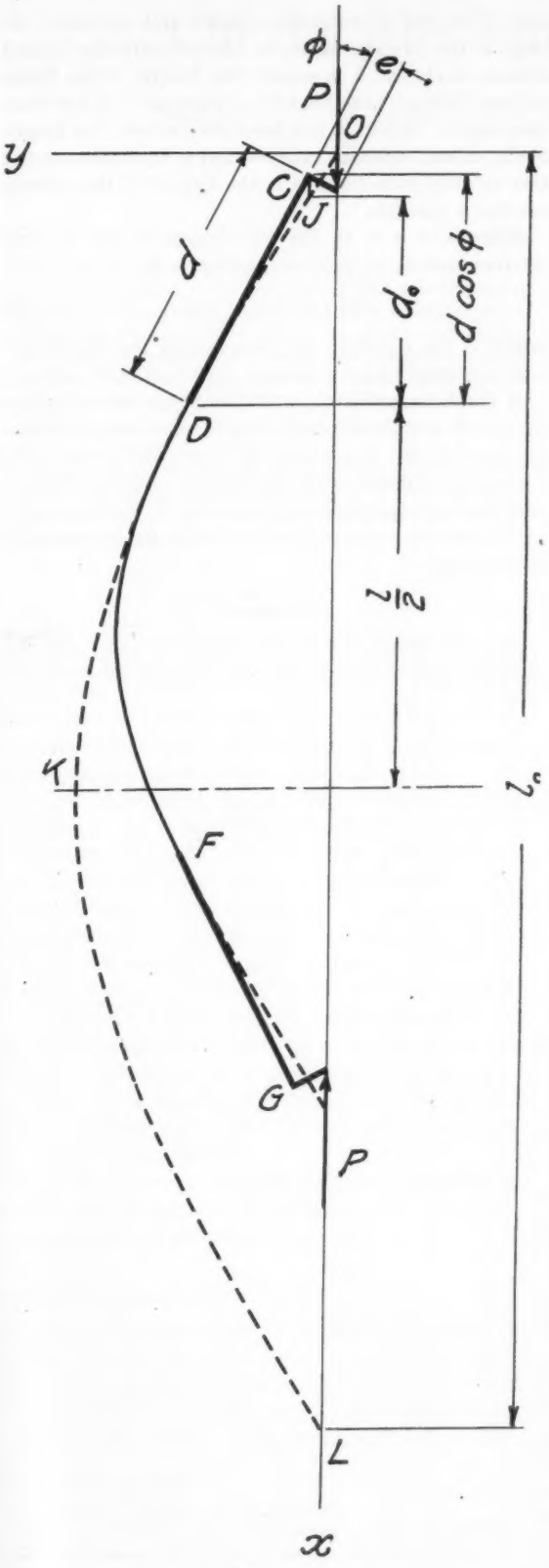

FIG. 1.

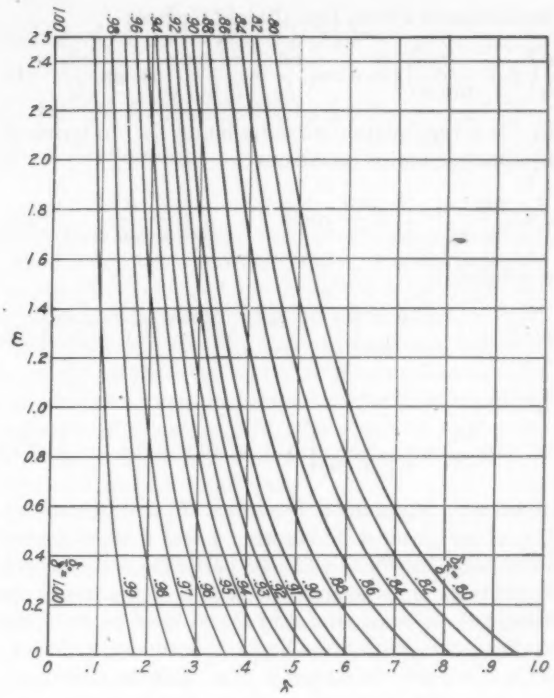

FIG. 2a.

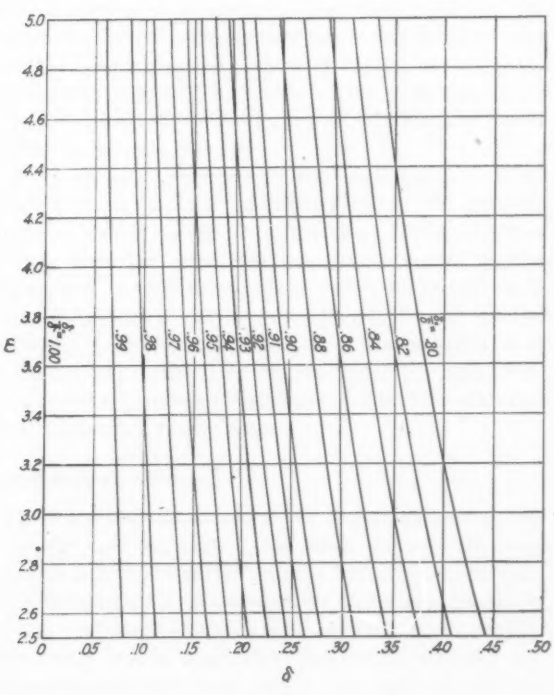

FIG. 2b.

or, when simplified,

$$\tan\phi = \frac{e}{d}\left\{\frac{\cos\left[\pi l/(2l_0)\right]}{\cos\left(\pi/l_0\right)(l/2+d_0)} - 1\right\}. \qquad (3)$$

Elimination of l from Eqs. (2) and 3 gives

$$\frac{\pi}{l_0}\left(d + \frac{e}{\tan\phi}\right)\cos\phi\cos\frac{\pi d_0}{l_0} = \frac{\pi e\cos\phi}{l_0\tan\phi} + \sin\frac{\pi d_0}{l_0} \quad (4)$$

Eq. (4) is the equation for determining d_0. In terms of the nondimensional quantities

$$\delta_0 = \frac{\pi d_0}{l_0} \qquad \delta = \frac{\pi d}{l_0}\cos\phi \qquad \epsilon = \frac{e}{d\tan\phi} \quad (5)$$

its solution is

$$\tan\delta_0 = \delta\,\frac{1+\epsilon}{1-\delta^2\epsilon^2}\left[1 - \frac{\epsilon}{1+\epsilon}\sqrt{1+\delta^2(1+2\epsilon)}\right] \quad (6)$$

or

$$\tan\frac{\delta_0}{2} = \frac{1}{\delta(1+2\epsilon)}\left[\sqrt{1+\delta^2(1+2\epsilon)} - 1\right] \quad (6a)$$

In order to determine d_0 from Eqs. (5) and (6) or (6a), d, e, ϕ, and l_0 must be known. d and e are measured dimensions, known as soon as a particular test has been decided on. ϕ is the angle of rotation of the end of the column at the maximum load P and must be measured at that load. Within the limits of accuracy of the correction, $\cos\phi = 1$ and $\tan\phi = \phi$. l_0 is the free length of a centrally loaded column that would fail at the same load P as the eccentrically loaded test column. So long as the average stress in the eccentrically loaded column is elastic, l_0 is simply the length of the Euler column failing at the load P. Otherwise l_0 is less than this length. When d_0 has been determined, the length of the column without carriers that is equivalent to the test column with carriers is the length of the column specimen plus $2d_0$.

When $e = \epsilon = 0$, Eq. (6) reduces to $\tan\delta_0 = \delta$; or since now $d_0 = {}^1/_2(l_0 - l)$ and $\phi = 0$,

$$\cot(\pi l/2l_0) = \pi d/l_0 \quad (7)$$

which is the equation for determining the free length l_0 of a centrally loaded column tested on rigid carriers.[1]

A graphic representation of Eq. (6) is shown in Figs. 2a and 2b and these figures may be used where extreme accuracy is not important, as it usually is not. The figures are entered with the known values of δ and ϵ, and the corresponding value of $\delta_0/\delta = d_0/(d\cos\phi)$ is read from the curves of constant δ_0/δ, by interpolation if necessary.

REFERENCE

[1] Osgood, William R., *Column Strength of Tubes Elastically Restrained Against Rotation at the Ends*, N.A.C.A. Report No. 615, 1938.

On the Mechanism of Friction

BERNHARD W. SAKMANN* AND JOHN T. BURWELL, JR.†
Massachusetts Institute of Technology

ABSTRACT

If two bodies slide over each other, matter is exchanged between the two surfaces. This exchange of material was studied by means of a radioactive method which made it feasible to detect small traces of material of 10^{-10} gram. Even under the smallest loads of a few grams transferred matter could be detected under dry as well as lubricated conditions. This fact indicated that the exchange of material might be of fundamental importance in all frictional processes, and it seemed desirable to investigate this exchange process systematically.

This paper reports the dependence of this transfer of material on various parameters such as normal load, distance of travel, roughness and hardness of the sliding surfaces, nature of the contacting materials, and lubrication.

INTRODUCTION

IN SPITE OF ITS FREQUENT OCCURRENCE the phenomenon of friction is little understood. Because of the importance of frictional effects an understanding of the nature of friction should be of value to the engineer both in controlling its detrimental effects and in making positive use of it where beneficial.

It is now known that the coefficient of friction of two substances is not a fundamental physical property in the sense in which, for instance, the thermoelectric power is characteristic for a pair of metals. The measured value of the coefficient of friction is the composite result of various other characteristics of the two contacting surfaces; many of these properties are difficult to specify accurately, such as surface contamination, previous history, surface roughness, and hardness. This statement about the uncertainty of the value of the friction force is substantiated by the fact that even in accurately controlled experiments the values of friction coefficients determined by different authors scatter considerably.

What, then, are the important factors influencing frictional effects and how do variations of these factors affect the frictional phenomena?

Factors Influencing Frictional Effects

The earliest theory[1] of the mechanism of dry friction maintains that the frictional force is due to the interlocking of the asperities of the two surfaces, and that work is required to push the minute protuberances of one surface over those of the other surface. While the surface irregularities may contribute appreciably to the friction between rough bodies, it is not probable that the interlocking of the asperities is the main factor in friction between the smooth surfaces encountered in most industrial applications. In support of this view one might mention the fact that friction does not decrease beyond a certain point if the surfaces are made progressively smoother. In some cases it may even be observed that the friction coefficient decreases if smooth surfaces are roughened.

A second theory[2,3] is based on the assumption that adhesion plays a major part, and that "cold welding" takes place over the area of contact. If two solid surfaces are in contact, they touch only at their highest points. Because of the fact that the true area of contact is very small the local pressures involved may be extremely high even under comparatively light loads. Under the influence of these high pressures the surfaces are welded together over the contact areas.

In a modified version of the adhesion theory[4] of kinetic friction it is assumed that during sliding the minute welds are continuously made and broken, and that the major part of friction is caused by the force required to rupture the welds. The fact that static friction is generally greater than sliding friction would appear to support this view.

More recently this theory has been further elaborated[5] to take account of differences in the relative hardness values of the two surfaces. If the slider is harder than the base, the roughness peaks of the former will plough through the softer material, small amounts of which will be left adhering to the harder surface. If, on the other hand, the slider is softer, it is locally welded to the base surface under the high pressures involved, and small globules of the rider material are left adhering to the base.

Experimental Evidence

The experimental evidence for any of these theories is scanty and indirect. For most smooth surfaces encountered in industrial practice the amount of material transferred is so minute as to escape detection by the ordinary experimental techniques available. Only under severe conditions does one obtain any experimental evidence from which one may extrapolate to the more ordinary cases. In the forced fits of collars, for instance, it is a common observation that the two surfaces become welded into a single piece. If the two surfaces are separated, large amounts of one surface are left adhering to the other one. This experience is

Received June 20, 1944.

* Department of Mechanical Engineering.

† Department of Mechanical Engineering. Now Lieutenant, U.S.N.R., stationed in the Office of the Coordinator of Research and Development, Navy Department, Washington, D.C.

particularly frequent if the two surfaces are of the same material. Whether this mechanism of friction operates in the region of light loads was until recently a matter of speculation.

The present work was undertaken with the aim of establishing the existence of material transferred from one surface to the other under light loads. Even the most refined microchemical techniques are not sensitive enough because the quantities of material involved are very small. In addition, chemical analysis cannot be used if the two surfaces are of the same material. For that reason a very sensitive method was developed which allows the study of exchange of material between similar as well as dissimilar surfaces. This method, which is described below, employs the activation of one surface by means of artificial radioactivity.

Method

A few of the 92 elements are naturally radioactive, emitting beta rays and gamma rays; the former are negatively charged particles, while the latter are electromagnetic waves whose wave lengths are considerably shorter than those of X-rays. Highly sensitive instruments have been developed for the detection of the rays emitted by the radioactive elements. In recent years it has become possible to induce artificial radioactivity in many ordinarily stable elements. The activation of the inert elements is achieved by bombardment of the material with various particles such as neutrons, protons, or deuterons. The charged particles are accelerated under the action of the equivalent of several million volts; at these high speeds the particles are able to penetrate the nuclei of the bombarded atoms transforming them either to a different chemical element or to a different isotope of the same element.

In general, the new nuclei are not stable, but transform into another stable nucleus. This transformation is associated with the emission of corpuscular rays or gamma rays, both of which can be detected by suitable instruments.

Because of the high sensitivity of the recording instruments it is possible to detect the presence of even small amounts of artificially radioactivated material. If proper techniques are developed, one can quantitatively determine the amount of activated material from the intensity of the radiation recorded by the detecting instruments; the sensitivity of this method exceeds the microchemical analysis by several orders of magnitude. While the experimental technique will be reported in more detail elsewhere, the principles of the method are briefly outlined in the following:

Principles of the Method

A base surface of copper alloy was made radioactive by deuteron bombardment in the M.I.T. cyclotron. After the activation of the copper alloy spherical or hemispherical friction samples were slid over the base surface under various conditions of load and distance of travel. During the friction tests a certain amount of radioactive base material was deposited on the surface of the rider. After the friction experiments the initially inert riders were tested for the presence of radioactive material and the amount of transferred material could be determined from the intensity of the emitted radiation. Of all the materials of technical importance copper was found to be the most suitable for the radioactive method. Because pure copper is softer than most of the copper alloys used for bearings, a flat surface of copper-beryllium was used for most of the measurements. Besides copper and copper alloy targets flats of manganese steel were used; however, the sensitivity which was attained by deuteron bombardment of manganese steel was considerably less than that achieved with copper alloys.

During deuteron bombardment of copper-beryllium targets some of the copper nuclei are transformed into unstable zinc nuclei while others are transformed into unstable isotopes of copper. The unstable nuclei decompose with the emission of beta rays and gamma rays. Since the intensity of radiation originating from the target decayed in an exponential fashion, it had decreased to such an extent within several hours after the bombardment that further measurements were not possible. As a result, only a limited number of friction experiments could be performed for each activation of the base surface.

Friction Equipments

In the friction experiments small spheres were slid over the base surface with a velocity of about 3 mm. per sec. If flat riders were used, the uncertainty in locating the area over which the transferred material was distributed caused considerable inaccuracy in determining the amount of deposited material. The use of spherical riders made it possible to locate the position of the transferred material. Commercial steel and phosphor bronze balls provided a convenient source of uniform reproducible sliders. After preliminary measurements had shown that a detectable amount of material was transferred under ordinary sliding conditions, a more careful investigation of the effect of load, distance of travel, hardness, surface roughness, and nature of the material was made.

The complexity of frictional effects mentioned in the beginning was substantiated. However, the results given below should throw some light on the fundamental mechanisms involved and should permit an evaluation of the various proposed theories.

Results

In the first series of experiments riders of different materials were slid over the copper-beryllium base surface under identical conditions of load and distance

of travel. The amounts of material transferred from the base to the different riders are shown in Table 1.

TABLE 1

Copper-Beryllium Deposited on Riders of Various Materials

Material of Rider	Transferred Copper-Beryllium, Microgram
Phosphor bronze	0.043
Steel	0.0084
Glass	0.0053

The table shows that phosphor bronze riders picked up the greatest amount of copper-beryllium, but it should be noted that even glass, although very dissimilar to the copper alloy, took up small amounts of base metal. The effect of load on the amount of deposited material was studied next for both phosphor bronze and steel. The results, which are shown in Fig. 1, indicate that within the accuracy of the measurements the amount of transferred material is proportional to the applied load.

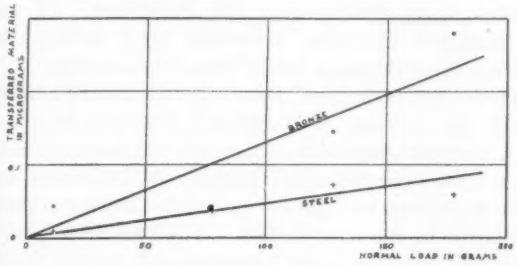

FIG. 1. Amount of transferred material in micrograms versus normal load in grams.

Influence of Distance of Travel

The influence of the distance of travel was studied next. In Fig. 2 the amount of transferred material in micrograms is plotted versus the distance of travel in centimeters. For both types of rider the amount of deposited material is roughly proportional to the distance of sliding. The results show similar behavior for phosphor bronze and steel riders although the quantities of transferred material involved are quite different.

However, the two materials were found to behave quite differently when the effect of surface finish was studied. In Fig. 3 the material transferred to steel riders is plotted versus the surface roughness in root mean square microinches. From this plot it is evident that the rough specimens took up more material than the smooth ones. With phosphor bronze riders, on the other hand, substantially the same amount of material was transferred over a range of surface roughness from 2 to 13 microinches. There was even some indication that less material was deposited on the rough specimens.

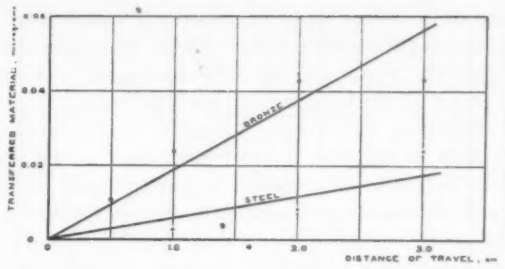

FIG. 2. Amount of transferred material in micrograms versus distance of travel in centimeters.

The steel riders were harder than the copper-beryllium base, while the phosphor bronze specimens were softer. This difference in behavior with respect to surface roughness might, therefore, be ascribed to either of two causes: difference in hardness or dissimilarity of the two materials. In order to eliminate one of the two effects, it was decided to anneal the steel riders to the same hardness as the phosphor bronze specimens. When this was done, it was found that the steel riders of surface roughness from 1 to 11 micro-inches picked up approximately equal amounts of base material. As in the case of phosphor bronze riders slightly less base material was found on the rough specimens. From these tests one may therefore conclude that surface roughness is of major importance only if the riders are harder than the base.

Influence of Hardness

Since the results of these measurements demonstrated that hardness is an important factor, it was decided to investigate the influence of this parameter more thoroughly. Steel riders were prepared for these measurements because of all materials of technical importance steel covers the widest hardness range. The results are shown in Fig. 4 in which the transferred material is plotted versus the inverse of the Brinell hardness of the rider. It is evident from this plot that, within the accuracy of the measurements, the

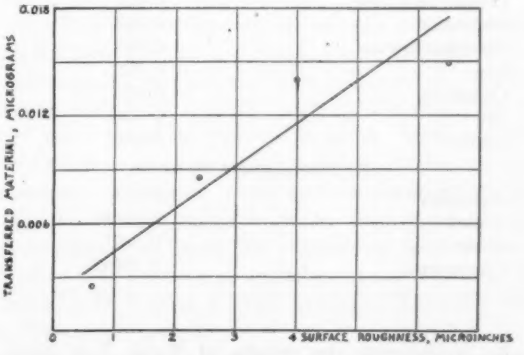

FIG. 3. Amount of transferred material in micrograms versus surface roughness in microinches for steel riders.

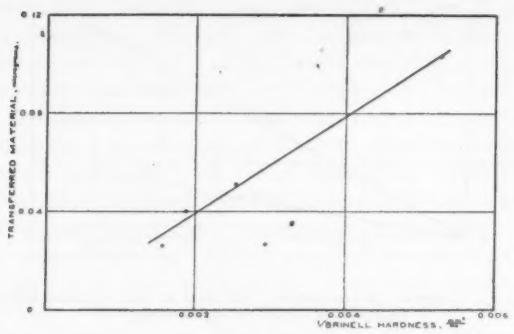

FIG. 4. Amount of transferred material in micrograms versus inverse of Brinell hardness in mm.²/kg. for steel riders.

deposited material is inversely proportional to the Brinell hardness which in its turn is inversely proportional to the area of the Brinell depression. The area of the Brinell depression is closely related to the true area of contact between spherical rider and flat base surface. One might thus interpret the measurements with the assumption that the transferred material is proportional to the true area of contact.

Nature of the Material

The nature of the material is another factor distinguishing steel riders from phosphor bronze specimens, and it is to be expected that, all other things being equal, the rider material is of importance in frictional behavior. To investigate this parameter, several riders of different materials were prepared. Some of the riders were cut from solid stock, while other materials had to be electroplated onto steel balls. The latter surfaces were in general much harder. Table 2 shows the results of the measurements.

TABLE 2

Copper-Beryllium Transferred to Riders of Different Materials

Material of Rider	Deposited Copper-Beryllium, Microgram
(A) Cut from Solid Stock	
Copper-beryllium	0.025
Aluminum	0.013
Phosphor bronze	0.091
Zinc	0.022
Cadmium	0.023
Tin	0.026
Lead	0.036
(B) Electroplated Materials	
Antimony	0.014
Nickel	0.0028
Silver	0.0073
Chromium	0.00012

In considering the results of Table 2 it must be borne in mind that it was impossible to control the hardness of the various materials. It is interesting that even soft metals such as lead, tin, and cadmium of Brinell hardness 3.8, 5.5, and 21 kg./mm.², respectively, took up material from the much harder copper-beryllium base of 310 Brinell. In general the electroplated materials picked up less base metal.

Difference of Hardness

The effect of difference in hardness between the various materials of Table 2 can be eliminated to some extent by considering the apparent area of contact between spherical rider and flat base; this area can be estimated visually under the microscope. One can obtain a value for the average thickness of the deposit by dividing the product of the apparent area of contact and the specific gravity of copper-beryllium into the amount of transferred material listed in Table 2. It was found that the copper-beryllium riders showed the greatest layer thickness of 1000 Ångströms or 10^{-5} centimeters. Likewise the deposit on phosphor bronze riders extended to a depth nearly equal to that found on copper-beryllium specimens. On the other hand, of all the materials cut from solid stock, lead had the smallest layer thickness of 100 Ångströms. Of the electroplated materials chromium steel showed an average layer thickness of less than 10 Ångströms.

These results suggest that, all other things being equal, the amount of transferred material increases with the solid solubility of the two metals in contact. To test these results more conclusively, measurements were made with two pairs of materials differing in their similarity to the base surface. The two materials of each pair had the same hardness and surface finish while their solid solubilities in copper were very different. The tests were performed under identical conditions of load and distance of travel. Phosphor bronze and annealed chromium steel were chosen as the materials of the first pair. The second pair of materials consisted of nickel and a low-carbon steel. Nickel and copper are completely soluble in the copper-beryllium base while the copper-iron phase diagram indicates only a limited solid solubility of copper in iron. Table 3 shows the results of these measurements.

TABLE 3

Material Transferred to Dissimilar Riders of the Same Hardness

Material of Rider	Brinell Hardness	Deposited Material, Microgram
Annealed chromium steel	195	0.046
Phosphor bronze	185	0.072
Low-carbon steel	220	0.022
Nickel	220	0.047

From the values of Table 3 it is evident that appreciably more material is transferred to phosphor bronze and nickel than to chromium steel and low-carbon steel.

Lubrication Effects

Finally the effect of the presence of a lubricant was studied by sliding the riders over the base under dry and lubricated conditions. Under conditions of hydrodynamic lubrication the two sliding surfaces are completely separated by a liquid film. In this case no material is transferred from one surface to the other. In actual operating conditions it is seldom possible to maintain a liquid film completely covering the entire surface at all times. When machines are started, conditions of boundary lubrication prevail, and some metal-to-metal contact takes place. For that reason it seemed to be of interest to see how partial lubrication would affect the exchange of matter.

For these tests the base surface was copiously covered with pure mineral oil. It was found that the difference of the material transferred under dry and lubricated conditions depended on the nature of the material of the rider and on the value of the normal load. The difference was found to be greater for lighter loads. Table 4 shows the amount of material deposited on steel and phosphor bronze riders under a normal load of 25 grams.

TABLE 4

Material Transferred to Riders Under Dry and Lubricated Conditions

Material of Rider	Transferred Copper-Beryllium, Microgram	
	Dry	Lubricated
Phosphor bronze	0.021	0.010
Steel	0.0025	0.0006

Finally an attempt was made to measure the material picked up by a rider when pressed against the base surface without lateral displacement. In all cases some deposited material could be detected on the rider. However, studies of the effect of normal load were inconclusive because the amount of deposited material was near the limit of the sensitivity of the method. Furthermore, in spite of all precautions, it was impossible to avoid small lateral displacements, a difficulty already pointed out by Claypoole and Cook.[6]

CONCLUSION

In summarizing it may be said that riders of all the materials studied took up some bulk material from the base. W. B. Hardy's postulate[7] that seizure and wear are characteristic of all frictional phenomena is thus corroborated by experiment. Base material was taken up by metals as soft as lead and by substances as dissimilar to the base material as glass. In the case of the soft metals it was evident from visual inspection under the microscope that some of the rider material had been smeared over the base surface.

Even under the smallest loads matter was transferred under dry as well as under lubricated conditions. This fact suggested that the exchange of material between sliding surfaces might be of fundamental importance in all frictional phenomena including the operation of machinery and it was hoped that systematic investigation of the transfer of matter might lead to a better understanding of frictional effects.

It was found that the amount of material transferred under otherwise identical conditions was proportional to the load and to the distance of travel.

For steel riders it was found that the material picked up from the copper-beryllium base was inversely proportional to the Brinell hardness of the rider. If the deformation of the rider during the friction test was plastic rather than elastic, the results of these measurements could be explained on the assumption that the amount of deposited material was proportional to the area of contact.

The amount of transferred material increased with the surface roughness of the rider if the latter was harder than the base. If, on the other hand, the riders were softer than the base material, surface finish was of minor importance.

This dependence on surface roughness can be understood on the basis of Bowden's[5] picture of friction between materials of different hardnesses according to which the hard rider ploughs up the soft base material. For rough surface riders the furrows in the base are deep, and it is to be expected that more base metal adheres to the rider. If, on the other hand, the rider is softer, its roughness peaks are flattened until a contact area is reached which is characteristic of the hardness of the softer material and the normal load. Measurements of the dependence on the hardness of the rider seemed to indicate that the transferred material was proportional to the area of contact.

It was shown that for identical conditions of hardness and surface finish the transferred matter was greater for phosphor bronze and nickel than for annealed chromium steel and low-carbon steel. Copper, the chief constituent of phosphor bronze, as well as nickel, is completely soluble in the base material while iron is practically insoluble in copper.

Thus it is interesting to note that the measurements reported here can, to a certain extent, be interpreted in terms of the properties of the bulk material such as hardness and solid solubility despite the fact that no steps were taken to remove invisible surface films. However, it is difficult to say to what extent one can generalize the limited experimental results thus far obtained. Furthermore, it is to be expected that surface films often mask the relationship between solid solubility and amount of transferred material, and it is probable that more metal is transferred if these surface films are removed.

Lubrication with pure mineral oil reduced the amount of deposited material. It was shown that the reduction

depended on load and, for the same load, on the nature of the material of the sliding surfaces.

While the picture of the frictional process is far from being complete, it can be concluded from the present work that in dry and lubricated metallic friction appreciable material transfer takes place even under smaller loads than those occurring in ordinary mechanical machinery. The radioactive method provides a useful tool for studying the frictional effects in various cases of practical importance.

The conclusion that transfer is least if the solid solubility of the two materials is small is only a more precise formulation of the well-known empirical rule of machine designers which states that bearing and journal should be made of dissimilar materials in order to minimize galling and seizure. The work of metallurgists and physical chemists on solid solubility relationships might well be turned to practical use in machine design.

The somewhat complex dependence of metal transfer on hardness and surface roughness may explain the rather conflicting current opinions on the best methods for surface finishing cylinder barrels and piston rings. It appears that not only the surface roughness, but also the relative hardness must be considered.

It is hoped that further work along these lines may contribute to an understanding of friction in industrial machinery, particularly in the internal combustion engine.

References

[1] Coulomb, C. A., *Théorie des Machines Simples*, Nouvelle Edition, pp. 99–105; Bachelier, Paris, 1821.

[2] Tomlinson, G. A., *A Molecular Theory of Friction*, Philosophical Magazine, Vol. 7, Series 7, pp. 905–939, June, 1929.

[3] Hardy, W. B., and Hardy, J. K., *Note on Static Friction and on the Lubricating Properties of Certain Chemical Substances*, Philosophical Magazine, Vol. 38, Series 6, pp. 32–48, July, 1919.

[4] Bowden, F. P., and Leben, L., *The Nature of Sliding and the Analysis of Friction*, Proceedings of the Royal Society of London, Series A, Vol. 169, No. A 938, pp. 371–391, February, 1939.

[5] Bowden, F. P., and Tabor, D., *Friction and Lubrication*, Report No. 1, Council for Scientific and Industrial Research, Bulletin No. 145, Commonwealth of Australia, Melbourne, 1942.

[6] Claypoole, W., and Cook, D. B., *The Nature of Static Friction*, Journal of the Franklin Institute, Vol. 233, No. 5, pp. 453–463, May, 1942.

[7] Hardy, W. B., *Problems of Lubrication*, Proceedings of the Royal Institution of Great Britain, Vol. 23, pp. 65–72, February, 1920.

The Response of Helicopters with Articulated Rotors to Cyclic Blade Pitch Control

A. F. DONOVAN* AND M. GOLAND†

Curtiss-Wright Corporation

SUMMARY

Results are obtained which permit calculation of the response of rotary wing aircraft to arbitrary control displacements. The type of craft specifically dealt with is equipped with a single lifting rotor, whose blades are hinged so as to possess freedom in flapping. Control of the craft is effected by cyclically varying the pitch of the rotor blades.

A criterion for the stability of such machines is derived, taking into account seven degrees of freedom. These are (a), (b) longitudinal and transverse motion of the center of gravity of the fuselage; (c), (d) rolling and pitching about the center of gravity of the fuselage; (e) tilt of the rotor cone in a pitching sense relative to the fuselage; (f) tilt of the cone in a rolling sense relative to the fuselage; and (g) coning of the rotor blades.

The suitability of cyclically varying the pitch of the rotor blades to obtain control of the craft is investigated, and the response of the machine to abrupt control displacements is studied in detail.

Numerical calculations are carried out for a particular machine in an initial hovering, or near hovering, condition. The present criterion indicates that the single rotor craft (of conventional design) is dynamically unstable; however, the period of the unstable oscillation is found to be almost twice as long, and the rate of amplification very much smaller, than is indicated by the previously published results of Hohenemser. Hence, the present treatment indicates the machine to be less unstable than has heretofore been assumed.

It is found that a condition of neutral stability is attained if the drag forces on the rotor are eliminated.

The response of the machine to an imposed cyclic pitch is traced through the first several seconds of motion, starting from the hovering state. The results are shown in graphic form.

INTRODUCTION

IT IS THE PURPOSE of this paper to outline methods for calculating the response of rotary wing aircraft to arbitrary control displacements. The mathematical analysis presented here deals only with machines that are in a hovering or near hovering state. Methods for extending the theory to include cases where the machine is in an initial state of steady translation are discussed in the Appendix. The stability of such craft, equipped with articulated rotors, is investigated thoroughly, and a study is made of the control characteristics obtainable by cyclically varying the pitch of the rotor blades. The load factors resultant from an abrupt stick displacement for a machine in an initial hovering condition are also computed.

The type of rotary wing craft specifically dealt with in this treatment is a single rotor helicopter. (Extension of the work to cover multiple rotor designs is not difficult, often resulting in some simplification of the theory. See later discussion of Hohenemser.[4]) The blades are mounted on the rotor hub by means of horizontal hinges, so as to possess freedom of flapping. For simplicity, it is assumed that there is no kinematical relationship between the blade pitch and blade flapping. Vertical hinges and dampers may be provided to permit blade leading (or lagging). Although neglected in the present treatment, their presence affects the results to only a negligible extent. Since only a single lifting rotor is employed, suitable torque correction for the rotor driving torque must be provided when necessary. Control of the craft is effected by cyclically varying the pitch of the rotor blades. The cyclic pitch variation of a particular blade follows a sinusoidal relation, with a period equal to one revolution of the rotor. Suitable controls are provided to enable the operator to govern both the maximum amount of the variation and the azimuth angle of blade rotation at which this maximum occurs.

Previous studies of somewhat similar nature have been carried out by several investigators. Their work, in general, has been based on the original development of rotary wing theory by Glauert,[1] later extended by Lock[2] and Wheatley.[3] Hohenemser[4] has investigated the stability and control of hovering machines with two coaxial, counterrotating articulated rotors, a topic similar to the one under discussion here. Von Kármán[5] and Küssner[6] have discussed the stability of helicopters with blades fitted rigidly to the rotor shaft. Miehl,[7] in an exhaustive work, deals with articulated rotors that are constrained to roll and pitch with either a constant angular velocity or a constant angular acceleration. His treatment is particularly applicable to autogyro rotors when the autogyro is provided with controls that operate independently of the rotor.

Although the work of Hohenemser[4] is similar in scope to that of the present paper, it does not possess the same degree of generality. The development presented here considers the craft response in terms of the following degrees of freedom: (a), (b) longitudinal and transverse motion of the center of gravity of the fuselage, (c), (d) pitching and rolling about the center of gravity of the fuselage, (e) tilt of the rotor cone in a pitching

Presented at the Rotating Wing Aircraft Session, Twelfth Annual Meeting, I.A.S., New York, January 25–27, 1944.

* Chief of Structures Department, Research Laboratory, Airplane Division.

† Section Head, Structural Design, Airplane Division.

sense relative to the fuselage, (f) tilt of the rotor cone in a rolling sense relative to the fuselage, and (g) coning of the rotor blades. Hohenemser considers (a) and (c) and only partially takes into account (e). Since his work is concerned mainly with the longitudinal stability of a dual rotor machine, it is proper for him to neglect the remaining two degrees of freedom, with the advantage of considerably simplifying the results. Also, no attempt is made by Hohenemser to consider the effects on the craft response of cyclically varying the blade pitch as is done here. A continued discussion of Hohenemser[4] is reserved for a later section of this paper, following the mathematical development (see "Comparison with Hohenemser's Solution").

In the work to follow, the aerodynamic forces and moments acting on the rotor are calculated by methods similar to those used by Glauert.[1] More accurate theoretical relations have been obtained by Sissingh;[3] however, their use here would introduce excessive complication.

Results and Conclusions

The results of the mathematical analysis derived in the succeeding sections of this paper are given here. It is to be kept in mind that all results and conclusions based on the present mathematical treatment are strictly applicable only for machines that are in a hovering or near hovering state. It is shown in the Appendix, however, that the theory can be extended without difficulty to include cases where the craft is in an initial condition of steady translation. An approximate upper limit on the machine speed, below which the present results remain valid, is equal to one-tenth of the rotor tip speed. In conventional machines, this limit would be approximately 40 m.p.h.

The mathematical analysis demonstrates that cyclically varying the pitch of the rotor blades is a powerful and effective means of controlling both the machine's horizontal translational velocity components and its roll and pitch orientation in space. It is also concluded that conventionally arranged helicopters, of the type described in the introduction, are characteristically dynamically unstable. Although dynamic instability is indicated, it is shown that the instability is unimportant from a practical operational standpoint. By properly proportioning the dimensions and masses of the machine's components, the period of the instability can be arranged to be of the order of $^1/_2$ min. or longer. Proper design will also make the rate of amplification of the unstable oscillation extremely small.

When the period of the oscillation is long with respect to the reaction time of the pilot and the amplification is small, the unstable characteristic will not be noticed by the operator. Normal reactions will cause the pilot automatically to correct the attitude of the disturbed machine in a small fraction of a period of oscillation. The type of corrections necessary is analogous to that required to avoid phugoid-type oscillations in an airplane subjected to random disturbances. Only if the pilot deliberately holds the controls fixed for several minutes and permits the oscillation to build up will the instability be noted.

The results indicate that the instability arises because of the fact that the vector describing the resultant aerodynamic force on the rotor is not perpendicular to the plane described by the tips of the rotor blades. The nonperpendicularity is caused by the presence of a drag force that acts parallel to the rotor tip plane and opposes the rotor motion. It is found that a condition of zero amplification of the oscillation is attained if the drag force is eliminated or if other means are taken to insure that the vectorial representation of the resultant rotor force remains perpendicular to the plane of the blade tips. A concrete manner of overcoming the inherent dynamic instability of single (or dual) rotor machines is thus suggested. In this connection it should be noted that refinement of the prevalent poor aerodynamic design of the rotor hub mechanism will improve the stability characteristics as well as the performance.

Calculations of the response to an abrupt control displacement were made assuming the machine initially statically balanced in the hovering condition. When a sudden change in cyclic pitch is made on a hovering machine, the analysis indicates that there are two principal effects.

The first is a change in the trim condition from one of hovering to steady translation. The new trim condition also requires that the rotor cone and, to a lesser extent, the fuselage be tilted in the direction of motion. Eqs. (35) show that the change in trim for a given amount of imposed cyclic pitch increases with the distance e_b of the hinges from the rotor center. Hence, the sensitivity of the control system improves as the hinge distance e_b is made larger.

The second effect arises as a result of the change in trim condition. The character of this part of the response is determined by the nature of the roots of the stability determinant Eqs. (36) and the initial conditions. These roots describe various modes of oscillation of the machine. Each mode may be of a damped or divergent character depending on the construction of the machine. For the machine whose properties are tabulated later in this paper, the roots of Eqs. (36) are

$$-0.166,\ -0.52 \pm 1.86i$$
$$-0.42 \pm 0.20i,\ 4.42 \times 10^{-4} \pm 0.0118i$$

The first three sets of roots describe two rapidly converging oscillations and one relaxation motion. The last pair of roots describe a dynamic instability with a period of 21 sec. The time required for the unstable oscillation to double its amplitude is 63 sec.

The response of the machine to an imposed 1.5° cyclic pitch θ_1 (decreasing the pitch of blades at the rear of the machine and increasing it for the forward blades) is shown graphically in Fig. 1. The conditions under which the machine is in trim with this cyclic pitch are computed from Eqs. (35) as: forward tip a_1 of rotor cone = 0, sidewards cone tip a_2 to starboard = $1^1/_2°$, forward velocity U of machine = 0, starboard velocity V = 84 m.p.h., angle of pitch α_p of fuselage = 0, and angle of roll α_r of fuselage = 0. In addition to the notation already specified, the following definitions apply to Fig. 1: t = time in seconds from instant of displacing controls, ψ = azimuth angle of blade rotation measured from the straight rearward position, μ_y = ratio of starboard speed V to rotor peripheral tip speed. For time previous to $t = \psi = 0$, the machine is in trim in the hovering state. For the details of the calculations for Fig. 1 see "Method of Solution and a Typical Numerical Calculation" later in this paper.

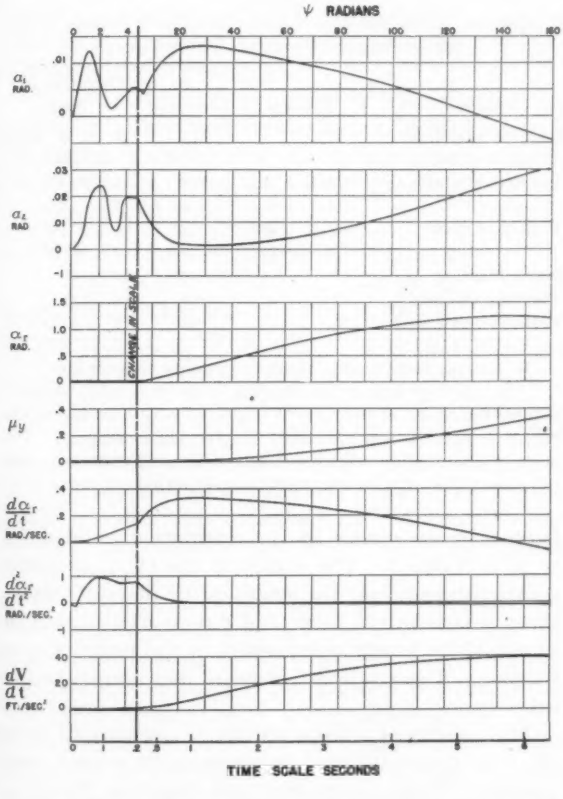

FIG. 1. Response of helicopter described in text to abrupt cyclic pitch change, $\theta_1 = 1^1/_2°$.

It will be noted that the velocity obtained from Eqs. (35) is unreasonably large. This condition arises because the drag of the machine is assumed to be linearly proportional to the velocity for purposes of mathematical simplification. A drag coefficient is chosen which is approximately correct in the speed range where the equations are valid ($\mu_y \lesssim 0.10$) but which is too small at higher speeds. The calculations are carried out only for the low-speed region, since only the first few seconds of the response are usually of interest. The results presented are, therefore, unaffected by this simplification. The fuselage trim condition of zero angle of roll likewise arises from an assumption made for analytic convenience—namely, that the fuselage drag force acts at the rotor hub. The calculations for Fig. 1 have been extended somewhat beyond their range of validity in order to more clearly illustrate the response trends. It is clear from the various plots that the long period oscillation has a pronounced effect on the motion. This oscillation is the controlling factor in determining the angular orientation of the machine and results in a rapid roll to starboard. The smooth increase of starboard velocity is of interest. The divergent character of the long period oscillation cannot be detected on the curves because of the small rate of amplification and the short length of time considered.

The coning angle a_0 of the rotor blades is found to remain unchanged throughout the motion. This is a result of the assumption that the rotor thrust is always equal to the weight of the machine. The angular components of the tilt of the rotor cone a_1 and a_2 are seen to increase fairly steadily in the first part of the motion.

Fig. 1 shows that the angular velocity of the fuselage does not exceed 0.3 rad. per sec. during the first several seconds of motion. The angular acceleration in roll has its maximum value of approximately 1.0 rad. per sec.^{2} during the first few instants following the control displacement. The starboard acceleration builds up to a maximum of 38 ft. per sec.^{2} at the end of the first 6 sec. It is of particular interest to note that an imposed cyclic pitch of only $1^1/_2°$ is sufficient to cause these relatively high values of acceleration.

It is suggested that the significance of the results of this work can be greatly increased by a program of systematic calculation of the responses for machines of various size and mass proportions and for various conditions of initial steady translation of the craft. The most efficient means for accomplishing this would seem to be through the use of a differential analyzer.

In a later part of the paper, a comparison is made between the results of the present work and that of Hohenemser.[4] Both solutions indicate that the machine in this section is dynamically unstable. Hohenemser's results, however, predict a more serious instability than does the present treatment. Whereas a period of 21 sec. is predicted by the present work, calculations based on Hohenemser's solution indicate a period of 10.6 sec. According to the present work, 63 sec. are required for the unstable oscillation to double its magnitude; Hohenemser predicts the same effect in only 11.6 sec.

Blade Dynamics and Aerodynamics

To determine the motion of the blades, it is necessary to equate their inertial forces to the aerodynamic blade loads. The subsequent development utilizes the following notations:

U = longitudinal velocity at time t of fuselage center of gravity (positive forward)

V = lateral velocity at time t of fuselage center of gravity (positive to starboard)

α_p = angle of fuselage pitch at time t, rad. (positive nose upwards)

α_r = angle of fuselage roll at time t, rad. (positive for bank to starboard)

ψ = azimuth angle of blade rotation at time t, rad. (measured from downwind position of blade, positive for counter-clockwise rotation looking down on rotor)

$\Omega = d\psi/dt$ = angular velocity of rotor, rad. per sec.

β = blade flapping angle at time t, rad. (measured relative to plane perpendicular to rotor axis, positive upwards)

If the angular velocity Ω of the rotor remains constant, then $\psi = \Omega t$. The pitching and rolling angular velocities of the machine and the angular velocity of blade flapping are then, respectively,

$$\left.\begin{aligned} d\alpha_p/dt &= \Omega(d\alpha_p/d\psi) = \Omega\dot{\alpha}_p \\ d\alpha_r/dt &= \Omega\dot{\alpha}_r,\quad d\beta/dt = \Omega\dot{\beta} \end{aligned}\right\} \qquad (1)$$

where each dot represents a differentiation with respect to the blade azimuth angle ψ. Similarly, the angular accelerations become

$$\left.\begin{aligned} d^2\alpha_p/dt^2 &= \Omega^2(d^2\alpha_p/d\psi^2) = \Omega^2\ddot{\alpha}_p \\ d^2\alpha_r/dt^2 &= \Omega^2\ddot{\alpha}_r,\quad d^2\beta/dt^2 = \Omega^2\ddot{\beta} \end{aligned}\right\} \qquad (1')$$

It is to be noted that the rolling and pitching motions are referred to axes fixed in space; the flapping of the blades is measured from a plane that is fixed relative to the machine.

The kinematics of a particular blade, considering both the machine and blade to be displaced from their initial positions, is conveniently studied with the aid of the five coordinate systems described in Table 1. The frame $(\bar{x}, \bar{y}, \bar{z})$ is fixed in space; the others are not. The coordinate $\bar{x}$ is along the longitudinal axis of the craft at the start of motion and is positive in the forward direction. The coordinate $\bar{y}$ is positive to the starboard; the third coordinate $\bar{z}$ of the right-handed frame is positive vertically downwards. The other systems are obtained by reorienting the $(\bar{x}, \bar{y}, \bar{z})$ frame in the manner described in Table 1. The $(\bar{x}, \bar{y}, \bar{z})$ system is first tipped backward about the $\bar{y}$ axis by an amount α_p; a starboard bank of amount α_r is next imposed. What was originally the vertical $\bar{z}$ axis is now coincident with the direction of the rotor shaft. A further rotation of the frame by an amount $(90 - \psi)$ about this last-mentioned axis and by $-\beta$ in the flapping sense results in the orientation notated (x, y, z) in Table 1. The y axis of the (x, y, z) frame points outward along the length of the (flapped) blade; the x axis is in the tangential direction—i.e., normal to the blade length and parallel to the plane of zero flapping. The z axis is downward and normal to the other two.

Table 1

Coordinate Axes Used in Discussion

Frame	Obtained by	Remarks
$(\bar{x}, \bar{y}, \bar{z})$	See discussion of axial directions in text	Frame fixed in space
(x', y', z')	Obtained from $(\bar{x}, \bar{y}, \bar{z})$ by rotation $+\alpha_p$ about $\bar{y}$	Frame rotating about $\bar{y}$ with velocity $d\alpha_p/dt$
(x'', y'', z'')	Obtained from (x', y', z') by rotation $+\alpha_r$ about x'	Frame rotating about x' with velocity $d\alpha_r/dt$ relative to (x', y', z')
(x''', y''', z''')	Obtained from (x'', y'', z'') by rotation $+(90 - \psi)$ about z''	Frame rotating about z'' with velocity $-\Omega$ relative to (x'', y'', z'')
(x, y, z)	Obtained from (x''', y''', z''') by rotation $-\beta$ about x'''	Frame rotating about x''' with velocity $-d\beta/dt$ relative to (x''', y''', z''')

Table 2

Components of the Absolute Velocity of a Blade Section at the Radial Distance r from the Rotor Center

Source	Amount	Direction	Relative to Axes
Longitudinal flight	U	$\bar{x}$	$(\bar{x}, \bar{y}, \bar{z})$ fixed
Transverse flight	V	$\bar{y}$	in space
Pitching of craft	$\Omega\dot{\alpha}_p(l + \beta r)$	$-x'$	(x', y', z')
	$\Omega\dot{\alpha}_p r\cos\psi$	z'	(x', y', z')
Rolling of craft	$\Omega\dot{\alpha}_r(l + \beta r)$	y''	(x'', y'', z'')
	$\Omega\dot{\alpha}_r r\sin\psi$	z''	(x'', y'', z'')
Rotor rotation	Ωr	x	(x, y, z)
Flapping of blade*	$\Omega r\dot{\beta}$	$-z$	(x, y, z)
Induced down-wash	w	$-z'''$	(x''', y''', z''')

l = distance from machine center of gravity to rotor hub.

* The effect of having the flapping hinge at a small distance e_b from the center of the rotor is neglected both here and in the terms of Table 3 which likewise involve blade flapping. The neglect is permissible when the length e_b is small compared with the rotor radius R, as is always the case in actual machines.

The velocity of a blade section at a distance r from the rotor center is found by summing its several components. These components are listed in Table 2, together with a specification of their directions. It is to be noted that the five coordinate systems of Table 1 are used to advantage for the latter purpose. For simplicity, it is assumed in Table 2 that the axis of the rotor shaft passes through the center of gravity of the machine; the notation l is introduced for the distance between the machine center of gravity and the rotor hub. The down-wash velocity induced at the blade section is written as w.

It remains to resolve the variously directed velocities into components along the coördinates of a single axial frame and to sum up the directionally related contributions. In accomplishing this, some terms are obtained which contain products of the angular displacements α_p, α_r, β and/or their time derivatives. Since it is desirable that the theory remain linear throughout, these terms are not taken into account. It is assumed that α_p, α_r, β and their time derivatives are of sufficiently small magnitude to permit neglect of their products in comparison with the quantities themselves. Furthermore, if the later work is to be kept linear, it is necessary to assume that the machine velocities U and V, and the down-wash velocity w are small compared with the tip speed ΩR of the blades (R being the rotor radius). The ratios $U/\Omega R$, $V/\Omega R$, and $w/\Omega R$ are then of the same order of magnitude as the angular displacements α_p, α_r, β (i.e., first order), and second order products involving them can be neglected.

Because of these restrictions, it must be concluded that all results of the present development are limited in their application to the analysis of flight responses that do not involve large disturbances of the craft from an initial hovering condition.

To facilitate the calculation of the aerodynamic blade loads, the absolute velocities of the blade sections are desired in the directions of the x and z axes. At the radial distance r from the rotor center these velocities are, to the first order,

$$\left.\begin{aligned} v_x &= \Omega r + U\sin\psi + V\cos\psi + l\Omega(\dot{\alpha}_r\cos\psi - \dot{\alpha}_p\sin\psi) \\ v_z &= -w - \Omega r\dot{\beta} + \Omega r(\dot{\alpha}_p\cos\psi + \dot{\alpha}_r\sin\psi) \end{aligned}\right\} \quad (2)$$

The velocity v_x is normal to the blade length and parallel to the plane of zero flapping; v_z is downwards, normal to both v_x and the blade length. The expression for the velocity v_y is not given. Since v_y is directed along the blade length, its small effect on the magnitude of the blade loading is neglected. Eqs. (2) are for the blade velocities relative to the earth and, hence, the air stream; their opposites are for the air stream relative to the blades.

The components which make up the absolute acceleration of a blade section are given in Table 3. Their directions are again specified in terms of the five axial systems of Table 1. In addition to terms of the usual type, several Coriolis accelerations appear.

They arise as a result of the motion of the blades relative to the fuselage—i.e., due to the blade rotation Ω and flapping $\Omega\dot{\beta}$. These supplementary accelerations are brought into play whenever a particle translates relative to a set of axes that are themselves rotating in space. [Let (ξ, η, ζ) be a right-handed frame. If a particle has the velocity v in the η direction, measured relative to a system that is rotating about the ξ axis with an angular velocity ω, then the Coriolis acceleration of the particle is $2v\omega$ in the ζ direction. See Timoshenko and Young.[9]]

TABLE 3

Components of the Absolute Acceleration of a Blade Section at the Radial Distance r from the Rotor Center

Source	Magnitude	Direction
Longitudinal flight	dU/dt	$\bar{x}$
Transverse flight	dV/dt	$\bar{y}$
Rotor rotation	$\Omega^2 r$	$-y'''$
Blade flapping	$\Omega^2 r\beta$	$-z$
Craft pitching	$\Omega^2\ddot{\alpha}_p(l+\beta r)$	$-x'$
	$\Omega^2\ddot{\alpha}_p\, r\cos\psi$	z'
	$\Omega^2\dot{\alpha}_p{}^2(l+\beta r)$	z'
	$\Omega^2\dot{\alpha}_p{}^2\, r\cos\psi$	$+x'$
Craft rolling	$\Omega^2\ddot{\alpha}_r(l+\beta r)$	y''
	$\Omega^2\ddot{\alpha}_r\, r\sin\psi$	z''
	$\Omega^2\dot{\alpha}_r{}^2(l+\beta r)$	z''
	$\Omega^2\dot{\alpha}_r{}^2\, r\sin\psi$	$-y''$
Coriolis Accelerations		
←coupled→		
Angular Velocity	Linear Velocity	Magnitude	Direction
$\Omega\dot{\alpha}_r\cos\psi$	Ωr	$2\Omega^2\dot{\alpha}_r\, r\cos\psi$	z'''
$\Omega\dot{\alpha}_p\sin\psi$	Ωr	$2\Omega^2\dot{\alpha}_p r\sin\psi$	$-z'''$
$\Omega\dot{\alpha}_r$	$\Omega r\dot{\beta}$	$2\Omega^2 r\dot{\beta}\dot{\alpha}_r$	$\bar{y}$
$\Omega\dot{\alpha}_p$	$\Omega r\dot{\beta}$	$2\Omega^2 r\dot{\beta}\dot{\alpha}_p$	$-\bar{x}$
$\Omega\dot{\alpha}_r\sin\psi$	$\Omega r\beta\dot{\beta}$	$2\Omega^2 r\dot{\alpha}_r\beta\dot{\beta}\sin\psi$	$-z'''$
$\Omega\dot{\alpha}_p\cos\psi$	$\Omega r\beta\dot{\beta}$	$2\Omega^2 r\dot{\alpha}_p\beta\dot{\beta}\cos\psi$	$-z'''$
Ω	$\Omega r\beta\dot{\beta}$	$2\Omega^2 r\beta\dot{\beta}$	$-x'''$

It is convenient to continue to use the directions of the (x, y, z) axes for reference. Again omitting all terms that are of second order importance, the absolute accelerations of the blade sections at r are found from Table 3 to be, respectively,

$$\left.\begin{aligned} a_x &= \Omega(\dot{U} - l\Omega\ddot{\alpha}_p)\sin\psi + \Omega(\dot{V} + l\Omega\ddot{\alpha}_r)\cos\psi \\ a_y &= \Omega(\dot{V} + l\Omega\ddot{\alpha}_r)\sin\psi - \Omega^2 r - \Omega(\dot{U} - l\Omega\ddot{\alpha}_p)\cos\psi \\ a_z &= -\Omega^2 r(\ddot{\beta} + \beta - \ddot{\alpha}_p\cos\psi - \ddot{\alpha}_r\sin\psi + 2\dot{\alpha}_p\sin\psi - 2\dot{\alpha}_r\cos\psi) \end{aligned}\right\} \quad (3)$$

where $\Omega\dot{U} = dU/dt$ and $\Omega\dot{V} = dV/dt$ are the longitudinal and transverse accelerations, respectively, of the machine center of gravity. Although the work here requires a knowledge of the acceleration a_z only, the other components are given for the convenience of future investigators. The accelerations in the x and y directions would have to be known when discussing such matters as blade lagging (and leading), the power input to the rotor, and the blade stresses during maneuvering flight.

[An alternative method that can be used to obtain Eqs. (3) consists of first writing the components of the absolute velocity of a blade element in the directions $(\bar{x}, \bar{y}, \bar{z})$ fixed in space. These velocities are then differentiated with respect to time, thus giving the blade element accelerations in the directions $(\bar{x}, \bar{y}, \bar{z})$. An axial transformation to the (x, y, z) directions results in Eqs. (3). This method has the advantage of automatically introducing the Coriolis terms. It is not necessary that they receive special consideration.

Both methods, however, involve nearly the same amount of labor.]

Let M_b represent the moment about the flapping hinge of the aerodynamic and gravity forces on a rotor blade. Then, from dynamical considerations,

$$M_b = -\int_{e_b}^{R} (r - e_b) a_z \, q \, dr \tag{4}$$

where q is the blade mass per unit of length and e_b is the distance of the flapping hinge from the center of the rotor. Since e_b is always small compared with R, the error introduced by neglecting the effect of e_b on the integral of Eq. (4) is negligible. Accordingly, with $e_b = 0$ this equation becomes

$$M_b = -\int_{0}^{R} r a_z \, q \, dr \tag{5}$$

Substituting for a_z from Eq. (3) and setting I_b equal to the mass moment of inertia of the blade about its flapping hinge, then from Eq. (5) results,

$$M_b = \Omega^2 I_b(\ddot{\beta} + \beta - \ddot{a}_p \cos\psi - \ddot{a}_r \sin\psi + 2\dot{a}_p \sin\psi - 2\dot{a}_r \cos\psi) \tag{6}$$

The aerodynamic portion of M_b is made up of the moment of the blade lift forces plus an unimportant contribution from the drag force components. The lift force on a blade element of length dr and chord c is

$$dL = {}^1/_2 \rho v_x^2 m \alpha c dr \tag{7}$$

where ρ is the mass density of the air, m is the slope of the lift versus angle-of-attack curve for the particular blade airfoil section employed, α is the blade angle of attack relative to the plane of zero lift, and the velocity v_x is used as a close approximation for the velocity $\sqrt{v_x^2 + v_z^2}$. As has been previously mentioned, the effect of the radial velocity v_y on the aerodynamic loading (causing a "yawing" flow across the blade) is neglected. The value of M_b is then,

$$M_b = {}^1/_2 \int_{0}^{BR} \rho v_x^2 m \alpha c r \, dr - G \tag{8}$$

The factor B is introduced in the upper integration limit, in the manner of Wheatley,[3] to account for the loss of lift at the blade tip. The notation G is used to denote the gravity moment of the blade about its flapping hinge.

The blade angle of attack α is made up of three parts: (a) a mean component θ_0 which does not vary with time; (b) the cyclically varying component $-(\theta_1 \cos\psi + \theta_2 \sin\psi)$; and (c) the induced angle φ. For the type of machine being studied, both the mean component θ_0 and the amount of cyclic pitch imposed can be controlled by the operator of the craft. By writing the cyclic component in terms of the two arbitrary constants θ_1 and θ_2, control of the maximum amount of blade pitch variation, as well as the azimuth angle of blade rotation ψ at which this maximum occurs, is left to the discretion of the operator. Since the induced angle is equal to

$$\varphi = v_z/v_x \tag{9}$$

the complete expression for the blade angle of attack becomes

$$\alpha = \theta_0 - \theta_1 \cos\psi - \theta_2 \sin\psi + (v_z/v_x) \tag{10}$$

It is assumed that the magnitude of α is comparable with those of the other first-order quantities that appear in the work.

The integral of Eq. (8) can be evaluated by using Eqs. (2) and (10) for the blade velocities and angle of attack. The integration is accomplished here only for the special case of a blade of constant profile and constant chord along its entire length. It is also convenient to assume that the down-wash velocity w does not vary along the blade length.

Eq. (8) then yields, neglecting terms of higher order than first,

$$M_b = \frac{1}{2}\rho m c R^4 \Omega^2 \left(\frac{B^4}{4}\right)\left(\theta_0 - \theta_1 \cos\psi - \theta_2 \sin\psi - \dot{\beta} - \frac{4}{3B}\frac{w}{\Omega R} + \dot{a}_p \cos\psi + \dot{a}_r \sin\psi\right) - G \tag{11}$$

and the dynamical equation for blade flapping, obtained by equating Eqs. (6) and (11) is

$$\ddot{\beta} + \nu\dot{\beta} + \beta - \ddot{a}_p \cos\psi + (2\sin\psi - \nu\cos\psi)\dot{a}_p - \ddot{a}_r \sin\psi - (2\cos\psi + \nu\sin\psi)\dot{a}_r = \nu(\theta_0 - \theta_1 \cos\psi - \theta_2 \sin\psi) - (4\nu/3B)(w/\Omega R) - (G/I_b\Omega^2) \tag{12}$$

where $\nu = \rho m c (BR)^4/8I_b$. It is to be noted that Eq. (12) is a differential equation with variable coefficients between β, α_p, and α_r. Because of neglect of higher order terms, the longitudinal and transverse velocities of the center of gravity of the fuselage disappear from this particular equation. However, they enter as variables in equations which are written later, thus causing the machine velocity and blade flapping to become interdependent.

Following the lead of previous investigators, the flapping angle β is written as

$$\beta = a_0 - a_1 \cos\psi - a_2 \sin\psi \tag{13}$$

where a_0 represents the coning angle of the blades, a_1 is the tilt of the rotor cone in the downwind direction, and a_2 is the rotor cone tilt to the starboard. Since the present work considers both steady and unsteady flight responses, the coefficents a_0, a_1, and a_2 cannot be regarded as constants. Instead, they are presumed to be functions of the blade azimuth angle ψ. (Since $\psi = \Omega t$, it is to be noted that a dependence on ψ is equivalent to a dependence on the time t.) The precise form of the three functions for a_0, a_1, and a_2 are yet to be determined.

Substituting Eq. (13) in the left side of Eq. (12), terms are obtained on the left which have: (a) sin ψ affixed; (b) cos ψ affixed; or (c) neither sin ψ nor cos ψ affixed. The terms on the right being similarly classified, equating the corresponding terms from the two sides causes Eq. (12) to be automatically satisfied.

The three equations resulting from this procedure are:

$$\ddot{a}_0 + v\dot{a}_0 + a_0 = v\theta_0 - (4v/3B)(w/\Omega R) - (G/I_b\Omega^2) \quad (14)$$

$$(\ddot{a}_2 + v\dot{a}_2) - (2\dot{a}_1 + va_1) + (\ddot{\alpha}_r + v\dot{\alpha}_r) - 2\dot{\alpha}_p = v\theta_2 \quad (15)$$

$$(2\dot{a}_2 + va_2) + (\ddot{a}_1 + v\dot{a}_1) + 2\dot{\alpha}_r + (\ddot{\alpha}_p + v\dot{\alpha}_p) = v\theta_1 \quad (16)$$

By adding the equations of motion for the center of gravity of the fuselage to these relations, a solution for the response and stability problem is obtained.

Dynamics of the Fuselage

Eqs. (14), (15), and (16) contain the five variables a_0, a_1, a_2, α_p, and α_r. If the equations of motion for the center of gravity of the fuselage are written, the additional variables U and V enter. Since the vertical and yawing motions of the machine are not taken into account, four equations are sufficient to describe the fuselage motion. The necessary condition is then fulfilled of having the total number of available equations equal to the number of variables considered (seven).

The external loads on the fuselage arise from three sources: (a) blade forces that are transmitted to the rotor hub by means of the flapping hinges; (b) gravitational forces having a resultant equal to the fuselage weight and acting at its center of gravity; and (c) aerodynamic drag forces acting on the fuselage and tending to restrain its translational and rotational motion. The resultant moment and force due to these external loads, referred to the fuselage center of gravity, must at any instant be equal to the fuselage inertial moment and force.

Using the results derived above, it is possible to precisely calculate the hinge forces. The blade weight, the air loads on the blade, and the blade accelerations must be taken into account. The hinge load is divided into components as follows: (a) thrust force—normal to the blade tip plane and acting upwards; (b) drag force—parallel to the blade tip plane and normal to the blade, tending to oppose the rotor rotation; and (c) radial force—parallel to the blade tip plane and acting outwards along the blade projection on this plane. The inertial loads of interest are due to the acceleration of the blade elements relative to the rotor hub. The air loads are calculable from Eq. (7) for the lift and a similar expression for the aerodynamic drag on a blade element.

If the exact expressions for the hinge loads are found in this manner, the results indicate that the thrust component is equal to the difference between the blade lift and blade weight, while the hinge drag force is made up of the aerodynamic blade drag and a component of the blade lift. The radial hinge force arises because of the centrifugal acceleration $\Omega^2 r$ of the blade elements relative to the hub and has the steady value $^1/_2(W_b/g)\Omega^2 R$ (W_b = blade weight, g = acceleration due to gravity).

Since both the blade lift and drag vary periodically with the azimuth angle ψ, the hinge thrust and drag forces also vary with time. In order to obtain the total thrust of the rotor on the fuselage, the thrust force per hinge must be averaged over one complete blade revolution and this mean hinge thrust multiplied by the number of blades comprising the rotor. For small departures of the machine from a hovering state, the total rotor thrust remains nearly equal to the fuselage weight. It is assumed here that the rotor thrust is always exactly equal to the fuselage weight W_f, thus eliminating any vertical motion of the machine.

At any instant, the thrust force at a single hinge is equal to

$$T_b = {}^1/_6\,\rho mc\Omega^2(BR)^3\Big(\theta_0 - \theta_1\cos\psi - \theta_2\sin\psi - \dot{\beta} + \frac{3}{2B}\,\frac{w}{\Omega R} + \dot{\alpha}_p\cos\psi + \dot{\alpha}_r\sin\psi\Big) - W_b \quad (17)$$

If the hinges are located a distance e_b from the rotor axis, the hinge thrust induces a pitching moment of amount $-T_b e_b\cos\psi$ and a rolling moment $-T_b e_b\sin\psi$, both about the fuselage center of gravity. If the pitching moment is averaged for one complete rotor revolution, its mean value is found to be

$$(e_b/12)\rho mc\Omega^2(BR)^3(\theta_1 - \dot{a}_1 - a_2 - \dot{\alpha}_p)$$

and for a rotor with n blades, the total pitching moment induced by the hinge thrust forces is

$$\epsilon W_f(\theta_1 - \dot{a}_1 - a_2 - \dot{\alpha}_p) \quad (18)$$

where $\epsilon = ne_b\rho mc\Omega^2(BR)^3/12W_f$. The total rolling moment from the same cause is determined in a similar manner and is equal to

$$\epsilon W_f(\theta_2 - \dot{a}_2 + a_1 - \dot{\alpha}_r) \quad (19)$$

The work of Glauert[1] indicates that the drag forces at the various hinges combine to produce a resultant drag force that opposes translation of the rotor through space. The exact magnitude of this force can be calculated by the same method as previously outlined for the thrust; the drag force at a single hinge is averaged for a complete rotor revolution, and this mean force is increased according to the number of rotor blades. Glauert has shown that the magnitude of the total drag force on the rotor is proportional to the speed of advance of the rotor. For the present analysis, the rotor hub moves forward with a velocity ($U - h\Omega\dot{a}_p$) and travels to the starboard at the rate ($V +$

$l\Omega\dot{a}_r$). Accordingly, the down-wind and port total drag forces on the rotor are taken equal to, respectively,

$$k_x W_f \left(\frac{U}{\Omega R} - \frac{l}{R}\,\dot{a}_p\right) \quad \text{and} \quad k_y W_f \left(\frac{V}{\Omega R} + \frac{l}{R}\,\dot{a}_r\right)$$

where k_x and k_y are rotor drag coefficients and W_f is the fuselage weight. With $\mu_x = U/\Omega R$ and $\mu_y = V/\Omega R$, the total drag forces become

$$k_x W_f \left(\mu_x - \frac{l}{R}\,\dot{a}_p\right) \quad \text{and} \quad k_y W_f \left(\mu_y + \frac{l}{R}\,\dot{a}_r\right) \tag{20}$$

The radial hinge forces are always arranged to have a zero force resultant. No unbalance of force on the rotor shaft due to radial hinge loads is tolerated. To accomplish this aim, it is sometimes necessary (as in the case of single blade rotors) to add dynamic balancing weights off the rotor axis. The radial forces do, however, contribute a moment about the rotor hub when the hinge distance e_b is not zero and the rotor cone is displaced. At any instant, the down-wind and starboard components of the radial force on a single hinge are, respectively,

$$\frac{1}{2}\,\frac{W_b}{g}\,\Omega^2 R\cos\psi \quad \text{and} \quad \frac{1}{2}\,\frac{W_b}{g}\,\Omega^2 R\sin\psi$$

The moment arm of these components about the rotor hub is

$$e_b(a_1\cos\psi + a_2\sin\psi)$$

The instantaneous pitching moment about the rotor hub is then

$$^1/_2(W_b/g)\Omega^2 R e_b(a_1\cos\psi + a_2\sin\psi)\cos\psi$$

and averaged for a complete rotor revolution this becomes $^1/_4(W_b/g)\Omega^2 R e_b a_1$. For a rotor with n blades the total pitching moment is then

$$+(n/4)(W_b/g)(\Omega^2 R e_b a_1) \tag{21}$$

Similarly, the total rolling moment due to the radial hinge loads is

$$+(n/4)(W_b/g)(\Omega^2 R e_b a_2) \tag{22}$$

The aerodynamic drag force on the fuselage is induced by the translational and rotational motion of the fuselage. At low speeds, the magnitude and line of action of this force are linearly dependent on the angular velocity and speed of the fuselage center of gravity. Four drag coefficients are required to describe the resistance of the fuselage to longitudinal and transverse translation and to rolling and pitching. Instead of introducing four additional constants into the theory, however, the fuselage drag is accounted for by slightly increasing the rotor drag coefficients k_x and k_y. This approximation is permissible since the effect of the fuselage drag on the results is small, and Eqs. (17) possess the proper linear dependence of the drag forces on the translational and rotational fuselage velocities.

The total forward force on the fuselage (in the direction of the $\bar{x}$ axis of Table 1) is then

$$F_{\bar{x}} = -W_f\{a_1 + \alpha_p + k_x[\mu_x - (l/R)\dot{a}_p]\} \tag{23}$$

The total force in the starboard ($\bar{y}$) direction is

$$F_{\bar{y}} = W_f\{a_2 + \alpha_r - k_y[\mu_y + (l/R)\dot{a}_r]\} \tag{24}$$

The total pitching moment about a transverse ($\bar{y}$) gravity axis of the fuselage is

$$M_{\bar{y}} = W_f l\{a_1 + k_x[\mu_x - (l/R)\dot{a}_p]\} + \epsilon W_f(\theta_1 - \dot{a}_1 - a_2 - \dot{a}_p) + (n/4)(W_b/g)\Omega^2 R e_b a_1 \tag{25}$$

The total rolling moment about a longitudinal ($\bar{x}$) gravity axis of the fuselage is

$$M_{\bar{x}} = W_f l\{a_2 - k_y[\mu_y + (l/R)\dot{a}_r]\} + \epsilon W_f(\theta_2 - \dot{a}_2 + a_1 - \dot{a}_r) + (n/4)(W_b/g)\Omega^2 R e_b a_2 \tag{26}$$

The equations of motion for the fuselage are then

$$\left.\begin{aligned} F_{\bar{x}} &= \frac{W_f}{g}\,\frac{dU}{dt} = \frac{W_f}{g}\,\Omega R\,\frac{d\mu_x}{dt} = \frac{W_f}{g}\,\Omega^2 R\dot{\mu}_x \\ F_{\bar{y}} &= \frac{W_f}{g}\,\frac{dV}{dt} = \frac{W_f}{g}\,\Omega R\,\frac{d\mu_y}{dt} = \frac{W_f}{g}\,\Omega^2 R\dot{\mu}_y \end{aligned}\right\} \tag{27}$$

and

$$\left.\begin{aligned} M_{\bar{y}} &= I_y(d^2\alpha_p/dt^2) = I_y\Omega^2\ddot{a}_p \\ M_x &= I_x(d^2\alpha_r/dt^2) = I_x\Omega^2\ddot{a}_r \end{aligned}\right\} \tag{28}$$

where I_x and I_y are the mass moments of inertia of the fuselage about its longitudinal and transverse gravity axes, respectively.

Substituting the complete expressions for the external forces and moments in the equations of motion leads to the set of relations,

$$a_1 - \left(k_x\,\frac{l}{R}\,\dot{a}_p - \alpha_p\right) + \left(\frac{\Omega^2 R}{g}\,\dot{\mu}_x + k_x\mu_x\right) = 0 \tag{29}$$

$$a_2 - \left(k_y\,\frac{l}{R}\,\dot{a}_r - \alpha_r\right) - \left(\frac{\Omega^2 R}{g}\,\dot{\mu}_y + k_y\mu_y\right) = 0 \tag{30}$$

$$\left[\frac{\epsilon}{l}\,\dot{a}_1 - \left(1 + \frac{n}{4}\,\frac{W_b}{W_f}\,\frac{\Omega^2 R}{g}\,\frac{e_b}{l}\right)a_1\right] + \frac{\epsilon}{l}\,a_2 + \left[\frac{I_y\Omega^2}{W_f l}\,\ddot{a}_p + \left(\frac{\epsilon}{l} + k_x\frac{l}{R}\right)\dot{a}_p\right] - k_x\mu_x = \frac{\epsilon}{l}\,\theta_1 \tag{31}$$

$$\left[\frac{\epsilon}{l}\,\dot{a}_2 - \left(1 + \frac{n}{4}\,\frac{W_b}{W_f}\,\frac{\Omega^2 R}{g}\,\frac{e_b}{l}\right)a_2\right] - \frac{\epsilon}{l}\,a_1 + \left[\frac{I_x\Omega^2}{W_f l}\,\ddot{a}_r + \left(\frac{\epsilon}{l} + k_y\,\frac{l}{R}\right)\dot{a}_r\right] + k_y\mu_y = \frac{\epsilon}{l}\,\theta_2 \tag{32}$$

These equations, plus Eqs. (14), (15), and (16) are seven differential equations with the same number of variables. Each equation is linear and has constant coefficients. Methods for solving for the variables under these conditions are well known.[10]

Method of Solution and a Typical Numerical Calculation

Eq. (14) is solved by taking

$$a_0 = v\theta_0 - \frac{4v}{3B}\frac{w}{\Omega R} - \frac{G}{I_b\Omega^2} + \sum_{n=1}^{2} A_n e^{r_n\psi} \tag{33}$$

where r_n are the roots of the quadratic

$$r^2 + vr + 1 = 0 \tag{34}$$

and the A_n are arbitrary constants to be fixed by the starting conditions of the problem. Letter e is the base of natural logarithms.

Eqs. (15), (16), (29), (30), (31), and (32) are solved by taking

$$\left.\begin{aligned}
a_1 &= -\theta_2 + \sum_{n=1}^{10} B_n e^{\lambda_n\psi} \\
a_2 &= \theta_1 + \sum_{n=1}^{10} C_n e^{\lambda_n\psi} \\
\mu_x &= \frac{\theta_2}{k_x}\left(1 + \frac{n}{4}\frac{W_b}{W_f}\frac{\Omega^2 R}{g}\frac{e_b}{l}\right) + \sum_{n=1}^{10} D_n e^{\lambda_n\psi} \\
\mu_y &= \frac{\theta_1}{k_y}\left(1 + \frac{n}{4}\frac{W_b}{W_f}\frac{\Omega^2 R}{g}\frac{e_b}{l}\right) + \sum_{n=1}^{10} E_n e^{\lambda_n\psi} \\
\alpha_p &= -\frac{n}{4}\frac{W_b}{W_f}\frac{\Omega^2 R}{g}\frac{e_b}{l}\theta_2 + \sum_{n=1}^{10} F_n e^{\lambda_n\psi} \\
\alpha_r &= +\frac{n}{4}\frac{W_b}{W_f}\frac{\Omega^2 R}{g}\frac{e_b}{l}\theta_1 + \sum_{n=1}^{10} G_n e^{\lambda_n\psi}
\end{aligned}\right\} \tag{35}$$

where B_n, C_n, . . ., G_n are constants and the λ_n are the ten roots of the equation, expressed in determinant form.

$$\begin{vmatrix}
P_1(\lambda) & -P_2(\lambda) & P_1(\lambda) & 0 & -2\lambda & 0 \\
P_2(\lambda) & P_1(\lambda) & 2\lambda & 0 & P_1(\lambda) & 0 \\
P_3(\lambda) & -\epsilon/l & P_4(\lambda) & k_y & 0 & 0 \\
1 & 0 & P_5(\lambda) & P_6(\lambda) & 0 & 0 \\
\epsilon/l & P_3(\lambda) & 0 & 0 & P_7(\lambda) & -k_x \\
0 & 1 & 0 & 0 & P_8(\lambda) & P_9(\lambda)
\end{vmatrix} = 0 \tag{36}$$

where

$$P_1(\lambda) = \lambda^2 + v\lambda;\quad P_5(\lambda) = 1 - k_y\frac{l}{R}\lambda$$

$$P_2(\lambda) = 2\lambda + v;\quad P_6(\lambda) = -\left(\frac{\Omega^2 R}{g}\lambda + k_y\right)$$

$$P_3(\lambda) = \frac{\epsilon}{l}\lambda - \left(1 + \frac{n}{4}\frac{W_b}{W_f}\frac{\Omega^2 R}{g}\frac{e_b}{l}\right);\quad P_7(\lambda) = \frac{I_y\Omega^2}{W_f l}\lambda^2 + \left(\frac{\epsilon}{l} + k_x\frac{l}{R}\right)\lambda$$

$$P_4(\lambda) = \frac{I_x\Omega^2}{W_f l}\lambda^2 + \left(\frac{\epsilon}{l} + k_y\frac{l}{R}\right)\lambda;\quad P_8(\lambda) = 1 - k_x\frac{l}{R}\lambda$$

$$P_9(\lambda) = \frac{\Omega^2 R}{g}\lambda + k_x$$

Methods for solving systems of linear differential equations of the type treated here are discussed by von Kármán and Biot.[10] They show that only ten of the constants B_n, C_n, . . ., G_n in Eqs. (35) are arbitrary. Hence, only ten starting conditions need be known to fix the values of all constants appearing in the summation of Eqs. (35). Two additional starting conditions are necessary to enable the values of the two unknown constants in Eq. (33) to be determined. Since the craft is initially in a hovering state, the twelve starting conditions are, at $t = \psi = 0$,

$$\left.\begin{aligned}
a_0 &= \left(v\theta_0 - \frac{4v}{3B}\frac{w}{\Omega R} - \frac{G}{I_b\Omega^2}\right)^* \\
\dot{a}_0 &= 0 \quad a_1 = \dot{a}_1 = 0 \quad a_2 = \dot{a}_2 = 0 \\
\alpha_p &= \dot{\alpha}_p = 0 \quad \alpha_r = \dot{\alpha}_r = 0 \quad \mu_x = \mu_y = 0
\end{aligned}\right\} \tag{37}$$

The particular solution to the system of seven differential equations is represented by the constant portions (not dependent on ψ) of Eqs. (33) and (35). These terms describe the steady-state response of the machine to an abrupt control displacement. They are, therefore, indicative of the suitability of cyclically varying the pitch of the blades in order to obtain control of the craft. This matter is discussed in some detail in the "Results and Conclusions" section of the paper, where control sensitivity is also investigated. Although the present work is concerned only with abrupt control displacements, no great difficulty is involved in extending the theory to deal with control displacements which are arbitrary functions of time.

The determinant of Eq. (36) is recognized to be the stability determinant for the craft. If all roots of Eq. (36) represent convergent (decaying) oscillations, the machine is stable. Small displacements of the craft from the hovering state will be damped out. If, however, one or more of the roots describe a divergent oscillation, the craft is unstable. Small disturbances will be magnified and will eventually cause the machine to upset.

In order to obtain some idea of the practical significance of the results, sample response calculations have been made for a typical machine. In order to simplify the work, two of the degrees of freedom, longitudinal translation and pitching, are not taken into account. This is done by setting $\alpha_p = \mu_x = 0$ in

* See Glauert.[1]

all of the developed theory. The equations of motion, Eqs. (29) and (31), relating to longitudinal translation and pitching, are no longer of importance and can be neglected. This results in the disappearance of the last two columns and rows from the determinant of Eq. (36) and considerably reduces the labor involved in solving for the roots λ_n. Instead of ten roots, only seven are obtained for the modified solution; the reduction is accounted for by the smaller number of starting conditions which are applicable to the problem. The degree of freedom described by the longitudinal tip a_1 of the rotor cone is not discarded in order to study the effects on a_1 of small displacements of the machine from a hovering state.

It is clear that α_p and μ_x can be set equal to zero only providing no disturbing forces tending to cause longitudinal motion are introduced by the cyclic pitch control. This condition is fulfilled when the cyclic pitch $\theta_2 = 0$. The steady-state responses of a_1, μ_x, and α_p are then zero, and only the oscillatory portions of the last two degrees of freedom are neglected.

The hypothetical machine for which response calculations have been made has the following characteristics:

W_f	= 2,200 lbs.	m	= 5.56 per rad.
W_b	= 55 lbs.	B	= 0.95
R	= 18.75 ft.	I_x	= 230 lbs. ft. sec.^{2}
c	= 14 in.	l	= 4.2 ft.

$$k_y = 0.10$$

The rotor is assumed to rotate at $\Omega = 25$ rad. per sec. (240 r.p.m.), and a cyclic pitch of amount $\theta_1 = 1.5°$ is imposed on the rotor blades.

For this case, the roots of Eq. (36) are found to be

$$-0.166, \quad -0.52 \pm 1.86i$$
$$-0.42 \pm 0.20i, \quad 4.42 \times 10^{-4} \pm 0.0118i \qquad (38)$$

The first five roots represent decaying oscillations. The pair of complex roots with a positive real part describe a divergent oscillation and, hence, indicate that the machine is unstable. It is to be noted that the period of the unstable oscillation is

$$2\pi/(0.0118 \times 25) = 21 \text{ sec.}$$

and the time required for it to double its amplitude is

$$0.693/(4.42 \times 10^{-4} \times 25) = 63 \text{ sec.}$$

The unstable motion is, therefore, not rapidly amplified and has a fairly long period. By suitably modifying the design of the machine, the period of the instability can be even further lengthened and the rate of amplification reduced.

The response of the machine to the imposed cyclic pitch is shown graphically on Fig. 1. The time scale is expanded for the first instants of motion in order to show how the damped oscillations become ineffectual within a fraction of a second. The complete range of the figure, covering several seconds of motion, shows the influence of the divergent roots on the responses.

A detailed discussion of the significance of the analytical and calculated results is given under "Results and Conclusions" in this paper. It is mentioned there that the instability can be eliminated completely if the rotor drag force can be nullified. Thus, if k_y is set equal to zero in the determinant of Eq. (36), a condition of neutral stability results.

Comparison with Hohenemser's Solution

Hohenemser[4] deals with the longitudinal stability and response of a hovering machine having two coaxial, oppositely rotating, identical rotors. The articulation of the rotors and the general constructional features of the craft are the same as described in the first part of this paper. It is of interest, therefore, to compare Hohenemser's results with those obtained here.

Because of the counterrotating arrangement, movement of the dual rotor craft in a particular direction does not introduce air loads transverse to the direction of motion. Hence, for this special case, longitudinal and lateral stability can be studied separately. In terms of the degrees of freedom utilized in the present development, this implies that the transverse cone tip a_2 need not be considered in a discussion of longitudinal stability and response. Conversely, a study of lateral motion does not require that the longitudinal tip a_1 of the rotor cone be taken into account.

Since no air loads are introduced transverse to the direction of motion, only two equations for the fuselage motion are significant. Thus, for investigating longitudinal stability and response, only the equations of motion for longitudinal translation and for pitching yield interesting results.

Hohenemser does not consider the effects of imposed cyclic pitch on the response of the machine. In terms of the present solution, this is equivalent to neglecting the parameters θ_1 and θ_2.

Setting $a_2 = \dot{a}_2 = \ddot{a}_2 = 0$, $\alpha_r = \dot{\alpha}_r = \ddot{\alpha}_r = 0$, and $\theta_1 = \theta_2 = 0$ in Eq. (15), this equation becomes

$$+(2\dot{a}_1 + \nu a_1) + 2\dot{\alpha}_p = 0 \qquad (39)$$

If $\dot{a}_1$ is arbitrarily set equal to zero, a relation between a_1 and $\dot{\alpha}_p$ is obtained in the form

$$a_1 = -(2/\nu)\dot{\alpha}_p \qquad (40)$$

Eq. (40) is identical with the relation used by Hohenemser to define the rotor cone tip (save for different notation and a different positive convention for α_p). It is clear, then, that Hohenemser has chosen to neglect the dynamical effects due to motion of the rotor cone relative to the fuselage.

A consequence of the previous assumptions is the vanishing of the factor ϵ from the equations of motion, Eqs. (29) and (31). With $\dot{a}_2 = a_2 = \theta_1 = 0$, these

equations are in agreement with those written by Hohenemser. Use of these equations, together with Eq. (40), for stability and response calculations give results that are identical with those of Hohenemser.

A further comparison between the present treatment and that of Hohenemser is obtained by comparing the roots of the stability determinants, computed from the results of the two solutions for similar machines. For the craft whose characteristics are tabulated in the section on "Method of Solution and a Typical Numerical Calculation," Hohenemser's work gives for the roots of the stability determinant,

$$-0.119, \quad 0.0024 \pm 0.0237i \tag{41}$$

These consist of a negative real root, representing a decaying motion, and a pair of complex conjugates with positive real parts, describing a dynamically unstable oscillation. The fact that only three roots are obtained, compared with the seven (or more generally, ten) that result from the present treatment, is due to the smaller number of degrees of freedom which Hohenemser has taken into account.

Considering the magnitudes of the unstable oscillations predicted by the two solutions, comparison of roots (38) and (41) shows that the present solution indicates the machine to be less unstable than does that of Hohenemser. The period of the instability from roots (41) is 10.6 sec., compared with a period of 21 sec. for the present treatment (see previous section). The amplification factor predicted by Hohenemser's work is much larger than that resulting from roots (38); whereas the present solution requires 63 sec. for the unstable oscillation to double its magnitude, Hohenemser's results predict the same effect in only 11.6 sec.

References

[1] Glauert, H., *A General Theory of the Autogyro*, R. & M. No. 1111, British A.R.C., 1926.

[2] Lock, C. N. H., *Further Development of Autogyro Theory*, R. & M. No. 1127, British A.R.C., 1927.

[3] Wheatley, J. B., *An Aerodynamic Analysis of the Autogiro Rotor with a Comparison between Calculated and Experimental Results*, N.A.C.A. Report No. 487, 1934.

[4] Hohenemser, K., *Dynamic Stability of a Helicopter with Hinged Rotor Blades*, Ingenieur-Archiv, Vol. 9, pp. 419–428, December, 1938. (For English translation see N.A.C.A. T.M. No. 907, 1938.)

[5] von Kármán, Th., *Helicopter Theory*, Zeitschrift für Flugtechnik und Motorluftschiffahrt, Vol. 12, No. 24, 1921. (For English translation see Aircraft Engineering, Vol. 12, No. 139, pp. 271–276, September, 1940.)

[6] Küssner, H. G., *Helicopter Problems*, Luftfahrtforschung, Vol. 14, No. 1, 1937. (For English translation see N.A.C.A. T.M. No. 827, 1937.)

[7] Miehl, M. L., *The Aerodynamics of the Lifting Airscrew with Hinged Blades in Curvilinear Motion*, Trans. Inst. Aero-Hydrodynamics, No. 465, 1940, pp. 1–60. (For English translation see R.T.P. Translation No. 1533, Ministry of Aircraft Production, England.)

[8] Sissingh, G., *Contribution to the Aerodynamics of Rotating-Wing Aircraft*, Luftfahrtforschung, Vol. 15, No. 6, 1938. (For English translation see N.A.C.A. T.M. No. 921, Parts I and II, 1939.)

[9] Timoshenko, S., and Young, D. H., *Engineering Mechanics*, Chap. VII; McGraw-Hill Book Company, Inc., New York, 1937.

[10] von Kármán, Th., and Biot, M. A., *Mathematical Methods in Engineering*, Chap. I; McGraw-Hill Book Company, Inc., New York, 1940.

Appendix

It has been pointed out by H. Reissner* that the solution given here need not be restricted to the case of hovering or near hovering machines. The stability under any condition of steady state motion, such as uniform translation, can be studied if minor revisions in the present theory are made.

If the case of steady translation is studied, terms are introduced into the equations which are composed of products of the translational velocity components, such as the forward speed U, and other variables. When the variable velocity U is not of small magnitude compared with the tip speed ΩR of the blades, these products are not of second order, and the terms cannot be considered to be of unimportant magnitude when formulating the pertinent equations. This results in the appearance of differential equations with variable coefficients in the theory. The exact solution of these differential equations is of extreme mathematical complication.

However, it is to be recalled that a study of stability requires merely that the behavior of the machine be investigated when it is undergoing small departures from an initial steady state condition. If the response calculations are likewise limited to small departures from an initial steady state condition, a solution to the stability and response problem for nonhovering machines can be obtained without difficulty.

Consider the forward velocity U to be written as the sum of a relatively large, constant component U_s and a component U_d, describing a small disturbance from the initial steady state condition. Then $U = U_s + U_d$ and products such as U^2 and βU (which enter, for example, in the calculation of the aerodynamic blade forces) become $U_s^2 + 2U_sU_d + U_d^2$ and $\beta U_s + \beta U_d$, respectively. Neglect of the second order terms U_d^2 and βU_d makes these equal to $U_s^2 + 2U_sU_d$ and βU_s, respectively. It is to be noted that these last expressions do not contain products of variables.

If this type of reasoning is incorporated into the development given in this paper, it is found that the

* Professor of Aeronautical Engineering, Polytechnic Institute of Brooklyn.

differential equations governing the stability and response of nonhovering machines are of exactly the same form as Eqs. (14), (15), (16), (29), (30), (31), and (32). Only the values of the constant coefficients are changed, through the addition of terms involving steady state velocity components, such as the constant velocity U_s. If these additional terms are caused to vanish, the equations describing the stability and response near the hovering state are obtained identically. (It is to be noted that the magnitudes of the rotor drag coefficients k_x and k_y must be varied according to the initial steady state condition chosen for investigation. Average values must be chosen which are applicable for drag calculations at and near the initial steady state velocities.)

Since the form of the differential equations do not change, the form of the solutions for the seven variables in the case of nonhovering machines remain likewise unchanged.

The form of the solutions are similar to those of Eqs. (33) and (35); the values of the roots r_n and λ_n are obtained from algebraic equations of exactly the same form as Eqs. (34) and (36). Although the values of the constant coefficients change, no increased complications are introduced in the methods of solution. The starting conditions are altered slightly from those of Eqs. (37) and are obtainable from the solutions of Glauert[1] and others.

It is evident that the extension of the work to include the case of nonhovering helicopters is of great practical interest and it is hoped that the stability and response characteristics under such conditions will become known as the result of a future program of calculation.

Letter to the Editor

Dear Sir:

The paper by Paul E. Sandorff on "Notes on Columns" (JOURNAL OF THE AERONAUTICAL SCIENCES, Vol. 11, No. 1, p. 1, January, 1944) contains certain statements which lead to the following comments:

(1) It may be presumed, in relation with the second paragraph of "Critical Loads of Elastically Restrained Columns," that the paper deals only with failure by lateral buckling, exclusive of torsional instability.

(2) The case considered after Eq. (23), which corresponds to the hypothesis $\alpha_2 = 0$, $M_1' = M_2$, $M_2 = M_3$, solution of which is given by Eqs. (24) and (25), is a condition of multiple-bay column, with spans alternatively defined by the quantities L_1, D_1 and L_2, D_2 and not a condition of two-bay column as indicated by the author. For the latter case, extending the author's assumption $\alpha_2 = 0$ to the end restraints ($\alpha_3 = \alpha_3 = 0$), the solution of the problem is given by the following equation:

$$\sqrt{\frac{D_2}{D_1}}\left(\frac{1}{2u_1} - \cot 2u_1\right) + \left(\frac{1}{2u_2} - \cot 2u_2\right) = 0$$

For both problems of two- and three-bay columns, complete charts are given by Ratzersdorfer.[1]

(3) Interpretation of Eq. (31) is to be corrected. That equation gives the failure of the whole continuous column, and if the operations leading to the critical load in bay $(n, n + 1)$ are repeated for other bays, the same critical load is found. That load corresponds to the value zero for the determinant constituted by the successive equations of the type (14) to (17). Reference (1), page 284, can be consulted for clarification of that point.

(4) It is desirable to complete Figs. 5 and 6 for negative values of α', since at a support the sign of α' can be negative as well as positive.

(5) The reference 14 of the formula for the active width is incorrect, since that formula has been given by S. Timoshenko[2] at an earlier date, and the writer has extended that result, valid only for infinitely wide flanges, to flanges of finite width.[3]

(6) There is a confusion between the end fixity, which refers to a span, and the end-restraint, which refers to a support. In the table on page 9, coefficients c_1 and c_4 are indicated. They are without significance with such notation, since end restraints only may have indexes referring to the support and not to the span. They must be replaced by a unique coefficient c defined as "test end fixity for a single bay."

(7) It is to be noted that with a two-bay column specimen, the error is reduced to one-half in comparison with a one-bay specimen. Moreover, combining the results of a one-bay test and a two-bay test, the end restraints can be actually determined, together with the actual values of the end fixity.

REFERENCES

[1] Ratzersdorfer, J., *Die Knickfestigkeit von Stäben und Stabwerken Wien*, p. 280, 1936.

[2] Timoshenko, S., *Theory of Elasticity*, p. 161.

[3] Beskin (Beschkine), L., *Determination of the Effective Width of the Compression Flanges of T-Beams*, International Association for Bridge and Structural Engineering, Publications, Vol. 5, p. 65, Zurich, 1938.

LEON BESKIN
Structures Engineer
Consolidated Vultee Aircraft Corporation

Buckling Loads of Beams or Plates on Continuous Supports

EDWARD SAIBEL*

Carnegie Institute of Technology

SUMMARY

A method is developed for finding the buckling loads of beams or plates over continuous rigid or elastic supports. These loads are found as the roots of characteristic equations that are developed in terms of the known characteristic modes of buckling and corresponding characteristic buckling loads of the beam or plate without the rigid or elastic supports. The method is an application of the direct method of the Calculus of Variations and consists of minimizing the potential energy of the system subject to the constraints that are the inner supports, rigid or elastic.

The object of this paper is to develop a method whereby the buckling loads of beams or plates, having simply supported, fixed, or free boundaries, and subject to inner constraints in the form of intermediate rigid or elastic supports, may readily be calculated. These buckling loads are the roots of the characteristic equations that arise from the condition that the potential energy of the system shall be a minimum subject to the constraints. By developing the buckled shape of the system as a Generalized Fourier Series in terms of the characteristic (or eigen) functions of the unrestrained system, in many cases known or easily found, it is possible to express the potential energy in a simple and compact form from which there is no difficulty in deriving the characteristic equation. Few terms of these equations need be used to obtain reasonably accurate results in most problems. The beam has been previously solved,[1] but the present treatment will be found to have advantages in some cases over the existing method. This is particularly evident if the beam is uniform. In the case of the plate results believed to be new are found.

BEAM WITH RIGID INTERMEDIATE SUPPORTS

LET THE BEAM of flexural rigidity $B(x)$, not necessarily uniform, be restrained from deflecting at any number of intermediate points. The ends may be simply supported, fixed, or free. The load on the beam is axial, and the problem is to determine the smallest value of this load (P) which will produce buckling. The change V in potential energy, in passing from the straight to the buckled state of equilibrium, may be expressed[1]

$$V = V_1 - V_2 \tag{1}$$

where

$$V_1 = \tfrac{1}{2}\int_0^l B(x)(d^2y/dx^2)^2dx$$

and

$$V_2 = (P/2)\int_0^l (dy/dx)^2dx$$

Applying the principle of minimum potential energy—that is, setting δV equal to zero—leads to

$$\delta V = \int_0^l B(x)\frac{d^2y}{dx^2}\frac{d^2(\delta y)}{dx^2}dx - P\int_0^l \frac{dy}{dx}\frac{d(\delta y)}{dx}dx = 0 \tag{2}$$

where δy is any admissible variation of y consistent with conditions at the ends of the beam. $B(x)$ is not varied. Corresponding to each characteristic mode of buckling, $\phi_k(x)$ where $k = 1, 2, \ldots$, there is a characteristic value P_k which is the buckling load for that particular mode. In Eq. (2), y may be set equal to $\phi_k(x)$, in which case P is equal to P_k. Since $\phi_j(x)$ is an admissible variation, it may be selected to be δy and Eq. (2) becomes

$$\int_0^l B(x)\frac{d^2\phi_k}{dx^2}\frac{d^2\phi_j(x)}{dx^2}dx - P_k\int_0^l \frac{d\phi_k(x)}{dx}\frac{d\phi_j(x)}{dx}dx = 0 \tag{3}$$

On the other hand, y may be set equal to $\phi_j(x)$ and δy taken as ϕ_k, in which case Eq. (2) becomes

$$\int_0^l B(x)\frac{d^2\phi_j}{dx^2}\frac{d^2\phi_k}{dx^2}dx - P_j\int_0^l \frac{d\phi_j}{dx}\frac{d\phi_k}{dx}dx = 0 \tag{4}$$

Subtracting Eq. (4) from Eq. (3) leads to

$$(P_k - P_j)\int_0^l (d\phi_k/dx)\ (d\phi_j/dx)dx = 0 \tag{5}$$

and if $k \neq j$,

$$\int_0^l (d\phi_k/dx)\ (d\phi_j/dx)dx = 0 \tag{6}$$

From Eq. (4) it follows that for $k \neq j$,

$$\int_0^l B(x)(d^2\phi_k/dx^2)\ (d^2\phi_j/dx^2)dx = 0 \tag{7}$$

If y is measured from a point of inflection of the elastic curve,[2] the differential equation of the beam in buckled states ϕ_k and ϕ_j, respectively, may be expressed

$$\left.\begin{aligned} B(x)(d^2\phi_k/dx^2) + P_k\phi_k &= 0 \\ B(x)(d^2\phi_j/dx^2) + P_j\phi_j &= 0 \end{aligned}\right\} \tag{8}$$

Substituting Eqs. (8) into Eq. (7) leads to the principle of orthogonality of the characteristic modes—namely,

$$\int_0^l \phi_k\phi_j dx/B(x) = 0 \qquad \text{for } k \neq j \tag{9}$$

Let the characteristic functions be normalized by making

$$\int_0^l \phi_k^2 dx/B = 1, \quad k = 1, 2, \ldots \tag{10}$$

Then

$$\int_0^l B(d^2\phi_k/dx^2)^2dx = P_k^2 \tag{11}$$

From Eq. (3), by setting $j = k$, it follows that

Presented at the Structures Session, Twelfth Annual Meeting, I.A.S., New York, January 25–27, 1944.

* Associate Professor of Mechanics.

$$\int_0^l (d\phi_k/dx)^2 dx = P_k \tag{12}$$

When the beam is buckled by a load P into any shape consistent with the end conditions, this shape may be approximated to any desired degree by means of the Generalized Fourier Series[3]

$$y(x) = \sum_{k=1}^{n} a_k \phi_k(x) \tag{13}$$

where the ϕ's are the characteristic functions or pure modes of buckling of the beam under the prescribed conditions at the ends. The substitution of Eq. (13) into Eq. (1) and the use of the orthogonal and normal properties of the ϕ's leads to

$$V = \frac{1}{2}\sum_{k=1}^{n} a_k^2 P_k^2 - \frac{P}{2}\sum_{k=1}^{n} a_k^2 P_k \tag{14}$$

Inner rigid supports or restraints may be taken care of as follows: Suppose that, in addition to the end restraints, the beam is supported at $x = b$ and $x = c$, then

$$\sum a_k \phi_k(b) = 0$$

and

$$\sum a_k \phi_k(c) = 0$$

These conditions may be introduced into the expression for the total potential energy, Eq. (14), by means of the undetermined multipliers β and γ as follows:

$$V = \frac{1}{2}\sum a_k^2 P_k^2 - \frac{P}{2}\sum a_k^2 P_k - \beta \sum a_k \phi_k(b) - \gamma \sum a_k \phi_k(c) \tag{15}$$

The necessary conditions that V be a minimum are

$$\partial V/\partial a_k = 0, \qquad k = 1, 2, \ldots . n \tag{16}$$

and

$$\left.\begin{aligned} \frac{\partial V}{\partial \beta} &= 0 \\ \frac{\partial V}{\partial \gamma} &= 0 \end{aligned}\right\} \quad \text{leading to} \quad \left\{\begin{aligned} \sum a_k \phi_k(b) &= 0 \\ \sum a_k \phi_k(c) &= 0 \end{aligned}\right\} \tag{17}$$

From Eq. (16),

$$a_k = [\beta \phi_k(b) + \gamma \phi_k(c)]/P_k(P_k - P)$$

This, substituted into Eqs. (17), results in a pair of linear homogeneous equations in β and γ:

$$\left.\begin{aligned} A\beta + B\gamma &= 0 \\ B\beta + C\gamma &= 0 \end{aligned}\right\} \tag{18}$$

where

$$\left.\begin{aligned} A &= \sum \phi_k^2(b)/P_k(P_k - P) \\ B &= \sum \phi_k(b)\phi_k(c)/P_k(P_k - P) \\ C &= \sum \phi_k^2(c)/P_k(P_k - P) \end{aligned}\right\} \tag{19}$$

The vanishing of the determinant of the coefficients β and γ in Eqs. (18), necessary for a nontrivial solution, gives the characteristic equation

$$\left[\sum \frac{\phi_k^2(b)}{P_k(P_k - P)}\right]\left[\sum \frac{\phi_k^2(c)}{P_k(P_k - P)}\right] - \left[\sum \frac{\phi_k(b)\phi_k(c)}{P_k(P_k - P)}\right]^2 = 0 \tag{20}$$

The lowest root of Eq. (20) is the lowest buckling load of the constrained system. In most cases it is necessary to consider only the first few terms to get this load accurately enough for practical purposes. The extension to any number of intermediate rigid supports is evident.

Beam with Elastic Intermediate Supports

The procedure may be illustrated without loss in generality by again assuming two supports at $x = b$ and $x = c$, both of which are elastic. Let α_1 and α_2 be the respective forces per unit displacement required to deflect the supports. As before, the buckled form of the beam may be represented in terms of the characteristic functions of the unrestrained beam—that is,

$$y(x) = \sum_{k=1}^{n} a_k \phi_k(x)$$

The strain energy stored in these elastic supports is $(\alpha_1/2)y^2(b)$ and $(\alpha_2/2)y^2(c)$. The total potential energy now takes the form

$$V = \frac{1}{2}\sum a_k^2 P_k^2 - \frac{P}{2}\sum a_k^2 P_k + \frac{\alpha_1}{2}\left[\sum a_k \phi_k(b)\right]^2 + \frac{\alpha_2}{2}\left[\sum a_k \phi_k(c)\right]^2 \tag{21}$$

Applying the necessary conditions to make V a minimum,

$$\partial V/\partial a_k = 0, \qquad k = 1, 2, \ldots . n$$

results in

$$\left.\begin{aligned} &a_1[P_1^2 + \alpha_1\phi_1^2(b) + \alpha_2\phi_1^2(c) - P_1 P] + \\ &\quad a_2[\alpha_1\phi_1(b)\phi_2(b) + \alpha_2\phi_1(c)\phi_2(c)] + \ldots . = 0 \\ &a_1[\alpha_1\phi_1(b)\phi_2(b) + \alpha_2\phi_1(c)\phi_2(c)] + a_2[P_2^2 + \\ &\quad \alpha_1\phi_2^2(b) + \alpha_2\phi_2^2(c) - P_2 P] + \ldots . = 0 \\ &\quad \ldots \ldots \ldots \ldots \ldots \ldots \ldots \ldots \ldots \ldots = 0 \end{aligned}\right\} \tag{22}$$

The vanishing of the determinant of the coefficients of the a's, the necessary condition for a nontrivial solution, is the characteristic equation. The lowest root of this equation is the smallest buckling load of the restrained system.

The elastically restrained beam, having both ends simply supported, has been treated before by the minimum energy principle.[1] The above treatment, however, is also valid for free or fixed ends. In all cases the ϕ's and the corresponding P's are known so that the determination of the characteristic equation is a simple matter. As a general rule it will suffice to consider only the determinant of the second order, which consists of

the four terms in the upper left-hand corner, to obtain reasonable accuracy.

Plate with Rigid Intermediate Supports

Consider a thin uniform plate with any combination of simply supported, built-in, or free edges. In addition, let the plate be restrained from deflecting along any number of lines parallel to either the X or the Y axis, where X and Y are the usual coordinate axes in the plane of the unbuckled plate. The plate is acted on by a uniform compressive force N_x per unit length in the X direction. The problem is to determine the smallest value of N_x at which instability occurs.

The change V in potential energy, in passing from the straight to the buckled state of equilibrium, may be expressed[1] by

$$V = V_1 - V_2 \tag{23}$$

where

$$V_1 = \frac{D}{2}\int\int\left\{(\nabla^2 w)^2 - 2(1-\nu)\left[\frac{\partial^2 w}{\partial x^2}\frac{\partial^2 w}{\partial y^2} - \left(\frac{\partial^2 w}{\partial x \partial y}\right)^2\right]\right\}dx\,dy$$

$$V_2 = (N_x/2)\int\int(\partial w/\partial x)^2 dx\,dy$$

$$D = Eh^3/12(1-\nu^2)$$

h being the thickness of the plate; E, the modulus of elasticity; and $\nabla^2 \equiv (\partial^2/\partial x^2) + (\partial^2/\partial y^2)$.

It will be convenient to introduce the quadratic functionals defined as follows:[3, 4]

$$H(u, v) = \int\int uv\,dx\,dy$$

$$F(u, v) = \int\int\left(\frac{\partial u}{\partial x}\frac{\partial v}{\partial x} + \frac{\partial u}{\partial y}\frac{\partial v}{\partial y}\right)dx\,dy$$

$$I(u, v) = \int\int\left[\nabla^2 u \nabla^2 v - (1-\nu)\times\left(\frac{\partial^2 u}{\partial x^2}\frac{\partial^2 v}{\partial y^2} + \frac{\partial^2 u}{\partial y^2}\frac{\partial^2 v}{\partial x^2} - 2\frac{\partial^2 u}{\partial x \partial y}\frac{\partial^2 v}{\partial x \partial y}\right)\right]dx\,dy$$

In this notation, the potential energy may be expressed

$$V = \frac{D}{2}I(w, w) - \frac{N_x}{2}H\left(\frac{\partial w}{\partial x}, \frac{\partial w}{\partial x}\right) \tag{24}$$

and

$$\delta V = DI(w, \delta w) - N_x H\left(\frac{\partial w}{\partial x}, \frac{\partial(\delta w)}{\partial x}\right)$$

The necessary condition that V be a minimum is that δV be zero or

$$I(w, \delta w) - \lambda H\left(\frac{\partial w}{\partial x}, \frac{\partial(\delta w)}{\partial x}\right) = 0 \tag{25}$$

where $\lambda = N_x/D$. Since δw is any admissible variation in w consistent with the boundary conditions, it may be set equal to ϕ_j, the characteristic shape of the plate in the jth mode of buckling. At the same time, w may be set equal to ϕ_k, for which $\lambda = \lambda_k$. Eq. (25) becomes

$$I(\phi_k, \phi_j) - \lambda_k H\left(\frac{\partial \phi_k}{\partial x}, \frac{\partial \phi_j}{\partial x}\right) = 0 \tag{26}$$

On the other hand, δw may be set equal to ϕ_k and w taken as ϕ_j, in which case Eq. (25) becomes

$$I(\phi_j, \phi_k) - \lambda_j H\left(\frac{\partial \phi_j}{\partial x}, \frac{\partial \phi_k}{\partial x}\right) = 0 \tag{27}$$

Since $I(u, v) = I(v, u)$ and $H(u, v) = H(v, u)$, subtracting Eq. (27) from Eq. (26) leads to

$$(\lambda_k - \lambda_j)\,H[(\partial\phi_k/\partial x), (\partial\phi_j/\partial x)] = 0$$

For $\lambda_k \neq \lambda_j$ it follows that

$$\int\int(\partial\phi_k/\partial x)(\partial\phi_j/\partial x)dx\,dy = 0 \tag{28}$$

Consequently, for $\lambda_k \neq \lambda_j$

$$I(\phi_k, \phi_j) = 0 \tag{29}$$

Furthermore, let the characteristic functions be normalized—that is, make

$$\int\int(\partial\phi_k/\partial x)^2 dx\,dy = 1$$

From Eq. (27) it is evident that

$$I(\phi_k, \phi_k) = \lambda_k \tag{30}$$

When the plate is buckled into any shape consistent with the boundary conditions, this shape may be approximated to any desired degree by means of the Generalized Fourier Series.

$$w = \sum_{j=1}^{n}\sum_{k=1}^{n} a_{jk}\phi_{jk}(x, y)$$

where the ϕ's are the characteristic functions expressing the various modes of buckling under the prescribed boundary conditions. By virtue of Eqs. (28), (29), and (30),

$$V = {}^1/_2\sum\sum a_{jk}{}^2\lambda_{jk} - (\lambda/2)\sum\sum a_{jk}{}^2$$

Restraints are introduced as before through undetermined multipliers. For example, if the plate is restrained from deflecting along the line $x = c$, then

$$0 = \sum\sum a_{jk}\phi_{jk}(c, y) \tag{31}$$

With β as the undetermined multiplier, the expression to be minimized takes the form

$$V = \frac{1}{2}\sum\sum a_{jk}{}^2\lambda_{jk} - \frac{\lambda}{2}\sum\sum a_{jk}{}^2 - \beta\sum\sum a_{jk}\phi_{j,k}(c, y) \tag{32}$$

From the conditions $\partial V/\partial a_{jk} = 0$ and $j, k = 1, 2, \ldots, n$, it is found that

$$a_{jk} = \beta\phi_{jk}(c, y)/(\lambda_{jk} - \lambda)$$

Substituting this value into $\partial V/\partial\beta = 0$, which is equivalent to Eq. (31), there results

$$\sum\sum\phi_{jk}^2(c, y)/(\lambda_{jk} - \lambda) = 0 \qquad (33)$$

Since this double sum must vanish for all values of y over the plate, n characteristic equations will be found. From these equations it will not be difficult in most cases to select the one from which the lowest root may be determined. This, of course, gives the smallest buckling load of the plate subject to the restraints. If more than one restraint is operative, say along the lines $x = c_1$ and $x = c_2$,

$$V = \frac{1}{2}\sum\sum a_{jk}^2\lambda_{jk} - \frac{\lambda}{2}\sum\sum a_{jk}^2 - \beta\sum\sum a_{jk}\phi_{jk}(c_1, y) - \gamma\sum\sum a_{jk}\phi_{jk}(c_2, y)$$

Minimizing V leads to a pair of homogeneous linear equations in β and γ from which the n characteristic equations may be found. The case of constraints along lines parallel to the Y axis is handled in the same manner.

No theoretical difficulties are introduced when the method is extended to the buckling of the constrained plate by compressive forces in both the X and Y directions or by shear forces along the edges. It is only necessary to make the appropriate changes in V_2. For example, under equal compressive forces N in both X and Y directions,[1]

$$V_2 = \frac{N}{2}\int\int\left[\left(\frac{\partial w}{\partial x}\right)^2 + \left(\frac{\partial w}{\partial y}\right)^2\right]dx\,dy = \frac{N}{2}\,F(w, w)$$

and with $\lambda = N/D$, $\delta V_2 = D\lambda F(w, \delta w)$.

As before, for $w = \phi_k$ and $\delta w = \phi_j$

$$\delta V_2 = \lambda_k DF(\phi_k, \phi_j) \qquad (34)$$

and for $w = \phi_j$ and $\delta w = \phi_k$

$$\delta V_2 = \lambda_j DF(\phi_j, \phi_k) \qquad (35)$$

Now δV_1 is the same in both cases, so when Eq. (35) is subtracted from Eq. (34), the orthogonality of the normal modes is again established—that is,

$$F(\phi_k, \phi_j) \equiv \int\int\left(\frac{\partial\phi_k}{\partial x}\frac{\partial\phi_j}{\partial x} + \frac{\partial\phi_k}{\partial y}\frac{\partial\phi_j}{\partial y}\right)dx\,dy = 0 \qquad k \neq j$$

and as before $I(\phi_k, \phi_j) = 0$. Normalizing, this time by making

$$\int\int[(\partial\phi_k/\partial x)^2 + (\partial\phi_k/\partial y)^2]dx\,dy = 1$$

it follows that $I(\phi_k, \phi_k) = \lambda_k$, and the procedure is as before. In the case of buckling due to shear forces N_{xy} along the edges and in the plane of the plate, it is easily shown that

$$\int\int[(\partial\phi_k/\partial x)(\partial\phi_j/\partial y) + (\partial\phi_j/\partial x)(\partial\phi_k/\partial y)]dx\,dy = 0 \qquad j \neq k$$

Normalizing brings about

$$2\int\int(\partial\phi_k/\partial x)(\partial\phi_k/\partial y)dx\,dy = 1$$

and again $I(\phi_k, \phi_k) = \lambda_k$.

An example that illustrates the method and at the same time is free of extraneous complications is furnished by the rectangular plate of sides a and b simply supported on all edges. Let it be subjected to a uniform compressive force N_x per unit length acting in the direction of the side a and in the plane of the plate. Taking the origin of the coordinate system at a corner of the plate, it is known that[1]

$$\phi_{jk} = (2/j\pi)\sqrt{(a/b)}\,\sin(j\pi x/a)\,\sin(k\pi y/b)$$

with the corresponding buckling load

$$\lambda_{jk} = (\pi^2a^2/j^2)[(j^2/a^2) + (k^2/b^2)]^2$$

The factor multiplying $\sin(j\pi x/a)\sin(k\pi y/b)$ in the expression for ϕ_{jk} has been introduced to make $\int\int(\partial\phi_{jk}/\partial x)^2dx\,dy$ equal to unity. Let the plate be restrained from deflecting along the line $x = c$. Eq. (33) becomes

$$\sin^2\frac{\pi y}{b}\left[\frac{(1/1^2)\sin^2(\pi c/a)}{\frac{\pi^2a^2}{1^2}\left(\frac{1}{a^2}+\frac{1}{b^2}\right)^2-\lambda} + \frac{(1/2^2)\sin^2(2\pi c/a)}{\frac{\pi^2a^2}{2^2}\left(\frac{2^2}{a^2}+\frac{1^2}{b^2}\right)^2-\lambda} + \cdots\right]$$
$$+ \sin^2\frac{2\pi y}{b}\left[\frac{(1/1^2)\sin^2(\pi c/a)}{\frac{\pi^2a^2}{1^2}\left(\frac{1}{a^2}+\frac{2^2}{b^2}\right)^2-\lambda} + \frac{(1/2^2)\sin^2(2\pi c/a)}{\frac{\pi^2a^2}{2^2}\left(\frac{2^2}{a^2}+\frac{2^2}{b^2}\right)^2-\lambda} + \cdots\right] + \cdots = 0$$
$$\cdots = 0$$

Since this must vanish for all values of y in the range $0 \leqslant y \leqslant b$, each of the expressions in the brackets must individually vanish. This leads to n characteristic equations. The first one corresponds to buckling with one half wave in the Y direction, the second to two half waves in the Y direction, etc. For a given ratio a/b it is not difficult to select the equation from which the lowest buckling load may be found.

If the restraint is along the line $y = d$, the characteristic equation is found to be

$$\sin^2\frac{\pi x}{a}\left[\frac{\sin^2(\pi d/b)}{\frac{\pi^2a^2}{1^2}\left(\frac{1}{a^2}+\frac{1}{b^2}\right)^2-\lambda} + \frac{\sin^2(2\pi d/b)}{\frac{\pi^2a^2}{1^2}\left(\frac{1}{a^2}+\frac{2^2}{b^2}\right)^2-\lambda} + \cdots\right]$$
$$+ \sin^2\frac{2\pi x}{a}\left[\frac{\sin^2(\pi d/b)}{\frac{\pi^2a^2}{2^2}\left(\frac{2^2}{a^2}+\frac{1^2}{b^2}\right)^2-\lambda} + \frac{\sin^2(2\pi d/b)}{\frac{\pi^2a^2}{2^2}\left(\frac{2^2}{a^2}+\frac{2^2}{b^2}\right)^2-\lambda} + \cdots\right] + \cdots = 0$$
$$\cdots = 0$$

And again each of the expressions in brackets must be set equal to zero, from which there results n characteristic equations.

Plate with Intermediate Elastic Supports

An approximate solution to the problem of the buckling of a plate reinforced by ribs may be obtained by considering the ribs as elastic restraints on the plate and including in the expression for the potential energy of the system the strain energy stored in the ribs in the buckled state. The procedure has been treated elsewhere for rectangular plates that are simply supported on all edges.[1] However, the methods described above enable the treatment to be extended to plates having any edge conditions for which the characteristic buckling modes and corresponding characteristic buckling loads for the plate without stiffening ribs are known or can be found.

For example, in the case of a plate reinforced by a single rib of uniform flexural rigidity B and subjected to a uniform compressive force N_x per unit length on the plate and P_x on the rib in the X direction, the potential energy takes the form

$$V = \frac{1}{2}\sum\sum a_{jk}^2\lambda_{jk} - \frac{N_x}{2}\sum\sum a_{jk}^2 + \frac{B}{2}\int_0^a \left[\frac{\partial^2 w(x, d)}{\partial x^2}\right]^2 dx - \frac{P_x}{2}\int_0^a \left[\frac{\partial w(x, d)}{\partial x}\right]^2 dx$$

when the shape of the plate in the buckled state has been represented by

$$w = \sum\sum a_{jk}\phi_{jk}(x, y)$$

and the rib is along the line $y = d$. It is easily seen that V is a function of the a's and minimizing V leads to a set of linear homogeneous equations in the a's, the determinant of which set equal to zero (for a nontrivial solution) gives the characteristic equation.

Conclusion

It is clear that in those cases for which the characteristic functions and corresponding characteristic buckling loads of a beam or plate are known it is a relatively simple matter to establish the equation from which the buckling load for the beam or plate subject to additional rigid or elastic restraints may be found. The solution of the equation in the case of several restraints may become quite involved arithmetically, but at least it is a straightforward procedure. It should be noted that even in those cases for which approximations to the characteristic functions must be used the method is applicable though the accuracy in such cases would be difficult to estimate. However, since it is much easier to find functions that satisfy only boundary conditions around the edges and to introduce the intermediate supports as constraints of the system than it is to find functions that satisfy both the conditions at the edges of the plate and the intermediate conditions, the above procedure would appear to have some advantages over the customary Rayleigh-Ritz method, even when the characteristic functions are unknown.

References

[1] Timoshenko, S., *Theory of Elastic Stability;* McGraw-Hill Book Company, Inc., New York, 1936.

[2] Prescott, J., *Applied Elasticity;* Longmans, Green and Co., London, 1924.

[3] Courant, R., and Hilbert, D., *Methoden der Mathematischen Physik I;* Julius Springer, Berlin, 1931.

[4] Weinstein, A., *Etude des spectres des equations aux derivées partielles de la théorie des plaques élastiques;* Gauthier-Villars, Paris, 1937.

EDITORIAL AND PROFESSIONAL ACTIVITIES COMMITTEE

HUGH L. DRYDEN, *Chairman*

Aerodynamics
William Bollay
Kenneth S. M. Davidson
Walter S. Diehl
Hugh L. Dryden
R. Paul Harrington
P. E. Hemke
Eastman N. Jacobs
Th. von Kármán
Alexander Klemin
W. B. Klemperer
Otto C. Koppen
A. M. Kuethe
John G. Lee
John R. Markham
Clark B. Millikan
Richard von Mises
Shatswell Ober
W. Bailey Oswald
Manfred Rauscher
Elliott G. Reid
H. J. E. Reid
Hans Reissner
Benjamin F. Ruffner
G. B. Schubauer
Abe Silverstein
R. H. Smith
Th. Theodorsen
M. J. Thompson
Starr Truscott
Michael Watter
K. D. Wood

Air Transport
Ralph S. Damon
Charles Froesch
Melvin N. Gough
J. A. Herlihy
William Littlewood
A. A. Priester
Paul E. Richter
N. F. Scudder

Aircraft Design
Karl Arnstein
Rex B. Beisel
B. C. Boulton
C. P. Burgess
C. H. Chatfield
J. W. Crowley, Jr.
R. C. Gazley
Leroy R. Grumman
Hall L. Hibbard
A. L. Klein
Otto C. Koppen
I. M. Laddon
John G. Lee
C. J. McCarthy
William H. Miller
R. H. Prewitt
Igor I. Sikorsky
E. A. Stalker
Th. Troller
Starr Truscott
R. H. Upson
Fred E. Weick
Robert J. Woods
T. P. Wright

Aircraft Production
John L. Atwood
W. E. Beall
Carl de Ganahl
W. K. Ebel
Fredric Flader
Hall L. Hibbard
Guy A. Luburg
C. J. McCarthy
A. E. Raymond
W. T. Schwendler
Harry A. Sutton
John Tjaarda
Robert J. Woods
T. P. Wright

Radio
C. S. Draper
Lloyd Espenschied
C. G. Fick
Lewis M. Hull
Haraden Pratt
F. X. Rettenmeyer

Physiologic Problems
H. G. Armstrong
Louis H. Bauer
David B. Dill
Eugene Du Bois
W. Randolph Lovelace, II
Ross A. McFarland
A. D. Tuttle

Power Plants and Propellers
M. A. Biot
George W. Brady
Frank W. Caldwell
Ivan H. Driggs
Louis H. Enos
David Gregg
L. S. Hobbs
Albert R. Jacobs
E. E. Johnson
Carleton Kemper
H. M. McCoy
W. C. Nelson
Arthur Nutt
Shatswell Ober
Elliott G. Reid
Hans Reissner
David R. Shoults
C. Fayette Taylor
E. S. Taylor
Th. Theodorsen
A. V. Willgoos
D. H. Wood

Structures and Materials
M. A. Biot
W. B. Bleakney
C. P. Burgess
E. W. Conlon
George W. DeBell
A. V. de Forest
L. H. Donnell
L. G. Dunn
Richard C. Gazley
W. C. Geer
E. C. Hartmann
J. P. Den Hartog
N. J. Hoff
Zay Jeffries
Th. von Kármán
W. B. Klemperer
E. E. Lundquist
C. J. McCarthy
C. F. Nagel, Jr.
J. S. Newell
Alfred S. Niles
Thomas D. Perry
W. Ramberg
E. Reissner
F. R. Shanley
H. W. Sibert
S. Timoshenko
H. S. Tsien
L. B. Tuckerman
George Tweney
J. A. Wise
J. E. Younger

Meteorology
C. F. Brooks
Karl O. Lange
D. M. Little
E. J. Minser
Sverre Petterssen
F. W. Reichelderfer
A. F. Spilhaus
P. V. H. Weems
H. C. Willett

Education
R. Paul Harrington
C. S. Jones
Alexander Klemin
Clark B. Millikan
W. C. Nelson
George B. Pegram
R. H. Smith
Ben D. Wood

Fuels and Oils
D. P. Barnard
A. L. Beall
J. H. Doolittle
Graham Edgar
Luis de Florez
R. Goodwin
Raymond Haskell
S. D. Heron
A. M. Rothrock
D. H. Young

Instruments
P. R. Bassett
W. G. Brombacher
Charles H. Colvin
C. S. Draper
Lucien L. Friez
Walter McKay
W. A. Reichel
C. F. Savage
A. F. Spilhaus
S. J. Zand

I.A.S. REPRESENTATIVES TO OTHER ORGANIZATIONS

Aeronautical Chamber of Commerce of America—CHARLES MARCUS
American Association for the Advancement of Science—J. C. HUNSAKER
American Institute of Mining & Metallurgical Engineers—A. V. DE FOREST
American Society of Mechanical Engineers—JOHN E. YOUNGER
American Standards Association—P. R. BASSETT
Greater New York Safety Council—WILLIAM LITTLEWOOD
Daniel Guggenheim Medal Board of Award—CHARLES H. COLVIN, RALPH S. DAMON, LESTER D. GARDNER
Institute of Radio Engineers—L. M. HULL
Manufacturers Aircraft Association—J. T. HARTSON
National Aeronautic Association—WILLIAM R. ENYART
National Safety Council—JEROME LEDERER
National Research Council Engineering Division—FRANK W. CALDWELL
New York Museum of Science and Industry—LESTER D. GARDNER
Society of Automotive Engineers—EDWARD P. WARNER

Index to Volume 11

Journal of the Aeronautical Sciences

Numbers 1–4, January–October, 1944

No. 1, January, 1944, pages 1– 94
No. 2, April, 1944, pages 95–188
No. 3, July, 1944, pages 189–282
No. 4, October, 1944, pages 283–408

Material that has appeared in the above volume has been indexed under a general subject heading and by author and has been further cross-indexed under various specialized subheadings.

ADAMS, J. C., B. GROESBECK, Jr., AND E. F. DUBOIS. Medical Activities in Naval Aviation 63
Aerodynamics—
Contracting Cones Giving Uniform Throat Speeds, Richard H. Smith and Chi-Teh Wang 356
Design of Elbows in Potential Motion, Boleslaw Szczeniowski 73
Directional Stability of Flying Boat Hulls During Taxiing, John D. Pierson 189
Drag of Airfoils in Grids of High Solidity, J. R. Weske 369
Effect of Dive Brakes on Airfoil and Airplane Characteristics, Philip G. Blenkush, Raymond F. Hermes, and Merle A. Landis 254
The Effects of a Fuselage upon the Stability of an Airplane, C. E. Pappas 174
Fuselage Influence on the Airflow at the Propellers of a Multiengined Airplane in Yawed Flight, R. P. Harrington and Victor Zadikov 205
An Iterative Method for Determining Dynamic Deflections and Frequencies, N. A. Boukidis and R. J. Ruggiero 319
Letters to the Editor
Lin, Chia-chiao 195
Tsien, Hsue-shen 91
The L.P.C. Method of Performance Computation, Joseph V. Foa and Bernard M. Leadon 329
Loss in Aileron Effectiveness Because of Wing Twist and Considerations Regarding the Internal-Pressure Balanced Aileron, Reinhardt Rosenberg 41
A New Method of Calculating Natural Modes of Uncoupled Bending Vibration of Airplane Wings and Other Types of Beams, N. O. Myklestad 153
Notes on Rudder Pedal-Force Characteristics, H. R. Pass 183
Prediction of Longitudinal Dynamic Stability, H. P. Liepman 307
Research for Aeronautics—Its Planning and Application, W. S. Farren 95
Some Two-Dimensional Adiabatic Compressible Flow Patterns, Hans Kraft and Charles G. Dibble 283
The Thermodynamics of Air at High Velocities, Neil P. Bailey 227
Aileron effectiveness, loss in, because of wing twist and considerations regarding the internal-pressure balanced aileron 41
Airflow, fuselage influence on the, at the propellers of a multiengined airplane in yawed flight 205
Airfoils in grids of high solidity, drag of 369

BAILEY, NEIL P. The Thermodynamics of Air at High Velocities 227
Beam-column, general, by the collocation method, analysis of the 165
Beams, continuous, vibration frequencies of 88
Beams or plates on continuous supports, buckling loads of 399
Beams with applications to multicellular sections, a theorem on the shearing stress in 272
Bending, plastic 213
BENSON, OTIS O., JR., DAVID B. DILL, AND W. RANDOLPH LOVELACE, II. Medical Activities in Military Aviation 21
BESKIN, LEON. Letter to the Editor (Stress Analysis and Structures) 398
———— Stress Analysis of Open Cylindrical Membranes 343
Blade pitch control, cyclic, the response of helicopters with articulated rotors to 387
Blade section variation on small-scale rotors 83
Blades, unbalanced lifting rotor, aero-elastic instability in 361
BLENKUSH, PHILIP G., RAYMOND F. HERMES, AND MERLE A. LANDIS. Effect of Dive Brakes on Airfoil and Airplane Characteristics 254
BOUKIDIS, N. A., AND R. J. RUGGIERO. An Iterative Method for Determining Dynamic Deflections and Frequencies 319
Brakes, dive, effect of, on airfoil and airplane characteristics 254
Buckling, inelastic, a note on 163
Buckling loads of beams or plates on continuous supports 399
BURWELL, JOHN T., JR., AND BERNHARD W. SAKMANN. On the Mechanism of Friction 381

CHRISTENSEN, N. B., AND TH. VON KÁRMÁN. Methods of Analysis for Torsion with Variable Twist 110
Column analogy, analysis of fuselage rings by the 137
Column with equal-spaced elastic supports 67
Columns, notes on 1
Columns tested between knife edges, corrections for lengths of 378
Cones, contracting, giving uniform throat speeds 356
CROWLEY, D. M. Causes of Nighttime Thunderstorms over the Middle West 313
Cylindrical membranes, open, stress analysis of 343

Deflections and frequencies, dynamic, an iterative method for determining 319
DEJUHASZ, KALMAN J. Graphical Analysis of Response Characteristics of Rate-of-Climb Indicators 48
DENKE, PAUL H. Strain Energy Analysis of Incomplete Tension Field Web-Stiffener Combinations 25
Design—
Directional Stability of Flying Boat Hulls During Taxiing, John D. Pierson 189
Radiant Energy Exchange as a Factor in Airplane Cabin Heating, B. F. Raber and F. W. Hutchinson 239

Stress Problems in the Design of Wooden Airplanes, Zbigniew Krzywoblocki... 76
DIBBLE, CHARLES G., AND HANS KRAFT. Some Two-Dimensional Adiabatic Compressible Flow Patterns... 283
DILL, DAVID B., OTIS O. BENSON, JR., AND W. RANDOLPH LOVELACE, II. Medical Activities in Military Aviation. 21
DONOVAN, A. F., AND M. GOLAND. The Response of Helicopters with Articulated Rotors to Cyclic Blade Pitch Control... 387
DORN, J. E., AND E. G. THOMSEN. The Effect of Combined Stresses on the Ductility and Rupture Strength of Magnesium-Alloy Extrusions... 125
Drag of airfoils in grids of high solidity... 369
DUBOIS, E. F., J. C. ADAMS, AND B. GROESBECK, JR. Medical Activities in Naval Aviation... 63
DUPLANTIER, DONALD A. Analysis of Fuselage Rings by the Column Analogy... 137

EASTMAN, E. J., AND F. A. RAPPLEYEA. Flexural Strength in the Plastic Range of Rectangular Magnesium Extrusions... 373
EIKENBERRY, ROBERT S. Letter to the Editor (Gliders)... 328
Elbows, design of, in potential motion... 73
Engines—
On the Mechanism of Friction, Bernhard W. Sakmann and John T. Burwell, Jr... 381
Study of Exhaust-Valve Design from Gas Flow Standpoint, Seng-chiu Hu... 13
Theory of the Centrifugally Tuned Vibration Absorber, Ralph J. Harker... 197
Extrusions, rectangular magnesium, flexural strength in the plastic range of... 373

FARREN, W. S. Research for Aeronautics—Its Planning and Application... 95
Flow patterns, some two-dimensional adiabatic compressible... 283
FOA, JOSEPH V., AND BERNARD M. LEADON. The L.P.C. Method of Performance Computation... 329
Friction, on the mechanism of... 381

Gliders—
Letters to the Editor
Eikenberry, Robert S... 328
Sawyer, Richard H... 196
Take-Off Distance of a Glider Train, Wieslaw Z. Stepniewski... 55
GOLAND, M., AND A. F. DONOVAN. The Response of Helicopters with Articulated Rotors to Cyclic Blade Pitch Control... 387
GOODIER, J. N. A Theorem on the Shearing Stress in Beams with Applications to Multicellular Sections... 272
GROESBECK, B., JR., J. C. ADAMS, AND E. F. DUBOIS. Medical Activities in Naval Aviation... 63

HARKER, RALPH J. Theory of the Centrifugally Tuned Vibration Absorber... 197
HARRINGTON, R. P., AND VICTOR ZADIKOV. Fuselage Influence on the Airflow at the Propellers of a Multiengined Airplane in Yawed Flight... 205
Heating, airplane cabin, radiant energy exchange as a factor in... 239
Helicopters with articulated rotors, the response of, to cyclic blade pitch control... 387
HERMES, RAYMOND F., MERLE A. LANDIS, AND PHILIP G. BLENKUSH. Effect of Dive Brakes on Airfoil and Airplane Characteristics... 254
HOFF, N. J. Letters to the Editor (Stress Analysis and Structures)... 318, 338
——— A Note on Inelastic Buckling... 163
HU, SENG-CHIU. Study of Exhaust-Valve Design from Gas Flow Standpoint... 13
Hulls, flying boat, during taxiing, directional stability of... 189
HUTCHINSON, F. W., AND B. F. RABER. Radiant Energy Exchange as a Factor in Airplane Cabin Heating... 239

Instruments—
Graphical Analysis of Response Characteristics of Rate-of-Climb Indicators, Kalman J. DeJuhasz... 48

KRAFT, HANS, AND CHARLES G. DIBBLE. Some Two-Dimensional Adiabatic Compressible Flow Patterns... 283
KRZYWOBLOCKI, ZBIGNIEW. Stress Problems in the Design of Wooden Airplanes... 76

LANDIS, MERLE A., PHILIP G. BLENKUSH, AND RAYMOND F. HERMES. Effect of Dive Brakes on Airfoil and Airplane Characteristics... 254
LEADON, BERNARD M., AND JOSEPH V. FOA. The L.P.C. Method of Performance Computation... 329
LIEPMAN, H. P. Prediction of Longitudinal Dynamic Stability... 307
LIN, CHIA-CHIAO. Letter to the Editor (Aerodynamics)... 195
LOVELACE, W. RANDOLPH, II, OTIS O. BENSON, JR., AND DAVID B. DILL. Medical Activities in Military Aviation. 21

Magnesium-alloy extrusions, the effect of combined stresses on the ductility and rupture strength of... 125
Materials—
The Effect of Combined Stresses on the Ductility and Rupture Strength of Magnesium-Alloy Extrusions, E. G. Thomsen and J. E. Dorn... 125
Flexural Strength in the Plastic Range of Rectangular Magnesium Extrusions, F. A. Rappleyea and E. J. Eastman... 373
McCOY, H. M. Propeller Design Requirements... 261
Medicine and Physiology—
Medical Activities in Military Aviation, Otis O. Benson, Jr., David B. Dill, and W. Randolph Lovelace, II... 21
Medical Activities in Naval Aviation, J. C. Adams, B. Groesbeck, Jr., and E. F. DuBois... 63
Meteorology—
Causes of Nighttime Thunderstorms over the Middle West, D. M. Crowley... 313
Military aviation, medical activities in... 21
MYKLESTAD, N. O. A New Method of Calculating Natural Modes of Uncoupled Bending Vibration of Airplane Wings and Other Types of Beams... 153

Naval aviation, medical activities in... 63
NUBAR, YVES. Analysis of the General Beam-Column by the Collocation Method... 165

OSGOOD, WILLIAM R. Corrections for Lengths of Columns Tested Between Knife Edges... 378
——— Letters to the Editor (Stress Analysis and Structures)... 91, 196
——— Plastic Bending... 213

Panels, efficiency of lateral stiffeners in... 299
Panels, strength of, effects of material distribution on... 247
PAPPAS, C. E. The Effects of a Fuselage upon the Stability of an Airplane... 174
PASS, H. R. Notes on Rudder Pedal-Force Characteristics 183
Performance computation, the L.P.C. method of... 329
PIERSON, JOHN D. Directional Stability of Flying Boat Hulls During Taxiing... 189

Propellers—
Propeller Design Requirements, H. M. McCoy 261
Theory of the Centrifugally Tuned Vibration Absorber, Ralph J. Harker 197

RABER, B. F., AND F. W. HUTCHINSON. Radiant Energy Exchange as a Factor in Airplane Cabin Heating 239
RAPPLEYEA, F. A., AND E. J. EASTMAN. Flexural Strength in the Plastic Range of Rectangular Magnesium Extrusions 373
Rate-of-climb indicators, graphical analysis of response characteristics of 48
RAZAK, KENNETH. Blade Section Variation on Small-Scale Rotors 83
Research for aeronautics—its planning and application 95
Rings, fuselage, analysis of, by the column analogy 137
ROSENBERG, REINHARDT. Aero-Elastic Instability in Unbalanced Lifting Rotor Blades 361
——— Loss in Aileron Effectiveness Because of Wing Twist and Considerations Regarding the Internal-Pressure Balanced Aileron 41
Rotary Wing Aircraft—
Aero-Elastic Instability in Unbalanced Lifting Rotor Blades, Reinhardt Rosenberg 361
Periodic Aerodynamic Forces on Rotors in Forward Flight, Charles Seibel 339
The Response of Helicopters with Articulated Rotors to Cyclic Blade Pitch Control, A. F. Donovan and M. Goland ... 387
Blade Section Variation on Small-Scale Rotors, Kenneth Razak 83
Rotors, small-scale, blade section variation on 83
RUGGIERO, R. J., AND N. A. BOUKIDIS. An Iterative Method for Determining Dynamic Deflections and Frequencies 319

SAIBEL, EDWARD. Buckling Loads of Beams or Plates on Continuous Supports 399
——— Vibration Frequencies of Continuous Beams 88
SAKMANN, BERNHARD W., AND JOHN T. BURWELL, JR. On the Mechanism of Friction 381
SANDORFF, PAUL E. Notes on Columns 1
SAWYER, RICHARD H. Letter to the Editor (Gliders) 196
SEIBEL, CHARLES. Periodic Aerodynamic Forces on Rotors in Forward Flight 339
SMITH, RICHARD H., AND CHI-TEH WANG. Contracting Cones Giving Uniform Throat Speeds 356
Stability of an airplane, the effects of a fuselage upon the .. 174
Stability, directional, of flying boat hulls during taxiing ... 189
Stability, longitudinal dynamic, prediction of 307
STEPNIEWSKI, WIESLAW Z. Take-Off Distance of a Glider Train 55
Stiffeners, lateral, in panels, efficiency of 299
Stress Analysis and Structures—
Analysis of Fuselage Rings by the Column Analogy, Donald A. duPlantier 137
Analysis of the General Beam-Column by the Collocation Method, Yves Nubar 165
Buckling Loads of Beams or Plates on Continuous Supports, Edward Saibel 399
Column with Equal-Spaced Elastic Supports, Shou-Ngo Tu 67
Corrections for Lengths of Columns Tested Between Knife Edges, William R. Osgood 378
Effects of Material Distribution on Strength of Panels, Adam Zahorski 247
Efficiency of Lateral Stiffeners in Panels, Adam Zahorski. 299
Flexural Strength in the Plastic Range of Rectangular Magnesium Extrusions, F. A. Rappleyea and E. J. Eastman 373
Letters to the Editor
Beskin, Leon 398
Hoff, N. J. 318, 338
Osgood, William R. 91, 196
Whitney, Charles S. 253
Wan, Conrad C. 312
Methods of Analysis for Torsion with Variable Twist, Th. von Kármán and N. B. Christensen 110
A Note on Inelastic Buckling, N. J. Hoff 163
Plastic Bending, William R. Osgood 213
Strain Energy Analysis of Incomplete Tension Field Web-Stiffener Combinations, Paul H. Denke 25
Notes on Columns, Paul E. Sandorff 1
Stress Analysis of Open Cylindrical Membranes, Leon Beskin 343
Stress Problems in the Design of Wooden Airplanes, Zbigniew Krzywoblocki 76
A Theorem on the Shearing Stress in Beams with Applications to Multicellular Sections, J. N. Goodier 272
Vibration Frequencies of Continuous Beams, Edward Saibel 88
SZCZENIOWSKI, BOLESLAW. Design of Elbows in Potential Motion 73

Thermodynamics of air at high velocities 227
THOMSEN, E. G., AND J. E. DORN. The Effect of Combined Stresses on the Ductility and Rupture Strength of Magnesium-Alloy Extrusions 125
Thunderstorms, nighttime, over the middle west, causes of. 313
Torsion with variable twist, methods of analysis for 110
TSIEN, HSUE-SHEN. Letter to the Editor (Aerodynamics) .. 91
TU, SHOU-NGO. Column with Equal-Spaced Elastic Supports 67

Valve design, exhaust-, from gas flow standpoint, study of .. 13
Vibration absorber, centrifugally tuned, theory of the 197
Vibration, uncoupled bending, of airplane wings and other types of beams, a new method of calculating natural modes of 153
VON KÁRMÁN, TH., AND N. B. CHRISTENSEN. Methods of Analysis for Torsion with Variable Twist 110

WAN, CONRAD C. Letter to the Editor (Stress Analysis and Structures) 312
WANG, CHI-TEH, AND RICHARD H. SMITH. Contracting Cones Giving Uniform Throat Speeds 356
Web-stiffener combinations, incomplete tension field, strain energy analysis of 25
WESKE, J. R. Drag of Airfoils in Grids of High Solidity ... 369
WHITNEY, CHARLES S. Letter to the Editor (Stress Analysis and Structures) 253
Wooden airplanes, stress problems in the design of 76

ZADIKOV, VICTOR, AND R. P. HARRINGTON. Fuselage Influence on the Airflow at the Propellers of a Multiengined Airplane in Yawed Flight 205
ZAHORSKI, ADAM. Effects of Material Distribution on Strength of Panels 247
——— Efficiency of Lateral Stiffeners in Panels. 299

Services of the Aeronautical Archives of the Institute of the Aeronautical Sciences

The services of the Aeronautical Archives are available to all members of the Institute, to Corporate Members, to advertisers in the Aeronautical Engineering Review and, under usual library limitations, to the public. Four specialized services are available.

The Paul Kollsman Library

This lending library service makes available, *without charge*, the latest and more important aeronautical books.

As far as the facilities permit, any person in the United States over 18 years of age who can furnish references which certify to his or her responsibility may become a member of the library.

Members may request the loan of any aeronautical or technical book they wish to borrow. Through an exchange agreement with the Engineering Societies Library, any book on general engineering may be borrowed from its great collection of over 160,000 volumes.

A photostating service is available at usual library rates.

Applications for membership in the library and further information will be sent on request.

The Burden Reference Library

This reference library contains over 14,000 aeronautical books, magazines, pamphlets, photographs, reports, and clippings gathered from world-wide sources and is one of the most complete aeronautical libraries in the world. Material from this library is not available for loan but may be used for reference purposes at the Aeronautical Archives.

The Pacific Aeronautical Library
6715 Hollywood Boulevard
Hollywood, California

Established in cooperation with the aircraft companies the library serves. The leading aircraft companies in or near Los Angeles participate in its support and operation.

This service library for aeronautical research is available to the public for reading privileges. Source material includes aerodynamic and structural research reports, as well as books on drafting, production methods, history, and allied sciences. It furnishes books, periodicals, and pamphlet material to the participating aircraft companies to supplement their engineering libraries.

The Aeronautical Archives Technical Information Service

This service has experienced personnel under the supervision of trained aeronautical engineers to compile any information desired. The services range from listing specialized reference books to the preparation of exhaustive bibliographies, digesting of reports, and general surveys of any aeronautical subject. Some of the available services are:

Bibliographies on any aeronautical subject.
Reports on any aeronautical subject.
Digests of aeronautical books, papers, periodicals, and references.
Translations.
Engineering investigations of special aeronautical subjects.
Biographies of individuals engaged in aeronautics.
Photostats of any aeronautical or general engineering material.
Microfilms made on special order.
Photographs made from the Institute's photographic collection.
Drawings and tracings made.

In addition to the services mentioned any commission which comes within the scope of the Service will be accepted. Special arrangements may be made for work requiring several weeks or months.

Translators are available for accurate transcriptions of all foreign language data. Translations are carefully edited by trained engineers.

Reproductions of any material in the Aeronautical Archives of the Institute may be ordered at standard photostat rates.

INSTITUTE OF THE AERONAUTICAL SCIENCES
1505 RCA BUILDING WEST
30 ROCKEFELLER PLAZA, NEW YORK 20, N. Y.

629

JOURNAL OF THE AERONAUTICAL SCIENCES

VOLUME 11 OCTOBER, 1944 NUMBER 4

CONTENTS

Some Two-Dimensional Adiabatic Compressible Flow Patterns . . . . . HANS KRAFT AND CHARLES G. DIBBLE 283
Efficiency of Lateral Stiffeners in Panels . . . . . ADAM ZAHORSKI 299
Prediction of Longitudinal Dynamic Stability . . . . . H. P. LIEPMAN 307
Causes of Nighttime Thunderstorms over the Middle West . . . . D. M. CROWLEY 313
An Iterative Method for Determining Dynamic Deflections and Frequencies . . . . . N. A. BOUKIDIS AND R. J. RUGGIERO 319
The L.P.C. Method of Performance Computation . . . . . JOSEPH V. FOA AND BERNARD M. LEADON 329
Periodic Aerodynamic Forces on Rotors in Forward Flight . . . CHARLES SEIBEL 339
Stress Analysis of Open Cylindrical Membranes . . . . . LEON BESKIN 343
Contracting Cones Giving Uniform Throat Speeds . . . . . RICHARD H. SMITH AND CHI-TEH WANG 356
Aero-Elastic Instability in Unbalanced Lifting Rotor Blades . . . . . REINHARDT ROSENBERG 361
Drag of Airfoils in Grids of High Solidity . . . . . J. R. WESKE 369
Flexural Strength in the Plastic Range of Rectangular Magnesium Extrusions . . . . . F. A. RAPPLEYEA AND E. J. EASTMAN 373
Corrections for Lengths of Columns Tested Between Knife Edges . . . . . WILLIAM R. OSGOOD 378
On the Mechanism of Friction . . . . . BERNHARD W. SAKMANN AND JOHN T. BURWELL, JR. 381
The Response of Helicopters with Articulated Rotors to Cyclic Blade Pitch Control . . . . . A. F. DONOVAN AND M. GOLAND 387
Buckling Loads of Beams or Plates on Continuous Supports . . . . EDWARD SAIBEL 399
Letters to the Editor 312, 318, 328, 338, 398
Index to Volume 11 405

Copyright, 1944, by the
INSTITUTE OF THE AERONAUTICAL SCIENCES, INC.

JOURNAL OF THE AERONAUTICAL SCIENCES

VOL. 11 OCTOBER, 1944 NO. 4

PUBLISHED QUARTERLY BY THE INSTITUTE OF THE AERONAUTICAL SCIENCES INC.

Chairman of the Editorial Board: HUGH L. DRYDEN, *Chief of Mechanics and Sound Division, National Bureau of Standards*

Editor: ROBERT R. DEXTER *Manager:* JOSEPH J. MAITAN

The Institute of the Aeronautical Sciences publishes the JOURNAL OF THE AERONAUTICAL SCIENCES quarterly, in January, April, July, and October, and the AERONAUTICAL ENGINEERING REVIEW monthly.

The JOURNAL OF THE AERONAUTICAL SCIENCES prints papers of scientific and technical interest to Institute members and subscribers. In general, it provides an opportunity for specialists to publish articles disclosing new knowledge and new applications in the field of the aeronautical sciences. The JOURNAL restricts itself to the aeronautical aspects of advances in science and engineering, and papers printed have either been submitted directly to the JOURNAL or have been previously presented at a meeting of the Institute.

The AERONAUTICAL ENGINEERING REVIEW keeps members and subscribers informed regarding the contents of new books and current periodicals in the field of aeronautics. It reviews new developments in the aircraft industry and reports on progress from house organs and catalogues published by aircraft and engine manufacturers and other companies engaged in aeronautical activities. It publishes papers on applied engineering and aircraft production. News of Institute activities is published in the REVIEW.

Statements and opinions expressed in the JOURNAL are to be understood as individual expressions of the authors and not those of the Institute.

SUBSCRIPTION RATES

Journal of the Aeronautical Sciences
Published Quarterly

United States and Possessions		Foreign Countries Including Canada (American Currency Rates)	
1 Year	$7.00	1 Year	$9.00
Single Copies	2.00	Single Copies	2.50

Aeronautical Engineering Review
Published Monthly

United States and Possessions		Foreign Countries Including Canada (American Currency Rates)	
1 Year	$3.00	1 Year	$3.50
Single Copies	0.30	Single Copies	0.35

Notices of change of address should be sent to the Institute at least 30 days prior to actual change of address.

Manuscripts for publication, proofs, and all correspondence should be addressed to the Editorial Office of the JOURNAL.

Correspondence regarding subscriptions may be addressed to Publication Office, 20th and Northampton Sts., Easton, Pa., or to the Editorial Office of the JOURNAL OF THE AERONAUTICAL SCIENCES, 1505 RCA Building West, 30 Rockefeller Plaza, New York 20, New York.

Entered as Second-Class Matter at the Post Office, Easton, Pa., May 1, 1937. Acceptance for mailing at a special rate of Postage provided for in the Act of August 24, 1912. Authorized April 20, 1937.

INSTITUTE of the AERONAUTICAL SCIENCES

President
R. H. FLEET

Vice-Presidents
WELLWOOD E. BEALL
WILLIAM K. EBEL
ELMER A. SPERRY, JR.
G. M. WILLIAMS

Executive Vice-President
BENNETT H. HORCHLER

Past-Presidents
J. C. HUNSAKER
CHARLES L. LAWRANCE
D. W. DOUGLAS
GLENN L. MARTIN
CLARK B. MILLIKAN
T. P. WRIGHT
GEORGE W. LEWIS
JAMES H. DOOLITTLE
FRANK W. CALDWELL
HALL L. HIBBARD
HUGH L. DRYDEN

Assistant to the President
GEORGE R. FORMAN

Secretary
ROBERT R. DEXTER

Treasurer
CHARLES H. COLVIN

Controller
JOSEPH J. MAITAN

COUNCIL

LESTER D. GARDNER, *Chairman*

P. R. BASSETT
W. A. M. BURDEN
RALPH S. DAMON
CHARLES FROESCH
R. T. GOODWIN
R. PAUL HARRINGTON
C. S. JONES
ROGER WOLFE KAHN
JOHN C. LESLIE
ALFRED MARCHEV
ROBB C. OERTEL
EARL D. OSBORN

ADVISORY BOARD

JOHN D. AKERMAN
WALTER BEECH
LAWRENCE D. BELL
DON R. BERLIN
LYMAN J. BRIGGS
CLAIRE L. EGTVEDT
JACK FRYE
ROBERT E. GROSS
TH. VON KÁRMÁN
J. H. KINDELBERGER
F. K. KIRSTEN
PAUL KOLLSMAN
ARNOLD M. KUETHE
I. M. LADDON
WILLIAM LITTLEWOOD
THOMAS A. MORGAN
JOHN K. NORTHROP
W. A. PATERSON
E. T. PRICE
A. E. RAYMOND
F. W. REICHELDERFER
FRED H. ROHR
T. CLAUDE RYAN
J. T. TRIPPE
J. G. VINCENT
RAYCROFT WALSH
EDWARD P. WARNER
E. E. WILSON
BURDETTE S. WRIGHT

HONORARY MEMBERS

GRIFFITH BREWER
LYMAN J. BRIGGS
W. A. M. BURDEN
FRANK O. CARROLL
ARTEMUS L. GATES
HARRY F. GUGGENHEIM
ROBERT A. LOVETT
JOHN S. MCCAIN
CLEMENTS MCMULLEN
GEORGE B. PEGRAM
L. WELCH POGUE
J. LAURENCE PRITCHARD
D. C. RAMSEY
F. W. REICHELDERFER
EUGEN E. REINARTZ
C. G. A. ROSSBY
T. P. WRIGHT

HONORARY FELLOWS

H. H. ARNOLD
D. W. DOUGLAS
HUGH L. DRYDEN
W. F. DURAND
C. R. FAIREY
A. H. R. FEDDEN
J. C. HUNSAKER
B. MELVILL JONES
TH. VON KÁRMÁN
GEORGE W. LEWIS
GLENN L. MARTIN
GEORGE J. MEAD
D. R. PYE
IGOR I. SIKORSKY
G. I. TAYLOR
ORVILLE WRIGHT

BENEFACTOR MEMBERS

EDWARD E. ALDRIN
HART O. BERG (Deceased)
E. L. CORD
D. W. DOUGLAS
SHERMAN M. FAIRCHILD
C. R. FAIREY
R. H. FLEET
FLORENCE GUGGENHEIM (Deceased)
C. D. HANSCOM
JOHN P. V. HEINMULLER
ALEXANDER KLEMIN
PAUL KOLLSMAN
BELLA C. LANDAUER
WILLIAM LANDAUER
GROVER LOENING
EDMUND C. LYNCH (Deceased)
F. W. MAGIN
GLENN L. MARTIN
GEO. J. MEAD
S. A. REED (Deceased)
L. S. ROCKEFELLER
EDWARD P. WARNER

AMERICAN FELLOWS

EDWIN E. ALDRIN
KARL ARNSTEIN
J. L. ATWOOD
RALPH S. BARNABY
P. R. BASSETT
WELLWOOD E. BEALL
REX B. BEISEL
G. M. BELLANCA
DON R. BERLIN
HENRY A. BERLINER,
B. C. BOULTON
GEORGE W. BRADY
LYMAN J. BRIGGS
W. G. BROMBACHER
CHARLES P. BURGESS
FRANK W. CALDWELL
CHARLES H. CHATFIELD
ALLAN CHILTON
V. E. CLARK
CHARLES H. COLVIN
KARL T. COMPTON
JOHN W. CROWLEY, JR.
LUIS DE FLOREZ
A. V. DE FOREST
RALPH S. DAMON
SMITH J. DE FRANCE
J. P. DEN HARTOG
WALTER S. DIEHL
JAMES H. DOOLITTLE
C. S. DRAPER
IVAN H. DRIGGS
WILLIAM K. EBEL
C. L. EGTVEDT
FREDERIC FLADER
JACK FRYE
GARLAND FULTON
R. F. GAGG
LESTER D. GARDNER
RICHARD C. GAZLEY
MICHAEL E. GLUHAREFF
MELVIN N. GOUGH
LEROY R. GRUMMAN
R. M. HAZEN
ALBERT F. HEGENBERGER
EDWARD H. HEINEMANN
S. D. HERON
HALL L. HIBBARD
L. S. HOBBS
PAUL E. HOVGAARD
WILLIAM HOVGAARD
ROBERT INSLEY
EASTMAN N. JACOBS
CLARENCE L. JOHNSON
PAUL H. KEMMER
J. H. KINDELBERGER
ARTHUR L. KLEIN
ALEXANDER KLEMIN
W. B. KLEMPERER
PAUL KOLLSMAN
OTTO C. KOPPEN
B. V. KORVIN-KROUKOVSKY
S. M. KRAUS
I. M. LADDON
E. S. LAND
CHARLES L. LAWRANCE
JOHN G. LEE
CHARLES A. LINDBERGH
WILLIAM LITTLEWOOD
GROVER LOENING
EUGENE E. LUNDQUIST
R. D. MACCART
WM. H. MCAVOY
C. J. MCCARTHY
RICHARD VON MISES
CLARK B. MILLIKAN
ROBERT J. MINSHALL
JOSEPH S. NEWELL
ALFRED S. NILES
JOHN K. NORTHROP
ARTHUR NUTT
ROBERT R. OSBORN
W. BAILEY OSWALD
GEORGE A. PAGE, JR.
F. W. PAWLOWSKI
F. W. PENNOYER, JR.
A. A. PRIESTER
A. E. RAYMOND
F. W. REICHELDERFER
ELLIOTT G. REID
H. J. E. REID
H. C. RICHARDSON
C. E. ROSENDAHL
WILLIAM T. SCHWENDLER
JAMES M. SHOEMAKER
MAC SHORT
IGOR ALEXIS SIKORSKY
ELMER A. SPERRY, JR.
JOHN STACK
WILLIAM B. STOUT
HARRY A. SUTTON
C. FAYETTE TAYLOR
EDWARD S. TAYLOR
PHILIP B. TAYLOR
TH. THEODORSEN
T. E. TILLINGHAST
S. TIMOSHENKO
STARR TRUSCOTT
L. B. TUCKERMAN
RALPH H. UPSON
J. G. VINCENT
EDWARD P. WARNER
P. V. H. WEEMS
FRED E. WEICK
R. D. WEYERBACHER
JOHN B. WHEATLEY
ANDREW V. WILLGOOS
DONALD H. WOOD
ROBERT J. WOODS
T. P. WRIGHT
JOHN E. YOUNGER
STEPHEN J. ZAND
ALBERT F. ZAHM

An Appreciation
to Corporate Members of the
Institute of the Aeronautical Sciences

Listed below are the leading aeronautical and industrial companies that make possible the publication of the *Journal of the Aeronautical Sciences*.

They enable the Institute to publish scientific and technical papers in the *Journal* and to devote its pages exclusively to editorial material.

Dues from individual members which would normally be used to publish this scientific and engineering quarterly are thus released for additional services to the profession and industry.

Advertising defrays the cost of publishing the *Aeronautical Engineering Review* and the *Aeronautical Engineering Catalog*.

These publications provide a comprehensive technical information service for the benefit of the aircraft and related industries.

ACADEMY OF AERONAUTICS
ADEL PRECISION PRODUCTS CORPORATION
AERO INSURANCE UNDERWRITERS
AEROJET ENGINEERING CORPORATION
AERONAUTICAL PRODUCTS, INC.
AEROQUIP CORPORATION
AIRCHOX COMPANY DIVISION, JOYCE AVIATION, INC.
AIRCRAFT ACCESSORIES CORPORATION
AIRCRAFT ACCESSORIES CORPORATION OF MISSOURI
AIRCRAFT RADIO CORPORATION
AIRESEARCH MANUFACTURING COMPANY
AIRESEARCH MANUFACTURING COMPANY OF ARIZONA, INC.
AIREX MANUFACTURING COMPANY, INC.
ALLIS-CHALMERS MANUFACTURING COMPANY
ALLISON DIVISION, GENERAL MOTORS CORPORATION
ALUMINUM COMPANY OF AMERICA
AMERICAN AIRLINES, INC.
AMERICAN BOSCH CORPORATION
AMERICAN CENTRAL MANUFACTURING CORPORATION
AMERICAN EXPORT AIRLINES, INC.
AMERICAN PHENOLIC CORPORATION
THE AMERICAN ROLLING MILL COMPANY
AMERICAN TUBE BENDING COMPANY, INC.
ASSOCIATED AVIATION UNDERWRITERS
ASSOCIATED FOUNDRIES & MANUFACTURERS, INC.
BAKER STEEL & TUBE COMPANY
BALLARD AIRCRAFT COMPANY, INC.
BAUSCH & LOMB OPTICAL COMPANY
BEECH AIRCRAFT CORPORATION
THE BG CORPORATION
BELL AIRCRAFT CORPORATION
BENDIX AVIATION CORPORATION
BENDIX PRODUCTS DIVISION
BENDIX RADIO CORPORATION
ECLIPSE-PIONEER DIVISION
EXPORT DIVISION
JULIEN P. FRIEZ & SONS DIVISION
PACIFIC DIVISION
SCINTILLA MAGNETO COMPANY
BOEING AIRCRAFT COMPANY
BOEING SCHOOL OF AERONAUTICS
BOLTON MANUFACTURING CORPORATION
BOOTS AIRCRAFT NUT CORPORATION
BREEZE CORPORATIONS, INC.
ESSEX TOOL & DIE COMPANY
FEDERAL LABORATORIES, INC.
EDWARD G. BUDD MANUFACTURING COMPANY
CANADIAN PACIFIC AIR LINES LTD.
CESSNA AIRCRAFT COMPANY
CHANDLER-EVANS CORPORATION
CHASE NATIONAL BANK OF THE CITY OF NEW YORK
THE CLEVELAND GRAPHITE BRONZE COMPANY
THE CLEVELAND PNEUMATIC TOOL COMPANY
AUTOMOTIVE-AIRCRAFT DIVISION
CLIFFORD MANUFACTURING COMPANY
CONSOLIDATED VULTEE AIRCRAFT CORPORATION
NASHVILLE DIVISION
STINSON AIRCRAFT DIVISION
CONTINENTAL MOTORS CORPORATION
CULVER AIRCRAFT CORPORATION
CURTISS-WRIGHT CORPORATION
AIRPLANE DIVISION
PROPELLER DIVISION
WRIGHT AERONAUTICAL CORPORATION
DOAK AIRCRAFT COMPANY, INC.
DOUGLAS AIRCRAFT COMPANY, INC.
EL SEGUNDO PLANT
LONG BEACH PLANT
THE DOW CHEMICAL COMPANY
EASTERN AIR LINES, INC.
EATON MANUFACTURING COMPANY
THOMAS A. EDISON, INC., INSTRUMENT DIVISION
EDO AIRCRAFT CORPORATION
ELASTIC STOP NUT CORPORATION OF AMERICA
THE ELECTRIC AUTO-LITE COMPANY
ELECTROL INCORPORATED
EMBRY-RIDDLE COMPANY
ENGINEERING AND RESEARCH CORPORATION
ETHYL CORPORATION
THE FAFNIR BEARING COMPANY
FAIRCHILD CAMERA & INSTRUMENT CORPORATION
FAIRCHILD AERIAL SURVEYS, INC.
FAIRCHILD ENGINE & AIRPLANE CORPORATION
DURAMOLD AIRCRAFT CORPORATION
FAIRCHILD AIRCRAFT DIVISION
RANGER AIRCRAFT ENGINES DIVISION
FEDERAL TELEPHONE & RADIO CORPORATION
FIRESTONE AIRCRAFT COMPANY
FLEETWINGS DIVISION, KAISER CARGO, INC.
FLETCHER AVIATION CORPORATION
G & A AIRCRAFT, INC.
GENERAL AIRCRAFT EQUIPMENT, INC.
GENERAL AVIATION EQUIPMENT COMPANY, INC.
GENERAL ELECTRIC COMPANY
GENERAL INSTRUMENT CORPORATION
GENERAL MOTORS CORPORATION
AC SPARK PLUG DIVISION
AEROPRODUCTS DIVISION
BUICK MOTOR DIVISION
CADILLAC MOTOR CAR DIVISION
CHEVROLET MOTOR DIVISION
DELCO PRODUCTS DIVISION
DELCO-REMY DIVISION
EASTERN AIRCRAFT DIVISION
FISHER BODY DIVISION
FRIGIDAIRE DIVISION
HARRISON RADIATOR DIVISION
RESEARCH LABORATORIES DIVISION
ROCHESTER PRODUCTS DIVISION
GENERAL TIRE & RUBBER COMPANY
THE B. F. GOODRICH COMPANY
THE GOODYEAR TIRE & RUBBER COMPANY
GRAND CENTRAL AIRPORT COMPANY
THE GRAY MANUFACTURING COMPANY
GRUMMAN AIRCRAFT ENGINEERING CORPORATION
GUIBERSON DIESEL ENGINE COMPANY
W. & L. E. GURLEY
HAMMOND AIRCRAFT COMPANY
HANNA ENGINEERING WORKS
HASKELITE MANUFACTURING CORPORATION
HAYES INDUSTRIES, INC.
HIGGINS AIRCRAFT, INC.
HUB INDUSTRIES, INC.
THE INTERNATIONAL NICKEL COMPANY
INTERSTATE AIRCRAFT & ENGINEERING CORPORATION
WILSHIRE DIVISION
EL SEGUNDO DIVISION
DE KALB DIVISION
IRVING AIR CHUTE COMPANY, INC.
JACK & HEINTZ, INC.
JACOBS AIRCRAFT ENGINE COMPANY
CASEY JONES SCHOOL OF AERONAUTICS, INC.
JORDANOFF AVIATION CORPORATION
KELLETT AIRCRAFT CORPORATION
KENYON INSTRUMENT COMPANY, INC.
WALTER KIDDE & COMPANY, INC.
KOLLSMAN INSTRUMENT DIVISION, SQUARE D COMPANY
LAISTER-KAUFFMANN AIRCRAFT CORPORATION
LANGLEY CORPORATION
LAVELLE AIRCRAFT CORPORATION
LEAR INCORPORATED
LIBERTY AIRCRAFT PRODUCTS CORPORATION
LIGHTS, INCORPORATED
LINK AVIATION DEVICES, INC.
LOCKHEED AIRCRAFT CORPORATION
LONGINES-WITTNAUER WATCH COMPANY, INC.
MAGNAFLUX CORPORATION
THE MARQUETTE METAL PRODUCTS COMPANY
THE GLENN L. MARTIN COMPANY
WARREN McARTHUR CORPORATION
McDONNELL AIRCRAFT CORPORATION
MENASCO MANUFACTURING COMPANY
MICROMATIC HONE CORPORATION
MINNEAPOLIS-HONEYWELL REGULATOR COMPANY
MOORE DROP FORGING COMPANY
NASH-KELVINATOR CORPORATION
NATIONAL CITY BANK OF NEW YORK
NATIONAL CREDIT OFFICE, INC.
NATIONAL MACHINE PRODUCTS
THE NATIONAL SCREW & MANUFACTURING COMPANY
NOORDUYN AVIATION LIMITED
NORMA-HOFFMANN BEARINGS CORPORATION
NORTH AMERICAN AVIATION, INC.
NORTH AMERICAN AVIATION, INC., OF TEXAS
NORTHEAST AIRLINES, INC.
NORTHROP AIRCRAFT, INC.
NORTHWEST AIRLINES, INC.
OTTO AVIATION CORPORATION
PACKARD MOTOR CAR COMPANY
PAN AMERICAN AIRWAYS SYSTEM
THE PARKER APPLIANCE COMPANY
PENNSYLVANIA-CENTRAL AIRLINES CORPORATION
PHILLIPS PETROLEUM COMPANY
PIONEER PARACHUTE COMPANY, INC.
PRATT, READ & COMPANY, INC.
PESCO PRODUCTS COMPANY DIVISION, BORG-WARNER CORPORATION
THE PURE OIL COMPANY
REPUBLIC AVIATION CORPORATION
RIDGEFIELD MANUFACTURING CORPORATION, AIRCRAFT DIVISION
JOHN A. ROEBLING'S SONS COMPANY
ROHR AIRCRAFT CORPORATION
ROOSEVELT FIELD, INC.
THE RYAN AERONAUTICAL COMPANY
SCOTT AVIATION CORPORATION
SHAKESPEARE PRODUCTS COMPANY
SHELL OIL COMPANY, INC.
SIMMONDS AEROCESSORIES, INC.
SOCONY-VACUUM OIL COMPANY
SOLAR AIRCRAFT COMPANY
SOUTHERN AVIATION SCHOOL
SPERRY GYROSCOPE COMPANY, INC.
SQUARE D COMPANY
STANDARD OIL COMPANY OF CALIFORNIA
STANDARD OIL COMPANY (INDIANA)
STANDARD OIL COMPANY OF NEW JERSEY
STEEL IMPROVEMENT & FORGE COMPANY
STEWART-WARNER CORPORATION, INC.
SUMMERILL TUBING COMPANY
SWEDLOW AEROPLASTICS CORPORATION
SWITLIK PARACHUTE COMPANY
TELEFLEX LIMITED
THE TEXAS COMPANY
THOMPSON PRODUCTS, INC.
TINNERMAN PRODUCTS, INC.
TITEFLEX, INC.
TRANSCONTINENTAL & WESTERN AIR, INC.
TRIPLETT & BARTON, INC.
UNITED AIRCRAFT CORPORATION
CHANCE VOUGHT AIRCRAFT DIVISION
HAMILTON STANDARD PROPELLERS DIVISION
PRATT & WHITNEY AIRCRAFT DIVISION
PRATT & WHITNEY AIRCRAFT CORPORATION OF MISSOURI
SIKORSKY AIRCRAFT DIVISION
UNITED AIR LINES TRANSPORT CORPORATION
UNITED STATES AVIATION UNDERWRITERS, INC.
UNITED STATES RUBBER COMPANY
DOMINION RUBBER COMPANY, LTD.
UNIVERSAL MOULDED PRODUCTS CORPORATION
VICKERS, INC.
VICTOR ADDING MACHINE COMPANY
VIDAL RESEARCH CORPORATION
WARNER AIRCRAFT CORPORATION
THE WEATHERHEAD COMPANY
WESTERN AIRLINES, INC.
WESTINGHOUSE ELECTRIC & MANUFACTURING COMPANY
WESTON ELECTRICAL INSTRUMENT CORPORATION
WYMAN-GORDON COMPANY
YOUNG RADIATOR COMPANY

es

rnal

y to

y are

alog.

ated

MPANY

AS

TION

ARNER

N, AIR-

ON

TION OF

N

ING.

TION

TURING

ATION

SUGGESTIONS FOR CONTRIBUTORS TO THE PUBLICATIONS *of the* INSTITUTE *of the* AERONAUTICAL SCIENCES

The Institute of the Aeronautical Sciences invites both members and nonmembers from any country to submit papers for publication in the JOURNAL OF THE AERONAUTICAL SCIENCES and the AERONAUTICAL ENGINEERING REVIEW. The Institute, following the practice of other societies, does not pay for contributions.

The following directions for the preparation of papers, if followed by authors, will save correspondence, avoid the return of papers for changes, minimize the work of preparation for the printer, and save the expense due to the charges made for "author's corrections."

MANUSCRIPTS: Papers must be written in English, in original typewriting on one side only of white paper sheets, consecutively numbered, and be double or triple spaced with wide margins. Manuscripts should be prepared with great care so that they will be typographically accurate. Paragraphing should be given special attention. Papers should be written in the third person, reference to the writer being made as "the author." Avoid the use of the words "I," "we," and "you." Blueprint copies of papers are unacceptable as it is impossible to mark directions to the printer on them. Correcting, changing, or adding to papers after they are in type is costly. It is, therefore, imperative that papers submitted be in final form. Typographical errors may be corrected on proofs, but if authors wish to add material, they may do so at their own expense. In mailing, drawings may be rolled, but manuscripts should be sent flat. Send by first class mail (register if you wish for your own protection) to the Editorial Office, Institute of the Aeronautical Sciences, 1505 RCA Bldg. West, 30 Rockefeller Plaza, New York 20, N. Y. All manuscripts will be examined by the Editorial Committee and by the Editor. Authors will be advised as promptly as possible whether the paper is acceptable for publication.

TITLES: The title of the paper should be brief. The name and initials of the author should be written as he prefers. The use of the full name of an author is advocated because of the frequent duplication of initials and surnames which sometimes makes it difficult to establish the identity of the author. This is particularly important for large annual indexing and abstracting services. All titles and degrees or honors are omitted. The name of the organization with which the author is associated should be placed after his name on a separate line. The date on which the paper is received will be inserted by the Editor.

SUMMARIES OR ABSTRACTS: An abstract to be printed at the beginning should accompany each article. It should be adequate as an *index* and as a *summary*. It should contain a statement of major conclusions reached, since summaries in many cases constitute the only source of information used in compiling scientific reference indexes. Abstracts printed in other journals, especially foreign, in most cases, consist of summaries from printed papers. The summary should explain as adequately as possible the major conclusions to a nonspecialist in the subject. The summary should contain from 100 to 300 words, depending on the length of the paper.

SUBHEADINGS: Subheadings should be inserted by the author at frequent intervals. The work of editorial preparation will be simplified by the author providing many subheadings. Owing to the breaking of columns and the insertion of illustrations, some of the subheadings may have to be omitted.

SHORTENING OF PAPERS: Some papers, at the end, fill in only a portion of a page. This leaves much wasted blank space as succeeding articles are started at the top of a page. Authors should indicate by notation on the left-hand side of the page what matter may be omitted when "runovers" occur. This request is important as the Journal cannot afford in the future, as it has in its earlier issues, to have blank half pages or more at the end of papers.

MATTER USUALLY DELETED: Acknowledgments of assistance in preparation of paper, except by collaborators. Photographs or illustrations of little technical interest and not showing advances in general practice. Too detailed tabular matter (general results of such tables may be included in the text). Lengthy descriptions of materials or processes or of preliminary experiments or theories that preceded final results; salient features only are of interest.

REFERENCES AND FOOTNOTES: References should appear as footnotes only, numbered consecutively, grouped together at the end of the manuscript. The arrangement should be as follows: (for books)—[1] Durand, W. F., *Aerodynamic Theory*, 1st Edition, Vol. 1, p. 23; Julius Springer, Berlin, 1934. (For magazines)—

[1]Englund, C. R., Crawford, A. B., and Mumford, W. W., *Some Results of a Study of Ultra-Short-Wave Transmission Phenomenon*, Proc. I. R. E., Vol. 20, No. 12, pp. 481 and 482, March, 1933. Please give author, title, edition, volume, page, publisher and date of publication as indicated. Omission of one required fact causes much extra editorial work and possible inaccuracies. All references are grouped at the end of the article.

ILLUSTRATIONS: Illustrations should accompany manuscripts and each should always be referred to in the text, preferably by number. Drawings or graphs should not be larger than 12 × 16 inches, and must be made with jet black India Ink on white paper or tracing cloth, the latter being preferred. *Do not use typewriter for lettering.* The smallest lettering on 8 × 10 inch figures should be no less than $^1/_4$ inch high. Cross-section paper (white with black lines) may be used, but should not have more than 4 lines per inch. If finer ruled paper is used, the major division lines should be drawn in with black ink, omitting the finer divisions. In the case of finely ruled paper, only blue-lined paper can be accepted. *Tracing paper and blueprints* are not acceptable. Lettering and all markings must be large enough to be readable after reduction. Mail rolled or flat, never fold. Drawings that cannot be reproduced (including pencil drawings) will be returned to the author for redrawing, thus delaying publication of the paper. Photographs should be very distinct and show clear black and white contrasts. They must be on glossy white paper. Avoid round and oval photographs.

CAPTIONS AND LEGENDS: Legends or captions must accompany each drawing or photograph submitted. If written on the drawing or photograph, they should be placed below and well outside the part to be reproduced. It is better to place them on separate sheets of paper pasted to the back of the drawings or photographs. Each table should have a caption such as Table 1, Table 2, Table 3, etc. Captions should be complete in themselves so as to make the data intelligible to the reader without reference to the text. A duplicate list of captions for figures should be included as the last page of the manuscript. Use "Fig. 1" (not Figure 1), Figs. 3 and 4, etc., in both the text and the numbering of illustrations. In the text, "Eq. (1)," or "Eqs. (1) and (2)" are preferable to "Equation (1)." In captions and legends, except for "Fig." and "Eq." and table headings, write all words in full; do not abbreviate. Avoid placing explanatory written matter in the drawings; it should be in the text.

MATHEMATICAL WORK: Only the simplest formulas should be typewritten; all others should be carefully written in pen and ink, the writing to be large enough so that ample room is provided to mark mathematical matter for the printer. A considerable space for marking should be allowed above and below all equations. All complicated equations should be repeated on separate sheets with plenty of space left for marking. The solidus should be used for simple fractions appearing within the text. Make all expressions clear to the typesetter. Greek letters used in formulas should be clearly designated by name on the margin of the manuscript. All symbols should be clearly written and carefully checked. The difference between capital and lower-case letters should be clearly distinguished and care taken to avoid confusion between zero (0) and the letter (o), between the numeral (one) and the letter (ell) and the prime ('), between alpha and a, kappa and k, u and mu, v and nu, n and eta. All subscripts and exponents should be clearly marked and dots and bars over letters or mathematical expressions should be avoided. Avoid complicated exponents and subscripts. When it is necessary to repeat a complicated expression, it should be represented by some convenient symbol.

NOMENCLATURE AND ABBREVIATIONS: The National Advisory Committee for Aeronautics Nomenclature should be used in preference to any others. Standard abbreviations should be used, and it should be noted that most abbreviations are lower case, such as m.p.h., b.m.e.p., i.hp., b.hp., hp., . . . etc.

INSTITUTE *of the* AERONAUTICAL SCIENCES
1932–1944

Since its incorporation in October, 1932, as a scientific membership society to advance the art and science of aeronautics, the Institute of the Aeronautical Sciences, in over ten years of service to aviation, has become the representative technical society for the aviation industry and profession. It is the only organization in the United States which brings together all of the sciences and branches of engineering and technology which are applied to aeronautics.

Activities

In this year, coincident with the great increase in aeronautical production and research in the nation's war effort, the Institute is expanding its membership and activities in keeping with the greater demands made upon its services. Beginning with aeronautical students, the Institute has increased the number and activities of Student Branches. Members of the Institute in aeronautical centers are organized in local Sections which hold their own meetings. More of these Sections are being formed this year and additional services provided for members. The Annual Meeting and other national meetings provide forums where specialists in all the aeronautical sciences may present and receive reports on progress made in their particular fields and learn of developments in other fields that have a bearing on their own work. Several annual awards and honors are conferred by the Institute to recognize and encourage outstanding achievement in the aeronautical sciences.

Publications

Papers presented at meetings or submitted to the Editorial Board are published in the JOURNAL OF THE AERONAUTICAL SCIENCES or the AERONAUTICAL ENGINEERING REVIEW. The JOURNAL prints in each issue several full length scientific papers on new research and developments in various fields applied to aviation. The REVIEW keeps members and subscribers up to date on aeronautical news and literature through reviews of new books and periodical articles, government publications and trade literature and publishes papers on applied engineering and aircraft production.

The AERONAUTICAL ENGINEERING CATALOG, published yearly, is a guide to sources and specifications of materials, parts, and accessories used in the design and production of aircraft, aircraft engines, and parts.

Research Facilities

Through the Aeronautical Archives of the Institute, members have for their use the most complete aeronautical library and reference research facilities maintained by any technical society. At Institute headquarters in New York, the W. A. M. Burden Reference Library of books, reports and periodicals, the Aeronautical Index of subject files, biographic files and bibliography, and the historical and art collections in the Archives are available for study. The Pacific Aeronautical Library at 6715 Hollywood Boulevard, Los Angeles, maintains a reference collection and reading room for members and loans books to company libraries in the area. Through The Paul Kollsman Library, aeronautical books are lent by mail without charge to members anywhere in the continental United States. In addition to a very complete collection of standard aeronautical reference works, the Kollsman Library has available for loan new aviation books as they are reviewed in the AERONAUTICAL ENGINEERING REVIEW.

Membership

In addition to membership in professional societies representing their particular fields, specialists applying their knowledge and experience to aeronautics find membership in the Institute of great value in the contacts made with others engaged in aeronautical work and in the broad coverage of all aeronautical problems furnished through its meetings and publications. All applications for membership are carefully reviewed by the Admissions Committee, which recommends the grade of membership for which the applicant is found eligible. There are advanced grades of membership—Associate Fellow, Fellow, Honorary Fellow—to which members may be elected as their experience warrants. Thus, a member receives due recognition—more valuable because it is given by his colleagues—for his contributions to the progress of aeronautics. New applicants may be elected initially by the Admissions Committee to the grade of MEMBER if they are engineering graduates with at least three years of experience or have had over five years' experience in research, engineering, or other special work applied to aviation; to the grade of Industrial Member if they have acquired a recognized standing in an administrative capacity in the aviation industry; to the grade of Technical Member if they are recent engineering school graduates or are engaged in technical aeronautical work. For those interested or engaged in aeronautics or fields related to aeronautics who wish to participate in the activities of the Institute, the grade of Affiliate is provided. Student Members are admitted by application through Student Branches organized at their schools. Aeronautical companies, as well as individuals, are affiliated with, and participate in, the support of the Institute through Corporate Membership.

Dues

An entrance fee of $5.00 is required of all new members who apply for admission to a grade of membership to be specified by the Admissions Committee (Corporate Members, Student Members, and those who apply specifically for the grade of Affiliate being excepted).

Annual membership dues for the various grades of membership are as follows: Fellows—$15; Associate Fellows—$11; MEMBERS—$9.00; Industrial Members—$9.00; Technical Members—$5.00; Affiliates—$5.00.

The regular subscription price for the JOURNAL OF THE AERONAUTICAL SCIENCES and the AERONAUTICAL ENGINEERING REVIEW is $7.00 and $3.00 per year, respectively. Members may subscribe to the JOURNAL or the REVIEW or both at one-half the regular subscription rates.

Those who are engaged in aeronautical work or who have an interest in any technical phase of aviation will find the services of the Institute to be a necessary aid in keeping abreast of developments in these times of such rapid progress. An application form and further information about membership can be obtained from an Institute member or by writing to the Secretary.

INSTITUTE OF THE AERONAUTICAL SCIENCES
1505 RCA BUILDING WEST
30 ROCKEFELLER PLAZA
NEW YORK 20, N. Y.